Macromolecular design for viscoelasticity and thoughness in polyelectrolyte complexes

Alexei Dmitrievitsj Filippov

Propositions

1. Self-assembly in aqueous milieu can be prevented by unintentional hydrophobic impurities (this thesis)

2. Linear viscoelasticity is an inadequate marker of material performance (this thesis)

3. The inverse Laplace transform method (CONTIN) leads to over-interpretation of data

4. Sci-hub is illegal, but not illegitimate

5. Squatting is an appropriate response to the failure of the state to provide safe and affordable housing

6. Earth is far from overpopulated: it is overpolluted

7. The criminalization of recreational substances is at the expense of public health

8. The militarization of Europe's border is a crime against refugees

Propositions belong to the thesis, entitled *Macromolecular design for viscoelasticity and toughness in polyelectrolyte complexes.*

Alexei Dmitrievitsj Filippov
Wageningen, 16 November 2021

Macromolecular design for viscoelasticity and toughness in polyelectrolyte complexes

A.D. Filippov

Thesis committee

Promotor
Prof. Dr Joris Sprakel
Personal chair, Physical Chemistry and Soft Matter
Wageningen University & Research

Co-promotor
Prof. Dr Marleen Kamperman
Professor, Faculty of Science and Engineering
University of Groningen

Other members
Dr M. M. K. Włodarczyk-Biegun — University of Groningen
Prof. Dr H. Zuilhof — Wageningen University & Research
Prof. Dr D. Hourdet — ESPCI Paris
Dr M.E. Aubin-Tam — Delft University of Technology

This research was conducted under the auspices of the Graduate School VLAG (Advanced studies in Food Technology, Agrobiotechnology, Nutrition and Health Sciences).

Macromolecular design for viscoelasticity and toughness in polyelectrolyte complexes

Alexei (Aljosha) Dmitrievitsj Filippov

Thesis
submitted in fulfilment of the requirements for the degree of doctor
at Wageningen University
by the authority of the Rector Magnificus,
Prof. Dr A. P. J. Mol,
in the presence of the
Thesis Committee appointed by the Academic Board
to be defended in public
on Tuesday 16 November 2021
at 4 p.m. in the Aula.

Alexei Dmitrievitsj Filippov
Macromolecular design for viscoelasticity and toughness in polyelectrolyte complexes
189 pages

PhD thesis, Wageningen University, Wageningen, The Netherlands (2021)
With bibliography, with summary in English

DOI: 10.18174/555339
ISBN: 978-94-6395-924-7

Юле и Диме

Contents

Chapter 1

Introduction

Polymers perform a dazzling array of duties throughout the kingdom of life. DNA stores the instructions for the assembly of all living beings, enzymes enable the biochemical processes from which life emerges, and collagen builds tissues as soft as lungs and as tough as blood vessels. Thus, macromolecules can routinely act as information carriers, catalysts, and structural materials. Given the scope of possibilities that this class of molecules offers, it is unsurprising that it has not escaped the attention of human enterprise. Indeed, the produced volume of even a subset of plastics already exceeded 0.4 GT in 2019,[1] which surpasses the estimated mass of the carbon in all terrestrial animals on Earth.[2] Despite the vast utility of polymer materials and the remarkable progress in polymer technology since the recognition of macromolecules as the building blocks of life, anthropogenic polymers are nowhere as versatile and adapted as their natural inspirations.

1.1 Learning from nature: bio-adhesion in marine animals

A striking lesson of how carefully optimized polymer properties enable organisms to adapt to severe conditions can be learned from the common mussel, *Mytilus edulis*. Mussels are able to anchor themselves to rocks by constructing threads (Figure 1.1a). The formation and maintenance of a robust, adhesive bond in a humid or even underwater milieu, where surfaces are predominantly hydrophilic, requires to satisfy a challenging cocktail of contradictions: first, the adhesive must be hydrophilic to compete with the water bound by hydrophilic interfaces, yet, simultaneously, the bulk of the material has to be insoluble in water. Second, the adhesive has to be delivered as a liquid or very soft solid to be able to conform to the irregularities of the underwater substrates to which underwater animals must attach, yet must develop enough cohesive strength to handle the long-term disturbance of life in the harsh hydrodynamics of the intertidal zone. Neither adhesion nor cohesion are trivial underwater.

To fit the narrow space in which the requirements for underwater adhesion are satisfied, mussels construct byssal threads (holdfasts) by layering at least 20 proteins,

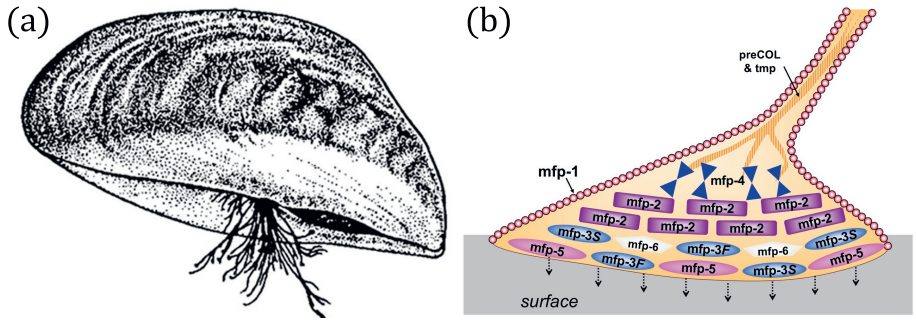

Figure 1.1: (a) Illustration of *M. edulis* (public domain) (b) A "protein atlas" of a mussel-built thread sticking to a surface, where mfp stands for mussel foot protein, and PreCOL and TMP (thread matrix protein) are collagens. Adapted from Waite et al.[3] ©The Company of Biologists.

out of which 12 have been extensively characterized.[4] The proteins vary substantially in their amino acid composition, as well as in their localization in the plaque, but are essentially all positively charged at physiological and ambient (ocean) pH.[4] Figure 1.1b shows the localization of various mussel foot proteins in the thread.

Directly at the interface, two proteins are present: mfp-3 and mfp-5, where mfp stands for mussel foot protein. The sequence of mfp-5 is drawn in Figure 1.2. Two amino acids are conspicuously represented in the sequences: lysine, which possesses a positively charged ammonium group at physiological pH, and the post-translationally hydroxylated 3,4-dihydroxytyrosine, which is often called Dopa in literature due to its close similarity to the phenethylamine neurotransmitter dopamine. The mechanism of initial adhesion involves the displacement of interfacial water molecules by the lysine residues,[5] followed by surface bonding by the dihydroxytyrosine moiety, which has an impressive repertoire of ways to bond to mineral surfaces.[6]

It would be an oversimplification to regard mussel byssus as a single material, since multiple components present a distinct localization: a byssal thread is a building rather than just cement or stainless steel. Besides the adhesive "primer" proteins at the interface, byssal threads contain a densely crosslinked cuticle to protect the thread against the environment, and collagen-type fibers for bulk strength.[4] In other words, mussel adhesion emerges from the synergy of many components. Nevertheless, much of the earlier work on mussel-inspired adhesion centered on the fabrication of synthetic or recombinant structures that mimic the polarity signature of the amino acid distribution of the interfacial mussel foot proteins. Through the combination

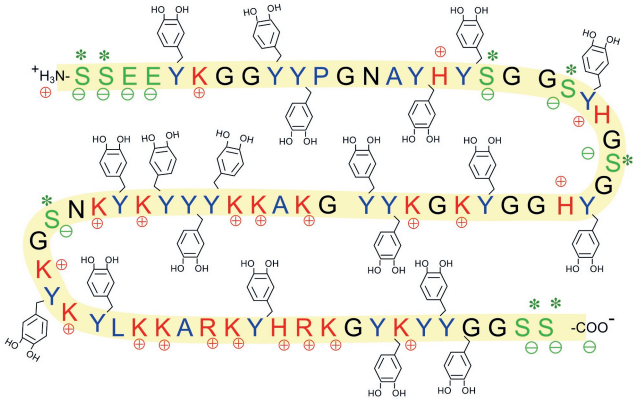

Figure 1.2: Sequence of mfp-5. Adapted from Waite et al.[3] ©The Company of Biologists.

of cationic, anionic, hydrophilic and hydrophobic monomers with those that are catechol-functionalized in ratios that reflect the expression of such moieties in one of the mussel proteins, it has indeed been possible to arrive at a liquid that wets two underwater surfaces, and shows cohesive strength on the nanoscale.[7] However, there is no clear relationship between the structure of the molecules and properties that are relevant for building a robust adhesive.

In some sense, mussels do not truly secrete an adhesive: one of the surfaces that are joined is the byssus, an organ of the mussel itself. On the other hand, another inhabitant of the intertidal zone, the sandcastle worm *Phragmatopoma californica*, shows off a material that is indeed very close to what we would recognize as a glue. *P. californica* is one of several known polychaetes that construct robust, tubular shelters by gluing together sand grains underwater.[8] The strategy that *P. californica* uses is similar to mussels in the sense that some of the proteins that the worm secretes contain large fractions of lysine and 3,4-hydroxytyrosine residues. However, unlike mussel proteins, which are all cationic, *P. californica* packages some of its polycations together with poly(sulfates), which are highly dense in negative charge.

The role of the polyanion is two-fold: first of all, polyelectrolytes that carry net negative charge have the ability to complex divalent metal cations such as Mg^{2+} and Ca^{2+}. The presence of said ions is essential to the mechanics of the cement of tube-building worms.[8] Furthermore, polyanions form complexes with polycations

that allow to concentrate polyelectrolytes without the need for much further compartmentalization. Complexes between polyanions and polycations are called complex coacervates, and, as soon will become clear, they are at the center of interest of this thesis.

The cement of *P. californica* has also seen many attempts at mimicking its properties. Again, the initial attempts succeeded to mimic the distribution of chemical characters given by the residues of the protein sequences. Materials obtained in this way indeed function as adhesives that can be applied and subsequently cured underwater, with appreciable adhesive strengths.[9] However, again, it is not clear how to address the molecular structure of the constituent polymers to engineer new and better properties into the glues.

A further area in which biological polymers impress chemists is in the construction of the tissues of animals. Quite differently from the hydrophobic character that plastics and rubbers present, tissues contain a great deal of water, yet can be tough and strong. More importantly, tissues are adapted to their mechanical milieu by possessing an appropriate stiffness and allowing the right amount of deformation: longs are soft and deform easily,[10] whereas bones are stiffer and brittler. Two properties that stand out in particular is that tissues are often highly extensible and become stiffer as high deformations are applied, that is, they possess the property of hardening under strain.[11, 12]

Human-made water-rich solids are generally hydrogels, which are polymers that would normally dissolve in water that have been fixed into a network by more or less permanent bonds, which we refer to as crosslinks. In the last two decades methods have been found to imbue hydrogels with the high extensibility and strain hardening.[13] Only quite recently, for water-less gels, structure-property relationships have been established that robustly relate molecular characteristics to the property of extensibility and the extent of strain hardening.[14]

The aforementioned approaches at mimicking the distribution of chemical functionalities of selected proteins found in the adhesive secretions of marine animals are not equipped to establish structure-property relationships towards properties such as stiffness, extensibility and hardening on strain. In short, polymer chemists still have to learn much from the ways in which evolution has adapted biopolymers to the hostilities of existence on Earth. In this Introduction, I will present the central theme of this thesis, that concepts from marine animals and the water-rich tissues of animals in general are uniquely positioned to widen the specifications of hydrophilic polymer materials.

1.2 Four challenges for load-bearing biomaterials

Materials developed for use in the interior of animals are called *biomaterials*. Examples with a history of real-world use are metals in prosthetic joints, and nanostructures for the delivery of polynucleic acids and drugs. In this thesis, we will focus on load-bearing biomaterials, in particular on polymer-based wet adhesives. It has been a great challenge to adapt synthetic polymers towards uses in the medical field, specifically when load-bearing properties are required. The development of wet adhesives that are safe for internal use could render the utilization of sutures and staples a niche intervention,[15] which promises a smoother recovery for patients, and more convenient (thus safer) surgical techniques for surgeons. While the idea to use polymers rather than just metals for medical purposes has been around for several decades, there is no wide scale adoption of tissue adhesives, and metal implants for joint replacement are much preferred to polymer-derived ones.[16, 17]

What makes biomaterials based on polymers so challenging to design? In this introduction, I will focus on four challenges for arriving at tissue-compatible materials. First, biomaterials need mechanical properties that fit with the tissues in which they are applied. For instance, skin shows a range of stiffnesses and is highly anisotropic, with large differences in elastic moduli in tension (up to 140 MPa) versus indentation (starting from 5 kPa).[18, 19] Moreover, skin is viscoelastic, and becomes progressively stiffer as it is strained.[20] Comprising the same biopolymers that make up skin (collagens and elastin), cartilage shows a much higher stiffness in tension (approximately 7 GPa).[21] Thus, materials that would need to adhere to skin or cartilage, or even act as their replacements would need to at least match these moduli, and withstand the deformations that the tissues are exposed to.[22]

Second, next to being sufficiently strong internally, a material for use in medicine must have adhesive properties that are appropriate to the intervention towards which the material is designed. Variously, adhesion must be prevented, such as in passivizing coatings for implants, or, contrastingly, strong adhesion is crucial. The hydrophobic elastomers, plastics, and polymer melts that traditional polymer science has taught us so much about can not provide adequate adhesion in water-rich conditions, and thus we must advance the science of hydrophilic materials to provide tailored adhesion.

Third, biomaterials must not provoke adverse effects in organisms in which they are applied, be it through provoking immunological response (foreign body reaction) or through the toxicity of breakdown products. A more modern and complete statement of the third criterion is that biomaterials must *communicate appropriately* with tissues, for instance provoking a healing response, rather than just avoiding inflammation.[17] Finally, biomaterials use must be convenient to those in the medical

profession: adhesives or patches must be easy to apply, injectables must be not too viscous, and curing (settling, solidifying) of liquid materials must proceed at a reasonable rate. Additionally, it can be desired that solidification can be induced (triggered) through the application of a stimulus, such as light or a change in temperature. Much work towards biomaterials with a built-in response to the environment has been done in the field.[23]

In this thesis, we focus on material characteristics that are relevant for the development of medical adhesives — low surface energy towards water, insolubility in water, and appreciable internal strength. The current technology for wet adhesion is problematic due to the cytotoxicity of cyanoacrylates glues ("super" or "crazy" glue) and limited underwater bond strengths,[24] despite limited application in the field.[25] Alternatives to cyanoacrylates often present limited adhesion or cohesion.[15] Thus, improvements are direly needed. In the next section, we will make the case that complex coacervates — complexes of oppositely charged polyelectrolytes — are a uniquely suitable candidate for synthetic adhesives for "wet" use cases.

1.3 Complex coacervates as a candidate for wet materials

Polymer blends – equilibrium phases in which two species of polymers are blended together, resulting in a mixture with no tendency to separate – are typically challenging to achieve, since theta polymers segregate in the long-chain limit.[26] However, when the chains incorporate mutually attractive interactions, this 'xenophobia' can be overcome, and polymers can be blended — "opposites attract". An extreme case is the situation in which each monomer is charged, and the charges on the two polymer species are opposite: such polymers can indeed be expected to blend very well. If the above scenario unfolds in water, the situation is more complex: polymers can either be allowed to carry their charges with them, or expel them into the solution. Whereas expulsion generates many more microstates for the polymer/ion/solvent system, solution electrostatics favour the counter-ion to be in the vicinity of its neutralizing polymeric charge. However, if we now offer a polymer with opposite charge, our chain is free to let go of its counter-ions (with an associated entropy increase of ΔS), and can neutralize its charges with the counter-polymer. The process is drawn in Figure 1.3.

When oppositely charged polyelectrolytes associate through said attraction in water, the resulting material is called a polyelectrolyte complex. The complex (or "dense" phase) coexists with a phase that is dilute in polyelectrolytes. In older lit-

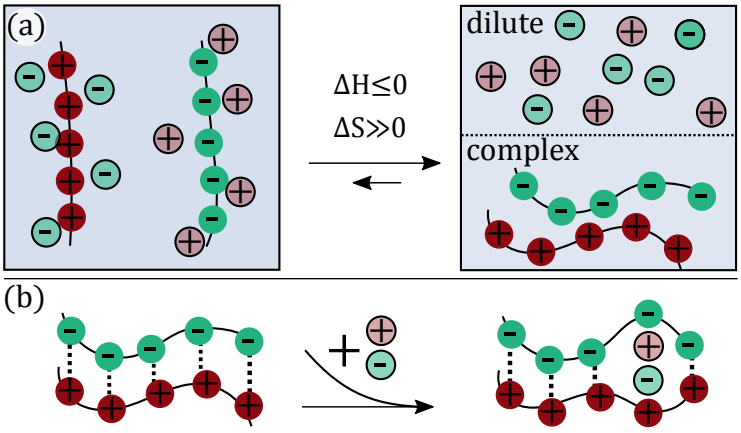

Figure 1.3: (a) Formation of a polyelectrolyte complex (right) from an aqueous solution of polyanions and polycations with their respective counter-ions (left). Complexes are most favourable for highly positive entropy changes ΔS and negative enthalpy changes ΔH. (b) Small ions such as Na^+ and Cl^- can be seen to act as a dopant, diluting out the friction-inducing interactions between polyanions and polycations. Saltier complexes are less viscous.

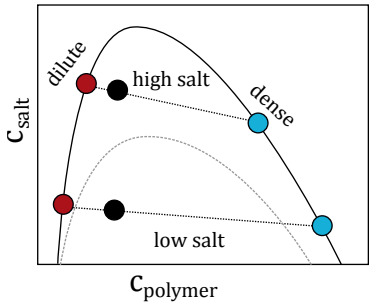

Figure 1.4: Phase diagrams for polyelectrolyte complexes of high (black line) and low (grey, dashed line) molecular weight, based on Tirrell et al.[29] The salt and polymer compositions indicated by the black dots decompose into two phases, one dilute (red dot) and one dense (blue dot) in polyelectrolytes.

erature, the term "complex coacervate" is used when emphasis is placed on the viscoelastic or liquid-like properties of a given polyelectrolyte complex. Complexes of polyanions and polycations in aqueous surroundings exist on a spectrum from dissipation- dominated to elasticity-dominated, and generally show a great deal of frequency dependence in their strain response.[27] As such, the distinction between a polyelectrolyte complex and a complex coacervate is no longer as emphasized in literature, and we use the terms fully interchangeably.

The viscoelasticity of coacervate complexes is strongly affected by the presence of salt (non-polymeric electrolytes). For complex coacervates that are driven by the entropy of liberation of soluble counter-ions, the addition of "background" salt reduces the friction that the polyelectrolytes experience: saltier coacervates show a reduced viscosity. Above a certain *critical* salt concentration c_s^*, there is no driving force towards coacervation, and the system exists as a single phase. The concentration of background salts also has an effect on phase composition (the concentrations of both polyelectrolytes in respectively the dense and dilute phase), and a modest effect on the phase boundaries when approaching c_s^*.[28] A representative phase diagram for coacervate complexes is given in Figure 1.4.

Recall that underwater adhesives need to, contradictorily, have low surface energies towards water and hydrophilic surfaces, yet be insoluble in water, and be liquid-like (or soft) for application, yet provide great resistance to deformation once set in a joint. In the language introduced in Figure 1.5, one needs a material with low interfacial tensions towards surface (low γ_{sa} enhances spreading) and water (low γ_{aw} avoids de-wetting) and a rather low complex modulus G^* upon application,

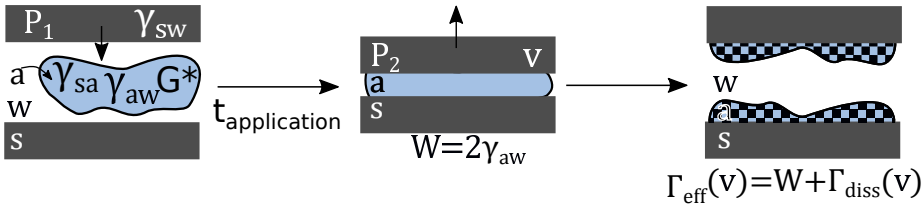

Figure 1.5: Requirements for an underwater adhesive. Take the pictured adhesion–detachment thought experiment: underwater, one applies an adhesive "a" characterized by complex modulus G^* between two surfaces "s", surrounded by water "w", by pushing together the plates with a pressure P_1. Subsequently, the surfaces are disjoined by some pressure P_2, for which one pays the work of adhesion W to create the interfaces, along with an extra penalty Γ_{diss}, which is dissipated during the deformation of the adhesive.

which provides the highest dissipated surface energy Γ_{diss} possible upon detachment, typically by having an appreciably large G^*. Do coacervates satisfy these preliminary demands? Unlike gels, coacervates are not crosslinked, and, unlike micellar assemblies, coacervates do not dissolve in water. Rather, they are "dissolved" (the system restricted to a single phase) by the addition of monovalent salts such as sodium chloride.[27,28] Consisting mostly of water (typically around 85% by mass), coacervates show an insignificant interfacial tension towards water (around 0.1 … 1 mJ m^{-2}). Thus, the phase diagrams that coacervates present satisfy an exacting demand for underwater adhesives: the material must present a hydrophilic interface, while being simultaneously insoluble.

Aside from providing appropriate interfacial properties, the internal or cohesive strength of coacervates can be tuned through a variety of methods, including by selection of various polyelectrolyte pairs,[30] those which dissolve at higher salt generally providing stronger complexes, by changing the water content,[31] or by the aforementioned manipulation of the salt concentration.[32] However, monomer chemistry, water content, and salt concentration are typically not degrees of freedom, and are generally constrained to what is physiologically tolerated when working in the context of biomaterials.

The adhesive of sandcastle worms is an example of a material in which control over the surface properties is achieved in a coacervate-like material. Unlike the adhesive "primer" of mussels, which contain primarily proteins with iso-electric points above the pH of sea water, *P. californica* secretes a substantial amount of anionic polysulfates, and as such complex coacervation has often be implicated as the mechanism that enables the features of low surface energy and water insolubility

in the adhesive.[33] In a more thorough description of the adhesion mechanism, lysine residues remove surface water, after which 3,4-dihydroxytyrosine moieties bind to the (mineral) surface.[34] However, dihydroxytyrosine has another quintessential role: to control the internal strength of the material. The moiety imparts cohesive strength to wet adhesives by covalent crosslinking, or through formation of crosslinking metal-ligand complexes.[3, 6, 35]

To summarize, Nature offers material chemists plenty of outstanding examples of functional adaptions in materials. These adaptations include mechanical strength of tissues and strong underwater adhesion of various underwater animals, and are regarded jealously by those who design materials to use for the repair of human tissues. I have described how the motives of polyelectrolyte complexation, (metal-ligand crosslinking), and assembly in hydrophilic milieus in general enables these adaptations.

1.4 This thesis – macromolecules to improve mechanical function of complex coacervates

In this thesis, we work towards filling the lack of chemical platforms to address mechanical features of complex coacervates. Thus, in the context of our four criteria (*vide supra*), we address mainly the criterion of strength (1), in a two-fold way: by tuning the linear viscoelasticity of complex coacervates, and by working towards improving the behaviour of coacervates at large deformations, the non-linear viscoelasticity. The criterion of biocompatibility, whilst crucial for application, is not treated in the research chapters of this thesis, but will be revisited in the General Discussion (Chapter 6).

The linear viscoelasticity of complex coacervates that have been strengthened by metal-ligand bonds is studied in Chapter 2. We deliberately chose a ligand that is not 3,4-dihydroxytyrosine, for concerns of oxidation, and the possibility of formation both bis and tris-linkages.[6] Rather, we worked with terpyridines, which result in well-defined "model" crosslinks, and turned out to suit our efforts to arrive at a fundamental understanding of the effect of metal-ligand bonding in complex coacervates.

In Chapter 3, we went beyond the linear regime, and studied the viscoelasticity of metal-ligand crosslinked coacervates at high strain rates at large deformations. "Strength" encompasses more than just the stiffness or viscosity of a material, and Chapter 3 provides a preliminary look into how one could achieve desirable mechanical characteristics such as strain hardening, or, conversely, shear thinning into

coacervates.

Progress towards macromolecules that modulate non-linear viscoelasticity in coacervates is presented in Chapter 4, where we build a semi-flexible polyelectrolyte according to the bottlebrush architecture. In such molecules, the backbone is rather stiff, and as a consequence, deformation of the chains results in the deformer "feeling" the finite length of polymer chains. We provide evidence of the semi-flexible nature of bottlebrush polyelectrolytes, and show that they participate in coacervate complexes.

In Chapter 5, we designed a molecule that could provide the triggered stiffening of coacervates that would fulfill the ease-of-use criterion (3) by incorporating temperature-responsive groups into a polyanion. Concurrently, we develop an improved synthesis of the ubiquitous polyanion poly(acrylic acid), which assures that the product residue is not contaminated with *tert*-butyl esters from an intermediate compound. We show that the *tert*-butyl contamination has a noticeable effect on the structure-forming potential of polymers.

While we do not actually test wet adhesion or tissue compatibility, the aim of this thesis aligns squarely with that field. We present tools to bring the futures biomaterials up to specification: here we present polyelectrolytes, their networks as achieved through telechelic assembly, metal-ligand complexation, and, their branching as design features of materials for use in water-rich environments.

Bibliography

[1] PlasticEurope - Association of Plastics Manufactures, "Plastics – the Facts 2020," 2020.

[2] Y. M. Bar-On, R. Phillips, and R. Milo, "The biomass distribution on Earth," *Proceedings of the National Academy of Sciences of the United States of America*, vol. 115, no. 25, pp. 6506–6511, 2018.

[3] J. H. Waite, "Mussel adhesion - Essential footwork," *Journal of Experimental Biology*, vol. 220, no. 4, pp. 517–530, 2017.

[4] Q. Guo, J. Chen, J. Wang, H. Zeng, and J. Yu, "Recent progress in synthesis and application of mussel-inspired adhesives," *Nanoscale*, vol. 12, no. 3, pp. 1307–1324, 2020.

[5] L. Petrone, A. Kumar, C. N. Sutanto, N. J. Patil, S. Kannan, A. Palaniappan, S. Amini, B. Zappone, C. Verma, and A. Miserez, "Mussel adhesion is dictated by time-regulated secretion and molecular conformation of mussel adhesive proteins," *Nature Communications*, vol. 6, p. 8737, 2015.

[6] J. Yang, M. A. Cohen Stuart, and M. Kamperman, "Jack of all trades: versatile catechol crosslinking mechanisms," *Chem. Soc. Rev.*, vol. 43, no. 24, pp. 8271–8298, 2014.

[7] S. Seo, S. Das, P. J. Zalicki, R. Mirshafian, C. D. Eisenbach, J. N. Israelachvili, J. H. Waite, and B. K. Ahn, "Microphase Behavior and Enhanced Wet-Cohesion of Synthetic Copolyampholytes Inspired by a Mussel Foot Protein," *Journal of the American Chemical Society*, vol. 137, no. 29, pp. 9214–9217, 2015.

[8] J. Fournier, S. Etienne, and J. B. Le Cam, "Inter- and intraspecific variability in the chemical composition of the mineral phase of cements from several tube-building polychaetes," *Geobios*, vol. 43, no. 2, pp. 191–200, 2010.

[9] H. Shao, K. N. Bachus, and R. J. Stewart, "A water-borne adhesive modeled after the sandcastle glue of P. californica," *Macromolecular Bioscience*, vol. 9, no. 5, pp. 464–471, 2009.

[10] B. Suki, A. Barabási, and K. R. Lutchen, "Lung tissue viscoelasticity : and its molecular basis a mathematical framework," *Journal of Applied Physiology*, vol. 76, no. 6, pp. 2749–2759, 1994.

[11] K. A. Erk, K. J. Henderson, and K. R. Shull, "Strain Stiffening in Synthetic and Biopolymer Networks," *Biomacromolecules*, vol. 11, pp. 1358–1363, 2010.

[12] C. Storm, J. J. Pastore, F. MacKintosh, T. C. Lubensky, and P. A. Janmey, "Nonlinear elasticity in biological gels," *Nature*, vol. 435, pp. 191–194, 2005.

[13] J. P. Gong, "Why are double network hydrogels so tough?," *Soft Matter*, vol. 6, no. 12, pp. 2583–2590, 2010.

[14] S. S. Sheiko and A. V. Dobrynin, "Architectural Code for Rubber Elasticity: From Supersoft to Superfirm Materials," *Macromolecules*, vol. 52, no. 20, pp. 7531–7546, 2019.

[15] L. P. Bré, Y. Zheng, A. P. Pêgo, and W. Wang, "Taking tissue adhesives to the future: from traditional synthetic to new biomimetic approaches," *Biomater. Sci.*, vol. 1, no. 3, pp. 239–253, 2013.

[16] B. D. Ratner, "Biomaterials: Been There, Done That, and Evolving into the Future," *Annual Review of Biomedical Engineering*, vol. 21, pp. 171–191, 2019.

[17] D. F. Williams, "On the mechanisms of biocompatibility," *Biomaterials*, vol. 29, no. 20, pp. 2941–2953, 2008.

[18] A. Kalra, A. Lowe, and A. M. Al-Jumaily, "Mechanical Behaviour of Skin: A Review," *Journal of Material Science & Engineering*, vol. 5, no. 4, 2016.

[19] C. T. McKee, J. A. Last, P. Russell, and C. J. Murphy, "Indentation versus tensile measurements of young's modulus for soft biological tissues," *Tissue Engineering - Part B: Reviews*, vol. 17, no. 3, pp. 155–164, 2011.

[20] J. Aziz, H. Shezali, Z. Radzi, N. A. Yahya, N. H. Abu Kassim, J. Czernuszka, and M. T. Rahman, "Molecular Mechanisms of Stress-Responsive Changes in Collagen and Elastin Networks in Skin," *Skin Pharmacology and Physiology*, vol. 29, no. 4, pp. 190–203, 2016.

[21] F. H. Silver, G. Bradica, and A. Tria, "Elastic energy storage in human articular cartilage: Estimation of the elastic modulus for type II collagen and changes associated with osteoarthritis," *Matrix Biology*, vol. 21, no. 2, pp. 129–137, 2002.

[22] J. Blume and W. Schwotzer, "Medical products and their application range," in *Biological Adhesive Systems: From Nature to Technical and Medical Application* (J. Blume and W. Schwotzer, eds.), pp. 213–224, SpringerWienNewYork, 2010.

[23] A. H. Hofman, I. A. van Hees, J. Yang, and M. Kamperman, "Bioinspired Underwater Adhesives by Using the Supramolecular Toolbox," *Advanced Materials*, vol. 1704640, p. 1704640, 2018.

[24] G. Pascual, S. Sotomayor, M. Rodríguez, B. Pérez-Köhler, A. Kühnhardt, M. Fernández-Gutiérrez, J. S. Román, and J. M. Bellón, "Cytotoxicity of cyanoacrylate-based tissue adhesives and short-term preclinical in vivo biocompatibility in abdominal hernia repair," *PLoS ONE*, vol. 11, no. 6, pp. 1–22, 2016.

[25] G. Bot, K. Bot, J. Ogunranti, J. Onah, A. Sule, I. Hassan, and E. Dung, "The use of cyanoacrylate in surgical anastomosis: An alternative to microsurgery," *Journal of Surgical Technique and Case Report*, vol. 2, no. 1, p. 44, 2010.

[26] P.-G. De Gennes, *Scaling concepts in polymer physics*. Cornell University Press (Ithaca and London), 1979.

[27] Q. Wang and J. B. Schlenoff, "The polyelectrolyte complex/coacervate continuum," *Macromolecules*, vol. 47, no. 9, pp. 3108–3116, 2014.

[28] E. Spruijt, A. H. Westphal, J. W. Borst, M. A. Cohen Stuart, and J. Van Der Gucht, "Binodal compositions of polyelectrolyte complexes," *Macromolecules*, vol. 43, no. 15, pp. 6476–6484, 2010.

[29] L. Li, S. Srivastava, M. Andreev, A. B. Marciel, J. J. De Pablo, and M. V. Tirrell, "Phase Behavior and Salt Partitioning in Polyelectrolyte Complex Coacervates," *Macromolecules*, vol. 51, no. 8, pp. 2988–2995, 2018.

[30] K. Sadman, Q. Wang, Y. Chen, B. Keshavarz, Z. Jiang, and K. R. Shull, "Influence of Hydrophobicity on Polyelectrolyte Complexation," *Macromolecules*, vol. 50, no. 23, pp. 9417–9426, 2017.

[31] R. F. Shamoun, A. Reisch, and J. B. Schlenoff, "Extruded saloplastic polyelectrolyte complexes," *Advanced Functional Materials*, vol. 22, no. 9, pp. 1923–1931, 2012.

[32] E. Spruijt, M. A. Cohen Stuart, and J. Van Der Gucht, "Linear viscoelasticity of polyelectrolyte complex coacervates," *Macromolecules*, vol. 46, no. 4, pp. 1633–1641, 2013.

[33] C. S. Wang and R. J. Stewart, "Multipart copolyelectrolyte adhesive of the sandcastle worm, Phragmatopoma californica (Fewkes): Catechol oxidase catalyzed curing through peptidyl-DOPA," *Biomacromolecules*, vol. 14, no. 5, pp. 1607–1617, 2013.

[34] R. J. Stewart, C. S. Wang, I. T. Song, and J. P. Jones, "The role of coacervation and phase transitions in the sandcastle worm adhesive system," *Advances in Colloid and Interface Science*, vol. 239, pp. 88–96, 2017.

[35] B. J. Sparks, E. F. T. Hoff, L. P. Hayes, and D. L. Patton, "Mussel-inspired thiol-ene polymer networks: Influencing network properties and adhesion with catechol functionality," *Chemistry of Materials*, vol. 24, no. 18, pp. 3633–3642, 2012.

Chapter 2

Complex coacervation and metal-ligand bonding as synergistic design elements for aqueous viscoelastic materials

Abstract

The application of complex coacervates in promising areas such as coatings and surgical glues requires a tight control of their viscous and elastic behaviour, and a keen understanding of the corresponding microscopic mechanisms. While the viscous, or dissipative, aspect is crucial at pre-setting times and in preventing detachment, elasticity at long waiting times and low strain rates is crucial to sustain a load-bearing joints. The independent tailoring of dissipative and elastic properties proves to be a major challenge that can not be addressed adequately by the complex coacervate motif by itself. We propose a versatile model of complex coacervates with customizable rheological fates by functionalization of polyelectrolytes with terpyridines, which provide transient crosslinks through complexation with metals. We show that the rheology of the hybrid complexes shows distinct footprints of both metal-ligand and coacervate dynamics, the former as a contribution very close to pure Maxwell viscoelasticity, the latter approaching a sticky Rouse fluid. Strikingly, when the contribution of metal-ligand bonds is dominant at long times, the relaxation of the overall complex is much slower than either the "native" coacervate relaxation time or the dissociation time of a comparable non-coacervate polyelectrolyte-metal-ligand complex. We recognize this slowing-down of transient bonds as a synergistic effect that has important implications for the use of complementary transient bonding in coacervate complexes.

This chapter is published eponymously as A. D. Filippov, J. Sprakel, M. M. G. Kamperman, *Soft Matter*, 2021, **17**, 3294-3305

2.1 Introduction

In synthetic coatings and adhesives, good adhesion and film formation is reliably found in hydrophobic, covalent bond-forming systems. Conversely, the polyelectrolyte-based adhesives of mussels and sandcastle worms are delivered in water-rich dispersions,[1, 2] and prominently feature transient bonds long into the curing process,[2, 3] whereas covalent bonds are important for long-term load bearing.[4] Associative strategies from Nature are diverse, and compelling arguments are made for their incorporation into novel water-based adhesives, biomaterials for tissue engineering and implants, and other novel viscoelastics for use in biological contexts. First, the requirement of low surface tension for effective contact formation is met by mussels and sandcastle worms through the choice of highly hydrophilic constituents.[3, 5] Second, the seemingly contradictory requirement of non-solubility in the medium of use (water) is overcome in the same systems by the modification of macromolecules with transiently binding groups.[2] Finally, Nature offers a vast range of bond strengths in transient bonds, allowing for the selection of appropriate stiffness and relaxation times. Unsurprisingly, the application of chemistry inspired by the underwater adhesion of water-dwelling animals is a tremendously active field.[1, 6, 7]

Since complex coacervation is a prominent feature in wet bio-adhesives,[3] the use of coacervate matrices in the development of novel water-rich materials represents a natural choice. Complex coacervates are complexes of oppositely charged polyelectrolytes with a salt-dependent terminal relaxation time τ_R,[8] and inevitably show creep when loaded for long times. Therefore, a central challenge of the field remains the incorporation of transient or covalent crosslinks into complex coacervates, ideally in response to a trigger. Examples are the thermostiffening block poly(*N*-*iso*propylacrylamide) (pNIPAm),[9–11] catechol chemistry,[12–14] or hydrophobic groups.[12] Despite the reassuring progress, substantial questions in the design of the networks remain.

For complex-coacervate based underwater adhesives, good adhesive performance occurs in a narrow range of salt concentration (c_s) and temperatures,[10] and it is not trivial to extend the parameter window towards arbitrary conditions, which has, for example, been attempted with extrusion.[15] Similarly, the thermostiffening transition is strongly dependent on the blocks lengths, some compositions favouring micelles rather than continuous phases.[16] Even in cases where a single lifetime τ_X can be ascribed to a crosslink, it is unknown how it impacts a pre-existing transient network of bonds of some lifetime τ_0, which is a property of the complex coacervate matrix. The design of previous studies makes the elucidation of exact contributions due to crosslinking difficult — in an ideal case, this would be done with a design element that is structurally and temporally orthogonal to the coacervate, an idea

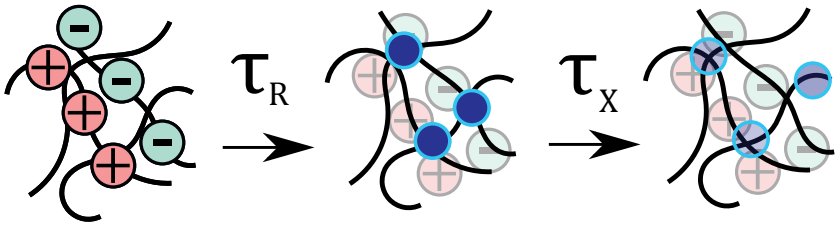

Figure 2.1: Transiently crosslinked complex coacervates show viscoelasticity on two different timescales: the sticky Rouse time τ_R and the metal-ligand dissociation time τ_X. In this Figure, the Rouse modes relax before the metal-ligand bonds dissociate. Depending on the metal-ligand pair, the polyelectrolytes and the amount of free electrolytes (plasticizer), the converse is also possible.

rooted in the work of Holten-Andersen et al.[17]

The targeted design of responsively strengthened coacervate complexes requires predictable models of the emergence of viscoelasticity and elasticity in "bimodal" networks — those with two modes of thickening or stiffening. Therefore, we present a strategy to tailor the flow of coacervate-forming polyelectrolytes with metal-ligand complexes. The pairing is ideally suited to explore the combined effect of τ_R and a longer crosslink-associated timescale τ_X on coacervate viscoelasticity, as drawn in Figure 2.1. We call the resulting materials transiently crosslinked complex coacervates (TC3s), in which the transient bonds we employ achieve transient crosslinks in the complex coacervate due to metal-ligand binding. To this end, we covalently attach terpyridines (tP) to polyelectrolytes poly(acrylic acid) (pA) and poly(N,N-dimethyl-aminoethyl methacrylate) (pD). The polyelectrolytes can then be bound to each other through complex coacervation, or by complexation with a range of metals, in which case a crosslink is formed by binding of one metal ion by two terpyridines. TC3s are models of underwater adhesives and their synthetic adaptations: instead of the complex behaviour of catechols[18] or thermoresponsive blocks,[9–11] we can analyze their phase behaviour and mechanics in terms of the well-defined relaxation times of coacervate and metal-ligand bonds. Furthermore, on account of the vast available range of terpyridine–metal ion equilibrium constants,[19] TC3s offer a highly ion-specific viscoelastic response that complex coacervates natively lack.

In this paper, we reveal the effect of independently changing the relative magnitude of two relaxational timescales on viscoelasticity. We address TC3 flow through macrorheological measurements. Specifically, we search for the circumstances in which the coacervate could be expected to act unaware of the transient bonds, and

vice versa. As such, we are able to assess to which extent transient bonds would suit to improve complex coacervate mechanics. The findings are relevant for those who seek to engineer novel water-rich materials, such as underwater glues and viscoelastics for use in a biological context. We show that the amount of transient crosslinks needed to thicken a complex coacervate is very low. Metal-ligand crosslinks are found to be able to entirely dominate the long-time mechanics of our hybrid complexes: TC3s can be tuned from low-viscosity fluids to indefinitely stable solids. Surprisingly, we find that the transient bonds are able to act over timescales that are often much longer than their "innate" lifetime, which we recognize as a form of synergy.

2.2 Experimental Section

Notation Throughout this work, we refer to polyelectrolytes as pX^{n}_{ϕ}, with X either A for acrylic acid, D for N,N-dimethylaminoethyl methacrylate, or AMPS for 2-acrylamido-2-methyl-1-propanesulfonic acid. ϕ represents the molar percentage of repeat units that express a tP moiety, and n the polyelectrolyte degree of polymerization. The symbol ∘ (instead of M^{2+}) denotes the absence of metal.

Materials Unless stated otherwise, chemicals were used as received. Hydroxybenzotriazole hydrate (HOBt, 14% water, 98%), ethyl α-bromoisobutyrate (98%), concentrated hydrochloric acid (HCl 37%, aqueous, ACS reagent), N-(3-Dimethylaminopropyl)-N'-ethylcarbodiimide hydrochloride (EDC, ≥ 98.0%), aluminum oxide (Al_2O_3, activated, basic), and, N,N-dimethylformamide (DMF, anhydrous, 99.8%) were obtained from Sigma-Aldrich, Germany. Tris[2-(dimethylamino)ethyl]amine (Me_6TREN, Alfa Aesar, ≥ 99.0%), ethylenediamine tetraacetic acid (EDTA, Millipore-Sigma), and, copper (II) bromide ($CuBr_2$, 99%), were obtained from VWR. 2-(dimethylamino)ethyl methacrylate (DMAEMA, stabilized with MEHQ, >98.5%), *tert*-butyl acrylate (*t*BuAc, stabilized with MEHQ, >98.0%), and, methyl α-bromophenylacetate (MBPA, ≥98.0%) were obtained from TCI Europe. Methanol (MeOH, HPLC, ≥ 99.9%), 1,1,1,3,3,3-hexafluoro-2-propanol (HFIP, AR, ≥ 99.8 %), acetonitrile (CH_3CN, anhydrous, 99.8%), di-*iso*-propyl ether (~ 0.001% BHT as stabilizer, ≥ 98.5 %), and, *n*-hexane (HPLC), were obtained from Biosolve.

CH_3CN and DMF were stored on molecular sieves (4Å). *t*BuAc and DMAEMA were stripped from inhibitor by filtration over a column of Al_2O_3. 3-Terpyridyloxy bromopropane and 4-terpyridyloxy butylamine were synthesized following literature procedures, and the corresponding Experimental Section can be found in Appendix 2.A.

Poly(N,N-dimethylaminoethyl methacrylate)–35 kDa (pD^{222}, Đ=1.12) and poly(acrylic acid)–17 kDa (pA^{234}, Đ=1.12) were obtained from Polymer Source, Canada. Com-

mercial pA was dried for several days on a high vacuum line, then dissolved in DMF and centrifuged at 2000g for 1h to remove insoluble impurities. Poly(N,N–dimethylaminoethyl methacrylate) (pD^{1k}, Đ=1.43) and poly(acrylic acid) (pA^{250}, Đ=1.13) were synthesized using copper-catalyzed polymerizations as reported below. pAMPs was obtained as is described in Appendix 2.A .

Terpyridylation of poly(N,N–dimethylaminoethyl methacrylate) In a representative example, pD (1.00 g, 6.36 mmol amines) was weighed into a round-bottomed flask and dissolved in dry acetonitrile (30 mL). To this was added 3-terpyridyloxy bromopropane (0.236 g, 0.64 mmol), and the mixture was stirred for three days at 55 °C. The mixture was concentrated *in vacuo* and purified by repeated precipitation in a mixtures of diethyl ether and hexane. pD_{10} was obtained as faintly yellow glassy solid, 1.06 g (85%). ^{1}H-NMR, 400 MHz: Figure 2.B.5.

pD_{01} was synthesized similarly, but precipitated in diisopropyl ether. It was obtained as a faintly yellow glassy solid, 0.80 g (50%). ^{1}H-NMR, 400 MHz: Figure 2.B.5.

Terpyridylation of poly(acrylic acid) pA was terpyridylated as described by Aamer and Tew.[20] In a representative example, pA (0.31 g, 4.3 mmol COOH) was dissolved in 10 mL dry DMF and bubbled with N_2(g). EDC (0.0815 g, 0.424 mmol), HOBT (0.0659 g, 0.424 mmol) were each dissolved in minimal DMF in separate vials, and also sparged with N_2(g). EDC and HOBT solutions were injected into the stirred pA solution, to which after 50 min was added a suspension of 4-terpyridyloxy butylamine (0.130 g) in minimal DMF. The mixture was left to stir for 16 h. pA with a terpyridylation extent of 10% (pA_{10}) was recovered as a mixture with the EDC urea after centrifugation, neutralization to pH 7 and dialysis against Milli-Q followed by lyophilization. 0.433 g, as a purple powder. ^{1}H-NMR, 400 MHz: Figure 2.B.3.

Synthesis of poly(N,N-dimethyl aminoethyl methacrylate) (pD^{1k}) To 60 mL of DMF in a round-bottomed flask fitted with a magnetic stirrer were added $Cu^{II}Br_2$ (5.68 mg, 25.4 μmol), Me_6TREN (40.8 μL, 152 μmol), and DMAEMA (60.0 mL, 0.356 mol), after which the solution was bubbled with Ar (g) for 15 min. MBPA was added (0.200 mL, 1.27 mmol), and the flask was sealed with a rubber septum and bubbled for 15 more min. The solution was then stirred for 37 h under UV light of 385 nm. The residue was precipitated thrice in hexane, and dried under high vacuum.

SEC-MALLS (HFIP, 0.02 M KTFA): M_n=161 kDa, M_w=230 kDa, Đ=1.43. The polymerization followed pseudo-first order kinetics strictly (Figure 2.B.1).

Synthesis of poly(*tert*-butyl acrylate)–32.5 kDa (pT^{250}) To a round-bottomed flask were added *tert*-butyl acrylate (57.1 mL, 0.390 mol), DMF (57 mL), ethyl α-bromoisobutyrate (0.229 mL, 1.56 mmol), $Cu^{II}Br_2$ (6.97 mg, 0.0312 mmol), and Me_6TREN (50.1 μL, 0.2520 mmol). While the green solution was bubbled with Ar (g) for 30 min, 50 cm of copper wire was activated in 37% aqueous HCl, and subsequently

rinsed with copious amounts of water. The wire was wrapped around a magnetic stirrer, and was added to the flask, which was then quickly sealed under postive Ar pressure with a rubber septum. The mixture was stirred for 5 h, after which a glassy residue was precipitated in ice-cold MeOH:water 2:1, which was redissolved in acetone and filtrated over a short plug of Al_2O_3. Thorough drying under high vacuum afforded a colourless, odorless glassy solid (38.2 g, 76%), which was de-*tert*-butylated to afford poly(acrylic acid).

SEC-MALLS (HFIP, 0.02 M KTFA): M_n=32.511 kDa, M_w=36.694 kDa, Đ=1.13. Polymerization kinetics are given in Figure 2.B.1.

Synthesis of poly(acrylic acid)–18 kDa (pA^{250}) Poly(*tert*-butyl acrylate (38.15 g, 0.2977 mol butyl ester) was dissolved in 220 mL of HFIP in a round-bottomed flask fitted with a magnetic stirrer. HCl (27.3 mL, 0.327 mol) in 100 mL of HFIP was slowly added using a dropping funnel. Immediately, a white precipitate formed, which was stirred for 3 d. The precipitate was collected by filtration, washed with fresh HFIP, and dried *in vacuo* to yield poly(acrylic acid) quantitatively. For use with terpyridines, it was further dialysed against large quantities of aqueous EDTA (10 mM) and then water.

Size exclusion chromatography with multi-angle light scattering detection Unmodified polyelectrolytes were characterized using size exclusion chromatography in tandem with multi-angle light scattering detector and viscometry, on an Omnisec Reveal system fitted with two PSS PFG columns. The mobile phase was HFIP with 0.02 M KTFA, at 0.7 ml min^{-1}.

Preparation of complexes We added half an equivalent of MCl_2 (with respect to terpyridyl content) to a solution of the non-modified polyelectrolyte, since two terpyridyl groups complex one metal ion. M^{2+} was either Mn^{2+}, Zn^{2+}, Co^{2+} or Ni^{2+}. The polyelectrolyte was subsequently brought into a complex with the oppositely charged, terpyridylated chain. Polyelectrolytes were pipetted from stocks with a monomer concentration of 0.25 M with a background salt concentration of 0.1 M. After addition of a NaCl solution of a suitable concentration (between 0.5 and 1.5 M), the final polyelectrolyte concentration was brought to 0.1 M by addition of Milli-Q water. The protocol encourages a uniform concentration of M^{2+}, minimizing distance from equilibrium. Complexes were equilibrated until transparent, which took an overnight wait for complexes with Mn^{2+} and Zn^{2+}, but required prolonged centrifugation for Co^{2+} and Ni^{2+} at low gravitational fields. In the latter case, flat tubes with a diameter of 10 mm were used to allow yieldless loading of the sample, and the temperature was kept at 20 °C.

To prepare polyelectrolyte gels of only pD, water was evaporated from a stock solution of pD with a terpyridyl content of 1% using a stream of nitrogen. Then, a quarter of an equivalent of either Mn^{2+}, Zn^{2+}, Co^{2+} or Ni^{2+} was added. The com-

plexes were mixed on a turning rack for one week, and equilibrated as described above. The mass-over-volume fraction was chosen to match the fraction of polymers in a high-salt coacervate. To this end, we measured the coacervate volume using photographs of equilibrated samples. Subsequently we assumed that all of the polymer travels to the coacervate phase, setting the polymer mass-over-volume fraction to 16%.

Rheology For mechanical characterization, we applied around 0.3 mL of dense phase onto the glass plate of an MCR-301 or MCR-501 (Anton Paar, Austria). For complexes that relaxed sufficiently fast, a 10 mm cone was used. For complexes characterized by a slow relaxation, a 10 mm plate was employed. After bringing the tool to trim gap and trimming, the dilute phase was poured over the geometry, and the tool was brought to gap. Geometries were closed off with a Peltier hood. Frequency sweeps between $0.1-100\,\mathrm{Hz}$ were performed at small strains in the linear viscoelastic regime (LVR, for our complexes, $\gamma < 1$). Step strain relaxation measurements were done at strains of $0.1-.25$. For samples that required prolonged measurement, a final frequency sweep was then recorded to assure evaporation did not alter the properties. Amplitude sweeps were conducted posteriorly, up to yield, to confirm that the prior measurements sampled the LVR.

2.3 Results and Discussion

We acquire unmodified polyelectrolytes pA and pD either commercially, or through synthesis under Cu-catalyzed conditions. We subsequently install tP groups by well-established derivatization chemistries. Complete experimental methods for synthesis of tP building blocks, polymerizations, and derivatization chemistry are given in Appendix 2.A, as well as characterization data for all polymers used (Figures 2.B.5, 2.B.3). Figure 2.2 portrays the resulting polymer inventory.

We prepare four families of complex: (1) complexes of unmodified polyelectrolytes (pA/pD), (2) complexes of divalent transition metals ions with only a single modified polyelectrolyte ($\mathrm{pD}_{01}-\mathrm{M}^{2+}$), (3) complexes in which one of the polyelectrolyte partners is modified ($\mathrm{pA}_{01}/\mathrm{pD}-\mathrm{M}^{2+}$, $\mathrm{pA}/\mathrm{pD}_{01}-\mathrm{M}^{2+}$), and (4) complexes in which both are terpyridylated ($\mathrm{pA}_{01}/\mathrm{pD}_{01}-\mathrm{M}^{2+}$). Non-TC3 complexes of families (1) and (2) know an extensive literature,[20–22] whereas (3) and (4) have not been prepared nor studied.

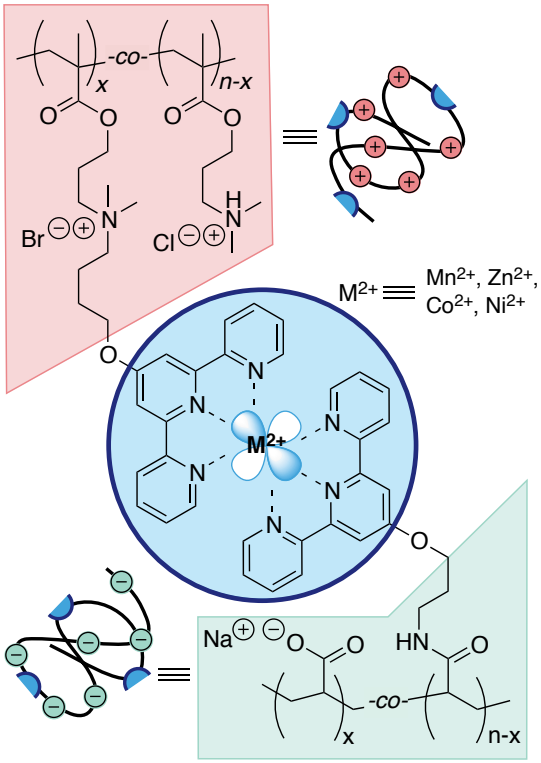

Figure 2.2: A chemical toolbox for studying transiently crosslinked complex coacervates: coacervate-forming polyelectrolytes pA and pD, metal ions M^{2+}, and terpyridines attached covalently to the polyelectrolytes allow to explore the dynamics sketched in Figure 2.1.

Transient crosslinking of complex coacervates alters the phase diagram for $\phi_{\mathrm{tP}} \geq 10\%$

For a given pair of pA and pD, complex coacervation was found to occur up to some critical salt concentration c_s^*, typical for complexes of flexible polyelectrolytes, as is consistently reported in literature.[21, 23] For the pair $\mathrm{pA}^{250}_{\phi,A}/\mathrm{pD}^{1\mathrm{k}}_{\phi,B} - \mathrm{Ni}^{2+}$, with $\phi_A = 0, 0.42\,\mathrm{or}\,1\%$ and $\phi_B = 0\,\mathrm{or}\,1\%$, we did not observe macroscopic complexes at salt strengths $c_s \geq 1.0$ M, regardless of the degree of terpyridylation on either polyelectrolyte or the addition of Ni^{2+}. Similarly, for the pair $\mathrm{pA}^{234}_{01}/\mathrm{pD}^{222}_{01} - \mathrm{M}^{2+}$, we observed coacervation up to a c_s of 0.9 M, regardless of the addition of even the stronger-binding Zn^{2+} or Ni^{2+} as metals. Thus, the added crosslinks do not strongly widen the two-phase region in the phase diagram, and neither do metal ions show any significant influence on complexes that present no terpyridine.

However, we observed that even the addition of Mn^{2+} (the weakest-binding ion) to $\mathrm{pA}^{234}/\mathrm{pD}^{222}_{10}$, which is non-complexing at 1.0 M NaCl, separated a viscous phase. Hence, a plenitude of enthalpically attractive bonds can overrule the entropic unfeasibility[24] of complex coacervation above c_s^*. The possibility to manipulate complex coacervate phase behaviour with even the weakest-binding metal ion suggests that TC3s have a particularly rich flow behaviour as well, the study of which is covered by the remainder.

Rouse-like rheological signatures of complexes with short-lived transient crosslinks

We employ rheology to quantify the effect of non-covalent crosslinks on the transient network formed in coacervate complexes with added salt. The complexes are in the non-entangled regime (*vide infra*). Complex coacervates are distinguished from non-charged viscous polymer solution by the presence of inter-chain electrostatic interactions, the strength of which is controlled by the salt concentration. Non-crosslinked coacervates resist flow at short times because each chain forms multi–ion "ladder" bonds to several other chains,[25] which act as a crosslink. Over time, the multi–ion pairs exchange between chains, initially enabling diffusion of small chain sections ("monomers") at τ_0, then larger chunks (τ_p), and finally entire chains at τ_R. The collective exchange act, at least for times longer than a few ms, yields behaviours consistent with the sticky Rouse model.[8, 26–28]

At long times, or low angular frequencies ($\omega < 2\pi\tau_R^{-1}$), only whole-chain friction can contribute to the viscoelasticity. The coil density sets the modulus level G_R, and for times much longer than τ_R, the shear relaxation modulus tends to a (Maxwellian) exponential decay

$$G(\mathrm{t}) = G_R \exp\left(-\frac{t}{\tau_R}\right) \tag{2.1}$$

The Fourier conjugate of $G(t)$ is the frequency-dependent shear relaxation modulus $G(\omega)$, with real (storage) and imaginary (loss) parts $G'(\omega)$ and $G''(\omega)$. Maxwell relaxation manifests itself as $G' \propto \omega^2$ and $G'' \propto \omega^1$ at low frequencies. At a certain ω_c, G becomes equal to G''. For a liquid with only one relaxation mode, ω_c is the inverse of a characteristic relaxation time τ_C. For shorter times (higher frequencies), G' plateaus at G_0 and G'' decreases rapidly with increasing frequency. However, viscoelastics with a broad relaxation spectrum typically give weak power laws in both $G^*(\omega)$ and $G(t)$.[29, 30] Such is also the case for complex coacervates.

Complex coacervates are Rouse-like, with signatures near to $G(t) \propto t^{-\frac{1}{2}}$ and $G(\omega) \propto \omega^{\frac{1}{2}}$ above the crossover frequency.[8, 31–34] The occurence of power laws of slope one-half is a feature of (sticky) Rouse theory,[28] and can be seen as a result of the superposition of an array of Maxwell modes ($G(t) = \sum_p G_p \exp(-\tau_p^{-1} t)$), with $\omega_{\mathrm{c},p}$ evolving according to

$$\left(\frac{2\pi}{\omega_p}\right) = \tau_p = \tau_0 \left(\frac{N}{p}\right)^2, \tag{2.2}$$

with $1 > p > N$, where τ is taken as the time needed to completely an entire oscillation period at the corresponding angular frequency. The Rouse modes p collectively describe bead motion, and the important consequence is that no single relaxation time characterizes the dynamics. Whilst based on a microscopic picture, there is no agreement on whether Rouse modes have a physical significance.[35]

The above slowest-mode analysis suffers from the weakness that only one relaxation time τ_R is treated (Equation 2.1). At frequencies below ω_c, this reproduces the frequency-dependent moduli sufficiently well to estimate the frequency of crossover. However, complex coacervates have a broad relaxation spectrum.[8, 32] Later, we will see that the effect of metal-ligand bonds on complex coacervates is profound when τ_X significantly outlives τ_R, broadening the relaxation spectrum even further. A number of previous authors has demonstrated the utility of Prony series, in which one takes the sum of a large number of Maxwell elements, which for complex coacervates can be viewed as having their origin in Rouse modes.[8, 17] Despite providing excellent agreement to data, the procedure requires iterative fitting, and is an ill-posed problem.

Here, we employ the fractional Maxwell liquid model (FMM). In the model, both stress and strain are fractional derivatives of time, which lead to forms for $G(t)$ and

$G', G''(\omega)$ that are able to capture highly broad relaxation spectra with excellent agreement with rheological data for complex liquids.[29] Rouse dynamics are consistent with FMM in the sense that the Rouse model can be cast as a constitutive equation with a fractional time derivative of the stress of order one-half[29, 32] – Rouse relaxation can then be captured in only three parameters, without the need for a Prony series of N Rouse modes, and thus $2N$ free parameters. Moreover, recent work[32] reveals that the scaling of the frequency-dependent storage and loss moduli deviates quite strongly from the $\omega^{\frac{1}{2}}$ required by Rouse theory, whereas an FMM model provided an excellent fit. Whilst microscopic models and properties based on fractional constitutive equations reconcile uneasily,[36] FMM proved more useful in our work than microscopic theories precisely because its flexibility allows a facile comparison between complex coacervate-dominated and metal-ligand dynamics.

The fractional Maxwell model characterizes complex coacervate flow in three parameters

Sadman et al.[32] outline the application of the fractional Maxwell model to complex coacervate rheology. For the complex modulus $G(\omega)$, FMM gives

$$G(\omega) = \frac{\mathbb{V}(i\omega)^{\alpha} \cdot \mathbb{G}(i\omega)^{\beta}}{\mathbb{G}(i\omega)^{\alpha} + \mathbb{V}(i\omega)^{\beta}}, \tag{2.3}$$

in which α and β are between zero and unity, and $\mathbb{V}$ and $\mathbb{G}$ are quasi-viscosities with units Pa s$^{\alpha}$ and Pa s$^{\beta}$. As previously shown for complex coacervates,[32] α can be set to unity, which results in a simpler formulation of the model in terms of a viscosity (since then the power in $\mathbb{V}$ is unity), a timescale and a modulus. Here, we use the traditional quasi-property[36] formulation of Equation 2.3, but with $\alpha = 1$, as suggested by Jaishankar.[29] For $\beta = 0$, the equation reverts to the Maxwell model with $\mathbb{G} = E$ and $\mathbb{V} = \eta_0$, with E a plateau modulus and η_0 a zero-shear viscosity. With $\alpha = 1$ and $\beta = \frac{1}{2}$, the model gives Rouse dynamics.

The time τ_c corresponding to the crossover frequency ω_c can be written

$$\tau_c = 2\pi\omega^{-1} = \left[\frac{\mathbb{G}}{\mathbb{V}}(\cos\pi\beta/2 - \sin\pi\beta/2)^{-1}\right]^{\frac{1}{\beta-1}} \tag{2.4}$$

as long as $\beta < 0.5$. For $\beta > 0.5$, there is no crossover, and for $\beta = 1$ the model is purely viscous (with $\eta_0 = \frac{\mathbb{V}\mathbb{G}}{\mathbb{G}+\mathbb{V}}$). The corresponding G_c can be calculated with Equation 2.3. τ_c equals the time that corresponds to the frequency $2\pi\tau_c^{-1}$ at which $G' = G''$, and at which the relaxation modulus $G(t)$ crosses over into an exponential decay. When a full measurement of either or both of these functions is not feasible due

to slow relaxation, we shall use Equation 2.4 to provide an estimate. The procedure is validated in the Section on frequency sweeps of coacervates at c_s^*.

FMM gives the relaxation modulus $G(t)$ as

$$G(t) = \mathbb{G} t^{-\beta} E_{\alpha-\beta,1-\beta}\left(-\frac{\mathbb{G}}{\mathbb{V}} t^{\alpha-\beta}\right) \tag{2.5}$$

in which E is the Mittag-Leffler (ML) function,

$$E_{a,b}(z) = \sum_{k=0}^{\infty} \frac{z^k}{\Gamma(ak+b)} \tag{2.6}$$

with Γ the gamma function, and parameters α, β, $\mathbb{V}$, $\mathbb{G}$ as defined for Equation 2.3. We used a Python implementation of the ML function for the numerical work.[37, 38]

Low-salt complexes at low terpyridyl content are largely unaffected by metal binding

We measure the mechanical relaxation spectrum of TC3s for different c_s, M^{2+} identities, and degrees of terpyridylation. First, we turn to the limiting case of low-c_s complexes with Mn^{2+}, a metal that is weakly bound, and thus fast to associate and dissociate. The complex $pA^{234}/pD^{222} - M^{2+}$ was prepared with various degrees of terpyridylation of pA and pD, and in presence and absence of Mn^{2+}.

At a c_s of 0.2 and 0.6 M NaCl, the frequency-dependent moduli exhibit features close to those expected for Rouse-like dynamics – loss and storage moduli tend to a scaling of respectively ω^1 and ω^2 at low frequencies, and cross at ω_c, from which point on they increase with a slope below $\omega^{\frac{1}{2}}$. Figure 2.3 shows $G', G''(\omega)$ of these complexes as black lines. At 0.2 M NaCl (Figure 2.3, two leftmost panels), we predominantly observe the effect of Rouse modes, whereas for 0.6 M NaCl we measure mostly in the terminal regime. Since Na^+ and Cl^- compete for bonds between the charges on pA and pD, the presence of salts speeds up polyelectrolyte complex relaxation.[24, 39] Multiple previous works have exploited this feature to access the entire relaxation spectrum[8, 33] through salt-time superposition: an increase in salt concentration is akin to an acceleration of dynamics through decrease of τ_0 (Equation 2.2).

Inspection of loss and storage moduli gives direct access to the crossover frequency that defines a relaxation time for a given complex, τ_C (Equation 2.2, leftmost equality). We fitted the frequency-dependent moduli to Equation 2.3. The fits were always excellent (Figure 2.3). We report the corresponding parameters in Table 2.1,

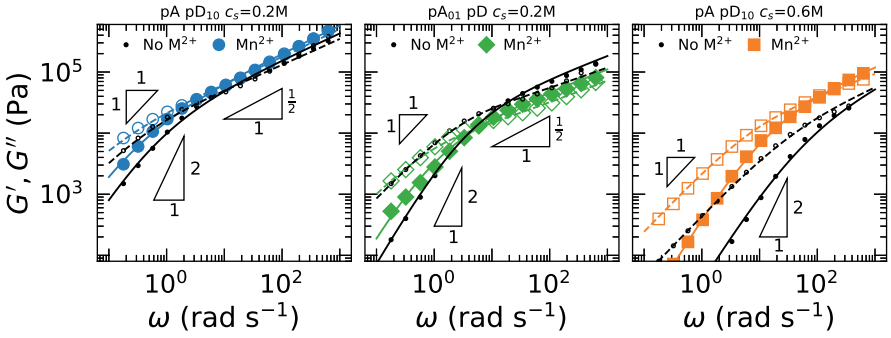

Figure 2.3: Storage (filled symbols) and loss (open symbols) moduli $G'(\omega)$ and $G''(\omega)$ for TC3s with at low (left and center) to moderate (right) c_s, with (large markers) and without (small dots) Mn^{2+}. All symbols represent recorded data, lines are fits to Equation 2.3, *vide infra*.

along with crossover times and moduli τ_c and G_c. The fits now allow us to extrapolate to τ_c through Equation 2.4, for those cases where the crossover lies beyond the rheometric range.

For complexes with no additional crosslinks, we can equate τ_C to τ_R, the whole-chain Rouse time, which at 0.2 M NaCl is 55 ms, and at 0.6 M NaCl is reduced to 0.8 ms for pA^{234}/pD^{222}_{10}. Reducing the amount of terpyridines on the chain reduces τ_R and G_R to the levels of an unmodified complex at the same c_s. Thus, we conclude that thickening of complexes due to hydrophobicity of terpyridine is a small yet significant effect.

We now turn to the question whether transient crosslinks with a lifetime τ_X *below* the coacervate relaxation time influence flow behaviour, i.e., whether transiently crosslinked coacervates are coacervate-like. At 0.2 M NaCl, the difference in terms of $G', G''(\omega)$ from the uncrosslinked complex is small for both lightly (1%) and heavily (10%) terpyridylated participants. However, at 0.6 M NaCl, as we approach c_s^*, the effect of Mn^{2+} is more pronounced. The transient bonds slow down relaxation, and contribute more strongly to the modulus at the crossover frequency. Figure 2.3 shows frequency sweeps for Mn^{2+}-crosslinked complexes with marked, colored lines. Nonetheless, short-lived transient crosslinks perturb pA/pD complexes only weakly.

Encouragingly, the addition of slower transient bonds did not hinder the ability of the FMM to capture the rheological behaviour over the complete frequency range employed. We see that the tPy–Mn^{2+} bonds are not consistently effective in slowing down relaxation at low salt strength. At higher salt (0.6 M), the effect of Mn^{2+} is to

Table 2.1: Complex coacervates with (Mn^{2+}) and without (∘) additional transient crosslinks at low-c_s: fractional Maxwell liquid ($\alpha = 1$) model fits and crossover times. $\mathbb{V}$ and $\mathbb{G}$ are in units of, respectively, (kPa s) and (kPa s^{β}). G_c is in kPa. Crossover times are defined as $2\pi\tau_c = \omega_c^{-1}$.

Complex	M^{2+}	[NaCl]	β	$\mathbb{V}$	$\mathbb{G}$	τ_c (ms)	G_c
pA^{234}/pD^{222}_{10}	∘	0.2 M	0.43	42.3	28.8	90	66
	Mn^{2+}	0.2 M	0.45	86.1	33.5	79	55
pA^{234}_{01}/pD^{222}	∘	0.2 M	0.35	9.0	19.3	55	32
	Mn^{2+}	0.2 M	0.36	10.8	11.8	176	12
pA^{234}_{10}/pD^{222}	∘	0.6 M	0.45	0.5	3.9	0.8	80
	Mn^{2+}	0.6 M	0.40	2.5	10.3	9.0	40

shift the crossover point slightly. β values were between 0.35 and 0.45, in accordance with the work of Sadman et al.[32]

The "ideal" case of Rousian chains corresponds to an FMM with $\alpha = 1$ and $\beta = 0.5$, which manifests itself as a $\propto \omega^{\frac{1}{2}}$ scaling in both loss and storage moduli (for "frozen" Rouse chains in between crosslinks, $\alpha = 0.5$ and $\beta = 1$). The inclusion of hydrodynamics (Zimm model) facilitates relaxation,[40] and increases β up to 0.67.[41] The discrepancy in our data from a Rouse fluid is thus not likely attributable to a contribution from hydrodynamics. Rather, the disagreement could stem from the bias towards predominantly fluid-like ($G'' > G'$) frequencies, which, however, is contradicted by the *decrease* of β as the bond lifetimes in the complex are lengthened by a decrease in salt. Alternatively, one could argue that we sample an excess of longer "ladder" bonds due to the slow equilibration of the complex coacervate. The suggestion of non-ergodicity does not agree with the near-Rouse dynamics of pA^{234}/pD^{222}_{10}, which should be the slowest sample to equilibrate on account of low c_s and high density of terpyridyl moieties.

Returning to the influence of metal-ligand transient crosslinks on the linear viscoelasticity of complex coacervates, we hypothesize that the distance between the Rousian relaxation time τ_R and metal-ligand crosslink time τ_X dictates the effect of the latter. In the following sections, we take the tools outlined so far to examine the case of near-c_s^* complexes, where the crosslink times can be expected to significantly outlast τ_R.

Table 2.2: Complex coacervates with (M^{2+}) and without ($\circ$) additional transient crosslinks near-critical salt strength c_s: fractional Maxwell liquid ($\alpha = 1$) model fits and crossover times. Crossover times are defined as $2\pi\tau_c = \omega_c^{-1}$. $\mathbb{V}$ and $\mathbb{G}$ are in units of, respectively, (kPa s) and (kPa s^{β}). G_c is in kPa. A minus sign (-) means that an estimate is not meaningful, since the data are dominated by inertial effects or slip, a smaller-than sign (<) means smaller than 0.01 kPa.

Complex	M^{2+}	[NaCl]	β	$\mathbb{V}$	$\mathbb{G}$	τ_c (s)	G_c
pA^{250}	$\circ$	0.9 M	-	-	-	$\leq 0.6 \cdot 10^{-3}$	<
$/pD_{01}^{1k}$	Mn^{2+}		0	$0.6{\cdot}10^{-3}$	0.4	$1.5 \cdot 10^{-3}$	0.2
	Zn^{2+}		0.103	0.340	1.0	$238 \cdot 10^{-3}$	0.6
	Co^{2+}		0.006	$4.6{\cdot}10^{4}$	2.2	$22.5 \cdot 10^{3}$	1.0
	Ni^{2+}		0.009	$2.8{\cdot}10^{5}$	1.9	$0.16 \cdot 10^{6}$	0.9
		0.8 M	0.015	$2.5{\cdot}10^{5}$	1.8	$0.16 \cdot 10^{6}$	0.8
pD_{01}^{1k}	Mn^{2+}	0 M	-	-	-	$\leq 1 \cdot 10^{-3}$	<
	Zn^{2+}		0.053	0.06	0.75	$68 \cdot 10^{-3}$	0.4
	Co^{2+}		0.014	$2.7{\cdot}10^{4}$	2.0	$13.6 \cdot 10^{3}$	0.9
	Ni^{2+}		0.015	$2.1{\cdot}10^{4}$	1.4	$20.9 \cdot 10^{3}$	0.5

Metal-ligand dissocation rates dictate relaxation times of complexes at high salt

We prepared complexes of pA^{250} and terpyridylated pD_{01}^{1k} at a salt concentration very near to dissolution (0.9 M). Metal ions were either Mn^{2+}, Zn^{2+}, Co^{2+}, or Ni^{2+}, and were introduced as pre-mixed with pA. We employed step strain measurements of $G(t)$ up to long waiting times (> 24 h), combined with frequency sweeps to address the widest range of relaxation times. $G(\omega)$ and $G(t)$ were recorded for all complexes but $pD_{01} - Mn^{2+}$, which did not give rise to enough torque to allow a meaningful measurement of $G(t)$.

Unlike the low-salt, fast-metal complexes seen in Figure 2.3, the high-salt complexes $pA/pD_{01} - M^{2+}$ were dramatically changed by the choice of metal ion in the transient metal-ligand bonds. Whereas fast metals Mn^{2+} and Zn^{2+} showed the tail of a decaying function, slow metals Co^{2+} and Ni^{2+} gave decay only after after prolonged waiting ($> 10^4$ s). Figure 2.4 (right) shows the pronounced effect of metal-ligand binding in terms of $G(t)$ (marks represent data).

Following literature on polymeric networks with metal-ligand crosslinks, we attempted to model the relaxations with Maxwell models (Equation 2.1),[42] and

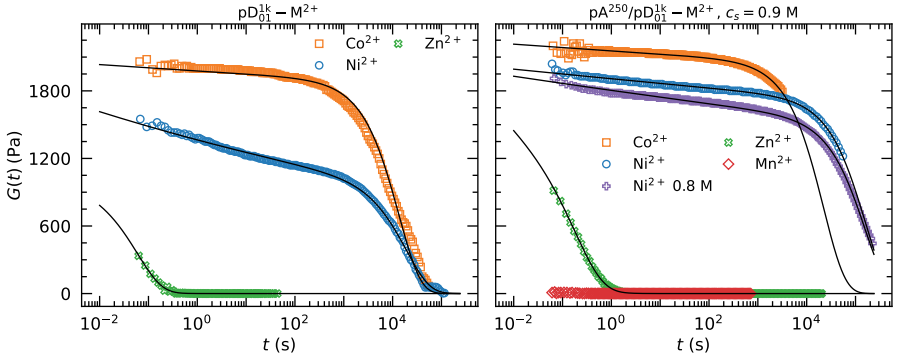

Figure 2.4: Relaxation moduli $G(t)$ for materials with different metal-ligand crosslinks for (left) non-coacervate samples and (right) coacervates at near-critical c_s. Symbols represent (part of) the collected data, while solid lines are fits to Equation 2.5.

stretched exponentials.[17] The Maxwell model approximated the data poorly, whereas the analysis with a sum of two stretched exponentials was complicated by multiple parameter sets offering similarly low residuals. The decays are not exponential, and are in fact power law-like in the initial several orders of magnitude in t. However, as is clear in the right-hand panel of Figure 2.4, we were able to capture the entire relaxation for all samples with the FMM form for $G(t)$ given by Equation 2.5.

As was the case for the mainly coacervate-like complex with Mn^{2+} and lower c_s, α was always kept at 1, meaning that the complexes are ultimately fluids, albeit with sometimes extreme viscosities. Unlike the coacervate-like complexes, β was much closer to 0, indicating Maxwell-like response. In the case of near-zero β, the pseudo-property $\mathbb{G}$ can be interpreted as close to a plateau modulus G_0. We list the parameters used to achieve the fits of $G(t)$ in Table 2.1. Using Equations 2.3 and 2.4, we calculated the crossover values for relaxation time and modulus. In the case of complexes with no metal-ligand bonds, an extrapolation was used, with τ_c assumed to be in exponential decay with c_s.[33] For Mn^{2+}, we used a fit to $G(\omega)$.

With all metals, the relaxation time is significantly lengthened by the presence of transient metal-ligand bonds. Figure 2.4 confirms that the relaxation times follow the order of binding affinities (equilibrium constants) $Mn^{2+} < Zn^{2+} < Co^{2+} < Ni^{2+}$.[19, 43] For the last three, the increase in measured τ_c is at least thousandfold. Ni^{2+} gives rise to particularly slow relaxation, $\frac{\tau_c}{\tau_R}$ approaching 10^9 (Table 2.2).

We attribute the increase of relaxation times in complexes that contain pD_{01} and

an M^{2+} species to the formation of a physical network inside the complex coacervate matrix, as pictured in Figure 2.1. With the help of simple scaling theories,,[44] knowledge of the form factor from neutron scattering of pD in a pA/pD complex of similar degrees of polymerization[45] allows to approximate the inter-terpyridine length R_x. Polyelectrolytes in coacervates obey Gaussian statistics,[45] $R_x^2 = N l_k^2$, with l_K the persistence length and N the amount of Kuhn segments between crosslinks.[45] Taking l_K at 16 nm, we arrive at an R_x of 20 nm for 1% terpyridylated chains (100 chemical monomers between terpyridine units). Given one elastically active chain per R_x^3, classical rubber elasticity predicts an elastic modulus of 0.5 kPa, which underestimates G_0' for complexes with the slow metals, but is a reasonable estimate for complexes with Mn^{2+} and Zn^{2+}.

Additionally, scaling theory allows to estimate whether intra-chain crosslinks are expected to play a role in the network. The possibility for polymers to crosslink with themselves is often overlooked, but results in crosslinks that are elastically inactive.[46–48] We assess the importance of self-crosslinks by counting the amount of terpyridines within one volume spanned by R_x – this is the bulk concentration of terpyridines c_{tPy} multiplied by R_x^3. Our coacervates near c_s^* have a c_{tPy} of 5 mM, which corresponds to 25 terpyridines within the volume, indicating a self-crosslinking efficiency of 4%. Thus, while present in the complexes, inactive, or "self", crosslinks do not likely have a dominant influence on G_0'.

Importantly, the rather large internode spacing suggests that there is ample space to guarantee appropriate binding geometry for the [2+1] complex, which is on the order of 2 nm. While no deviation from the expected stoichiometry due to strain[49] is expected, we did not quantify the stoichiometry, since the absolute number of crosslinks does not affect our comparison between metal identities. We note that the scaling analysis above is an order-of-magnitude estimate, and that a full structure study using deuterated "tracer" polyelectrolytes is appropriate to address the issue of structure fully. Since we focus on the dynamics of the hybrid complexes, such a study is beyond the scope of the present contribution.

In complex coacervates at high salt in which one polyelectrolyte is terpyridylated, the metal-ligand bond strengths dominate the rapid relaxation mechanisms that are native to complex coacervates. Only at frequencies so rapid to be inaccessible by rheology would one expect to retrieve a contribution of the coacervate. At frequencies measurable with a commercial rheometer, the linear viscoelasticity bears witness only to relaxation from metal-ligand dissocation. Transient bonds offer a salt-independent control over high-c_s polyelectrolyte complexes: they can be tuned from viscous to indefinitely mechanically stable at one and the same salt concentration.

Non-coacervate complexes experience less slowing-down than their coacervate counterparts

We then turned to the question whether the extreme response to metal ion identity is intrinsic to pD_{01}^{1k}, or a result of participation of both pA and pD. We inquired into whether the non-dominant contribution of the coacervate (at $\frac{\omega}{2\pi} \approx (0.6 \cdot 10^{-3})^{-1} s^{-1}$) is at all present in the rheology, or whether the coacervate merely provides a water-insoluble phase that then accepts metal-ligand viscoelasticity. First, we repeated the experiment with pA/pD$-Ni^{2+}$ at a slightly lower c_s of 0.8 M, which resulted in exactly the same relaxation time, and negligible differences in the FMM fits (Table 2.2). Thus, at long times, complexes with Ni^{2+} crosslinks are entirely dominated by the metal-ligand dissociation time.

Moreover, we made non-coacervate metal complexes with terpyridylated pD, denoted $pD_{01}-M^{2+}$ (note the absence of pA). The polymer mass-over-volume fraction of the coacervate complexes at 0.9 M was estimated at 0.16, which was subsequently used as the polymer concentration in the $pD_{01}-M^{2+}$ complexes (see Experimental Section for details).

Non-coacervate complexes $pD_{01}-M^{2+}$ showed strikingly similar linear viscoelasticity to the metalated coacervate samples (Figure 2.4, leftmost panel), and were amenable to the same FMM analysis with Equation 2.5. In the bottom part of Table 2.2, we list fit parameters and crossover features. For Mn^{2+}, it was difficult to assess the reliability of the data due to low torque: complexes with Mn^{2+} do not have a distinguishable contribution of terpyridylation at this level of analysis.

β values were close to zero for Zn^{2+}, Co^2 and Ni^{2+}, which means that the response is nearly Maxwellian, and $\mathbb{G}$ essentially a plateau modulus. Note that for an FMM liquid with $\beta > 0$, $G_c < \mathbb{G}$ – an analysis of crossover moduli in the Maxwellian sense is thus somewhat misleading. Rather, $\mathbb{G}$ is proportional to the $G(t)$ at $t = 0$ (Equation 2.5).

Due to the responses being close to Maxwellian, we can approximately compare τ_c and $\mathbb{G}$ for pA/$pD_{01}-M^{2+}$ to the corresponding non-coacervate $pD_{01}-M^{2+}$ systems. The values of $\mathbb{G}$ agree up to a factor of 1.3, which indicates that the effective crosslinking densities are sufficiently close to allow a comparison of τ_c. The striking similarities in β and $\mathbb{G}$ preclude major structural changes. Such a comparison of τ_c shows that each non-coacervate sample relaxes significantly faster than the corresponding high-salt coacervate sample. The difference is especially striking in the case of Ni^{2+}, where τ_c is slowed down more than tenfold. We analyze the short-time response of the complexes more closely using $G(\omega)$ in the subsequent section.

Entanglements have proven to be an important contribution to the slow relaxation of coacervate complexes of high molecular weight polyelectrolytes.[33] However, we do

not ascribe the plateaus in $G(t)$ and high τ to entanglement-like phenomenology, at least not at the polymer concentration of 16% $^{m}/_{v}$. The pD_{01} complex with Mn^{2+} is a liquid of poor viscosity, and the corresponding coacervate complex $pA/pD_{01}-Mn^{2+}$ shares a very similar flow behaviour. While the higher M_n of the poly[cation] suggests that entanglements could be important, the relaxation times of pA^{234}/pD^{222} and pA^{250}/pD^{1k} are in fact very close, more representative of the molecular weight derived from conversion during polymerization (see Figure 2.C.1 and the accompanying discussion). Thus, slowed-down $pA/pD_{01}-M^{2+}$ complexes do not have a significant contribution of entanglements to their viscoelasticity.

Frequency-dependent moduli agree with the parameters determined from relaxation fits

Given the wide separation between τ_R and τ_c for complexes with metals slower than Mn^{2+}, we would expect high similarities in the short-time responses in both families of complexes, $pD_{01}-M^{2+}$ and $pA/pD_{01}-M^{2+}$. On the other hand, any differences would signify a change in network structure on a rather short length scale. $G(t)$ data are not reliable below 100 ms, and therefore we measured $G', G''(\omega)$ using oscillatory shear.

Frequency sweeps were consistent with relaxation moduli. To demonstrate the correspondence on a quantitative level, we plotted graphs of G', $G''(\omega)$ calculated using Equation 2.3 with the parameters previously obtained for the same samples in step shear (Table 2.2). Figure 2.5, shows measured $G', G''(\omega)$ as marks, and calculated $G', G''(\omega)$ as black lines. Note that the black lines are not fits to the frequency-dependent data, they are merely the Fourier conjugate of Equation 2.5 with the appropriate parameters.

The agreement was excellent for Zn^{2+}, whereas it leaves something to be desired for the slower metals. This is a consequence of the fact that most of $G(t)$ captures exclusively plateau-like regimes for Co^{2+} and Ni^{2+}, so any sloping-up features are missed. Additionally, measurements of $G(\omega)$ were plagued by problems due to slip and inertia at higher frequencies, which manifests as the erratic increases in both curves at high frequencies. By using a sum of two FMM elements, we were able to fit the whole frequency range (colored lines in Figure 2.5). However, the extracted parameters are of very limited use for our analysis, since they indicate $\beta > 0.5$. Complex coacervates have finite relaxation times, and therefore we attribute the high-frequency anomalies to slip and inertia.

However, G' was reliably found to arrive to a plateau-like feature at the value predicted by the FMM fits of the step strain measurements. Additionally, we do not

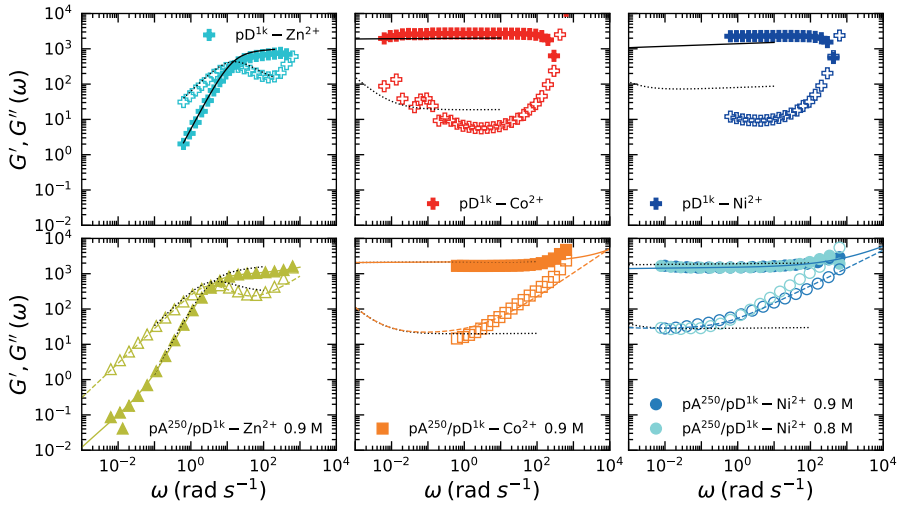

Figure 2.5: Real and imaginary parts of frequency-dependent moduli G' (filled symbols) and $G''(\omega)$ (open symbols). Symbols are measured data, one in two or three points is marked. Molarities refer to c_s. The high-frequency ends were *not* truncated, and the upturn in moduli is related to slip and tool inertia. Black lines are graphs of Equation 2.3 with parameters as fitted for the corresponding relaxation modulus $G(t)$, i.e. measured in the same run. Coloured lines (bottom panels) are fits to a two-component fractional Maxwell liquid.

see evidence for a different short-time relaxation mechanism for coacervate and non-coacervate complexes from the frequency sweeps, since features in $G(\omega)$ and $G(t)$ are highly similar.

Coacervate-metal-ligand synergy in transiently crosslinked complex coacervates

In the above, we have shown that metal-ligand complexation offers an attractive avenue to program the rheological fate of complex coacervates. Given the potential applicability of complex coacervates in underwater adhesives and other future technologies, ways of changing their modulus and relaxation behaviour "on demand" attract interest. For complex coacervates at low c_s, thus with a long τ_R, with quickly-dissociating metals, we find that metal-ligand binding gives only a modest contribution to the rheology. The timescale of tPy$-M^{2+}$-dissocation is not separated from the dissocation time of a carboxylate-dimethylammonium bond. However, when the distance between the coacervate relaxation time and the metal-ligand dissociation time is clearly separated, the linear viscoelasticity is strongly dominated by the latter.

At near-critical salt concentrations, where the complex coacervate contributes to viscoelasticity only at extremely high frequencies, we retrieve similar behaviour for metal-ligand-only complexes of pD_{01} (without poly[anion] partner) and the coacervate-metal-ligand complexes. However, the relaxation times are vastly different, despite similar instantaneous and short-time moduli. Given the obvious benefits of having two faster (i.e. easily injectable) building blocks assemble into a much slower one for e.g. underwater adhesion, we identify the slowing-down effect of the coacervate on metal-ligand network formation as a synergistic effect. However, the elucidation of the structural cause is beyond the scope of the present contribution, and is a topic of ongoing investigation.

To widen the scope of the idea of metal-ligand-coacervate synergy, we took the tPy$-Zn^{2+}$ motif into a complex of pD_{01} with not pA but poly(2-acrylamido-2-methylpropylsulfonic acid) (pAMPS), prepared near the critical salt strength (1.3 M for this pair) and at much lower salt (0.6 M). $G(t)$ measurements again showed that coacervates without additional transient bonds have short relaxation times, untractable (<1 ms) at c_s^*, but easily estimable at 0.6 M (10 ms) (see Table 2.3 for relaxation times and FMM fit parameters and Figure 2.6 for measured and fit $G(t)$ data).

Both critical and medium-salt complexes were significantly slowed down by addition of Zn^{2+} with respect to the native relaxation time of the metal-less complex.

Table 2.3: Complex coacervates with Zn^{2+} and without (∘) at medium and near-critical salt strength c_s: fractional Maxwell liquid ($\alpha = 1$) model fits and crossover times. Crossover times are defined as $2\pi\tau_c = \omega_c^{-1}$. $\mathbb{V}$ and $\mathbb{G}$ are in units of, respectively, (kPa s) and (kPa s^{β}). A hyphen (–) means that any estimate is not meaningful, since the data are dominated by inertial effects or slip.

Complex	M^{2+}	[NaCl]	β	$\mathbb{V}$	$\mathbb{G}$	τ_c (s)
$pAMPS^{800}$	∘	0.6 M	0.211	0.29	6.6	$10 \cdot 10^{-3}$
$/pD_{01}^{1k}$	Zn^{2+}	0.6 M	0.094	$53.5 \cdot 10^{3}$	6.6	8.3
	∘	1.3 M	-	-	-	$\leq 1 \cdot 10^{-3}$
	Zn^{2+}	1.3 M	0.078	0.36	0.66	$453 \cdot 10^{-3}$

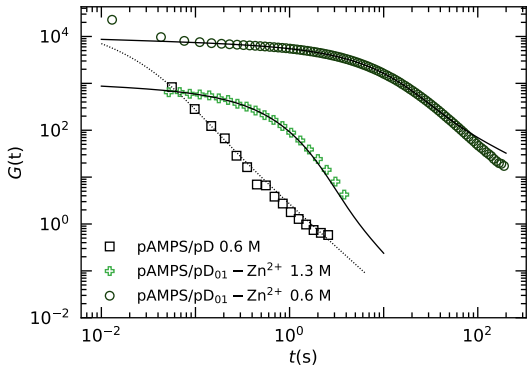

Figure 2.6: Relaxation moduli $G(t)$ at medium high c_s for metal-ligand-coacervate system pAMPS–pD_{01}–Zn^{2+}. Symbols correspond to collected data, solid lines are fits to Equation 2.5.

The c_s^*-complex closely resembled the 0.9 M scenario for pA/pD–Zn^{2+} (compare Figure 2.4, left), which shows that complex coacervates generally slow down tPy-metal bonds, even at the critical salt concentration. For the lower c_s of 0.6 M, we witness a slowdown of almost three orders of magnitude in time with respect native dynamics, and a twenty-fold change as compared to the complex at critical salt.

Thus, the relaxation time of a coacervate-metal-ligand complex is *not* solely set by the dissociation time of the metal-ligand complex. Instead, the dissociation time is a limiting value that complexes approach as their viscosity decreases. Throughout two different poly(anion) chemistries, we show that the relaxation time of a complex can outlast both the native complex coacervate relaxation time, as well as the relaxation time of a complex with only one of the polyelectrolyte partners.

2.4 Conclusion

We demonstrate with pA/pD complexes in which tP groups are incorporated that complex coacervates can be stiffened through the use of metal-ligand complexes. While low tP contents do not increase the salt tolerance of the pA/pD complex, we show that the incorporation of 10% tP widens the complex coacervation window. This is attributable to the hydrophobic effect, given that terpyridine is insoluble in water. The effect of tP–M^{2+} complexes on the dynamics of the coacervate-metal-ligand complex depends on the stability of the metal-ligand bond, but also on the "native" relaxation time inherent in the coacervate. When the "native" timescale is longer than the metal-ligand dissociation time, effects are only seen for high tPy contents, which again could be explained by the hydrophobic effect. However, for metal-ligand bonds that significantly outlast the native relaxation times, we find a dramatic slowing-down of the coacervate-metal-ligand complex. This is attributed to the metal-ligand bonds now acting as an impermanent crosslink. In fact, the transient bonds can appear as rather permanent, with relaxation times in excess of 1 day for Ni^{2+} at a tPy content of only 1% on one of the coacervating partners.

Owing to the far slower time signature of such bonds, the coacervate's native dynamics are mostly invisible in the rheology, and coacervate-metal pA/pD_{01}–M^{2+} and non-coacervate-metal pD_{01}–M^{2+} complexes appear highly similar in their high-frequency dynamics. However, we see unaccounted-for slowing-down in the long-time behaviour of the coacervate complexes with respect to their non-coacervate counterparts. We see this as a form of coacervate-metal-ligand synergy, in which two relatively fast elements come together to flow much more slowly together. The requirements of on-demand setting adhesives are highly compatible with the synergistic characteristics of transiently crosslinked complex coacervates. Future studies

should point out whether ligands that offer better biocompatibility (such as histidine) or responsivity (catechols) offer similar benefits. A wider choice of ligands would also allow to address the influence of hydrophobicity.

In addition, we expose the utility of the fractional Maxwell model in capturing viscoelastic phenomena encountered in complex liquids with diverse mechanisms accounting for their constrained flow. All our results can be fitted with equations derived from one and the same constitutional equation. Thus, fractional Maxwell models can be successfully applied in the design of complex fluids.

Appendix

2.A Synthesis and spectroscopy of terpyridylated polyelectrolytes

Materials & Methods

Unless stated otherwise, chemicals were used as received. Acetonitrile (CH_3CN, anhydrous, 99.8%), KOH (powdered, for synthesis, ≥ 85.0%), 1,4-dibromobutane (99%), dimethylformamide (DMF, anhydrous, 99.8%), 2-acrylamido-2-methyl-1-propanesulfonic acid (AMPS, 99%), 4-cyano-4-[(dodecylsulfanylthiocarbonyl)sulfanyl]pentanoic acid (4CDTPA, 97%), 2,2'-azobis(2-methylpropionitrile) (AIBN, 98%), and, dimethylsulfoxide (DMSO, anhydrous, ≥99.9%) were obtained from Sigma-Aldrich, Germany. 4'-Chloro-2,2':6',2"-terpyridine (>98.0%), 3-amino-1-propanol (>98.0%) and, 2,6-bis(2-pyridyl)-4(1*H*)-pyridone (>98.0%) were obtained from TCI Europe. Dichloromethane (DCM, stabilized with ethanol, ≥ 99.9%), and, methanol (MeOH, HPLC, ≥ 99.9%) were procured from Biosolve. AIBN was recrystallized from methanol thrice. AMPS was crystallized from ethanol twice and freshly used. Dibromobutane was distilled at low pressure, and stored over molecular sieves (4Å). CH_3CN and DMSO were stored on molecular sieves (4Å).

Poly(N,N-dimethylaminoethyl methacrylate)–35 kDa (pD^{222}, Đ=1.12) and poly(acrylic acid)–30 kDa (pA^{416}, Đ=1.12) were obtained from Polymer Source, Canada. Commercial pA was dried for several days on a Shlenk line, then dissolved in DMF and centrifuged at 2000g for 1h to remove insoluble impurities. Poly(N,N-dimethylaminoethyl methacrylate)–161 kDa (pD^{1k}, Đ=1.43) and poly(acrylic acid)–30 kDa (pA^{250}, Đ=1.13) were synthesized using copper-catalyzed polymerizations as reported in the Experimental Section of the main text.

Methods

Synthesis of 3-aminopropoxyterpyridine The synthesis of 3-aminopropoxyterpyridine by Williamson ether synthesis was adapted from literature.[20] Under N_2 (g), 4'-chloro-2,2':6',2"-terpyridine (1.64 g, 6.36 mmol), powdered KOH (1.65 g, 29 mmol), and 3-amino-1-propanol (0.50 mL, 6.7 mmol) were added to 25 mL of dry DMSO in a round-bottomed flask. The mixture was stirred at 60 °C for 30 h, after which it was added to 300 mL saturated aqueous K_2CO_3 and extracted into DCM. The DCM

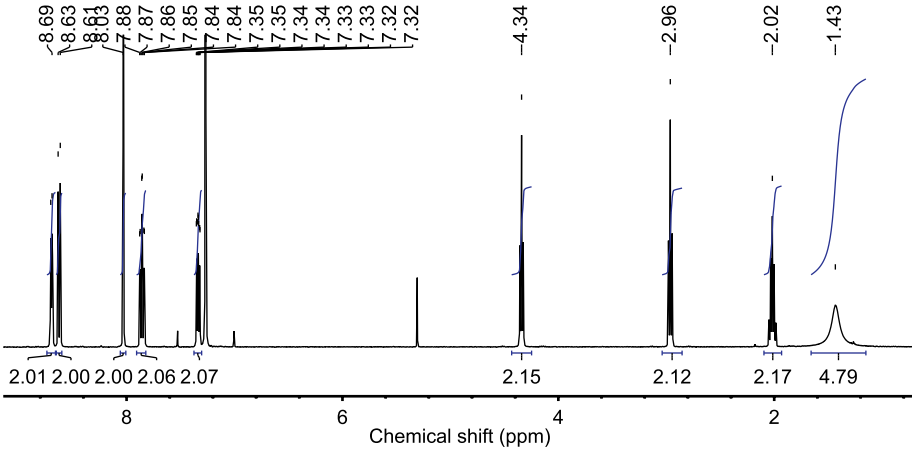

Figure 2.A.1: ^{1}H-NMR (400 MHz, $CDCl_3$ of 3-aminopropoxyterpyridine.)

solution was washed with 0.1 M NaOH and thrice with K_2CO_3, and dried over Na_2SO_4. After filtration and concentration *in vacuo*, 3-aminopropoxyterpyridine was obtained as a yellow solid. (1.04 g, 3.39 mmol, 53%).

^{1}H-NMR (400 MHz, $CDCl_3$: Figure 2.A.1. ^{13}C-NMR (101 MHz, $CDCl_3$): δ (ppm) 167.07, 157.14, 156.10, 149.03, 136.78, 123.82, 121.34, 107.32, 67.09, 33.26, 29.35, 27.65. MS (ESI): $[M+K]^+$ found at 345.1109, expected 345.1111, $[M+Na]^+$ at 329.1369, expected 329.1369.

Synthesis of 4-bromobutoxyterpyridine The synthesis of 4-bromobutoxyterpyridine was adapted from literature.[50] 2,6-bis(2-pyridyl)-4(1H)-pyridone (0.867 g, 3.48 mmol) was added to 50 mL of dry CH_3CN in a round-bottomed flask. Dibromobutane (4.1, 34 mmol) and K_2CO_3 (1.0 g, 7.0 mmol) were introduced into the white suspension, which was left to reflux overnight. The caramel-coloured crude was left to cool down, was filtrated and then concentrated *in vacuo*. The brown oil was chromatographed over SiO_2 and eluted with 5% MeOH in DCM, yielding 4-bromobutoxyterpyridine (0.78 g, 2.0 mmol, 59%).

^{1}H-NMR (400 MHz, $CDCl_3$: Figure 2.A.2. ^{13}C-NMR (101 MHz, $CDCl_3$): δ (ppm) 167.07, 157.14, 156.10, 149.03, 136.78, 123.82, 121.34, 107.32, 67.09, 33.26, 29.35, 27.65. MS (ESI): $[M+K]^+$ found at 422.0261 and 424.0241, expected 422.0261 and 424.0241.

Synthesis of poly(2-acrylamide-2-methylsulfonic acid) To a round-bottomed flask was added 5.0 g of AMPS (24.2 mmol, 500 eq), 19.5 mg (0.048 mmol, 1 eq) of 4CDTPA, and 1.6 mg of AIBN (0.2 eq). To this was added 10 mL of DMF, and a septum

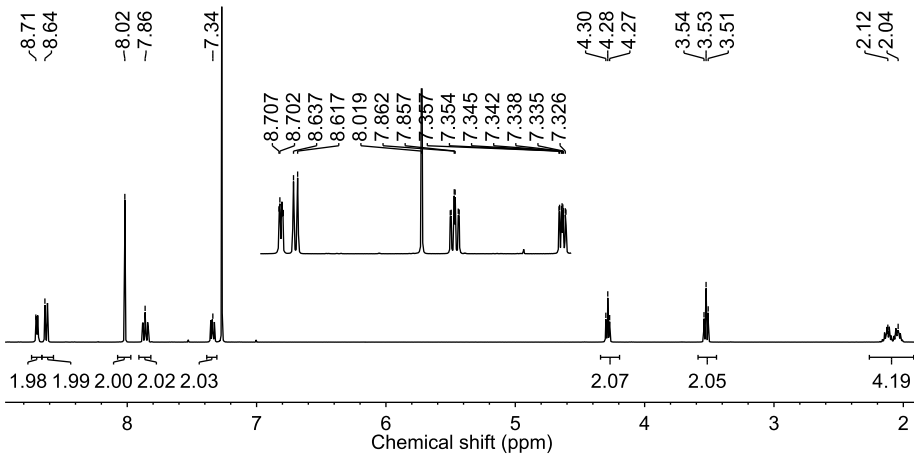

Figure 2.A.2: ^{1}H-NMR (400 MHz, $CDCl_3$ of 4-bromobutoxyterpyridine.

was fitted into the neck of the flask. The mixture was bubbled for 30 min. with N_2, after which the flask was submerged into a pre-heated oil bath at 70 ° C. After 4 h, polymerization was stopped by admitting oxygen and placing the flask on ice. The residue was purified by reprecipitation, thrice in acetone.

SEC-MALLS (HFIP, 0.02 M KTFA): M_n=165 kDa, M_w=186 kDa, Đ=1.13.

2.B Synthesis of homopolymer polyelectrolytes

The nature of this work required access to larger quantaties of relatively monodisperse polyelectrolytes at low price. Therefore, we based our synthetic practice on copper-based polymerization techniques from the recent literature,[51, 52] albeit with minor optimizations towards the reactivity of *tert*-butyl acrylate and N,N-dimethylamino-ethyl methacrylate. We believe these modifications to be of some merit to the polymer chemist, and report them in detail here.

Synthesis of poly(acrylic acid)

Poly(acrylic acid) was obtained through de-*tert*-butylation of poly(*tert*-butyl acrylate). The latter was made using Cu(0)-catalyzed polymerization, following Haddleton et al. with substitution of *n*-butyl acrylate for *tert*-butyl acrylate.[52] In this procedure, initiating radicals derived from a halide are generated by a complex of Cu(0) and a

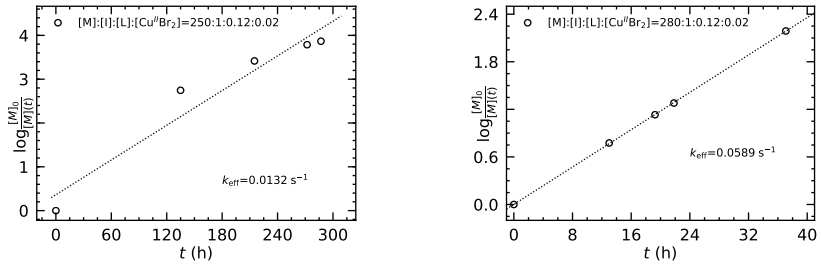

Figure 2.B.1: Pseudo-first order kinetics of (left) *tert*-butyl acrylate and (right) *N,N*-dimethylaminoethyl methacrylate

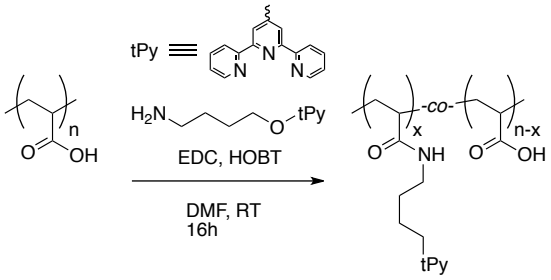

Figure 2.B.2: Synthesis of terpyridylated pAA copolymers by carbodiimde-driven peptide formation of pAA and an aminoalkyl terpyridine.

strongly ligating tertiary amine, whereas the corresponding Cu^{II} complex catalyzes formation of halogen caps from radical chain ends, forming Cu^{I} simultaneously. The latter then proceeds to generate radicals from halogenated polymers or unused initiator. For appropriate combinations of monomers, ligand, and initiator, a uniform rate of propagation is thus achieved.

The ligand used was Me_6TREN, the initiator ethyl α-bromoisobutyrate. The reaction is elementary to set up, yet rivals anionic methods in terms of dispersity (Đ=1.13 without any optimization). We used the condition 50% $^{v}/_{v}$ *tert*-butyl acrylate in DMF with [M]:[I]:[L]:[$Cu^{II}Br_2$] being 250:1:0.12:0.02. Kinetics did not follow the pseudo-first order rate law (Figure 2.B.1), but HFIP-SEC showed excellent agreement to nominal molecular weight and narrow dispersities. The slow-down in the effective addition rate constant is likely due to termination at the rather high conversions employed, and can easily be avoided by an earlier termination of the polymerization.

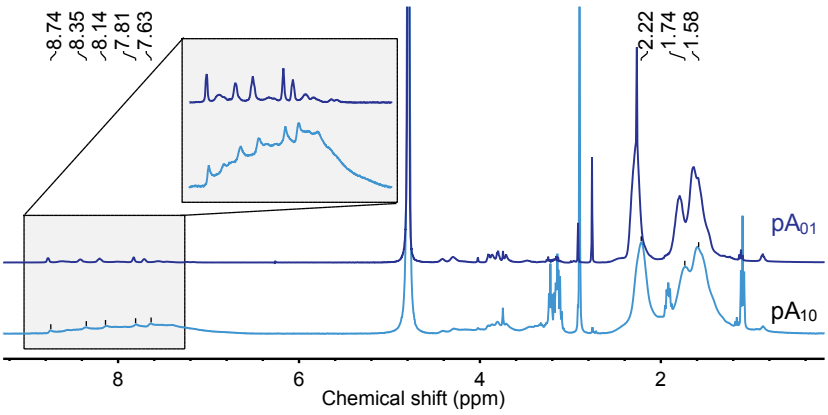

Figure 2.B.3: Proton NMR spectra (400 MHz, D_2O) of solutions of 1% and 10% terpyridylated pAA, pA_{01} and pA_{10}. The inset shows a magnification of the aromatic (terpyridine) region.

Synthesis of poly(N,N-dimethylaminoethyl methacrylate)

Poly(N,N-dimethylaminoethyl methacrylate) (pD) was synthesized using copper-based photocatalysed polymerization. To this end, we extended the work of Haddleton et al.[51] in which poly(acrylates) are conveniently synthesized by photocatalysis of a Cu(II)-Me_6TREN complex, towards methacrylates. However, we found that the suggested conditions do not allow photocatalyzed polymerization of DMAEMA, since the polymerizations terminate at low conversions. We also note a brown discoloration of the reaction medium. Following another work by Haddleton et al.[52] we swapped the initiator for methyl α-bromo phenylacetate (MBPA).

Copper(II)-Me_6TREN-catalyzed photopolymerization of DMAEMA yielded the polymer straightforwardly, at a convenient (50 g) scale. The kinetics adhered to the pseudo-first order rate law strictly (Figure 2.B.1), eliminating concerns over end of chain-end reactivity due to Menschutkin coupling with polymeric or monomeric DMAEMA. SEC-MALLS in HFIP (see main text) revealed a rather high dispersity (Đ=1.43) and a five-fold deviation from the conversion-based molecular weight (DP=216, M_{nominal} = 34 kDa). However, since we did not seek to compare relaxation times between complexes of polyelectrolytes of various molecular weights as has already been done,[8] but rather between complexes with different *added* transient bonds, we deemed the molecular weight to be sufficiently defined.

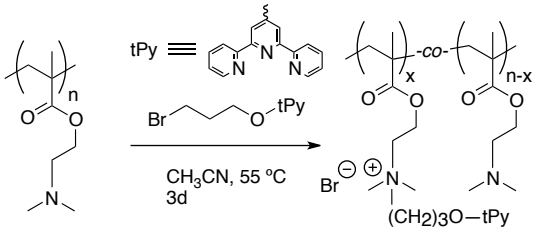

Figure 2.B.4: Synthesis of terpyridylated pDMAEMA copolymers by Menschutkin reaction of a terpyridyl alkylbromide with pDMAEMA.

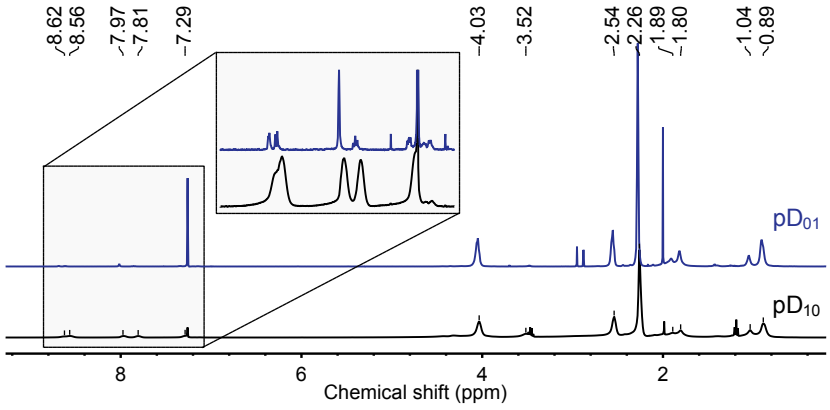

Figure 2.B.5: Proton NMR spectra (400 MHz, $CDCl_3$) of solutions of 1% and 10% terpyridylated pDMAEMA, pD_{01} and pD_{10}. The inset shows a magnification of the aromatic (terpyridine) region.

2.C "Native" viscoelasticity of coacervate complexes used in this work

To alleviate concerns about the presence of entanglements, we compare the viscoelasticity of two "native" coacervate complexes (i.e., no additional transient crosslinks): one made from commercial polymers (see Table 1 of the main text), and the other from polymer synthesized as described here (*vide supra*). Figure 2.C.1 shows frequency sweeps for the two coacervate pairs at similar salt concentrations. It can be readily seen that both samples have a strikingly similar viscoelasticity: most of the points lie in the terminal (viscous) regime, where $G' \propto \omega^2$ and $G'' \propto \omega^1$. The frequencies of crossover also appear similar, excluding serious slow-down in the dynamics as required by the presence of entanglements.

We estimate the crossover frequency using a fit to the fractional Maxwell model (see main text). The corresponding crossover times (here defined as $2\pi\tau_R = \omega_c^{-1}$) are 0.8 ms for pA^{234}/pD^{222} at 0.6 M NaCl and 1.2 ms for pA^{250}/pD^{1k} at 0.5 M NaCl, the superscripts denoting the degrees of polymerization. We can account for the difference in salt concentration c_s by noting that τ_R scales with $\exp -\sqrt{c_s}$ and carrying out an interpolation.[8, 53] This estimates τ_R at 1.3 ms for pA^{234}/pD^{222} at 0.5 M NaCl, versus a measured τ_R of 1.2 ms for pA^{250}/pD^{1k} at the same c_s. In short, the relaxation times of the two complexes are essentially indistinguishable, despite the difference in M_n reported by SEC. Thus, we do not find evidence for the presence of entanglements, which would result in a severe increase of τ_R.

For unentangled monodisperse polyelectrolytes, $\tau_R \propto N^2$, which does not support the finding of similar relaxation times for chains with a four-fold difference in M_n. We reconcile the discrepancy by noting the increased polydispersity of pD^{1k}, and speculate that the lower molecular weight fraction of the residue acts to plasticize the coacervates. Alternatively, noting that the conversion-based degrees of polymerization of both poly(cations) are essentially identical (216 and 222), M_n or M_w could have been overestimated by SEC due to absorption of pD on the column. Again, we do not directly compare relaxation times between complexes derived from the two distinct pA/pD pairs, and thus the residue is defined enough in terms of molecular mass. Instead, we focus on the very strong effect of added transient bonds in unentangled coacervate complexes.

Bibliography

[1] A. H. Hofman, I. A. van Hees, J. Yang, and M. Kamperman, "Bioinspired Underwater Adhesives by Using the Supramolecular Toolbox," *Advanced Materials*,

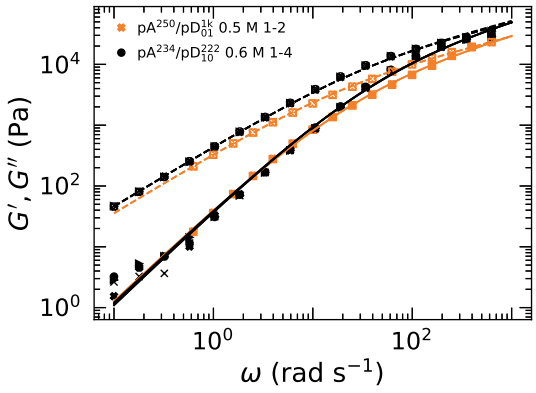

Figure 2.C.1: Storage (filled symbols) and loss (empty symbols) moduli G', G'' as function of ω, the frequency of oscillation for two complex coacervate pairs. The symbols are measured data, whereas the lines are fits to the fractional Maxwell model (Equation 3 of the main text).

vol. 1704640, p. 1704640, 2018.

[2] C. S. Wang and R. J. Stewart, "Multipart copolyelectrolyte adhesive of the sandcastle worm, Phragmatopoma californica (Fewkes): Catechol oxidase catalyzed curing through peptidyl-DOPA," *Biomacromolecules*, vol. 14, no. 5, pp. 1607–1617, 2013.

[3] R. J. Stewart, C. S. Wang, and H. Shao, "Complex coacervates as a foundation for synthetic underwater adhesives," *Advances in Colloid and Interface Science*, vol. 167, no. 1-2, pp. 85–93, 2011.

[4] H. G. Silverman and F. F. Roberto, "Understanding marine mussel adhesion," *Marine Biotechnology*, vol. 9, no. 6, pp. 661–681, 2007.

[5] R. J. Stewart, T. C. Ransom, and V. Hlady, "Natural underwater adhesives," *Journal of Polymer Science, Part B: Polymer Physics*, vol. 49, no. 11, pp. 757–771, 2011.

[6] M. Cui, S. Ren, S. Wei, C. Sun, and C. Zhong, "Natural and bio-inspired underwater adhesives: Current progress and new perspectives," *APL Materials*, vol. 5, no. 11, p. 116102, 2017.

[7] W. C. Blocher and S. L. Perry, "Complex coacervate-based materials for biomedicine," *Wiley Interdisciplinary Reviews: Nanomedicine and Nanobiotechnology*, vol. 9, no. 4, pp. 76–78, 2017.

[8] E. Spruijt, M. A. Cohen Stuart, and J. Van Der Gucht, "Linear viscoelasticity of polyelectrolyte complex coacervates," *Macromolecules*, vol. 46, no. 4, pp. 1633–1641, 2013.

[9] I. van Hees, A. H. Hofman, R. Fokkink, and M. Kamperman, "In Preparation," 2020.

[10] M. Dompé, F. J. Cedano-serrano, O. Heckert, N. V. D. Heuvel, J. V. D. Gucht, Y. Tran, D. Hourdet, C. Creton, and M. Kamperman, "Thermoresponsive Complex Coacervate-Based Underwater Adhesive," *Advanced Materials*, vol. 31, p. 1808179, 2019.

[11] M. Dompé, F. J. Cedano-serrano, M. Vahdati, L. V. Westerveld, D. Hourdet, C. Creton, J. V. D. Gucht, T. Kodger, and M. Kamperman, "Underwater Adhesion of Multiresponsive Complex Coacervates," *Advanced Materials Interfaces*, vol. 7, p. 1901785, 2020.

[12] Q. Zhao, D. W. Lee, B. K. Ahn, S. Seo, Y. Kaufman, J. Israelachvili, and J. H. Waite, "Underwater contact adhesion and microarchitecture in polyelectrolyte complexes actuated by solvent exchange," *Nature Materials*, vol. 15, no. 4, pp. 407–412, 2016.

[13] L. Zhang, V. Lipik, and A. Miserez, "Complex coacervates of oppositely charged co-polypeptides inspired by the sandcastle worm glue," *J. Mater. Chem. B*, vol. 4, no. 8, pp. 1544–1556, 2016.

[14] S. Seo, S. Das, P. J. Zalicki, R. Mirshafian, C. D. Eisenbach, J. N. Israelachvili, J. H. Waite, and B. K. Ahn, "Microphase Behavior and Enhanced Wet-Cohesion of Synthetic Copolyampholytes Inspired by a Mussel Foot Protein," *Journal of the American Chemical Society*, vol. 137, no. 29, pp. 9214–9217, 2015.

[15] M. Dompe, M. Vahdati, F. V. Ligten, F. J. Cedano-serrano, D. Hourdet, C. Creton, M. Zanetti, P. Bracco, J. V. D. Gucht, T. Kodger, and M. Kamperman, "Enhancement of the Adhesive Properties by Optimizing the Water Content in PNIPAM-Functionalized Complex Coacervates," *ACS Applied Polymer Materials*, vol. 2, pp. 1722–1730, 2020.

[16] I. A. V. Hees, P. J. M. Swinkels, R. G. Fokkink, A. H. Velders, I. K. Voets, J. V. D. Gucht, and M. Kamperman, "Polymer Chemistry Self-assembly of oppositely charged polyelectrolyte block copolymers containing short thermoresponsive blocks," *Polymer Chemistry*, vol. 10, no. 23, pp. 3127–3134, 2019.

[17] S. C. Grindy, R. Learsch, D. Mozhdehi, J. Cheng, D. G. Barrett, Z. Guan, P. B. Messersmith, and N. Holten-Andersen, "Control of hierarchical polymer mechanics with bioinspired metal-coordination dynamics," *Nature Materials*, vol. 14, no. 12, pp. 1210–1216, 2015.

[18] J. Yang, M. A. Cohen Stuart, and M. Kamperman, "Jack of all trades: versatile catechol crosslinking mechanisms," *Chem. Soc. Rev.*, vol. 43, no. 24, pp. 8271–8298, 2014.

[19] R. H. Holyer, C. D. Hubbard, S. F. Kettle, and R. G. Wilkins, "The Kinetics of Replacement Reactions of Complexes of the Transition Metals with 2,2',2"-Terpyridine," *Inorganic Chemistry*, vol. 5, no. 4, pp. 622–625, 1966.

[20] K. A. Aamer and G. N. Tew, "Supramolecular Polymers Containing Terpyridine - Metal Complexes in the Side Chain," *Macromolecules*, vol. 40, pp. 2737–2744, 2007.

[21] E. Spruijt, A. H. Westphal, J. W. Borst, M. A. Cohen Stuart, and J. Van Der Gucht, "Binodal compositions of polyelectrolyte complexes," *Macromolecules*, vol. 43, no. 15, pp. 6476–6484, 2010.

[22] J. Brassinne, F. D. Jochum, C. A. Fustin, and J. F. Gohy, "Revealing the supramolecular nature of side-chain terpyridine-functionalized polymer networks," *International Journal of Molecular Sciences*, vol. 16, no. 1, pp. 990–1007, 2015.

[23] L. Li, S. Srivastava, M. Andreev, A. B. Marciel, J. J. De Pablo, and M. V. Tirrell, "Phase Behavior and Salt Partitioning in Polyelectrolyte Complex Coacervates," *Macromolecules*, vol. 51, no. 8, pp. 2988–2995, 2018.

[24] J. Fu and J. B. Schlenoff, "Driving Forces for Oppositely Charged Polyion Association in Aqueous Solutions: Enthalpic, Entropic, but Not Electrostatic," *Journal of the American Chemical Society*, vol. 138, no. 3, pp. 980–990, 2016.

[25] J. A. Jaber and J. B. Schlenoff, "Mechanical properties of reversibly cross-linked ultrathin polyelectrolyte complexes," *Journal of the American Chemical Society*, vol. 128, no. 9, pp. 2940–2947, 2006.

[26] F. G. Hamad, Q. Chen, and R. H. Colby, "Linear Viscoelasticity and Swelling of Polyelectrolyte Complex Coacervates," *Macromolecules*, vol. 51, no. 15, pp. 5547–5555, 2018.

[27] C. S. Y. Tan, G. Agmon, J. Liu, D. Hoogland, E. R. Janeček, E. A. Appel, and O. A. Scherman, "Distinguishing relaxation dynamics in transiently crosslinked polymeric networks," *Polymer Chemistry*, vol. 8, no. 35, pp. 5336–5343, 2017.

[28] M. Rubinstein and A. N. Semenov, "Thermoreversible Gelation in Solutions of Associating Polymers. 2. Linear Dynamics," *Macromolecules*, vol. 31, no. 4, pp. 1386–1397, 1998.

[29] A. Jaishankar and G. H. McKinley, "Power-law rheology in the bulk and at the interface: Quasi-properties and fractional constitutive equations," *Proceedings of the Royal Society A: Mathematical, Physical and Engineering Sciences*, vol. 469, p. 20120284, 2013.

[30] P. Patricio, "Power law rheology of generalised Maxwell and Kelvin-Voigt models," *arXiv:1506.01934 (physics.bio-ph)*, 2015.

[31] P. C. Suarez-Martinez, P. Batys, M. Sammalkorpi, and J. L. Lutkenhaus, "Time-Temperature and Time-Water Superposition Principles Applied to Poly(allylamine)/Poly(acrylic acid) Complexes," *Macromolecules*, vol. 52, no. 8, pp. 3066–3074, 2019.

[32] K. Sadman, Q. Wang, Y. Chen, B. Keshavarz, Z. Jiang, and K. R. Shull, "Influence of Hydrophobicity on Polyelectrolyte Complexation," *Macromolecules*, vol. 50, no. 23, pp. 9417–9426, 2017.

[33] M. Yang, J. Shi, and J. B. Schlenoff, "Control of Dynamics in Polyelectrolyte Complexes by Temperature and Salt," *Macromolecules*, vol. 52, no. 5, pp. 1930–1941, 2019.

[34] K. Sadman, Q. Wang, and K. R. Shull, "Guanidinium Can Break and Form Strongly Associating Ion Complexes," *ACS Macro Letters*, vol. 8, no. 2, pp. 117–122, 2019.

[35] P.-G. De Gennes, *Introduction to Polymer Dynamics*. Cambridge University Press, 1990.

[36] G. W. Blair, B. C. Veinoglou, and J. E. Caffyn, "Limitations of the Newtonian time scale in relation to non-equilibrium rheological states and a theory of quasi-properties.," *Proceedings of the Royal Society of London. Series A, Mathematical and physical sciences*, vol. 189, pp. 69–87, 1947.

[37] R. Garrappa, "The Mittag-Leffler function," 2020.

[38] K. Hinsen, "The Mittag-Leffler function in Python," 2020.

[39] Q. Wang and J. B. Schlenoff, "The polyelectrolyte complex/coacervate continuum," *Macromolecules*, vol. 47, no. 9, pp. 3108–3116, 2014.

[40] P. G. De Gennes, "Dynamics of Entangled Polymer Solutions. II. Inclusion of Hydrodynamic Interactions," *Macromolecules*, vol. 9, no. 4, pp. 594–598, 1976.

[41] R. L. Bagley and P. J. Torvik, "A Theoretical Basis for the Application of Fractional Calculus to Viscoelasticity," *Journal of Rheology*, vol. 27, no. 3, pp. 201–210, 1983.

[42] T. Rossow and S. Seiffert, "Supramolecular polymer gels with potential model-network structure," *Polymer Chemistry*, vol. 5, no. 8, pp. 3018–3029, 2014.

[43] R. Hogg and R. G. Wilkins, "Exchange Studies of Certain Chelate Compounds of the Transitional Metals. Parts VIII. 2,2',2"-Terpyridine Complexes.," *Journal of the Chemical Society (Resumed)*, pp. 341–350, 1962.

[44] P.-G. De Gennes, *Scaling concepts in polymer physics*. Cornell University Press (Ithaca and London), 1979.

[45] E. Spruijt, F. A. Leermakers, R. Fokkink, R. Schweins, A. A. Van Well, M. A. Cohen Stuart, and J. Van Der Gucht, "Structure and dynamics of polyelectrolyte complex coacervates studied by scattering of neutrons, X-rays, and light," *Macromolecules*, vol. 46, no. 11, pp. 4596–4605, 2013.

[46] P. J. Skrzeszewska, F. A. De Wolf, M. W. Werten, A. P. Moers, M. A. Cohen Stuart, and J. Van Der Gucht, "Physical gels of telechelic triblock copolymers with precisely defined junction multiplicity," *Soft Matter*, vol. 5, no. 10, pp. 2057–2062, 2009.

[47] D. Xu, J. L. Hawk, D. M. Loveless, S. L. Jeon, and S. L. Craig, "Mechanism of shear thickening in reversibly cross-linked supramolecular polymer networks," *Macromolecules*, vol. 43, no. 7, pp. 3556–3565, 2010.

[48] M. Zhong, R. Wang, K. Kawamoto, B. D. Olsen, and J. A. Johnson, "Quantifying the impact of molecular defects on polymer network elasticity," *Science*, vol. 353, no. 6305, pp. 1264–1268, 2016.

[49] J. Wang, R. H. De Kool, and A. H. Velders, "Lanthanide-Dipicolinic Acid Coordination Driven Micelles with Enhanced Stability and Tunable Function," *Langmuir*, vol. 31, no. 44, pp. 12251–12259, 2015.

[50] P. V. Gorelkin, D. S. Mukhin, A. G. Majouga, R. B. Romashkina, E. K. Beloglazkina, I. V. Yaminsky, and N. V. Zyk, "New self-assembled monolayer coated cantilever for histidine-tag protein immobilization," *Mendeleev Communications*, vol. 20, no. 6, pp. 329–331, 2010.

[51] A. Anastasaki, V. Nikolaou, Q. Zhang, J. Burns, S. R. Samanta, C. Waldron, A. J. Haddleton, R. McHale, D. Fox, V. Percec, P. Wilson, and D. M. Haddleton, "Copper(II)/tertiary amine synergy in photoinduced living radical polymerization: Accelerated synthesis of ω-functional and α,ω-heterofunctional poly(acrylates)," *Journal of the American Chemical Society*, vol. 136, no. 3, pp. 1141–1149, 2014.

[52] G. R. Jones, R. Whitfield, A. Anastasaki, N. Risangud, A. Simula, D. J. Keddie, and D. M. Haddleton, "Cu(0)-RDRP of methacrylates in DMSO: Importance of the initiator," *Polymer Chemistry*, vol. 9, no. 18, pp. 2382–2388, 2018.

[53] E. Spruijt, J. Sprakel, M. Lemmers, M. A. Stuart, and J. Van Der Gucht, "Relaxation dynamics at different time scales in electrostatic complexes: Time-salt superposition," *Physical Review Letters*, vol. 105, no. 20, 2010.

Chapter 3

Transient bonds toughen polyelectrolyte complexes in shear

Abstract

The engineering requirements of complex coacervates in bioadhesives require to take charge of not only the linear viscoelasticity, but also the behaviour at large strain. The latter encompasses phenomena close to, at, and beyond failure. We characterized the high-strain behaviour of complex coacervates, and find that they fail as a brittle fluid. Since there is no way to address the failure mode of coacervate complexes, we fill this gap by adding transient crosslinks to the complexes. We show that terpyridine-metal bonds widen the linear viscoelastic regime of complex coacervates at high salt concentrations, and decrease the extent of brittle fracture at all salt concentrations studied. Furthermore, we investigate the effects of the distribution of terpyridines over the two polyelectrolyte partners in the complex. The results open avenues to improving the failure resistance of complex coacervates.

3.1 Introduction

Complex coacervates, viscoelastic phases that form upon complexation of polyelectrolytes of opposing charge, offer a promising platform for the development of bioadhesives,[1, 2] implants,[3] nucleic acid encapsulation and other drug delivery platforms.[4] In light of these applications, two key characteristics distinguish coacervates from more traditional, hydrophobic, polymer materials: their hydrophilicity[5] and salt-dependent viscoelasticity (saloplasticity).[6] The linear viscoelasticity of complex coacervates is elucidated in a sizable bibliography, and several authors show that it is essentially Rouse-like,[5, 7–10] whereas others have refined this picture by noting the role of entanglements when high-molecular weight polyelectrolytes take part in the complex.[11] Furthermore, the viscoelasticity of coacervates has been tuned by introducing further crosslinking modalities, such as catechols,[12] terpyridines (Chapter 2), and other transient bonds,[13, 14] a solution to enhance solidification that is inspired by the oxidative curing of mussels and sandcastle worms.[1, 15]

Linear viscoelasticity can be conveniently studied in shear,[16] and has enabled understanding of the temporal structure of "native" (unmodified) and various classes of "hybrid" coacervates, those that have been further outfitted with crosslinks. However, given the high mechanical demands of the applications foreseen for complex coacervates (prosthetics, cartilage replacement, surgical glues),[4] we argue that the mode and extent of failure of the material is an equally crucial object of study. Complex coacervates fail in fracture at high-amplitude shear, with the shear amplitude or shear rate at failure weakly increasing with salt concentration.[8] Thus, while salt postpones failure to higher strain amplitudes, it also strongly softens the complexes,[10] and as such there is no way to achieve improved failure resistance at a given modulus level. While failure in unaxial extension has been somewhat documented,[17] there is no further data on the failure of complex coacervates in shear, which impedes progress in improving their failure resistance.

Failure is non-linear.[18] Thus, the mode of failure is notoriously disconnected from the linear viscoelasticity,[19] except under very narrow criteria.[20] Materials with a similar viscoelasticity can show drastic differences in their resistance to fracture, and show diverse behaviour on the threshold of non-linearity, such as going from strain softening to strain hardening.[21, 22] Thus, optimizing linear viscoelastic targets such as the shear modulus and the relaxation spectrum, while indispensable in finding correct moduli level and viscosities, is doomed to fail to select those materials that will prove to be failure-resistant and relevant for the world outside laboratories.

In this Chapter, we discuss the extent of the linear viscoelastic regime, and the viscoelastic properties for deformations sufficiently large for stress to be no longer linear in strain. We prepared complex coacervates with terpyridine-metal crosslinks, and studied in detail their viscoelasticity, as described before (Chapter 2). The relaxation spectra discussed so far are representative for linear viscoelastic regime. This Chapter is structured as follows: first, we discuss the response of complex coacervates with no further transient bonds and of transiently bonded polyelectrolytes when subjected to shear deformations of an increasing amplitude. Then, we look into systems in which the two components are combined. As such, we are able to outline the parameter space in which more failure-proof complex coacervates could be achieved in future investigations.

3.2 Materials and methods

Polymers and complexes were prepared using various chemistries, which are described in Chapter 2.

Methods

Rheological characterization was performed on an Anton Paar MCR-301 and MCR-501, both fitted with an evaporation-blocking hood and a thermostat bath at 20 °C. For samples that relax within a practical time frame (< 10 s), we used a cone-plate setup with a 10 mm cone, whereas for slower samples we employed a 10 mm plate. For coacervates, around 0.3 mL of the dense phase was loaded onto the centre of the plate, and dilute phase was pipetted over it. Then, the cone or plate was brought to trim gap, the sample trimmed, and then brought to gap. For non-coacervate polyelectrolyte gels, only the gel phase was used without a surrounding liquid.

Frequency sweeps were recorded up to 10^2 rad s^{-1} in the linear range of strain amplitudes. Amplitude sweeps were taken at frequencies ω_0 of 20 or 70 rad s^{-1}, with the amplitudes ramped up from a small value (down to 10^{-5}) up to 10. Flow curves were recorded for a small selection of samples by ramping of the shear rate from a small value up to 10^3 rad s^{-1}.

3.3 Results and discussion

We discuss the onset of non-linear behaviour in terms of "failure signatures" in amplitude sweeps, by which we mean the evolution of G' and G'' with strain rate. Such a signature is, for instance, a certain decrease in the moduli. The energy dissipation rate upon failure is the integral of these moduli over the strain rate at which the material starts failing: when the failure is postponed to higher strain rates, one must invest more energy to break the bonds that constitute the material. Thus, a material that shows failure at a later strain rate than another with the same linear $|G^*|$ is taken to be more failure-resistant. Similarly, a material in which the moduli decrease less drastically beyond the onset of failure is more failure-resistant.

Complex coacervates with no additional crosslinks fail in catastrophic fracture

We characterized the non-linear viscoelasticity of complexes of pA and pD by recording storage and loss moduli $G', G''(\omega)$ as a function of the amplitude of an oscillatory shear at constant frequency (amplitude sweeps). The complexes were made from the polyelectrolyte pairs pA^{234}/pD^{222}, pA^{250}/pD^{1023}, and $pAMPS^{800}/pD^{1023}$, where A stands for acrylic acid, D stands for *N,N*-dimethylaminoethyl methacrylate, and AMPS for 2-acrylamido-2-methyl propylsulfonate. For transient crosslinking of the polymers with metal ions M^{2+}, we modified pA and pD with 0%, 1%, or 10% of

terpyridines. The percentual terpyridine loading is given in the subscript of the monomer: pA_{10} represents poly(acrylic acid) with 10% of its carboxylates amide-bonded to a terpyridine moiety. The range of salt concentrations c_s was between 0.2 M and 1.3 M. We sampled strain amplitudes between 10^{-6} and 10. In order to compare data recorded at different frequencies and to illustrate the connection to frequency sweeps, the storage and loss moduli were plotted against the maximum strain rate in each measurement point, given by $\dot{\gamma}_{\max} = \omega\gamma_0$.

For soft materials, G', G'' are independent of the strain rate (or strain amplitude) at low strain rates. The range of strain amplitudes at which G', G'' show no change is the linear viscoelastic envelope (LVE). At such small strains, the bonds that bind the chains together carry stress, but the amount of bonds is unchanged as the strain is increased. At a certain strain amplitude, the deformations exceed this threshold. The network structure is altered from equilibrium, and complex coacervates show a marked decrease of loss and storage modulus. The complex modulus turns from storage-dominated ($G' > G''$) to dissipation-dominated ($G'' > G'$) upon this event.

In Figure 3.1, we show the amplitude sweeps for the native (not crosslinked) complexes, where we have normalized the moduli with the linear viscoelastic values to allow a comparison between complexes of strongly different linear viscoelasticity. For salt strengths that place the constant oscillation frequency ω_0 (between 20 and 70 rad s^{-1}) above the crossover frequency (two leftmost panels), there is a rather broad LVE, followed by a regime in which the moduli decrease dramatically. At high salt strength, the terminal relaxation time goes to a value much below 0.5 ms (see Chapter 2), and the crossover frequency is unattainable. As a consequence, the response to oscillatory shear is dominated by dissipation ($G'' > G'$): the complexes are essentially liquids of a quite low viscosity on the order of 0.1 Pa s. While oscillatory shear is not appropriate for liquids, we include representative data in the rightmost panel of Figure 3.1 for the sake of facilitating comparison to complex coacervates with additional transient crosslinks (*vide infra*).

As long as salt strengths are not close to critical, the failure signature of native complex coacervates resembles fracture rather than yield (ductile failure). The decrease in storage and loss moduli with strain rate is sudden, whereas in ductile failure one sees an extended range of softening before fracture.[23] Additionally, in ductile failure, the gradual softening coincides with a peak in the loss tangent ($\tan\delta = \frac{G''}{G'}$), which reflects that ductile materials flow above the strain (rate) of onset.

In the case of flow curves (steady shear), previous work in our group[9] shows that the strain rate of onset of shear thinning is entirely set by the terminal relaxation time τ_R of the complex. Flow curves fall onto a master curve when plotted against a strain rate that is normalized with τ_R.[9] Thus, linear and non-linear behaviour can

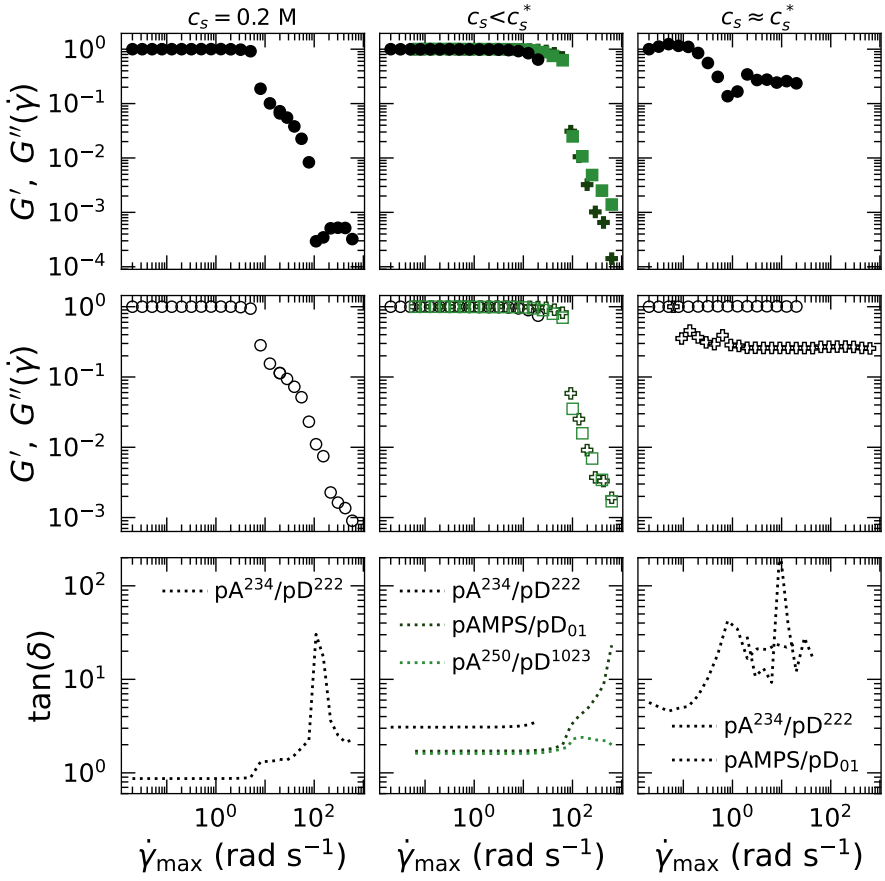

Figure 3.1: Storage and loss moduli G', G'' as a function of strain rate at the node of the shear cycle $\dot{\gamma}_{max}$ at (left) salt strength far below critical salt strength, (center) salt strength somewhat below critical and (right) salt strength closely approaching critical. The data were recorded at 20 or 63 rad s^{-1}.

be superimposed for the case of steady shear, which indicates that the flow curve is determinated by a single timescale at all accessible shear rates. For amplitude sweeps in oscillatory shear, we do not see such an opportunity in our and previous, unpublished results. The lack of a direct correspondence between the steady shear and oscillatory behaviour is unsurprising – in general, behaviour obtained from one flow profile can not be extrapolated to another once the flow is non-linear.[16]

For salt strengths at the critical level (0.9 M for the two pA/pD pairs and 1.3 M for the pAMPS/pD pair), we are not able to get reliable data from oscillatory shear, since the torque does not sufficiently exceed the threshold of the measurement system. Flow curves (see Appendix B) indicate that the flow is unstable at shear rates up to 10^0, above which it stabilizes at a rate-dependent viscosity of around 50 mPa s.

In oscillatory shear, the strain rate at which fracture sets in is only weakly dependent on the terminal relaxation time of the complex, as can be seen as the onset of fracture moving to the right upon an increase in salt concentration in Figure 3.1. Consequently, complex coacervates lack an intrinsic feature that allows for increased fracture resistance. In the following section, we motivate our choice for using metal-ligand complexes as an extrinsic feature for engineering fracture resistance into complex coacervates.

Failure signature of polyelectrolyte gels depends on choice of metal in the crosslink

We extended our analysis of amplitude sweeps in oscillatory shear to aqueous solutions of only the tertiary poly(amine) pD_{01}^{1023}. We quaternized 1% of the amines with a terpyridine-expressing alkyl bromide. Metal-ligand complexation between two terpyridines and one metal ion M^{2+} yields a transient bond of lifetime τ_X. We prepared complexes with the metals Mn^{2+}, Zn^{2+}, Co^{2+} and Ni^{2+}, which represent a wide window of bond lifetimes from below $1 \cdot 10^{-3}$ ms to beyond $20 \cdot 10^3$ s. The total polyelectrolyte content of $14\%^{w}/_{v}$ was chosen to match the polyelectrolyte concentration in complexes near c_s^*.

The pD_{01} complexes with Zn^{2+}, Co^{2+} and Ni^{2+} all gave rise to near-Maxwellian (Chapter 2) viscoelastic materials, with frequencies above 10 rad s^{-1} being storage-dominated. The polyelectrolyte gel crosslinked with Mn^{2+} was excluded from the amplitude sweep analysis, as all accessible frequencies gave rise to highly dissipative behaviour with low torque, and oscillatory shear did not provide reliable values for G' and G''. The absence of elasticity in both the Mn^{2+} polyelectrolyte gel and the native coacervate complex at c_s^* allows to infer that the rheology is dominated by metal-ligand bonding, and not by properties inherent to the polyelectrolyte itself. As

such, we can estimate the contribution of entanglements to be smaller than the effect of even Mn^{2+} – the metal that is fastest to dissociate and yields the weakest networks at all frequencies.

The non-coacervate nature of the polyelectrolyte gels $pD_{01}^{1023}-M^{2+}$ is reflected in a failure signature that is distinct from what we describe for the native coacervate. We recognize three features that distinguish the strain response of polyelectrolyte gels from that of native coacervates: a significant widening of the LVE from strain rates below 50 rad s^{-1} to above 100 rad s^{-1}, a peak in either or *both* of G' and G'', and, a lack of clear jumps in either G' or G'' with increasing strain rate. Figure 3.2 presents the amplitude sweeps for complexes with Zn^{2+}, Co^{2+} and Ni^{2+}.

If we define a strain rate of failure onset $\dot{\gamma}^*$, we can show that the polyelectrolyte gels outperform native coacervate complexes substantially. We approximate the onset individually for the storage ($\dot{\gamma}^*_{G'}$) and loss ($\dot{\gamma}^*_{G''}$) moduli by finding the strain rate at which either modulus loses 10% of its linear value (respectively G'_0 and G''_0). The distinction must not be overemphasized, since the losses in both quantities do not likely correspond to distinct mechanisms. However, the definitions prove useful when comparing complexes from different classes with distinct failure modes. Table 3.1 lists strain rates at failure threshold for native coacervates pA/pD and pAMPS/pD, polyelectrolyte gels $pD-M^{2+}$ and hybrid complexes (*vide infra*).

The polyelectrolyte gels crosslinked with Zn^{2+}, Co^{2+}, and Ni^{2+} are characterized by a broad LVE at a plateau (storage) modulus in the order of magnitude of 1 kPa. The choice of metal ion affects the distribution of the increase over G' and G''. For Ni^{2+} and Co^{2+}, there is thickening but no hardening, whereas for Zn^{2+} both contributions go through a peak. For Co^{2+}, we could not achieve failure of the complex within the range of strain amplitudes employed. Since the major distinction between the samples is the crossover frequency ω_c, we speculate that ω_c plays a role in determining whether the excess bonds formed in high shear lead to an increased elastic and/or viscous response.

For the Zn^{2+} polyelectrolyte gel, both G' and G'' go through a peak, which can be recognized as, respectively, strain hardening and thickening. We attribute the increase in the components of the complex modulus to either the effects of straining the chains into the part of the force-extension curve where finite extensibility is felt, or an interconversion from intra-chain crosslinks to inter-chain crosslinks.[24] In Chapter 2, we have estimated the fraction of intra-chain crosslinks at around 5%. Given the eight-fold increase in G'' for $pD_{01}^{1k}-Ni^{2+}$, the extent of intra-chain crosslinking must then have been severely underestimated.

Non-linear rheological signatures of the conversion of intra- to inter-chain crosslinks in transient networks have been reported in detail by the group of Craig.[22, 24, 25] Strain hardening due to an increase in the inter-chain crosslink fraction manifests in

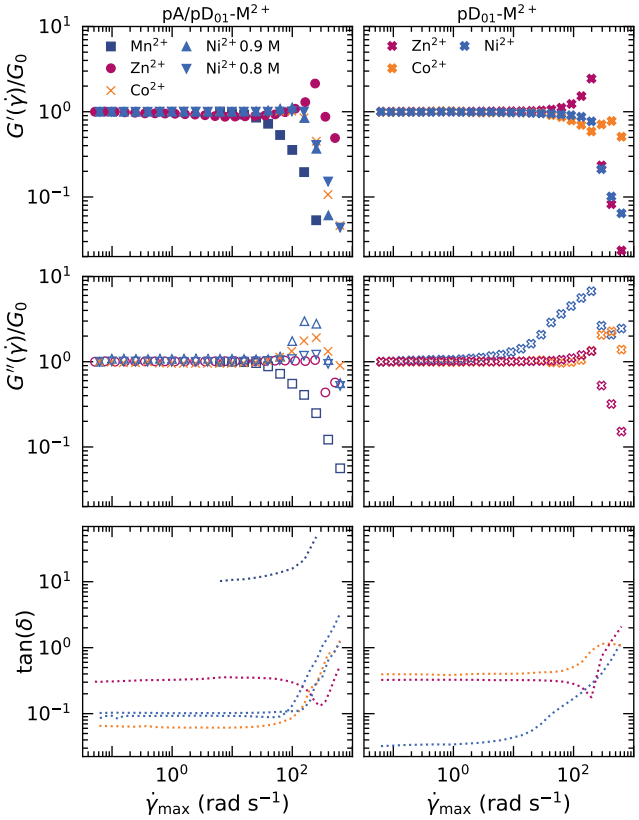

Figure 3.2: Storage and loss moduli G', G'' as function of strain rate, as recorded from an amplitude sweep with $\omega = 31.4$ rad s^{-1} on samples of the polyelectrolyte gel pD_{01}^{1023}-M^{2+} (left), and of the terpyridylated complex coacervate pA/pD_{01}^{1023}-M^{2+} (right).

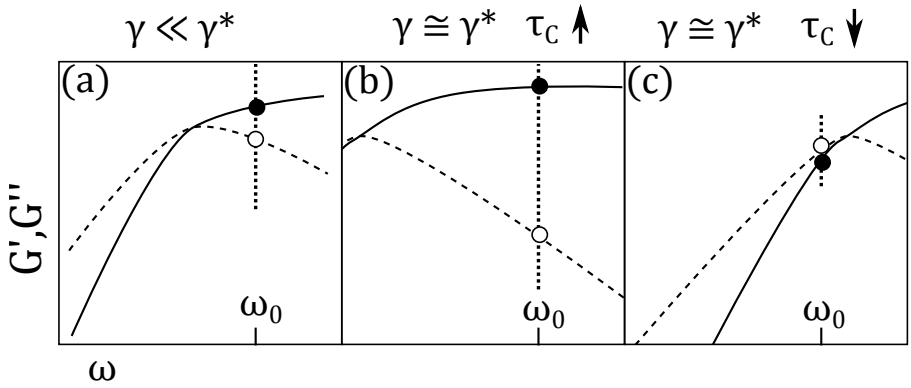

Figure 3.3: Storage (solid lines) and loss moduli (dashed lines) for a hypothetical Maxwell fluid: (a) linear viscoelastic spectrum, (b) high-strain frequency response with an increased relaxation time, and (c) high-strain frequency response with a decreased relaxation time. The loss tangent at a single frequency ω_0, at which, for instance, we are probing the amplitude response is given by $\tan\delta = \frac{\circ}{\bullet}$, and can provide the direction in which the relaxation time has changed: a decreased $\tan\delta$ reflects a lengthened τ_C (b), whereas an increased one a shortened τ_C (c).

strain thickening of G''.[22] In addition, the thickening coincides with an increase in the relaxation time τ_c, since the average cluster size held together by the transient crosslinks increases.[24]

Analysis of the evolution of the loss tangent gives an indirect measure of the change in the crossover time τ_c as the maximum strain (rate) is increased. Since $\tan\delta$ can be seen to increase as the strain amplitude exceeds the LVE, the loss modulus that would be measured at the corresponding frequency increases with respect to the storage modulus. If we assume that the crossover point is relatively nearby, and that the overall shape of the frequency sweep at that particular strain amplitude remains unchanged, then an increase in $\tan\delta$ should correlate with a shortening of τ_c. Figure 3.3 illustrates how the viscoelastic spectrum of a Maxwell fluid could change at high strain, and how respectively an increase (b) and a decrease (c) in τ_c is reflected in $\tan\delta$.

The decrease of τ_c with shear rate reflects the accelerating effect of external force on the dissociation kinetics of supramolecular bonds, also termed "slip bonding".[26] Slip bonding occurs in telechelic polymer networks and multiple other supermolecular constructs, and can be directly observed with parallel superposition rheology.[21]

In parallel superposition, one records frequency sweeps (to measure the crossover time) while subjecting the fluid to steady shear. The lack of an increase in τ_c in our data does not support intra- to inter-chain conversion of crosslinks as an explanation of the hardening in $|G^*|$. The exception is Zn^{2+}, which is also the only metal to satisfy the criterion of strain hardening in G'.

Furthermore, since the choice of metal is immaterial to the fraction of intra-chain crosslinks, the "conversion" hypothesis remains difficult to embrace. As explanations for strain hardening at high strain in transient networks, the importance of non-affine deformations due to the finite extensibility of real chains has been suggested.[25, 27] Since the scenario of finite extendibility aligns with a shortening of τ_c,[24] we identify the latter hypothesis as better supported by the data.

Metal-ligand complex coacervates are toughened at least up to the modulus given by the metal-ligand network

We will now see how the more "failure-proof" high-strain signatures of the polyelectrolyte gel motif $pD_{01}-M^{2+}$ impact the amplitude response in oscillation when it is brought into a hybrid coacervate complex. The coacervate samples at c_s^* were prepared with a concentration of active complexes ϕ_X of 2.5 mM, identical to ϕ_X in the polyelectrolyte gels, and had the same polyelectrolyte mass-over-volume fraction of 0.16.

Similarly to the polyelectrolyte gels, the strain response in oscillation shows an enhanced strain resistance. The amplitude sweeps for hybrid complexes $pA/pD_{01}-M^{2+}$ are plotted in the leftmost column of Figure 3.2, and again show a widening of the LVE, a peak in either or both components in G^*, and, a lack of obvious discontinuities in the moduli. The complex with Mn^{2+}, however, represents an exception, and has a rather low threshold strain rate (25-40 s^{-1}). In Chapter 2, we have shown that the Mn^{2+} is loss-dominated ($G'' > G'$) at all frequencies accessible by our rheometers. As a consequence, Mn^{2+} also forms the only complex in which the amplitude response was measured in the terminal regime, rather than in a plateau-like feature. It would be interesting to measure the amplitude sweep at different frequencies for a complex with a "crossover" metal: one in which both terminal and plateau behaviour are easily accessed. However, this is outside the scope of this Chapter, where we focus on the amplitude response of complexes close to and above crossover. Thus, at this stage we could attribute the low fracture threshold of Mn^{2+} to the (supposed) predominance of yield in the terminal regime, or simply to the fact that crosslinks of a lower equilibrium constant[28] are easier to break.

For the slower metals Zn^{2+}, Co^{2+} and Ni^{2+}, the amplitude sweeps sample the

strain response in a plateau-like regime ($G', G'' \propto \omega^{\beta}$ with $\beta < 0.1$ in the frequency sweeps). The features of the corresponding polyelectrolyte samples are retained qualitatively in all cases, including the strain hardening in G' for Zn^{2+}. In addition, softening in G' sets in 20−100 rad s^{-1} later for the hybrid complexes. Critical strain rates and linear moduli are printed in Table 3.1.

At c_s^*, the contribution of the coacervate to the *linear* shear moduli is shifted to frequencies $\omega > 10^3$ rad s^{-1}: the complexes are dominated by the metal-ligand crosslink time τ_X. With a comparison of the left and right panels of Figure 3.2, we have shown that the strain response in oscillation for τ_X-dominated hybrid complexes is similarly determined by the metal-ligand crosslinks. The effects of the presence of the near-critical coacervate are subtle: we note a further slight broadening of the LVE, and a simultaneous lowering of any peaks in G' and G''. At this stage, a simple hypothesis on the effect of metal-ligand bonds on the oscillatory strain response of a complex coacervate is the following: the metal-ligand bonding network provides a modulus level G_X at which the overall complex is toughened beyond the $\dot{\gamma}^*$ provided by the complex coacervate. If the zero-amplitude modulus of the coacervate G_N were to exceed G_T, then the material would fail at $\dot{\gamma}^*$, but only down to the plateau modulus of the metal-ligand network, G_X. Thus, the metal-ligand network then acts as a safety net at a lower modulus level.

For the $pA/pD_{01}-M^{2+}$ hybrid complexes at c_s^*, G_X is on the order of 1 kPa (Table 3.1), whereas that of the coacervate is essentially zero. As is in line with the "independent networks" hypothesis, only the failure signature of the metal-ligand network is evident for the hybrid complexes at critical salt strengths. In the following sections, we will explore the failure behaviour for hybrids at non-critical salt strengths, at which G_X is typically close to or even overwhelmed by G_N, and test the independent network hypothesis.

The presence of metal-ligand crosslinks enhances fracture resistance in medium and low-salt complexes

On failure, amplitude sweeps of native coacervates at lower c_s (Figure 3.1) present catastrophic drops for both components of G^* that follow a relatively narrow LVE of a weakly salt-dependent width. In contrast, polyelectrolyte gels and hybrid coacervates at c_s^* present a broader LVE, the width of which is not clearly correlated to τ_X above 1 s. In addition, the behaviour beyond the linear threshold is markedly different: the fracture-like drops are absent, whereas the decrease of the moduli is preceded by strain hardening in either or both of G' and G''. What happens if we introduce metal-ligand crosslinks into the fracture-prone low-c_s complexes?

Table 3.1: Linear and non-linear rheology of complexes pA/pD and pAMPS/pD: linear moduli for normalization in Figures 3.1–3.4 G_0', G_0'', relaxation times τ_c, and strain rate at failure threshold as extracted from storage ($\dot{\gamma}^*_{G'}$) and loss ($\dot{\gamma}^*_{G''}$) modulus.

Complex	M^{2+}	c_s (M)	G_0' (Pa)	G_0'' (Pa)	τ_c (s)	$\dot{\gamma}^*_{G'}$ (s^{-1})	$\dot{\gamma}^*_{G''}$ (s^{-1})
pA/pD^{222}	○	0.2	$3.4\cdot10^4$	$2.9\cdot10^4$	0.59	8.1	8.1
pA/pD^{222}	○	0.6	$2.0\cdot10^3$	$6.3\cdot10^3$	$5.2\cdot10^{-3}$	13	13
pA/pD^{222}	○	0.9	2.35	13.3	$3.8\cdot10^{-4}$	$\gg10^3$	$\gg10^3$
pA/pD	○	0.6	$4.9\cdot10^3$	$8.0\cdot10^3$	$7.4\cdot10^{-3}$	8	8
pAMPS/pD	○	0.6	$3.0\cdot10^3$	$5.1\cdot10^3$	0.015	43	63
pAMPS/pD	○	1.3	< 1	22.5	$\ll10^{-3}$	$\gg10^3$	$\gg10^3$
pD_{01}	Zn^{2+}	—	662	215	0.47	292	292
pD_{01}	Co^{2+}	—	882	348	$9.6\cdot10^4$	63	670
pD_{01}	Ni^{2+}	—	$1.6\cdot10^3$	50.6	$1.4\cdot10^5$	134	292
pA/pD_{01}	Mn^{2+}	0.9	3	30.6	$9.1\cdot10^{-3}$	25	40
pA/pD_{01}	Zn^{2+}		189	57.8	1.50	355	294
pA/pD_{01}	Co^{2+}		$2.4\cdot10^3$	158	$1.4\cdot10^5$	156	623
pA/pD_{01}	Ni^{2+}		$2.6\cdot10^3$	225	$1.0\cdot10^6$	160	499
pA/pD_{01}	Ni^{2+}	0.8	$3.4\cdot10^3$	346	$1.0\cdot10^6$	200	495
pA_{01}/pD^{222}	Mn^{2+}	0.2	$2.7\cdot10^4$	$2.2\cdot10^4$	0.757	5	5
pA_{01}/pD^{222}_{01}	Zn^{2+}	0.2	$6.6\cdot10^4$	$3.1\cdot10^4$	6.4	13	19
pA/pD^{222}_{01}	Zn^{2+}	0.6	$6.2\cdot10^3$	$5.2\cdot10^3$	2.1	13	13
$pAMPS/pD_{01}$	Zn^{2+}	0.6	$1.8\cdot10^4$	$8.1\cdot10^3$	53.34	18	41
$pAMPS/pD_{01}$	Zn^{2+}	1.3	760	106	3.04	135	291

At a c_s of 0.6 M, crosslinking of complexes of pA or pAMPS with pD_{01} and Zn^{2+} results in failure that resembles yield as a plasticity-dominated failure mode rather than fracture: there are no longer any discontinuous drops in the amplitude sweeps, as can be seen in the central column of Figure 3.4. In addition, the LVE is always broadened with respect to the corresponding native complex coacervate (compare lines and markers in Figure 3.4). Unlike the clear peaks in G' and G'' that we saw for τ_X-dominated complexes, we see no pronounced strain hardening. A close inspection of $G''(\dot{\gamma})$ for pAMPS/pD_{01}–Zn^{2+} suggests a marginal degree of strain hardening in G'', but the increase is preceded by an equal extent of softening earlier on.

At a c_s of 0.2 M, the complexes pA_{01}/pD_{01}–Zn^{2+} and pA_{01}/pD–Mn^{2+} were prepared. Surprisingly, even the low-salt (0.2 M) complex with 2.5 mM of Mn^{2+} crosslinks has a broadened LVE. However, fracture-like failure of the coacervate is not entirely avoided. Addition of ligands onto pA, increasing the concentration of complexes to 5.0 mM and lengthening the lifetime of the metal-ligand complex has a small, positive effect on the failure resistance: pA_{01}/pD_{01}–Zn^{2+} shows a failure signature closer to yield, and the LVE is broadened by another small margin with respect to the Mn^{2+} complex. Because the experiment did not specifically control for any of these features, we cannot definitively attribute the increase in failure resistance to any of the aforementioned parameters. However, we suggest that the choice for Zn^{2+} as a failure-avoidance agent is natural versus Mn^{2+}, given the strongly improved amplitude sweeps of polyelectrolyte gels and hybrid complexes at c_s^* for Zn^{2+} over Mn^{2+} (Figure 3.2).

Given the 10-fold difference in linear shear modulus between the metal-ligand and polyelectrolyte network, the enhancement of fracture resistance for the lowest c_s is a phenomenon that cannot be reconciled with the independent network hypothesis, which suggests that the material would only be tough at the modulus contributed by the metal-ligand network (see discussion accompanying Figure 3.2). Likewise, when c_s is 0.6 M, the linear modulus of the coacervate is at least two-fold higher than that of the hybrid complex (Table 3.1), and we expect the failure signature of the native coacervate to dominate.

In the last sections of this Chapter, we will suggest alternatives to the idea of independent networks by looking at the effect of architecture, and discussing the structure of the crosslinks. First, however, we will further study the scope of the observed increase in failure resistance that metal-ligand complexes impart on complex coacervates.

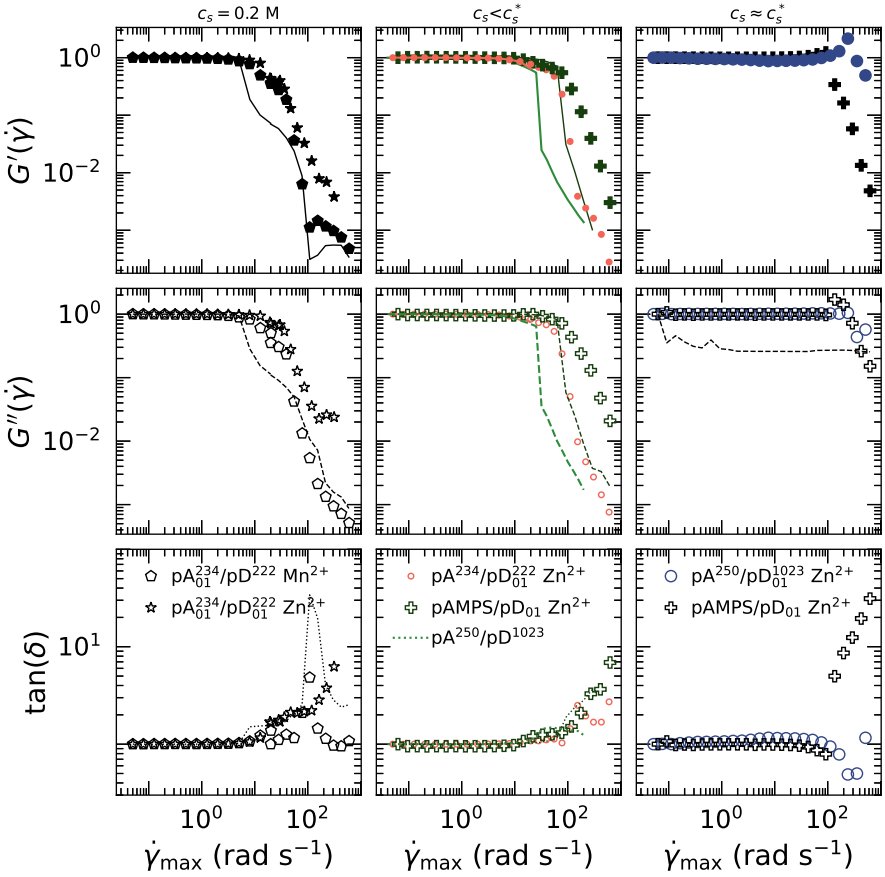

Figure 3.4: Storage and loss moduli G', G'' as function of strain rate, as recorded during an amplitude sweep at $\omega = 31.4$ rad s^{-1} (pA/pD) and $\omega = 60$ rad s^{-1} (pAMPS/pD). Samples at low salt (0.1 M) are in the leftmost column, at medium salt (0.5–0.6 M) in the central, and at critical salt in the rightmost. Data of complexes that contain M^{2+} species are represented by markers, "background" measurements on non-metalated complexes are drawn with lines.

Failure signatures depend on hybrid complex architecture

In the above, we made comparisons that included metalated complexes of terpyridylation architecture pA_{01}/pD, pA/pD_{01}, and pA_{01}/pD_{01}. The failure signature and critical strain rates were compared on the basis of the (terminal) relaxation times of the complexes, but no explicit discussion of the effect of architecture has so far been offered. In this section, we will provide a preliminary study of the effect of architecture. We will also consider preliminary data on "overmetalated" complexes, those with a larger-than-stoichiometric concentration of metal ions with respect to what would be required for a two-to-one complex with terpyridines, which allows to reject some ideas about the structure in the crosslinks.

Both viscoelasticity and high-strain failure in oscillatory shear are asymmetric in the terpyridylation architecture, as can be seen by the different behaviour in the frequency sweeps (left-hand panel) and the amplitude sweeps (right-hand panel) of Figure 3.5. pA_{01}/pD has a a τ_c of 0.2 ms, whereas pA/pD_{01} retains elasticity up to a time on the second scale. When the terpyridines are spread over the two polyelectrolyte partners (pA_{01}/pD_{01}), but the metal concentration is kept identical to the value of the former complexes (ϕ_X is unchanged), G at crossover is similar to the value for pA/pD_{01}, but the crossover is a full order of magnitude faster than for $pA/pD_{01}-Zn^{2+}$. Only when ϕ_X is doubled by supplying enough metal ions to form the maximum amount of active complexes do we see the expected effect of having more terpyridines in the complex: pA_{01}/pD_{01}-$Zn^{2+}_{0.5}$, where the subscript refers to the ratio of metal ions to terpyridines, shows an increased τ_C and G_C of 3 s and 2.1 kPa.

The ten-fold increase of G_C with a two-fold increase in ϕ_X, a change that encompasses both the inclusion of terpyridylated pA and a two-fold increase in availability of Zn^{2+}, needs two notes. First, the networks with 2.5 mM of active complex are perhaps slightly beneath the percolation point. Doubling ϕ_X then crosses the point, which then allows G_C to increase much more than as $G_C \propto \phi_X$. Furthermore, we argue that the presence of pA decreases the (arguably small) extent of intra-chain crosslinking, since two adjacent monomers that are not directly bonded have a high chance to be a pA/pD pair. The latter point should then be also visible in the amplitude sweep, since intra-chain crosslinks are known to facilitate strain hardening in oscillatory shear.[22] Indeed, the right-hand panel of Figure 3.5 shows only strain softening for pA_{01}/pD_{01}-$Zn^{2+}_{0.5}$, whereas some strain hardening is evident for pA/pD_{01}-$Zn^{2+}_{0.5}$.

Figure 3.5 reveals a further effect of an increase in ϕ_X for the pA_{01}/pD_{01} architecture – at the higher concentration of active complex, the failure shows an unsteady, abrupt failure with a sharp increase in the loss tangent. The complex with a lower ϕ_X fails gradually with an unchanged loss tangent. It is currently unclear why the increased ϕ_X gives rise to a brittler failure: while the scenario of a significant popu-

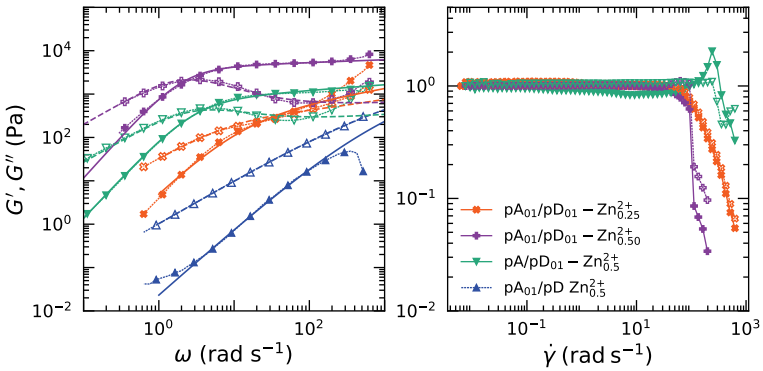

Figure 3.5: Frequency sweeps (left) and amplitude sweeps (right) plotted as G', G'' as function of strain rate $\dot{\gamma}$. Marked symbols are measured data, colored lines (left-hand panel) are fits to the fractional Maxwell model. The subscripted value x in Zn^{2+}_x refers to the ratio of metal ions to terpyridines.

lation of intra-terpyridine bonds is attractive, it is not supported by the arguments presented in Chapter 2. Since we limited our analysis to the aforementioned concentration, future work should elucidate the dependence of failure behaviour and linear viscoelasticity on ϕ_X and the network architecture.

Interestingly, the brittle fracture of the pA_{01}/pD_{01} architecture can be reversed by the addition of an excess of Zn^{2+}. We will, first, briefly discuss the linear viscoelasticity in this paragraph. The addition of a five-fold excess of Zn^{2+} to the complex pA_{01}/pD_{01} shifts the linear viscoelasticity to higher ω, as shown in Figure 3.6. We make the, admittedly anecdotal, observation that the modulus level at crossover *increases* by 70% (from 2.1 to 3.5 kPa). The increase of G_c clearly does not support the notion that the two-to-one complex crosslinks dissociate upon their conversion to one-to-one complexes. Thus, either the conversion to one-to-one complexes does not happen in our networks, the one-to-one Zn^{2+}-terpyridine moieties stack hydrophobically into a more transient bond, or Zn^{2+} interacts with the carboxylates of pA. The latter hypothesis is easily rejected: addition of an equal concentration of Zn^{2+} to a complex coacervate undecorated with complexes yields a poor viscoelasticity (Figure 3.6, black dots). Hydrophobic stacking into a network with a higher modulus also seems an unlikely explanation: one would not expect an increase in the modulus at crossover when two-to-one complexes convert into other two-to-one complexes. Additionally, hydrophobicity should allow several moieties to stack,

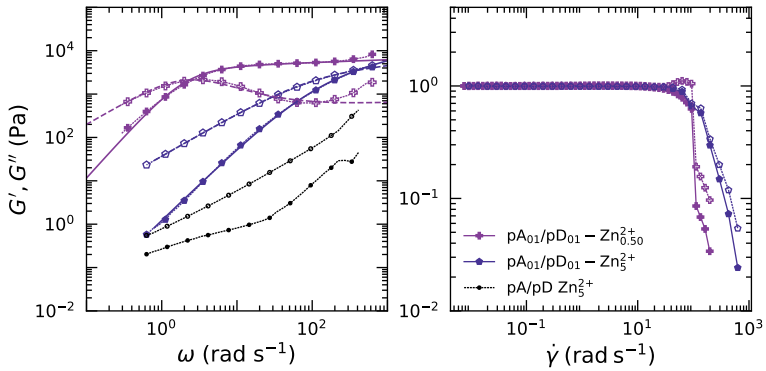

Figure 3.6: Frequency sweeps (left) and amplitude sweeps (right) plotted as G', G'' as function of strain rate $\dot{\gamma}$. Marked symbols are measured data, colored lines (left-hand panel) are fits to the fractional Maxwell model. The subscripted value x in Zn_x^{2+} refers to the ratio of metal ions to terpyridines.

further decreasing the prospective modulus. However, the first hypothesis violates thermodynamics, and is even more unlikely. The fact that complexes do not simply dissociate into a non-bonding state at metal superstoichiometry remains a puzzling observation.

Remarkably, the amplitude sweep in the right-hand panel of Figure 3.6 indicates that a five-fold excess of metal allows the complex to regain the failure resistance that was lost upon allowing pA to participate in the transient network. We note a remarkable consequence to this observation: an increase in G_c does not necessarily cause networks to fail earlier, such as was earlier seen in native complex coacervates (Table 3.1). Earlier, we saw that the strain (rate) at which a hybrid complex fails correlates weakly, if at all, with the terminal relaxation time τ. Thus, the increase in $\dot{\gamma}^*$ must be connected to a change in structure in the complex. The metal-to-ligand ratio is another parameter that determines the failure destiny of complex coacervates with additional metal-ligand complexes.

In the last part of the Chapter, we will further discuss the remarkable differences in the sensitivity of failure thresholds and the behaviour of G', G'' thereupon to linear viscoelastic parameters and choice of network (complex coacervate, metal-ligand, hybrid). For this purpose, we will first discuss a further class of hybrid complexes: those with a trace amount of Cu^{2+}, and with an additional metal.

Mixed-metal complexes with Cu^{2+}

Hybrid complexes of complex coacervates in which metal-ligand bonds are responsible for crosslinking can be conceptualized as dual networks. When the metal-ligand dissociation time τ_X is somewhat longer than the sticky Rouse time of the coacervate τ_R, we can envision the cationonomer-anionomer bond population to provide dissipation, and the metal-ligand bond population elasticity. The picture is then analogous to the dual networks discussed in a recent paper by Seiffert et al.,[28] with the reservation that the authors employ covalent crosslinks. The relaxation spectrum of the "dissipative" population is further tuned by incorporation of *two* populations of dissociation rates, as is achieved by providing two metal ions.[29] In this section, we present our preliminary data on the effect of a "triple"-τ relaxation spectrum on the failure signature.

We prepared a series of complexes pA_x/pD_y-Cu^{2+} in which a trace amount of Cu^{2+} was still present from the synthesis of pA or pA_{01} with ATRP (see Chapter 2). To a further family of complexes, half an equivalent to terpyridine of Mn^{2+}, Zn^{2+}, or Ni^{2+} was added, which accelerated the dynamics in all cases. As before, we analyze the linear viscoelasticity in terms of fractional Maxwell models. The full analysis of relaxation moduli $G(t)$ and $G(\omega)$ is given in Appendix A. The concentration of copper ions was not explicitly controlled for, but the linear moduli of a plateau-like feature allow for an estimate of the density of active crosslinks. We estimate that the concentration is of Cu^{2+} is much lower than the stoichiometric concentration of $\frac{1}{2}\phi_{tP}$, and interpret the relaxations measured in the linear viscoelastic spectra as disentanglement of non-percolating structures rather than as metal-ligand dissociation (Appendix A).

Figure 3.7 presents the amplitude sweeps for the Cu^{2+} and two-metal complexes with c_s at 0.5 M, 0.8 M or 0.9 M. As we have already shown with complexes with Zn^{2+} (Figure 3.5), and as is also discussed for the linear viscoelasticity (Appendix A), there is a strong effect on the rheology of the choice of which of the polyelectrolytes is terpyridylated. $pA_{01}/pD-Cu^{2+}$ fails at remarkably early strain rates, whereas failure is somewhat postponed in $pA/pD_{01}-Cu^{2+}$. In all cases, addition of half of an equivalent of Zn^{2+} moves the failure to higher strain rates, similar to what was seen for the other metal-ligand complex coacervate complexes (Figure 3.4). Similarly, the complexes show a failure signature that is closer to yield than to fracture.

At higher salt concentration failure is even more gradual, and loss tangents are essentially constant, disregarding the fluctuations in the right column of Figure 3.7 that we attribute to poor data quality at the low complex moduli that pA_{01}/pD complexes present near the critical salt concentration.

All complexes at $c_s = 0.5$ with Cu^{2+} underperform when compared to the unmetalated parent complex pA^{250}/pD^{1k} – the complexes with Cu^{2+} are unique in their early

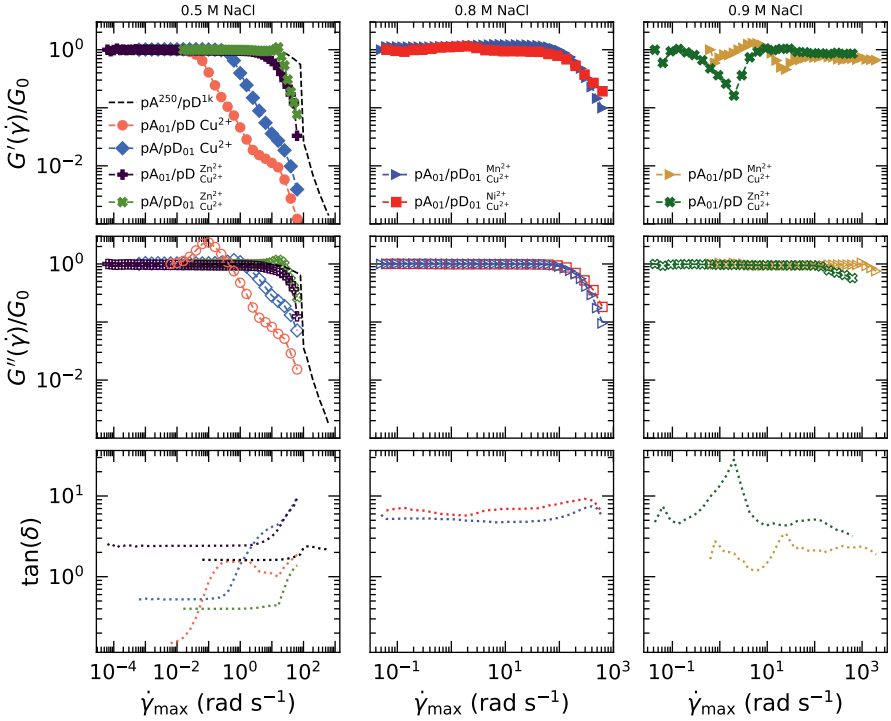

Figure 3.7: Amplitude sweeps for complex coacervates with additional terpyridine-metal crosslinks, with either one species of metal ion (Cu^{2+}), or two species ($^{Mn^{2+}}_{Cu^{2+}}$, $^{Zn^{2+}}_{Cu^{2+}}$ and $^{Ni^{2+}}_{Cu^{2+}}$). The concentration of the additional ion is always half that of the concentration of terpyridine, while the concentration of Cu^{2+} is not controlled (see Appendix A for details). Marked points are data points, unmarked lines for G' and G'' are data for an unmetalated complex given for comparison.

failure as compared to a native coacervate. We consider several explanations for the easy failure of the complexes with Cu^{2+}. In Appendix A, we have argued that the complexes with Cu^{2+} are strongly sub-stoichiometric, and the frozen dynamics are a consequence of entanglements of non-percolating structures. Craig and Xu report failure at lower strain amplitudes upon increasing the concentration of a transient network-forming polymer beyond the entanglement point, and rationalize the lack of strain hardening in the entangled networks by noting the crosslinks, once broken, are not open long enough for the entanglements to relax.[22]

Addition of Zn^{2+} at a higher concentration outcompetes the trace of Cu^{2+}, and results in an unfreezing of the dynamics. The amplitude response is close to that of the native coacervate, indicating that entanglements no longer dominate the strain response.

Near critical salt concentrations (0.8…0.9 M), complexes of pA_{01}/pD_{01} and pA_{01}/pD with Cu^{2+} and $\frac{M^{2+}}{Cu^{2+}}$ do not present frozen dynamics, and show a gradual failure at high strain rates. Due to the low degree of polymerization of pA, the dynamics are not controlled by the metal-ligand crosslinks, and there is no pronounced influence of metal choice on the failure signature. The asymmetry of linear and non-linear viscoelasticity to terpyridylation architecture is discussed in more detail in Appendix A.

Further discussion in terms of non-dimensional numbers and outlook

So far, we have studied the onset of non-linearities in oscillatory shear flow of viscoelastic materials with a broad (9 orders of magnitude) range of relaxation times, subjected to a shear rates up to 10^3 rad s^{-1}. The materials were sampled from three families: native complex coacervates (ie, with only those transient bonds that are provided by charge correlations[30]), metal-ligand polyelectrolyte gels and transiently crosslinked complex coacervates.

Oscillatory shear of a generic viscoelastic fluid can be described by two dimensionless numbers – the Deborah number, $De = \omega\tau$, which characterizes whether the frequency ω probes liquid-like ($De \ll 1$), viscoelastic ($De \approx 1$) or elastic ($De \gg 1$) response, and the Weissenberg number, $Wi = \dot{\gamma}\tau$, which captures the amplitude of the strain cycle.[31,32] By changing the coordinate (De, Wi), one explores the different signatures of the material at hand: let De decrease while keeping Wi constant, and one moves into non-linear viscoelasticity (on account of the strain amplitude γ_0 increasing past γ^*), let Wi increase while keeping De constant, and again one will find deviations from linearity (also on account of the strain amplitude increasing).

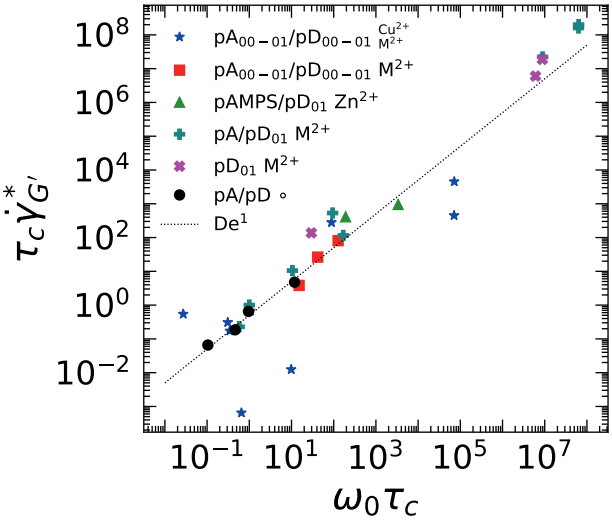

Figure 3.8: Weissenberg number at failure onset plotted versus Deborah number at crossover for all complexes in this Chapter. The line corresponds to the Wi = De.

For our set of data, we take the longest relaxation time τ as dominating the linear and non-linear viscoelasticity, and the critical strain rate $\dot{\gamma}^*$ where softening in G' is at least 10% as a representative onset of non-linearity. This allows to arrange all complexes into a (De,Wi)-frame, a Pipkin plot.[16] The x-axis can be seen as representative of the linear viscoelasticity, whereas the y-axis informs about the onset of non-linearity. Figure 3.8 shows that most families of complexes cluster around the line De = Wi, which is hardly surprising, since the same relaxation time is plotted on both axes. In a Pipkin plot, the region where rheology is described by linear viscoelasticity is bounded by a line with De $\propto$ Wi, which corresponds to our choice for $\dot{\gamma}$ of a "boundary" strain rate that is just beyond linearity.

Additionally, the Pipkin plot shows that the complexes with trace Cu^{2+} circumscribe a much smaller region in (De,Wi)-space, which relates to the tendency of this class of materials to fail at low strain rates. We have argued in the discussion of Figure 3.7 and in Appendix A that long-τ, low-ϕ metals cause entanglements, which predispose transient networks to early failure and strain softening.[22]

Other classes of complexes are larger in (De,Wi)-space, in particular those that contain complexes with pD^{1k} and are dominated by metal-ligand dynamics. These

are indeed the complexes that have a wider LVE, and are thus more "failure-proof". We note that even for very high relaxation times, complexes of the pA/pD^{01}-M^{2+} fail at strain rates that are inaccessible to the linear viscoelasticity of native coacervates. The observation that all complexes lead to points on line in (De, Wi) implies that there is not too much systematic variation in $\dot{\gamma}^*$ with τ, and that larger moduli or relaxation times do not necessarily lead to a decrease of strain tolerance.

The strain response of the complexes in this Chapter have been analyzed at one frequency, with only the first harmonic taken into account. A more complete analysis of the non-linear flow would study the frequency dependence of large-strain behaviour, and would yield, in principle, an infinite series of odd stress harmonics (or Chebyshev coefficients) that together quantify the non-linear response.[33] The points in the Pipkin plot of Figure 3.8 could then reflect a measure of the degree of strain hardening of thickening above the onset of non-linearity. Such an analysis would, beyond doubt, provide a wealth of insight about the *rheology* of complex coacervates and polyelectrolyte gels.

However, given the initial context in which this Thesis is written, we would suggest to aim future studies at the *structure* of the coacervate complexes, and how it is impacted by further transient bonds. In the General Discussion, we will summarize what is already known, and how rheology and scattering would shed light on the remaining questions. Furthermore, it is recommendable to aim rheological studies at non-linear observables that are relevant to future applications of complex coacervates, such as in probe-tack tests or in extension. While there is no correspondence between the fracture signature in shear and in probe-tack, shear remains a highly accessible paradigm that is invaluable to study structural questions in polymer materials.

3.4 Conclusion

In short, we have characterized the effect of the incorporation of transient terpyridyl-metal crosslinks on the threshold of non-linearities in oscillatory shear, and the mode of failure. The effect of the transient crosslinks on amplitude sweeps at non-linear strain amplitudes is subtle, yet clear: in cases where the linear viscoelastic mode is exposed at the frequency at which the amplitude sweep is performed, the amplitude (and, thus, strain rate) at which the response becomes non-linear is increased. Additionally, the behaviour at the failure threshold is often changed from a fracture-like signature to a smoother decrease of the storage and loss modulus, with in some cases even a prominent strain hardening in either or both components. We account for the changes by noting the different structure of the metal-ligand network to the coacervate, and suggest two possible explanations – the increase of the propor-

tion of inter-chain to intra-chain crosslinks, and increased collision rates between metal and ligand. These "toughening" mechanisms are unavailable to coacervate complexes, and thus are especially noticeable when the coacervate contribution to the viscoelasticity is weakened by salt. However, we note that the move away from fracture-like failure, but not strain hardening, is evidenced in essentially all our complex coacervates in which further transient bonds were available.

The increase of the threshold strain amplitude or strain rate and the strain hardening is currently difficult to translate to real-world behaviour (such as in lap shear or adhesion) or to concrete design practices, which stems from the lack of fundamental understanding of the non-linear rheology of coacervates. Because salt-time superposition breaks down at high strains in oscillation, our analysis in terms of non-dimensional numbers is only partially useful to translate the findings to other strain rates (or frequencies). We suggest that a full characterization of the frequency dependence of the response to large-amplitude oscillations is in order. Knowledge of the frequency-dependence of the threshold strain (rate) will complement the findings in this Chapter to further illuminate how the presence of transient bonds enhances the linear and non-linear viscoelasticity of complex coacervates.

Appendix

3.A Linear viscoelasticity of mixed-metal complexes with Cu^{2+}

We follow the methodology outlined in Chapter 2 to establish the linear viscoelasticity of the mixed-metal complexes with Cu^{2+} and a further metal, $pA_x^{250}/pD_y^{1k}-{}^{M^{2+}}_{Cu^{2+}}$, with x and y 0 or 1, and the ion Mn^{2+}, Zn^{2+} or Ni^{2+}. Authors that study the dissociation rate of *mono*-terpyridyl complexes with metal dications disagree remarkably on the dissociation rate for the complex with Cu^{2+}: the complex is either indefinitely stable,[34] or it dissociates faster than Zn^{2+}.[35] Given the difficulty we had to separate the residual ions from our samples of pA_{01}, and the content of the following discussion, we maintain that the complex is highly stable.

Mixed-metal dynamics at moderate salt concentration

We recorded frequency-dependent moduli $G', G''(\omega)$ for mixed-metal complexes at salt concentrations 0.5, 0.8 and 0.9 M. The frequency sweeps at 0.5 M (Figure 3.A.1) show Maxwell-type behaviour for complexes ${}^{Zn^{2+}}_{Cu^{2+}}$, and can be captured in a single fit to the fractional Maxwell model (FMM, Equation 3, Chapter 2). For complexes with only Cu^{2+}, "frozen" dynamics are obtained, and a relaxation time can not be obtained from the frequency sweeps. $G(t)$ was recorded for the frozen complexes, and shows partial relaxation at the 10^3 s timescale. Again, we performed fits to the FMM equation for $G(t)$ (Equation 5, Chapter 2), and the parameters were re-inserted in the equation for $G(\omega)$, and plotted in Figure 3.A.1 as a frequency sweep.

We reconstructed frequency sweeps over a wide frequency range by combination of either the known response of pA/pD ∘ or a fit to the high-frequency component in $G(\omega)$ with the low-ω behaviour from the fits to Figure 3.A.2. We strived to use the least fitting to achieve reasonable agreement, and the protocols for reconstruction are indicated in the legend of Figure 3.A.1. Disregarding the mid-frequency regime at ($10^{-2}\ldots10^{-1}$ rad s^{-1}) for which there is no data, the reconstructed frequency sweeps for the frozen complexes show similar features: a crossover between $\omega \approx 10^{-4}\ldots10^{-3}$ rad s^{-1} and a high-ω feature where the moduli increase as a power law.

The modulus level at crossover G_c of the pA/pD_{01} complexes can be compared with G_c for a complex with a controlled concentration of M^{2+} to estimate the density

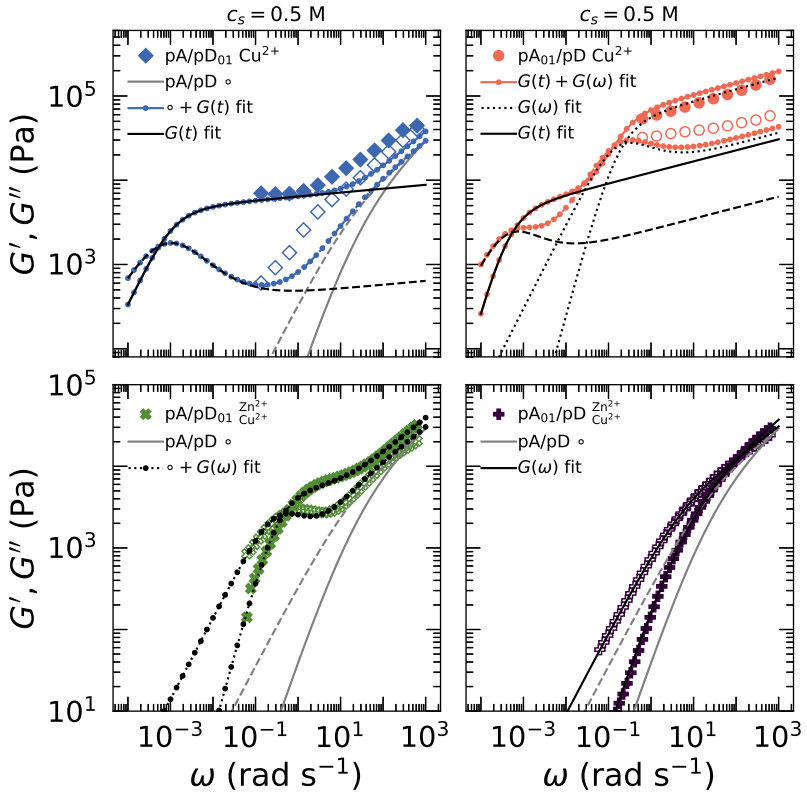

Figure 3.A.1: Frequency-dependent storage and loss moduli $G', G''(\omega)$ for pA/pD$_{01}$ (left) and pA$_{01}$/pD (right) with Cu^{2+} (top) and $\frac{Zn^{2+}}{Cu^{2+}}$ (bottom). Marked points are measured frequency sweeps for the hybrid complexes, grey lines are for the native coacervate pA/pD ∘ at 0.5 M. Black lines are fits to either $G(t)$ or $G(\omega)$ (see Figure 3.A.2), as specified in the legend. The colored, dotted lines are reconstructed curves, as indicated in the legend.

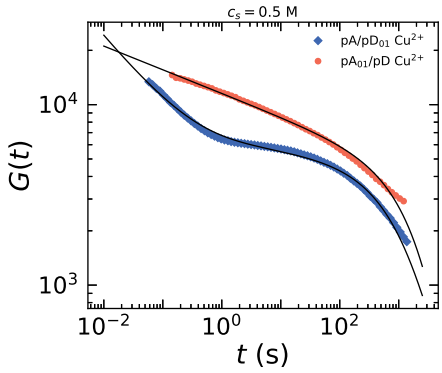

Figure 3.A.2: Relaxation modulus $G(t)$ for terpyridylated complex coacervates with Cu^{2+}. Marker points are measured values, black lines are fits to the fractional Maxwell model (Chapter 2, Equation 5).

of active complex ϕ_X. pA/pD$_{01}$-Cu^{2+} crosses over at 1.7 kPa, and pA$_{01}$/pD-Cu^{2+} at 2.4 kPa. The moduli of complexes pA/pD$_{01}$ with Co^{2+} and Ni^{2+} are close to 1 kPa (Chapter 2, Table 2), which suggests that our Cu^{2+} complexes have a crosslink density that is around twice the value for the other metals. However, in the following, we will see that the given analysis of ϕ_X is spurious. The increase in G_c is partially due to the increase of coacervate density associated with going from a c_s of 0.9 M to 0.5 M. Literature[36] shows that the polymer concentration varies from around 0.3 M to 1.0 M when the salt concentration is changed from background ($\approx$ 0.01 M) to critical ($\approx$ 1.0 M) - thus, a twofold increase in G_C can be entirely due to the polymer concentration.

However, the effect of addition of Zn^{2+} does not correspond to what we expect for a near-stoichiometric ratio between Cu^{2+} and terpyridine. The crossover frequencies are much shifted upwards, to 0.55 rad s^{-1} for pA/pD$_0$1$^{Zn^{2+}}_{Cu^{2+}}$ and even 114 rad s^{-1} for pA$_{01}$/pD$^{Zn^{2+}}_{Cu^{2+}}$. For the former, G_c increases somewhat to 2.7 kPa, while for the latter we can not interpret G_c, as it lies too close to the crossover point of the native coacervate (gray lines in Figure 3.A.3, 27 versus 12 kPa).

As we have seen in Chapter 2, Zn^{2+} is a weak terpyridine binder, whereas we consider Cu^{2+} to be stronger than Ni^{2+}.[34] It is thermodynamically inadmissible that the weaker ion displace one that is much stronger by a few orders of magnitude in K_{eq}. Thus, we conclude that Cu^{2+} is present at a trace concentration, and that the Zn^{2+} complex in the $^{Zn^{2+}}_{Cu^{2+}}$ samples is near-stoichiometric.

How can a strongly sub-stoichiometric concentration of metal ions freeze the

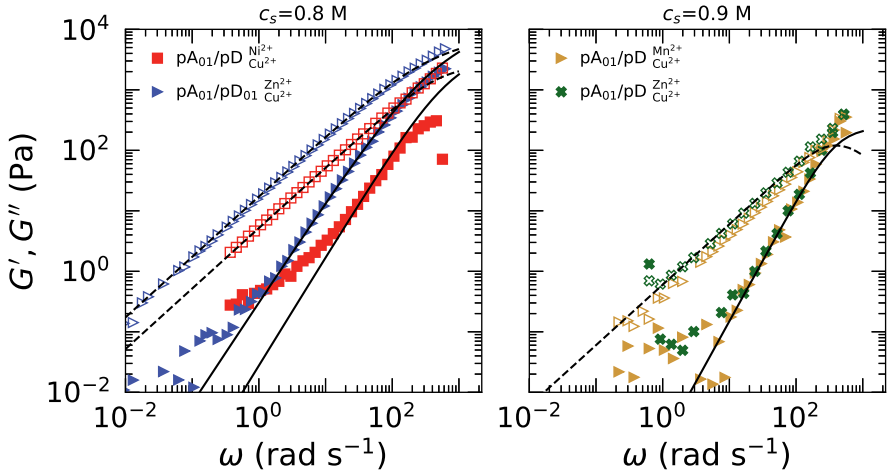

Figure 3.A.3: Frequency-dependent storage and loss moduli $G', G''(\omega)$ for mixed-metal complex coacervates at salt concentrations 0.8 M (left) and 0.9 M (right). The marked points are measured data, the black lines are fits to the fractional Maxwell model (Chapter 2, Equation 3).

dynamics to the extent evidenced by Figures 3.A.1 and 3.A.2? We suggest that the low metal load is enough to generate large yet non-percolating chains and cluster that entangle heavily. Due to the non-percolating nature of the clusters, the finite relaxation times do not reflect the "indefinite" stability of the complex.

Mixed-metal dynamics at high salt concentration

At higher salt concentrations, the response is always Maxwellian for complexes in which pA$_{01}$ presents terpyridines (Figure 3.A.3). We fitted the data to a single-mode FMM, which suggested the crossover to be on the order of 1 ms at critical salt, which is representative of non-crosslinked coacervates near c_s^*.

At $c_s = 0.8$ M, the crossover moves to even higher frequencies, and G_c increased as well. The shape of the curves, and the simultaneous increase of both crossover modulus and frequency are indications of the presence of superstoichiometric concentrations of metal ions, which could explain the lack of crosslinking in spite of the presence of, for example, Ni^{2+}, which binds nearly covalently. We will discuss some alternative hypotheses in the following section.

Asymmetry to terpyridylation architecture

For complexes with Cu^{2+} as well as $\binom{Zn^{2+}}{Cu^{2+}}$, the frequency response is highly asymmetric with the architecture of the terpyridine-metal network: when pA is terpyridylated (pA_{01}/pD), the crossover time is shorter ($\binom{Zn^{2+}}{Cu^{2+}}$), and the contribution to elasticity also seems higher (at least at 0.5 M). Terpyridylation of only pD (pA/pD_{01}) appears to be more effective in controlling (slowing down) the relaxation time of complex coacervates, which was used to reach the conclusions of Chapter 2.

The frequency response for samples that are mono-metalated and have a controlled metal concentration is also asymmetric to which of the polyelectrolyte partners is/are terpyridylated (Figure 3.5). We concluded that pA, due to its lesser degree of polymerization, has a smaller reach in the coacervate due to its smaller R_G, and has fewer terpyridines available (2.5 on average) to form crosslinks. Thus, complexes where the crosslinks are supplied by pD typically have a lower crossover frequency than when they are supplied by pA.

Similarly, the coacervates at high salt did not display the metal sensitivity described for pA/$pD_{01}-M^{2+}$ in Chapter 2. We clarify that this is neither due to the presence of Cu^{2+} with another metal. As discussed before, overmetalation would be a hypothesis. Alternatively, the lack of a strong metal response is due the use of a crosslinking polyelectrolyte of a relatively low degree of polymerization at a salt concentration at which the polymer, and thus crosslinker, density is also low. Thus, in "hybrid" complex coacervates, also the metal-ligand modality has a critical c_s^*, above which no effective bonds are formed. To systematically explore the viscoelasticity of pA_{01} with mixed metals and complement the data in Figure 3.A.1 with other mixes than $\binom{Zn^{2+}}{Cu^{2+}}$, a study at lower salt concentration than 0.8 M-0.9 M would be recommended.

3.B Behaviour of select complexes in ramped shear (flow curves)

After measurement of the quantities that characterize the linear viscoelastic response, we typically measured amplitude sweeps up to fracture. After fracture, measurements are no longer representative of the material in question, but rather of the history of the sample. Thus, we were prevented from measuring both flow curves and amplitude sweeps for most of the complexes in this work. However, we recorded ramped shear runs for a few cases in which the amplitude sweeps were deemed irrelevant due to strong loss-dominance of the linear spectrum. Figure 3.B.1 shows flow curves

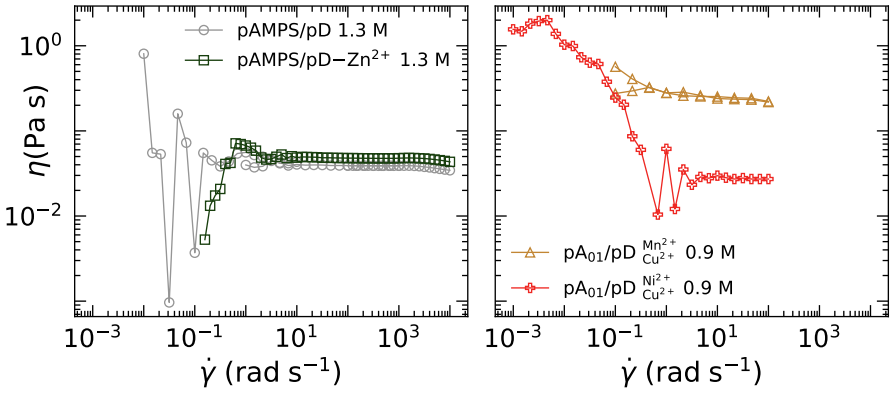

Figure 3.B.1: Rate-dependent viscosities calculated from flow curves of unterpyridylated complex (left) and terpyridylated complexes (right).

for non-terpyridylated complexes (left) and terpyridylated mixed-metal complexes (right) as graphs of rate-dependent viscosity η versus shear rate.

For pAMPS/pD at critical salt, the flow curves were unstable at low shear rates, with the stress fluctuating within three orders of magnitude. Wide fluctuations are also previous by Spruijt et al. in steady shear,[8] and were previously attributed to shear banding in telechelic networks.[21] The rate-dependent viscosity stabilized around 50 mPa s, with no significant change upon adding Zn^{2+} at 2.5 mM, which is unsurprising given that the polymers were unterpyridylated. The samples with 1% terpyridine on pA showed much higher low-shear viscosities around 10^3 mPa s, and strong shear thinning for $^{Ni^{2+}}_{Cu^{2+}}$ up to the viscosity of the corresponding native complex without terpyridines. For $^{Mn^{2+}}_{Cu^{2+}}$, we do not observe shear thinning, but it is quite likely that it is relegated to high $\dot{\gamma}$ due to the 10^2-fold increase of k_a of Mn^{2+} when compared to Ni^{2+}.[28]

Bibliography

[1] A. H. Hofman, I. A. van Hees, J. Yang, and M. Kamperman, "Bioinspired Underwater Adhesives by Using the Supramolecular Toolbox," *Advanced Materials*, vol. 1704640, p. 1704640, 2018.

[2] R. J. Stewart, C. S. Wang, and H. Shao, "Complex coacervates as a foundation for synthetic underwater adhesives," *Advances in Colloid and Interface Science*, vol. 167, no. 1-2, pp. 85–93, 2011.

[3] D. S. Hwang, J. H. Waite, and M. Tirrell, "Promotion of osteoblast proliferation on complex coacervation-based hyaluronic acid - recombinant mussel adhesive protein coatings on titanium," *Biomaterials*, vol. 31, no. 6, pp. 1080–1084, 2010.

[4] W. C. Blocher and S. L. Perry, "Complex coacervate-based materials for biomedicine," *Wiley Interdisciplinary Reviews: Nanomedicine and Nanobiotechnology*, vol. 9, no. 4, pp. 76–78, 2017.

[5] K. Sadman, Q. Wang, Y. Chen, B. Keshavarz, Z. Jiang, and K. R. Shull, "Influence of Hydrophobicity on Polyelectrolyte Complexation," *Macromolecules*, vol. 50, no. 23, pp. 9417–9426, 2017.

[6] R. F. Shamoun, A. Reisch, and J. B. Schlenoff, "Extruded saloplastic polyelectrolyte complexes," *Advanced Functional Materials*, vol. 22, no. 9, pp. 1923–1931, 2012.

[7] E. Spruijt, M. A. Cohen Stuart, and J. Van Der Gucht, "Linear viscoelasticity of polyelectrolyte complex coacervates," *Macromolecules*, vol. 46, no. 4, pp. 1633–1641, 2013.

[8] E. Spruijt, *Strength, structure and stability of polyelectrolyte complex coacervates*. PhD thesis, Wageningen University, 2012.

[9] E. Spruijt, J. Sprakel, M. Lemmers, M. A. Stuart, and J. Van Der Gucht, "Relaxation dynamics at different time scales in electrostatic complexes: Time-salt superposition," *Physical Review Letters*, vol. 105, no. 20, 2010.

[10] Y. Liu, H. H. Winter, and S. L. Perry, "Linear viscoelasticity of complex coacervates," *Advances in Colloid and Interface Science*, vol. 239, pp. 46–60, 2017.

[11] M. Yang, J. Shi, and J. B. Schlenoff, "Control of Dynamics in Polyelectrolyte Complexes by Temperature and Salt," *Macromolecules*, vol. 52, no. 5, pp. 1930–1941, 2019.

[12] Q. Zhao, D. W. Lee, B. K. Ahn, S. Seo, Y. Kaufman, J. Israelachvili, and J. H. Waite, "Underwater contact adhesion and microarchitecture in polyelectrolyte complexes actuated by solvent exchange," *Nature Materials*, vol. 15, no. 4, pp. 407–412, 2016.

[13] I. A. V. Hees, P. J. M. Swinkels, R. G. Fokkink, A. H. Velders, I. K. Voets, J. V. D. Gucht, and M. Kamperman, "Polymer Chemistry Self-assembly of oppositely charged polyelectrolyte block copolymers containing short thermoresponsive blocks," *Polymer Chemistry*, vol. 10, no. 23, pp. 3127–3134, 2019.

[14] M. Dompe, M. Vahdati, F. V. Ligten, F. J. Cedano-serrano, D. Hourdet, C. Creton, M. Zanetti, P. Bracco, J. V. D. Gucht, T. Kodger, and M. Kamperman, "Enhancement of the Adhesive Properties by Optimizing the Water Content in PNIPAM-Functionalized Complex Coacervates," *ACS Applied Polymer Materials*, vol. 2, pp. 1722–1730, 2020.

[15] J. Yang, M. Włodarczyk-Biegun, A. Filippov, S. Akerboom, M. Dompé, I. van Hees, M. Mocan, and M. Kamperman, "Functional Polymeric Materials Inspired by Geckos, Mussels, and Spider Silk," *Macromolecular Chemistry and Physics*, vol. 219, no. 16, 2018.

[16] C. W. Macosko, *Rheology principles, measurements and applications*. Wiley-VCH, 1994.

[17] H. H. Hariri and J. B. Schlenoff, "Saloplastic macroporous polyelectrolyte complexes: Cartilage mimics," *Macromolecules*, vol. 43, no. 20, pp. 8656–8663, 2010.

[18] C. Creton and M. Ciccotti, "Fracture and adhesion of soft materials: a review," *Reports on Progress in Physics*, vol. 79, no. 4, p. 046601, 2016.

[19] T. Tixier, H. Tabuteau, A. Carrière, L. Ramos, and C. Ligoure, "Transition from "brittle" to "ductile" rheological behavior by tuning the morphology of self-assembled networks," *Soft Matter*, vol. 6, no. 12, pp. 2699–2707, 2010.

[20] H. Tabuteau, S. Mora, G. Porte, M. Abkarian, and C. Ligoure, "Microscopic mechanisms of the brittleness of viscoelastic fluids," *Physical Review Letters*, vol. 102, no. 15, pp. 1–4, 2009.

[21] J. Sprakel, E. Spruijt, M. A. Cohen Stuart, N. A. Besseling, M. P. Lettinga, and J. Van Der Gucht, "Shear banding and rheochaos in associative polymer networks," *Soft Matter*, vol. 4, no. 8, pp. 1696–1705, 2008.

[22] D. Xu and S. L. Craig, "Strain hardening and strain softening of reversibly cross-linked supramolecular polymer networks," *Macromolecules*, vol. 44, no. 18, pp. 7478–7488, 2011.

[23] L. Ramos, A. Laperrousaz, P. Dieudonné, and C. Ligoure, "Structural signature of a brittle-to-ductile transition in self-assembled networks," *Physical Review Letters*, vol. 107, no. 14, pp. 1–5, 2011.

[24] D. Xu, J. L. Hawk, D. M. Loveless, S. L. Jeon, and S. L. Craig, "Mechanism of shear thickening in reversibly cross-linked supramolecular polymer networks," *Macromolecules*, vol. 43, no. 7, pp. 3556–3565, 2010.

[25] D. Xu and S. L. Craig, "Multiple Dynamic Processes Contribute to the Complex Steady Shear Behavior of Cross-Linked Supramolecular Networks of Semidilute Entangled Polymer Solutions," *Journal of Physical Chemistry Letters*, vol. 1, no. 11, pp. 1683–1686, 2010.

[26] E. Evans and K. Ritchie, "Dynamic strength of molecular adhesion bonds," *Biophysical Journal*, vol. 72, no. 4, pp. 1541–1555, 1997.

[27] R. D. Groot, A. Bot, and W. G. Agterof, "Molecular theory of the yield behavior of a polymer gel: Application to gelatin," *Journal of Chemical Physics*, vol. 104, no. 22, pp. 9220–9233, 1996.

[28] M. Ahmadi and S. Seiffert, "Thermodynamic control over energy dissipation modes in dual-network hydrogels based on metal-ligand coordination," *Soft Matter*, vol. 16, no. 9, pp. 2332–2341, 2020.

[29] S. C. Grindy, R. Learsch, D. Mozhdehi, J. Cheng, D. G. Barrett, Z. Guan, P. B. Messersmith, and N. Holten-Andersen, "Control of hierarchical polymer mechanics with bioinspired metal-coordination dynamics," *Nature Materials*, vol. 14, no. 12, pp. 1210–1216, 2015.

[30] E. Spruijt, F. A. Leermakers, R. Fokkink, R. Schweins, A. A. Van Well, M. A. Cohen Stuart, and J. Van Der Gucht, "Structure and dynamics of polyelectrolyte complex coacervates studied by scattering of neutrons, X-rays, and light," *Macromolecules*, vol. 46, no. 11, pp. 4596–4605, 2013.

[31] J. M. Dealy, "Weissenberg and Deborah Numbers - Their Definition and Use," *Rheology Bulletin*, vol. 79, no. 2, pp. 14–18, 2010.

[32] R. Poole, "The Deborah and Weissenberg numbers," *Rheology Bulletin*, vol. 53, no. 2, pp. 32–39, 2012.

[33] R. H. Ewoldt, A. E. Hosoi, and G. H. McKinley, "New measures for characterizing nonlinear viscoelasticity in large amplitude oscillatory shear," *Journal of Rheology*, vol. 52, no. 6, pp. 1427–1458, 2008.

[34] R. H. Holyer, C. D. Hubbard, S. F. Kettle, and R. G. Wilkins, "The Kinetics of Replacement Reactions of Complexes of the Transition Metals with 2,2',2"-Terpyridine," *Inorganic Chemistry*, vol. 5, no. 4, pp. 622–625, 1966.

[35] R. Hogg and R. G. Wilkins, "Exchange Studies of Certain Chelate Compounds of the Transitional Metals. Parts VIII. 2,2',2"-Terpyridine Complexes.," *Journal of the Chemical Society (Resumed)*, pp. 341–350, 1962.

[36] E. Spruijt, A. H. Westphal, J. W. Borst, M. A. Cohen Stuart, and J. Van Der Gucht, "Binodal compositions of polyelectrolyte complexes," *Macromolecules*, vol. 43, no. 15, pp. 6476–6484, 2010.

Chapter 4

Towards tuning the degree of semi-flexibility in polyelectrolyte complexes with the bottlebrush topology

Abstract

The study of complex coacervates, viscoelastic phases that form due to complexation of polyelectrolytes with opposite charges, mainly concerns flexible polyelectrolytes. Nonetheless, the inclusion of semi-flexible chains could allow to adjust the mechanical properties of polyelectrolytes complexes over a wider range. We present the synthesis of a macromolecule of the bottlebrush architecture, in which poly(acrylic acid) chains are grafted from a poly(*N*-hydroxyethyl acrylamide) backbone. The backbone is synthesized using RAFT, whereas the grafting is performed with termination-promoting ATRP, which was chosen to minimize crosslinking during grafting. As shown with GPC and AFM data, the resulting bottlebrushes are narrowly dispersed and reach a molecular weight of 2 MDa. The conformations are semiflexible with a long persistence length. Multi-angle DLS on aqueous samples of the bottlebrush revealed a robust bimodal decay at all accessible angles, with corresponding diffusion coefficients ten-fold apart. A study of the complexation behaviour of the polyanionic bottlebrush with a flexible polycation shows that the salt concentration at which the flexible-semiflexible complex dissolves is decreased with respect to flexible-flexible coacervates. The decrease in salt tolerance is in line with the tendency of weak anionic polymer brushes to charge-regulate due to a balancing of electrostatic repulsion with proton pressure. Finally, a DLS study on soluble complexes suggested that bottlebrush-flexible complexes form preferentially with polycations of lower degree of polymerization. Thus, the participation of bottlebrushes in coacervates modulates offers a different complexation profile.

4.1 Introduction

Since synthetic polymer materials such as plastics and rubbers presently fulfill demanding and diverse roles, the majority of the polymer science field concerns the preparation, behaviour, and utility of hydrophobic materials. Nevertheless, biomedicine has fostered a long-time ambition to take inspiration from the countless examples of highly-performing polymers that are central to the tissues and secretions of living beings, and apply them to synthetic creations such as implants, grafts, and adhesives.[1,2] Given their inherent hydrophilicity, and therefore adhesiveness to tissues, complexes of water-soluble polyelectrolytes (complex coacervates) have emerged as an important candidate for the development of surgical glues.[3] However, the application of complex coacervates as biomaterials also requires the opportunity to adjust the mechanics of complex coacervates to the demanding roles of tissues.

A framework for the stability and deformation behaviour of complex coacervates has been largely achieved by matching the results of rheological and structural measurements with theories derived for flexible polyelectrolytes.[4–8] Ubiquitous flexible polyelectrolytes include poly(*N*,*N*-dimethylethylamino methacrylate), poly(acrylic acid), poly(2-acrylamido methylpropyl sulfonate), and poly(diallyldimethylammonium chloride), which have persistence lengths ℓ_P of several nm when they are complexed in coacervates with salt concentrations in the 0.1 M range,[5,9] but are typically polymerized up to contour lengths L on the order of 10^2 nm. Whereas polymers at a high $\frac{\ell_P}{L}$-ratio can be described by Gaussian statistics, as confirmed by X-ray scattering studies of complexes of flexible polyelectrolytes,[5] polymers with $\ell_P \approx L$ show rod-like conformations, which deeply affects interactions and mechanical behaviour. The role of flexibility in complex coacervates has so far not been addressed, and semiflexible ($\ell_P \approx L$) polyelectrolytes are under-studied in polyelectrolyte complexes.

Chain stiffness is one of the few design parameters that one can address in polymer materials, and its relative neglect in the coacervate field is inopportune. Semi-flexibility is a key phenomenon in the mechanics of DNA, and the mechanical behaviour of DNA sequences has been recently shown to guide evolution.[10] Furthermore, large ℓ_P plays an important role in the strain hardening of collagen, actin and fibrin, which is a crucial feature for the mechanical integrity of organisms.[11,12] The persistence length strongly impacts the way in which polyelectrolytes engage in interactions, and the energetic consequences of their deformation, and therefore efforts towards a platform to study the effects of flexibility on complex coacervation is of crucial importance. While studies of coacervation of DNA and poly(cations) appear in the literature,[3,13] its scale-up is cost-prohibitive, and there is no opportunity for the facile tuning of ℓ_P.

In this Chapter, we present a polymer chemistry towards poly(acrylic acid) with

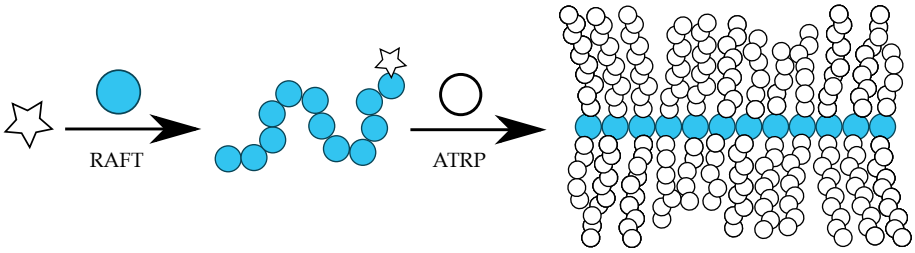

Figure 4.1: Cartoon of the synthesis presented in this Chapter. In the first step, 2-hydroxyethyl methacrylate (blue circles) is polymerized with RAFT polymerization to yield a flexible backbone chain. In the second pictured step, *tert*-butyl acrylate (white circles) is polymerized onto the backbone, resulting in a bottlebrush with a much stiffened backbone. For brevity, we pictured neither the attachment of an ATRP-initiating functionality, nor de-*tert*-butylation of the bottlebrush to yield poly(acrylic acid) grafted to the backbone.

tunable stiffness by targeting the bottlebrush architecture. A bottlebrush is a molecule in which side chains have been densely grafted onto a flexible backbone, and as a result macromolecules of varyingly high stiffness can be produced through variation of the density and polymerization degree of the grafted chains.[14] Our programme combines reversible addition-fragmentation transfer (RAFT) polymerization and atom transfer radical polymerization (ATRP), and is summarized in Figure 4.1. We explore the conformational properties of a dense poly(acrylic acid) bottlebrush through dynamic light scattering and atomic force microscopy. Finally, we present the first preliminary account of the complexation behaviour of a bottlebrush polyelectrolyte when it is brought into a solution of poly(cations). We urge to expand upon the techniques and methods presented here to address the question of chain flexibility in complex coacervates.

4.2 Materials and methods

Linear polymer fractions are notated pX^n, where X is D for *N*,*N*-dimethylaminoethyl methacrylate, HEAm for 2-hydroxyethyl acrylamide, and BiBEAm for the ester of poly(2-hydroxyethyl acrylamide, and where n is the degree of polymerization. The graft copolymer pBiBEAm-*g*-poly(acrylic acid) is written as gPA.

Materials

Chemicals were used as received, unless indicated otherwise. 2-methyl-2-propionic acid dodecyl trithiocarbonate (DMP, 98% HPLC), *N*,*N*-dimethyl formamide (DMF, anhydrous, 99.8%), pyridine (ACS reagent, ≥99.0%), basic aluminum oxide (Al_2O_3, activated, basic, Brockmann I), HCl (37% w/w, ACS reagent), and 1,4-dioxane (anhydrous, 99.8%) were obtained from Sigma-Aldrich (presently Merck), Germany. α-bromo *iso*-butyryl bromide (BrBiB, >98.0%, GC), 2-hydroxyethyl acrylamide (HEAm, stabilized with MEHQ, >98.0%, GC), tris[2-(dimethylamino)ethyl]amine (Me_6TREN, >98.0%, GC), *tert*-butyl acrylate (tBuAc, stabilized with MEHQ, >98.0%, GC), and $CuBr_2$ (>98.0%, titration) were obtained from TCI Belgium. CuBr (Alfa Aesar, ≥98.0%) was obtained from VWR, The Netherlands. Hexafluoroisopropanol (HFIP, AR, ≥99.8%) and MeOH (HPLC, ≥99.9%) were obtained from Biosolve BV, The Netherlands. Poly(*N*,*N*-dimethylaminoethyl methacrylate) (pD) was sourced from Polymer Source, Canada (pD^{32}), or prepared as described in Chapter 2 (pD^{1k}).

Pyridine was dried and stored over molecular sieves (4Å). HEAm and tBuAc were stripped of inhibitor by passing the liquids through a plug of Al_2O_3.

A M385LP1 LED (Thorlabs, UK) rated at 1650 mW was used as a UV source, which was mounted inside of a cardboard box covered with aluminum foil.

Methods

RAFT polymerization of poly(2-hydroxyethyl acrylamide) (1) To a 100 mL round-bottomed flask, we added DMP (47.5 mg, 0.130 mmol), 30 mL of DMF, and HEAm (10 mL, 78.2 mmol), and the yellow solution was bubbled with Ar for 30 m. The flask was sealed with a septum, and irradiated with 385 nm UV for 16h over a magnetic stirrer. Threefold precipitation into acetone afforded $pHEAm^{530}$ (**1**) as a yellow, glassy solid.

Synthesis of the ester of poly(2-hydroxyethyl acrylamide) and bromo-*iso*-butyrate (2) In an oven-dried round-bottomed flask, we dissolved $pHEAM^{530}$ (1.00 g, 8.69 mmol) in 15 mL of anhydrous DMF, to which pyridine (1.4 mL, 17 mmol) was added. The mixture was cooled on ice, and under a stream of Ar, BrBiB (1.1 mL, 8.7 mmol) was added dropwise. The sealed contents were stirred overnight, and threefold precipitation into Milli-Q afforded $pBiBEAm^{530}$ (0.24 g, 18%) (**2**) as a glassy solid.

Grafting of *tert*-butyl acrylate with ATRP (3) To a 50 mL two-necked flask, tBuAc (2.1 mL, 14.2 mmol), pBiBEAm (0.075 g, 0.284 mmol), ME_6TREN (28.5 μL, 0.1065 mmol), $CuBr_2$ (7.9 mg, 0.036 mmol), DMF (4 mL) and 1,4-dioxane (7 mL) were added. After the mixture was bubbled with Ar for 30m, CuBr (10.2 mg, 0.071 mmol) was added under a steady stream of Ar, and both necks of the flask were sealed. The lime mixture was stirred for 16h, after which it was passed through a column of Al_2O_3 and

concentrated on a rotary evaporator. Threefold precipitation into a 1:1 mixture of MeOH and Milli-Q afforded pBiBEAm-*g*-ptBuAc (**3**) as a rubbery off-white solid.

Removal of the *tert*-butyl esters In a 100 mL round-bottomed flask, we dissolved pBiBEAm-*g*-ptBuAc (0.50 g, 3.9 mmol) in HFIP (40 mL), and added 37% w/w HCl (0.33 mL, 3.9 mmol). After stirring overnight, the solvent was removed by rotary evaporation to yield pBiBEAm-*g*-pA (gPA, **4**).

Polymer characterization Molecular weight distributions were measured using size exclusion chromatography in tandem with multi-angle light scattering detector and viscometry. We used an Omnisec Reveal, with two PSS PFG columns. HFIP with 0.02 M KTFA was used as a mobile phase at 0.7 ml min^{-1}.

^{1}H-NMR spectra were recorded on a Bruker Avance 400 in deuterated chloroform ($CDCl_3$) or deuterated MeOH (MeOD). Chemical shifts δ are reported with respect to tabulated values[15] of trace hydrogenated solvent.

Atomic force microscopy (AFM) was performed on a Bruker MultiMode 8, using the ScanAsyst (peak force tapping) mode. Samples were prepared by spin-coating one or two droplets of a 0.01 g L^{-1} polymer solutions in chloroform on mica. Mica was freshly cleaved by three-fold exfoliation with office tape.

Dynamic light scattering We recorded the angle-dependent second-order intensity autocorrelation function $g_2(q,t) = \langle I(t)I(0)\rangle\langle I(t)^2\rangle$ of light scattered by solutions of polyelectrolytes and polyelectrolyte complexes, where the triangular brackets indicate an average over all possible $\tau = 0$. The dynamic light scattering (DLS) setup comprised an ALV-125 goniometer, a ALV5000/60X0 external correlator, a HIGH QE APD single detector, and a Cobolt Flamenco 300 mW DPSS laser operating at 660 nm. Measurements were performed at room temperature (19°C). Scattering angles were set between 30 and 150°.

Polyelectrolyte samples were prepared from stock solutions, which were made by neutralizing gPA with NaOH, or pD with HCl to pH 7, and subsequently diluting the samples with an NaCl solution and Milli-Q until a salt strength of 0.1 M and a polymer concentration of 0.25 M (monomer equivalents). Stocks were filtrated over a 0.45 μm (gPA) or 0.2 μm (pD) membrane filter. Subsequently, samples were prepared by adding a known amount of stock to 1 mL of filtrated salt solution.

4.3 Results and discussion

Synthesis of the poly(initiator)

In this section, we describe the full synthesis of a poly(initiator), the ester of poly(2-hydroxyethyl acrylamide) and bromo-*iso*-butyrate (pBiBEAm, **2**), starting from the

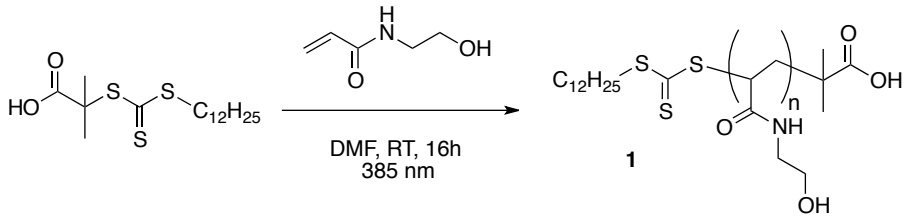

Figure 4.2: Synthesis of the hydroxyl-functional pHEAm with the help of photomediated RAFT polymerization.

polymerization of 2-hydroxyethyl acrylamide (HEAm) using photomediated RAFT polymerization. A recent review sums up the advantages of using light to mediate RAFT polymerizations, which offers the ability to polymerize at room temperature, without the need for an additional "free" initiator.[16] The latter would be a significant advantage, as free initiators (commonly azo compounds) inevitably lead to chains that have no RAFT functionality, and thus decrease the amount of control over the polymerization.[17]

We opted to control polymerization of HEAm with the widely available trithiocarbon compound 2-methyl-2-propionic acid dodecyl trithiocarbonate (DMP), mediated by low-intensity (1.7 W) long-wave UV radiation at 365 nm, as is displayed in Figure 4.2. We motivate the choice for a low-intensity source by the prevalence of such equipment in polymer laboratories, and reports that specify that high conversions can be reached even with light sources driven by powers P as low as a few watts.[18, 19] The polymerization rate k_{eff} increases as P^{α}, with Lewis et al. reporting an α of 0.73.[18] Since neither the dispersity Đ, nor the correspondence between conversion-based ("nominal") and GPC-based ("real") molecular weight averages are affected by P, we consider an improvised lighting setup adequate.

We performed polymerizations on the multigram scale, with monomer-to-DMP ratios between 600 and 15000. After assessing molecular weight averages based on conversion (ϕ_C) and GPC measurements, we found that only the ratio of 600 gave rise to well-defined polymers (Table 4.1). When higher M are targeted, we find high dispersities and discrepancies between molecular weight averages based on ϕ_C and GPC. Work by Wang et al. on UV-mediated polymerization with DMP, albeit on a different monomer (methyl acrylate) in a different solvent (benzene) and with UV long-passed at 320 nm, paints a familiar picture: Đ is around 1.2 until the monomer-to-DMP ratio is 6000, and then increases. The higher ratio at which we lose control over the polymerization can be attributed to our preference to have ϕ_C as close to

Table 4.1: Photomediated polymerization of HEAm controlled by DMP in DMF at RT. Number-averaged molecular weights M_n were obtained from GPC in hexafluoroisopropanol. The monomer concentration was 2 M. M_{NMR} and M_n are reported in kDa, k_{eff} in $M^{-1}s^{-1}$.

[M]/[DMP]	ϕ_c	M_{NMR}	M_n	Đ	t	k_{eff}
600	0.88	61	78	1.25	16h	0.053
2000	0.9	209	87	2.43	41h	0.038
15000	0.6	1039	>100	>2.5	48h	0.017

unity as possible, and due to the particularities of the monomer/solvent combination with the RAFT agent.[19] Further optimization could involve screening solvents (for instance water), or using a RAFT agent with a higher deactivation rate.[20] However, the obtained pHEAm^{530} was deemed sufficiently long and well-defined to serve as a backbone for the synthesis of molecular bottlebrushes.

On a side note, we report that the method reported above also gave rise to copolymers of dimethyl acrylamide (DMA) and HEAm, when DMA and HEAm were introduced in a one-to-one ratio. GPC in water and THF suggested a somewhat higher Đ of 1.5, but we have not pursued a measurement in HFIP. We note that such copolymers offer a backbone for bottlebrushes with more dilute side branches in future studies, and thus a lower rigidity.

Subsequently, we esterified pHEAm^{530} with α-bromo *iso*-butyryl bromide to afford the poly(initiator) pBiBEAm^{530}, **2**. We attempted the array of esterification conditions that is summarized in Table 4.2, and find that addition under a flow of Ar of 1 eq of the bromide to a solution of pHEAm with 2 eq of pyridine in DMF yields a clear solution, from which a glassy solid precipitated upon addition of water. ^{1}H-NMR confirmed successful esterification as a shift of the NH–C**H**$_2$– and –C**H**$_2$–O– protons from, respectively, 3.1 and 3.6 ppm to 3.5 and 4.2 ppm (Figure 4.3). Additionally, the methyl peak of the two methyl groups appears prominently at 1.93 ppm.

In earlier trials, we found that NEt_3 in DMF successfully mediated the esterification of the copolymer p(HEAm–*co*–DMA). The move to pyridine was prompted by the observation that NEt_3 acts as a co-nonsolvent for homopolymer pHEAm. Given the toxicity of pyridine and the difficulties of its removal, we can not recommend its use other than when specifically required. The latter seems to be the case here due the peculiar solubility of HEAm, and perhaps hydrophilic polyacrylamides in general. In the following section, we will report on the grafting of the thus obtained pBiBEAm (**2**) with *tert*–butyl acrylate (tBuAc) and its subsequent de-esterification to p(BiBEAm-*g*-[pAA]) (gPA, **4**).

Table 4.2: Conditions attempted for esterification of pHEAm^{530} with α-bromo *iso*-butyryl bromide (BBiB); "sim" means that the base was added simultaneously with the bromide.

Solvent	Base	*t*	BBiB	Results
DMF	Pyridine (1 eq)	24h	1 eq	Precipitation upon BBiB addition, no product
DMF	NEt_3 (3 eq)	16h	2 eq	Precipitation upon NEt_3 addition, no product
DMF	NEt_3 (2 eq, sim)	16h	1.5 eq	Precipitation upon NEt_3 addition, no product
H2O	KOH	30m	1 eq	Forms *iso*-butyrate, no product
DMF	Pyridine (2 eq)	24h	1 eq	Quantitative esterification

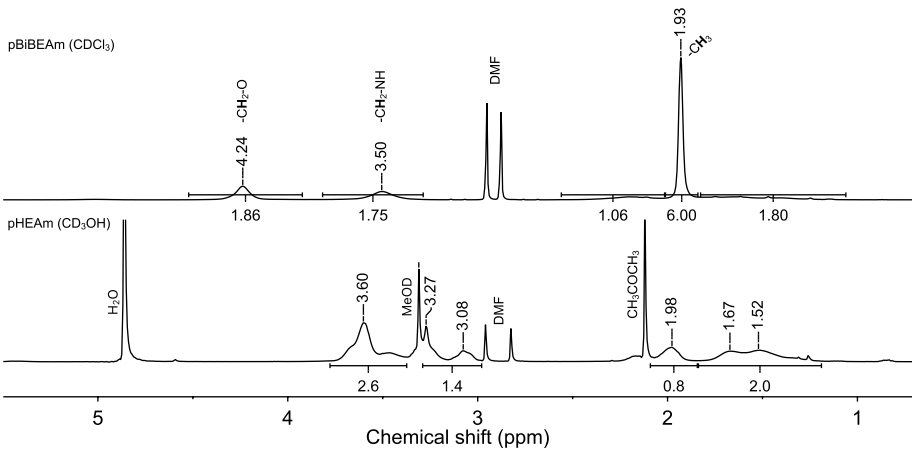

Figure 4.3: ^{1}H–NMR spectra of solutions of pHEAm (**1**) in MeOD (bottom) and pBiBEAm in $CDCl_3$ (top).

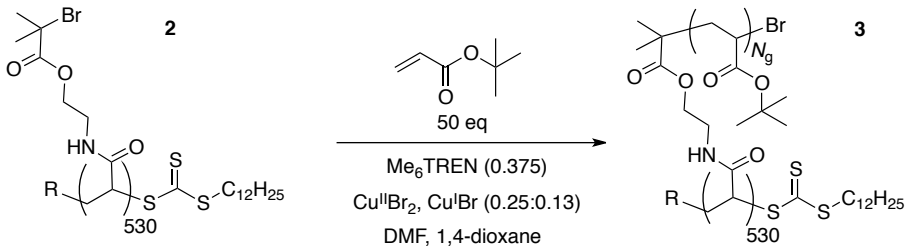

Figure 4.4: ATRP grafting of pBiBEAm with tBuAc and copper complexes of Me_6TREN at RT.

Synthesis of a poly(acrylic acid)-grafted bottlebrush

Initial screening of conditions for the grafting of tBuAc unto p(BiBEAm–*co*–DMA) in DMF revealed that the ATRP polymerization tends to be uncontrollably fast with typical reactant ratios [M]:[I]:[L]:[Cu^I]:[Cu^{II}]=50:1:1:1:0.05, in which [I] refers to concentration of initiator monomer, [M] to tBuAc, and [L] to the ligand Me_6TREN. Cu^I, when bound to an appropriate ligand, provides a catalyst for generation of radicals from the initiator, and $Cu^{II}Br$ catalyzes re-halogenation of active chains. Under these conditions, a gel formed within seconds, which resisted any attempts at dissolution. Dilution of the reaction mixture with solvent resulted in a crude that appeared soluble, however, the product was once again insoluble after precipitation. Reactions in MeOH led to similar disappointment, and so did attempts with an increased deactivator load ([Cu^I]:[Cu^{II}]=1:0.2).

Following the work of Matyjaszewski et al,[21] we were able to control the ATRP grafting of tBuAc to pBiBEAm. The authors suggest to promote Cu-catalyzed irreversible termination of growing chains to avoid branch–branch radical addition, which leads to crosslinking (and gelation). We found that a reactant load of [M]:[I]:[L]:[Cu^I]:[Cu^{II}]=100:1:0.375:0.13:0.25 in a mixed solvent of DMF and 1,4–dioxane gave rise to a mixture that gradually thickened over the course of 16h, and did not suffer precipitation. The reaction scheme is drawn in Figure 4.4.

^{1}H–NMR analysis confirmed the polymerization of tBuAc up to high conversion (ϕ_c =0.88 in 16h). The residue was precipitated thrice into ice-cold MeOH:H_2O, and took the form of a rubber-like solid that dissolved in chloroform, acetone and HFIP. A more detailed analysis of the ^{1}H–NMR spectrum of a $CDCl_3$ solution of the purified graft copolymer supports the formation of ptBuAc branches on the backbone. As shown in the spectrum of Figure 4.5, prominent resonances characterize ptBuAc (see Chapter 5), with chemical shifts around 1.4 and 2.2 ppm. Furthermore, broadened, faint signals from the methylene protons of the poly(initiator) persist near to 3.5

and 4.2 ppm. Around 4.1 ppm, another broad peak appears, which is characteristic of a terminal, brominated, methine, suggesting that a majority of chains was not terminated by chain-chain coupling or catalyzed radical termination.

The peak corresponding to NH–C$\mathbf{H}_2$– is isolated, and the proportion of its integral that of the *tert*–butyl methyl peak at 1.4 ppm provides an estimate of the mean degree of polymerization of the side-chains. In Figure 4.5, we normalized the resonance at 3.5 ppm to $\frac{2}{9} \approx 0.22$, so that the integral of the *tert*–butyl methyl peak suggests that the mean amount of tBuAc units added to the side-chains is 70. We note that the fact that the chains appear longer than as one would expect at full conversion (50) could suggest that the initiator efficiency (ie, brush density) lower than unity, as reported before in the literature.[21] Moreover, the protons at the interior of the molecule are much slower to relax, and thus the integrals should not be interprerated in a rigorously quantitative fashion.

"Absolute molecular weight" GPC with multi-angle light scattering detection and HFIP as a mobile phase further confirmed the formation of well-defined ultra-high M macromolecules. We report a number-averaged molecular weight M_n of 2.0 MDa, with Đ equal to 1.21, which is corroborated by AFM contour length analysis (*vide infra*). The latter is striking, as the apparent dispersity of the overall macromolecule is seen to *decrease* as side-chains are added. This should not be taken to mean that branches themselves are equally homogegenous, however. The value for M_n from GPC suggests around 30 units of tBuAc per side chain. However, the GPC estimate is hard to confirm, since the sizing method expects the chains to be spherical coils, which is not corroborated by AFM data (next section).

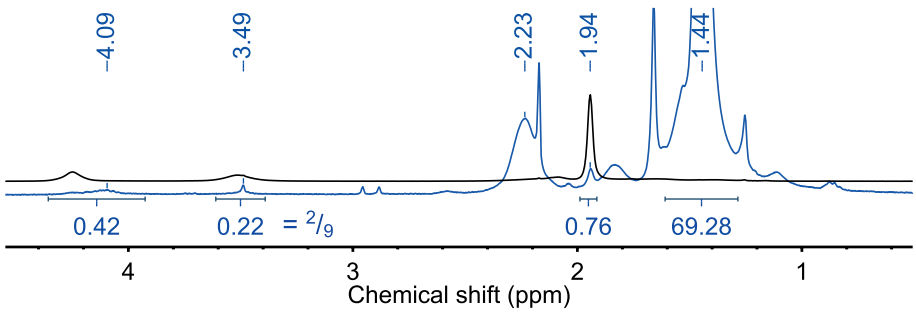

Figure 4.5: ^{1}H–NMR spectra of $CDCl_3$ solutions of ptBuAc-grafted pBiBEAm (**3**, bottom, blue), and the poly(initiator) (**2**, black, top). The integrals are for the grafted molecule, and are normalized to one methylene (2 protons) from an initiating unit being equal to $\frac{2}{9}$ - as a consequence, the integral of the peak at 1.4 ppm represents the NMR estimate of N_g.

With well-defined bottlebrushes in hand, we de-*tert*-butylated the material by the method developed in Chapter 5 to yield pBiBEAm-*g*-pA (gPA, **4**). ^{1}H–NMR confirmed the quantitative removal of the ester group as the disapperance of the peak at 1.4 ppm (Figure 4.6). The structure of the backbone is not readily discernible from the broadened peak downfield from the solvent signal, but assuming that the signal at 4.3 ppm corresponds to a backbone methylene, integration suggests a sidechain length of 54. Without cleavage essays, in which the side-chains are detached from the backbone, it is difficult to establish the exact value of N_g. However, we deem the obtained product to be well-defined enough to warrant a further study of the conformation of a densely anionic bottlebrush, and of its complexation with a poly(cation). First, however, we will present further evidence from AFM that the (neutral) ptBuAc precursor shows the stiff behaviour expected for bottlebrush molecules.

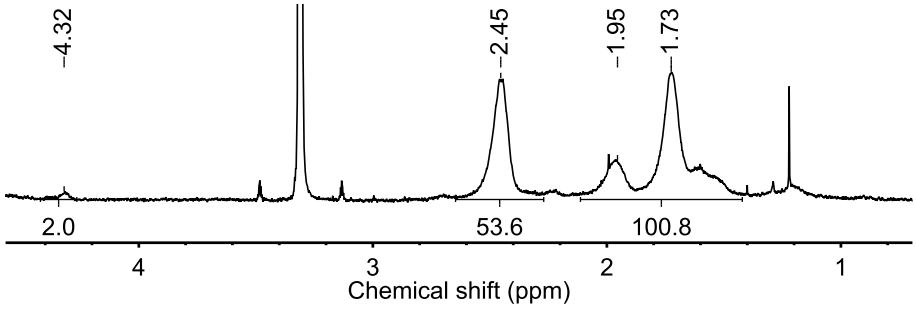

Figure 4.6: ^{1}–NMR spectrum of the de-*tert*-butylated bottlebrush with poly(acrylic acid) side-chains **4** in MeOD. The integrals are normalized such that the area under the peak at 2.5 ppm corresponds to an estimate of N_g.

AFM imaging of a bottlebrush with *tert*-butyl acrylate side chains

To confirm the bottlebrush structure of our materials, we performed AFM imaging of gPA. The molecules were deposited on freshly peeled mica by spin coating a 0.01 g mL^{-1} solution in chloroform. Scans of the resulting surfaces showed macromolecules of a high stiffness with lengths on the order of 10^{-7} m, a z-height of around 1.8 nm and a thickness between 20 and 40 nm. Two representatives scans can be viewed in Figure 4.7. We find no branched molecules, in line with the claims of Matyjaszewski et al. of low incidence of branch-branch termination reactions under conditions that promote catalyzed radical termination.[21]

Furthermore, we performed contour length analysis using the Python package

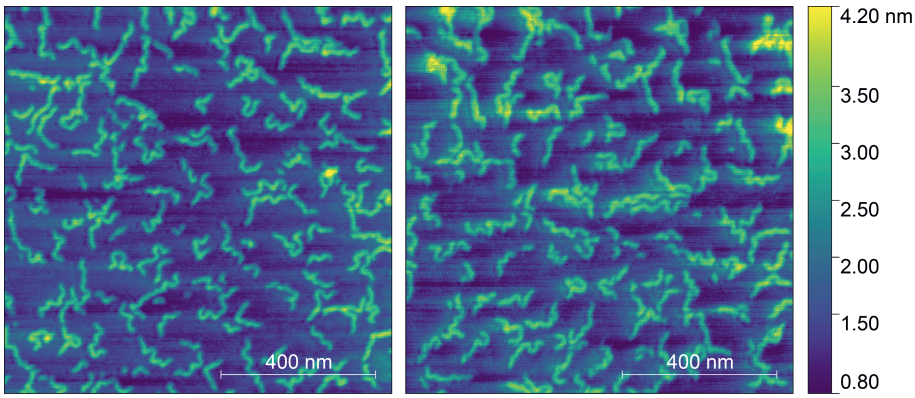

Figure 4.7: AFM scans of two 1 μm^2 areas of mica samples on which a 0.01 g mL^{-1} of poly(*tert*–butyl acrylate)-grafted pBiBEAm bottlebrushes was spin coated.

TopoStats provided by Pyne and co-workers,[22, 23] after a few modifications. As expected for polymers obtained from radical polymerization, the distribution of contour lengths resembles a log-normal function, as can be seen in the histogram of Figure 4.8,

$$P(L) = \frac{1}{x\sigma\sqrt{2\pi}} \exp\left(-\frac{(\ln x - \mu)^2}{2\sigma^2}\right) \tag{4.1}$$

in which μ is related to the mean by $\exp\left(\mu + \frac{\sigma^2}{2}\right)$ and σ is related to the variance and the skewness of the distribution.

For the distribution in Figure 4.8, the mean contour length is 92 nm. Since the contour length is directly proportional to M, the proportionality constant being $M_{\text{segment}} L_{\text{segment}}^{-1}$, we can compare L with the expected length $n_{\text{segments}} L_{\text{segments}}$. If we try to calculate the monomer length by dividing the mean contour length by the conversion-based degree of polymerization (530 backbone units), we obtain value of 0.17 nm, which is shorter than the chemical monomer length of 0.254 nm. The mismatch is a result of either an overestimation of the mean degree of polymerization, or undersampling of the longer chain population in the AFM images. However, given the appearance of the bottlebrushes, it is reasonable to conclude that our molecules are near-maximally stretched, as has been reported before for ATRP bottlebrushes made from backbones with an initiator on every acrylate residue.[24]

Furthermore, the degree of spreading in the distribution must relate to the dispersity. A convenient property of the log-normal distribution is Đ= $\exp\sigma^2$, which

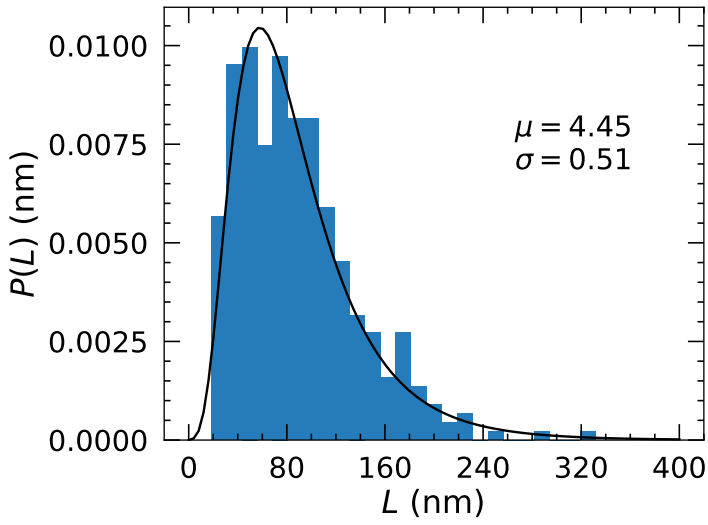

Figure 4.8: Histogram of contour lengths extracted from fitted splines of objects detected in AFM scans of ptBuAc bottlebrushes spincoated on mica (Figure 4.7) (bars), and a log-normal distribution fitted to the histogram (curve). The parameters μ and σ are as defined for Equation 4.1.

corresponds to a dispersity of 1.28, which is essentially identical to the value obtained from GPC sizing of the hydroxyl precursor to the initiator (Table 4.1).

Since AFM shows that our molecules are indeed semiflexible and not branched, we conclude that the synthetic protocol employed here successfully gives tBuAc bottlebrushes. Additionally, we tried to image the de-esterified polymers. To this end, the reaction product after de-esterification was neutralized with NaOH at 0.1 M NaCl, the salt added to prevent osmotic rupture[24] caused by further stretching due to electrostatic repulsion between the negatively charged carboxylates. However, the obtained images were of poor quality due to the presence of salt crystals, even after rinsing the mica surfaces with Milli-Q. Attempts to cast the bottlebrushes in pure water gave images of both globular and stiff structures of contour lengths on the scale of 10^{-7} m.

Thus, at present we can not conclusively claim the bottlebrush morphology of the de-*tert*-butylated polymers. In the rest of the Chapter, we first study the conformation of the presumed poly(anion) bottlebrushes with dynamic light scattering (DLS). Subsequently, we study the formation and light scattering of a polyelectrolyte complex between the presumed pA bottlebrush and a poly(cation).

Dynamic light scattering of poly(acrylic acid) bottlebrushes

We measured the second-order intensity autocorrelation function $g_2(t)$ of light scattered from a 1 g L^{-1} solution of neutralized gPA bottlebrushes using a fast correlator. Scattering experiments were performed at scattering vectors q from 6 to 24 10^6 m^{-1}, scattering angles θ between 30 and 150°. Ten curves were recorded for each q. Then, we calculated the first-order intensity autocorrelation function using the Siegert relation,

$$g_1(q,t) = \frac{1}{\sqrt{\beta^\dagger}}\sqrt{1-g_2(q,t)} \tag{4.2}$$

where $\beta^\dagger$ is the observed proportionality constant which was obtained simply by normalizing the correlations to the value at $t = 0.25$ μs.

We fitted the resulting correlations to a biexponential decay, yielding two decay rates Γ_A and Γ_B, both of which increased with increasing q, as can be seen by the accelerated decay of $\sqrt{1-g_2(q,t)}$ in Figure 4.9. Γ_A and Γ_B were on the order of, respectively 10^2 and 10^3 s^{-1}, and averages over ten measurements of the decay rates are plotted in the right-hand panel of Figure 4.9. Whereas the fits were satisfactory for times beyond 10^{-5} s, a small contribution ($\ll 0.1$) of an ultra-fast mode ($\Gamma \gg 10^6$)

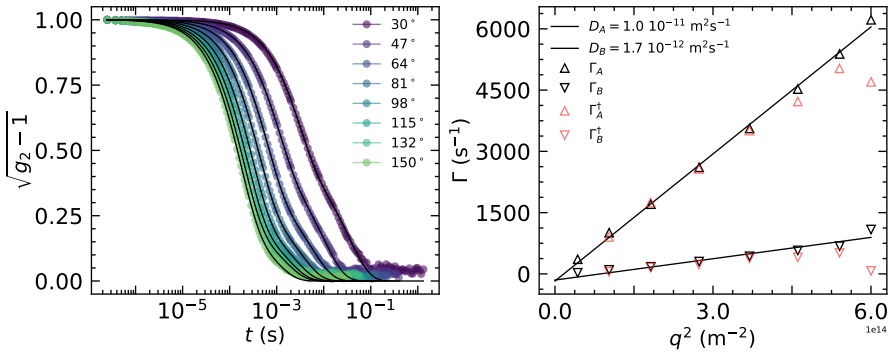

Figure 4.9: (left) Normalized first-order intensity correlation functions $\sqrt{g_2-1}$ as function of decorrelation time t for scattering angles between 30° and 150° for gPA solutions at 1.0 g L^{-1} polymer and 0.1 M NaCl concentration and (right) decay rates Γ_A and Γ_B as fitted from a biexponential decay model. Symbols represent measurements, whereas black lines are fits to biexponential decays (left) or to the equation $\Gamma = Dq^2$ (right). The values for the effective diffusion coefficients D are given in the legend.

was evident in less than the first 10 data points. We did not fit these due to the high uncertainty in the resulting decay rates.

We repeated the measurement with a lower attenuator setting (higher transmission). The decay rates found from the biexponential fit are given in Figure 4.9 as labeled $\Gamma^\dagger$. At the high end of the q-range, the high-transmission decays deviate from the lower-transmission ones, which is most likely due to detector overflow. At lower q, both runs yield the same decay rates, which shows that data acquisition and fitting are robust.

When plotted against q^2, *both* decay rates grow in a directly proportional fashion (Figure 4.9, right). Then, the modes can be characterized by diffusion coefficients D_A and D_B, which are about an order of magnitude apart. The large gap between D_A and D_B shows that the two modes are not due to translation and rotation of rigid rods, which would lead to two decays with the same slope of Γ versus q^2.[25,26] Indeed, the micrographs of Figure 4.7 suggest that the *tert*-butylated precursors to the gPA bottlebrushes are semiflexible.

A body of literature offers an analysis on the effect of persistence length ℓ_P of semiflexible molecules on the decay of the intensity correlation measured in DLS.[27–31] Given a large enough degree of polymerization, semiflexible molecules assume Gaussian statistics on length scales $\lambda \gg \ell_p$.[30] In our case, AFM strongly suggests that the

gPA bottlebrushes are at most a few times longer than their ℓ_P, and thus should be expected to be optically anisotropic. Fujime and Maeda[27] derive the dynamic structure factor in an integral form for semiflexible molecules as function of $\frac{L}{\ell_P}$ starting from a Langevin equation that takes into account the free energy of bending against a backdrop of thermal fluctuations. The authors do not present an exponential decomposition, but from the results it is clear that the decays would be very closely spaced. A score of more recent papers arrive at a stretched-exponential form for the decay, starting from the same Langevin equation.[29–31]

For our case in which the scattering wavelengths $\lambda = \frac{2\pi}{q}$ are larger than the contour length of the chains at all scattering angles, Reineker and co-workers suggest that the correlations be described by a single decay.[29] The theories referenced in the preceding paragraph appear to be valid for $\lambda \ll L$. Clearly, neither of these conditions are met in our case, given the ample evidence for biexponential decay for all scattering angles (Figures 4.9). We note that at the highest scattering angle ($\theta = 150°$) $\lambda \approx L$. Thus, the origin of the biexponential form with apparent D spaced around ten-fold is at present unclear. One might suppose that for cases in which $\lambda \approx L$, only the first bending mode comes into view, however, this is rather unlikely given the rather broad range of q.

Other possibilities might be related to either impurities or osmotic rupture. We note that, given the available data, it is not possible to completely exclude that modes A and B simply represent two populations of coils with hydrodynamic radii R_H of 24 nm (fast mode B) and 140 nm (slow mode A). However, the strictly exponential nature of the decays is at odds with the polydisperse nature that the coils would likely have, should they have their origin in osmotic rupture. Furthermore, the hydrodynamic radius that we measure for mode B is rather close to the expected contour length, whereas osmotically ruptured fragments should be neither large nor so monodisperse. We note that the smaller R_H value is on the order of the width of the *tert*-butylated precursors, whereas the larger radius is on the order of the contour length. An analysis of the depolarized component of the scattered light might reject the possibility of a globular origin of either or both the modes, and we recommend this analysis for future studies.

In short, the above shows that DLS at scattering wavelengths between 0.2 and 1 μm captures neither internal modes, nor rigid rotation of the presumed bottlebrushes. For visible light, typically $qL \leq 1$, and X-ray photocorrelation could perhaps be used to probe the relevant length scales. However, the appearance of two well-defined modes that scale with q^2 suggests that the molecules are stable in salt solution. In the final section of the Chapter we will form complexes with the poly(cation) poly(*N*,*N*-dimethylaminoethyl methacrylate), denoted gPA/pD, and also catalogue the low-q

dynamics of non-stoichiometric complexes.

Complexation of poly(acrylic acid) bottlebrushes with a polycation

Addition of an aqueous 0.25 M solution of pD^{32} (5.5 kDa) to an equal volume of gPA solution, both brought to pH 7 and c_s=0.1 M NaCl, gave a two-phase system at a total c_s of 0.225 M. The continuous phase was a clear liquid, whereas the complex precipitated as a white powder. Stepwise addition of a 0.75 M NaCl solution resulted in the powder first becoming sticky to glass (at 0.4 M NaCl), and then forming a cohesive phase (0.54 M NaCl). The complex never assumed a liquid state, but dissolved at 0.7 M. We estimate that, at a monomer *pair* concentration of 0.083 M, the critical salt strength lies between 0.55 and 0.7 M. Furthermore, we note that heating the solution at 0.7 M NaCl does not turbidify the liquid, which suggests that the system is no longer at a point close to the two-phase region in the phase diagram.

Several points in our, admittedly anecdotal, account of complex formation with a bottlebrush participant differ from what is described for flexible polyelectrolytes here and in literature.[7,8] First, we do not observe non-cohesive powder-like phases that do not stick to glass for flexible polyelectrolytes, not even at lower salt strengths. Furthermore, our flexible complexes have an extensive salt range in which they are poorly viscous liquids (around 10 mPa s). We cannot compare the critical salt strengths for gPA/pD to the flexible case, since the former is extremely asymmetric in molecular weight (5 kDa versus several MDa). Rather, we may say that c_s^* is close to what we would expect for such a short pD fragment, but lower than what is expected for a flexible pA of comparable molecular weight.[4,6,7]

Finally, we studied the effect of pD binding to gPA on the (apparent) diffusion coefficient using DLS. For the purpose of keeping the diffusing object soluble (unlike, for instance, the gels studied with DLS in Chapter 5) and at equilibrium, we made high-salt (c_s = 0.5 M), non-stoichiometric complexes at a low gPA concentration of 0.1 g L^{-1}, with a carboxylate concentration of 1.3 mM. Complexes were made with 0.2 molar equivalents of pD, of which we sampled two molecular weight distributions, monodisperse pD^{32} and the more polydisperse pD^{1k}.

Despite the small fraction of poly(cation) added, formation of a discontinuous phase was evident for all complexes, which took the form of fibers that sedimented to the bottom of the cell. We allowed ample time for the rest of the solutions to reach a steady state (1 month), even though the liquid phase of the samples appeared clear even briefly after mixing. Subsequently, we recorded intensity autocorrelation functions at $\theta = 90°$ ($1.8{\cdot}10^7$ m^{-1}) for solutions of only pD, only gPA, and of the complexes.

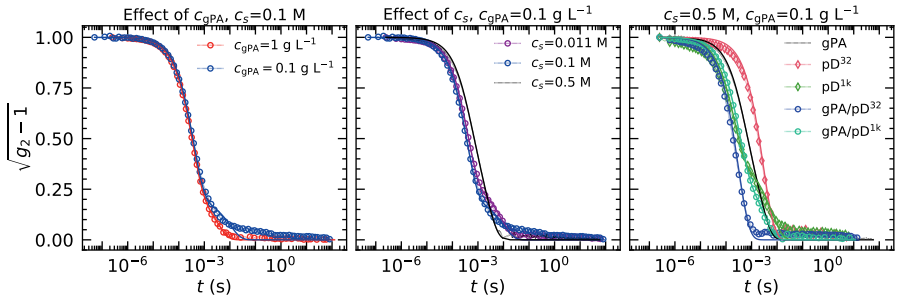

Figure 4.10: Normalized first-order intensity autocorrelation functions obtained with DLS of solutions of (left) gPA at 0.1 M NaCl, (center) 0.1 g L^{-1} of grafted polymer, and (right) pD and complexes of gPA with 0.2 equivalents of pD. Marked points represent averages over 10 correlation functions, lines are fits to (a sum of) one or two exponential decays. For gPA 0.5 M NaCl, we did not plot the marks for increased readability. The diffusion coefficients that correspond to the decay rates and pre-exponential weights of the optimum fits are given in Table 4.3.

First, we confirmed whether solutions of gPA still give sufficient scattering intensity after a ten-fold decrease in c_{gPA} with respect to the measurements described for Figure 4.9, and whether the intensity autocorrelations are still comparable. Second, we compared the correlations for three salt concentrations (0.011 M, 0.1 M and 0.5 M). The decrease to 0.1 g L^{-1} in c_{gPA} at 0.011 M and 0.1 M NaCl gave rise to a slow multi-exponential mode with $\Gamma_i \ll 100$ s^{-1}, which we did not fit. However, an increase in c_s to 0.5 M disabled the slow mode, and the correlation could be fitted with a biexponential decay, as described for the data in Figure 4.9. The effect of c_{gPA} can be viewed in the left panel of Figure 4.10, and the effect of c_s in the central one.

Given that, in solutions of gPA, the decay rates of the two modes scale as $\Gamma \propto q^2$, (Figure 4.9) the two fitted exponential decay rates at 90° were converted to diffusion constants using the relation $\Gamma_i = D_i q^2$, i being A, B. At all sampled c_s, D_A averaged to a robust $0.79 \cdot 10^{-11} \pm 0.01$ (see Table 4.3), which suggests a complete lack of a conformational effect of screening electrostatic repulsions. While this is surprising for a polyelectrolyte with a charge on every monomer, we interpret this as the backbone being maximally stretched due to steric hindrance even at high salt strength, which is perhaps reasonable given that our AFM data already suggested the backbones to be in the all-trans configuration (Figure 4.8 and accompanying discussion). D_B is not as robust for the lower salt concentrations due to slow modes, but returns to a value essentially identical to what we found for 1.0 g L^{-1} solutions in the multi-angle study.

Furthermore, salt-dependent charging might explain the absence of an effect of c_s on the diffusion coefficient of the slower mode. A recent contribution by the group of Dahlin[32] establishes clearly that, at low c_s, deprotonation of weak poly(acid) brushes is relegated to higher pH as a way to avoid the high energetic penalty of charged monomers in an already-densely packed brush. The trade-off between decreasing electrostatic repulsion but increasing deprotonation might contribute to a lack of salt sensitivity of gPA solutions. Either way, the response to c_s corroborates the semiflexible statistics of gPA in aqueous solution.

The effect of the decrease of c_{gPA} from 1.0 g L^{-1} to 0.1 g L^{-1} is a slight increase in D_A. This could be interpreted as a slight shrinking of the hydrodynamic radius of the scatterers, which would mean that inter-molecular interactions are already present at such a low concentration, and that we are not purely measuring the form factor at this q. The latter aligns with a bottlebrush morphology of the scatterers.

Having established the robustness with respect to changes in θ, c_s, and c_{gPA} of at least the faster mode (A), we now turn to the influence of added poly(cation) pD^{32} and pD$^{1\mathrm{k}}$. Scattering of either of the pure poly(cation) solutions (no bottlebrushes added) presents a somewhat mystifying picture, which is due to non-ideal sample composition. In particular, aqueous solutions of 0.1 g L^{-1} pD^{32} at 0.5 M NaCl seems to decay much *slower* than the corresponding samples of pD$^{1\mathrm{k}}$, which is evident in the rightmost panel of Figure 4.10, as well as in the (apparent) D in Table 4.3. Our interpretation is that the relevant diffusive mode of pD^{32} is relegated to the very early data points in the correlation, thus invisible. The fitted decay is hard to explain, and unlikely to result from impurities, given that the decay is neatly mono-exponential. For pD$^{1\mathrm{k}}$, D_A translates to a very reasonable R_H of 24 nm for pD at a degree of polymerization of around 10^3.[33]

The two gPA/pD complexes present very different correlations. Addition of pD$^{1\mathrm{k}}$ to gPA resulted in a modest (30%) decrease in scattering intensity, and gave a correlation function with shape and two decay rates similar to the uncomplexed gPA. In sharp contrast, presence of the smaller pD^{32} resulted in a decay that could be completely described by a single exponential decay, and a more marked decrease in scattered intensity of 80%.

We interpret the former observation as the scattering of largely uncomplexed gPA and pD left in the solution, with some pD$^{1\mathrm{k}}$ present in the precipitated fibres. Scattering of the sample with bottlebrush and pD^{32} is more likely to reflect an actual complex: the apparent D_A increased with 25%, and the second and potential further slow modes were completely suppressed. We interpret this as evidence of effective complex formation: the outer shell of the bottlebrushes have a lower monomer density, which allows poly(cations) to diffuse inside the brush, as long as their R_G is small enough. The result is a slight shrinking of the bottlebrush: assuming diffusive

Table 4.3: Fitted decay rates (presented as apparent diffusion coefficients, $D = \Gamma_i q^{-2}$ of the intensity autocorrelation functions given in Figure 4.10. A sum of two exponential decays was used in all cases, safe for those samples in which pD[32] – for the latter, a fit to a single decay described all data above the noise floor.

Complex	c_{gPA}	c_s (M)	D_A ($\mathrm{m^2\ s^{-1}}$)	D_B ($\mathrm{m^2\ s^{-1}}$)
gPA†	1	0.1	$1.0{\cdot}10^{-11}$	$1.7{\cdot}10^{-12}$
gPA	0.1	0.011	$0.79{\cdot}10^{-11}$	$3.6{\cdot}10^{-13}$
gPA	0.1	0.1	$0.77{\cdot}10^{-11}$	$2.9{\cdot}10^{-13}$
gPA	0.1	0.5	$0.78{\cdot}10^{-11}$	$1.4{\cdot}10^{-12}$
pD[32]	0.1	0.5	$0.11{\cdot}10^{-11}$	-
pD[1k]	0.1	0.5	$1.5{\cdot}10^{-11}$	$5.1{\cdot}10^{-13}$
gPA/pD[32]	0.1	0.5	$1.0{\cdot}10^{-11}$	-
gPA/pD[1k]	0.1	0.5	$1.0{\cdot}10^{-11}$	$0.98{\cdot}10^{-12}$

scaling of the fitted decay rates, the Stokes-Einstein R_H decreases from 31 to 24 nm.

Thus, DLS provides us with a preliminary account of complexation of bottlebrushes with a flexible counter-polyelectrolyte. To further establish the R_G-selectivity of complexation to a bottlebrush, we recommend to study the scattering of soluble complexes with a wider range of molecular weights of the flexible poly(cation). In particular, the transition from complexation to non-complexation should occur when the R_G of the flexible partner is on the order of the inter-side-chain distance at the depth at which the latter species intercalate into the brush. On a final note, we would urge towards the use of poly(cations) with a neutral water-soluble block, as its complexes with the bottlebrush will not precipitate.

4.4 Conclusion

In this Chapter, we paved the way towards the study of polyelectrolyte complexes with a semiflexible poly(anion) of bottlebrush architecture. We presented a synthetic pathway starting from a UV-mediated RAFT polymerization of a hydroxy-functional acrylamide, followed by a side-chain grafting-from using ATRP of *tert*-butyl acrylate. The intermediate is de-esterified to yield a backbone chain densely grafted with poly(acrylic acid). Gelation during grafting was prevented by selecting conditions that promote catalyzed radical termination, which was confirmed by the absence of cross-linked structures in chromatography (SEC) as well as in microscopy (AFM).

By quantifying the contour length distribution using automated image analysis on AFM micrographs, we confirmed that the poly(*tert*-butyl acrylate)-grafted molecule possessed a structure-conform stiffness, as well as the dispersity suggested by SEC.

Finally, we carried out a preliminary study of the conformation of the deprotonated poly(acrylic acid)-grafted bottlebrushes in both presence and absence of a poly(cation). We report that at the low q-range associated with DLS, no evidence of rigid rotation or internal (bending) modes is evident. Instead, the non-complexed bottlebrush displays two decay rates that scale robustly with q^2, and have diffusion coefficients on the order of, respectively, 10^{-12} and 10^{-11} m^2 s^{-1}. While scattering of non-stoichiometric (soluble) complexes with high-molecular weight pD did not result in strong evidence for a conformational change, small-molecular weight fragments of pD resulted in a change towards a monoexponential decay suggestive of a decrease in hydrodynamic radius.

Unlike flexible polyelectrolytes, the high side-chain density of bottlebrushes favours complexes with smaller counter-polyelectrolytes. Furthermore, the effect of said complexation is a slight decrease in the dimensions of the grafted molecule, which is an effect of the tempered electrostatics as a result of neutralized polymeric charge. To conclude, the authors await with keen anticipation the future studies of the behaviour of polyelectrolytes complexes in which one or both partners are semiflexible, in particular with regard to their linear and non-linear viscoelasticity.

Bibliography

[1] A. Kirillova, T. R. Yeazel, D. Asheghali, S. R. Petersen, S. Dort, K. Gall, and M. L. Becker, "Fabrication of Biomedical Scaffolds Using Biodegradable Polymers," *Chemical Reviews*, 2021.

[2] B. D. Ratner, "Biomaterials: Been There, Done That, and Evolving into the Future," *Annual Review of Biomedical Engineering*, vol. 21, pp. 171–191, 2019.

[3] W. C. Blocher and S. L. Perry, "Complex coacervate-based materials for biomedicine," *Wiley Interdisciplinary Reviews: Nanomedicine and Nanobiotechnology*, vol. 9, no. 4, pp. 76–78, 2017.

[4] E. Spruijt, M. A. Cohen Stuart, and J. Van Der Gucht, "Linear viscoelasticity of polyelectrolyte complex coacervates," *Macromolecules*, vol. 46, no. 4, pp. 1633–1641, 2013.

[5] E. Spruijt, F. A. Leermakers, R. Fokkink, R. Schweins, A. A. Van Well, M. A. Cohen Stuart, and J. Van Der Gucht, "Structure and dynamics of polyelectrolyte

complex coacervates studied by scattering of neutrons, X-rays, and light," *Macromolecules*, vol. 46, no. 11, pp. 4596–4605, 2013.

[6] E. Spruijt, J. Sprakel, M. Lemmers, M. A. Stuart, and J. Van Der Gucht, "Relaxation dynamics at different time scales in electrostatic complexes: Time-salt superposition," *Physical Review Letters*, vol. 105, no. 20, 2010.

[7] E. Spruijt, A. H. Westphal, J. W. Borst, M. A. Cohen Stuart, and J. Van Der Gucht, "Binodal compositions of polyelectrolyte complexes," *Macromolecules*, vol. 43, no. 15, pp. 6476–6484, 2010.

[8] Y. Liu, H. H. Winter, and S. L. Perry, "Linear viscoelasticity of complex coacervates," *Advances in Colloid and Interface Science*, vol. 239, pp. 46–60, 2017.

[9] M. Yang, J. Shi, and J. B. Schlenoff, "Control of Dynamics in Polyelectrolyte Complexes by Temperature and Salt," *Macromolecules*, vol. 52, no. 5, pp. 1930–1941, 2019.

[10] A. Basu, D. G. Bobrovnikov, and T. Ha, "DNA mechanics and its biological impact," *Journal of Molecular Biology*, vol. 433, no. 6, p. 166861, 2021.

[11] K. A. Erk, K. J. Henderson, and K. R. Shull, "Strain Stiffening in Synthetic and Biopolymer Networks," *Biomacromolecules*, vol. 11, pp. 1358–1363, 2010.

[12] C. Storm, J. J. Pastore, F. MacKintosh, T. C. Lubensky, and P. A. Janmey, "Nonlinear elasticity in biological gels," *Nature*, vol. 435, pp. 191–194, 2005.

[13] A. Brunet, C. Tardin, L. Salomé, P. Rousseau, N. Destainville, and M. Manghi, "Dependence of DNA Persistence Length on Ionic Strength of Solutions with Monovalent and Divalent Salts: A Joint Theory-Experiment Study," *Macromolecules*, vol. 48, no. 11, pp. 3641–3652, 2015.

[14] W. F. Daniel, G. Xie, M. Vatankhah Varnoosfaderani, J. Burdyńska, Q. Li, D. Nykypanchuk, O. Gang, K. Matyjaszewski, and S. S. Sheiko, "Bottlebrush-Guided Polymer Crystallization Resulting in Supersoft and Reversibly Moldable Physical Networks," *Macromolecules*, vol. 50, no. 5, pp. 2103–2111, 2017.

[15] G. R. Fulmer, A. J. Miller, N. H. Sherden, H. E. Gottlieb, A. Nudelman, B. M. Stoltz, J. E. Bercaw, and K. I. Goldberg, "NMR chemical shifts of trace impurities: Common laboratory solvents, organics, and gases in deuterated solvents relevant to the organometallic chemist," *Organometallics*, vol. 29, no. 9, pp. 2176–2179, 2010.

[16] S. Li, G. Han, and W. Zhang, "Photoregulated reversible addition-fragmentation chain transfer (RAFT) polymerization," *Polymer Chemistry*, vol. 11, no. 11, pp. 1830–1844, 2020.

[17] G. Moad and C. Barner-Kowollik, *The Mechanism and Kinetics of the RAFT Process: Overview, Rates, Stabilities, Side Reactions, Product Spectrum and Outstanding Challenges.* 2008.

[18] R. W. Lewis, R. A. Evans, N. Malic, K. Saito, and N. R. Cameron, "Ultra-fast aqueous polymerisation of acrylamides by high power visible light direct photoactivation RAFT polymerisation," *Polymer Chemistry*, pp. 60–68, 2017.

[19] H. Wang, Q. Li, J. Dai, F. Du, H. Zheng, and R. Bai, "Real-time and in situ investigation of living/controlled photopolymerization in the presence of a trithiocarbonate," *Macromolecules*, vol. 46, no. 7, pp. 2576–2582, 2013.

[20] R. N. Carmean, T. E. Becker, M. B. Sims, and B. S. Sumerlin, "Ultra-High Molecular Weights via Aqueous Reversible-Deactivation Radical Polymerization," *Chem*, vol. 2, no. 1, pp. 93–101, 2017.

[21] G. Xie, M. R. Martinez, W. F. Daniel, A. N. Keith, T. G. Ribelli, M. Fantin, S. S. Sheiko, and K. Matyjaszewski, "Benefits of Catalyzed Radical Termination: High-Yield Synthesis of Polyacrylate Molecular Bottlebrushes without Gelation," *Macromolecules*, vol. 51, no. 16, pp. 6218–6225, 2018.

[22] J. G. Beton, R. Moorehead, L. Helfmann, R. Gray, B. W. Hoogenboom, A. P. Joseph, M. Topf, and A. L. Pyne, "TopoStats – A program for automated tracing of biomolecules from AFM images," *Methods*, 2021.

[23] A. L. Pyne and J. G. Beton, "TopoStats," *https://github.com/AFM-SPM/TopoStats*, 2021.

[24] S. S. Sheiko, F. C. Sun, A. Randall, D. Shirvanyants, M. Rubinstein, H. I. Lee, and K. Matyjaszewski, "Adsorption-induced scission of carbon-carbon bonds," *Nature*, vol. 440, no. 7081, pp. 191–194, 2006.

[25] R. Pecora, "Dynamic light scattering studies of rodlike particles," *Pure and Applied Chemistry*, vol. 56, no. 10, pp. 1391–1395, 1984.

[26] B. J. Berne and R. Pecora, *Dynamic Light Scattering with Applications to Chemistry, Biology, and Physics.* Dover Publications, dover ed., 2000.

[27] T. Maeda and S. Fujime, "Effect of Filament Flexibility on the Dynamic Light-Scattering Spectrum with Special Reference to fd Virus and Muscle Thin Filaments," *Macromolecules*, vol. 14, no. 3, pp. 809–818, 1981.

[28] R. Pecora, "DNA: A model compound for solution studies of macromolecules," *Science*, vol. 251, no. March 1991, pp. 893–898, 1991.

[29] L. Harnau, R. G. Winkler, and P. Reineker, "Dynamic structure factor of semiflexible macromolecules in dilute solution," *Journal of Chemical Physics*, vol. 104, no. 16, pp. 6355–6368, 1996.

[30] R. Götter, K. Kroy, E. Frey, M. Bärmann, and E. Sackmann, "Dynamic light scattering from semidilute actin solutions: A study of hydrodynamic screening, filament bending stiffness, and the effect of tropomyosin/troponin-binding," *Macromolecules*, vol. 29, no. 1, pp. 30–36, 1996.

[31] T. B. Liverpool and A. C. Maggs, "Dynamic scattering from semiflexible polymers," *Macromolecules*, vol. 34, no. 17, pp. 6064–6073, 2001.

[32] G. Ferrand-Drake Del Castillo, R. L. Hailes, and A. Dahlin, "Large Changes in Protonation of Weak Polyelectrolyte Brushes with Salt Concentration-Implications for Protein Immobilization," *Journal of Physical Chemistry Letters*, vol. 11, no. 13, pp. 5212–5218, 2020.

[33] L. N. Andreeva, S. V. Bushin, M. A. Bezrukova, T. N. Nekrasova, R. T. Imanbaev, V. D. Pautov, O. V. Nazarova, Y. I. Zolotova, and E. F. Panarin, "Conformation properties of poly(N,N-dimethylaminoethyl methacrylate) macromolecules in various solvents," *Russian Journal of Applied Chemistry*, vol. 85, no. 3, pp. 417–425, 2012.

Chapter 5

Rapid and quantitative de-*tert*-butylation for poly(acrylic acid) block copolymers and influence on relaxation of thermoassociated transient networks

Abstract

The synthesis of charged polymers often requires the polymerization of protected monomers, followed by a polymer-analogous reaction to the polyelectrolyte product. We present a mild, facile method to cleave *tert*-butyl groups from poly(*tert*-butyl acrylate) blocks that yields poly(acrylic acid) (pAA) blocks free of traces of the ester. The reaction utilizes a slight excess of HCl in hexafluoroisopropanol (HFIP) at room temperature, and runs to completion within four hours. We compare deprotection in HFIP with the common TFA/DCM method, and show that the latter does not yield clean pAA. We show the effect of complete *tert*-butyl cleavage on a ABA triblock copolymer, where poly(*N*- isopropylacrylamide) (pNIPAM) is A and pAA is B, by means of viscosimetry, DLS and SAXS on solutions above overlap. The pNIPAM blocks dehydrate, and their increased self-affinity above the lower critical solution temperature (LCST) results in network formation by the triblocks. This manifests itself as an increase in viscosity and a slowing-down of the first-order correlation function in light scattering. However, this stickering effect manifests itself exclusively when the pAA block is *tert*-butyl-free. Additionally, SAXS shows that the conformational properties of *tert*-butyl free pAA copolymers are markedly different from those with residual esters. Thus, we illustrate a surprising effect of hydrophobic impurities that acts across blocks, and assert the usefulness of HCl/HFIP in pAA synthesis.

This chapter is published eponymoulsy as A. D. Filippov, I. A. van Hees, R. Fokkink, I.K. Voets, M. M. G. Kamperman, *Macromolecules*, 2018, **51**, 8316-8323

5.1 Introduction

Acrylic acid (AA) is the smallest unsaturated carboxylic acid, and can be polymerized radically. By virtue of the carboxylic moiety, the resulting polymers are polyelectrolytes and have a pH-dependent charge and H-bonding capacity. In copolymers, AA is used to tailor responsive behavior of other polymeric building blocks, such as the swelling of hydrogels[1, 2] and the lower critical solution temperature (LCST) of poly(*N*-isopropylacrylamide) (pNIPAm) and its copolymers.[3] pAA is one of the most studied polyanions in polyelectrolyte complexes, owing to its ability to form complexes with many polycations.[4, 5]

In radical polymerizations, acrylic acid is unusually inclined to transfer reactions to solvent,[6] transfer to polymer,[7] and formation of Michael dimers.[8] These side reactions result in diminished control over linearity, molecular weight distribution, and end-group fidelity of the polymer products.[8, 9] There are many reports that detail pAA synthesis with the help of controlled radical polymerization (CRP) techniques, in particular reversible addition-fragmentation chain transfer (RAFT).[6, 10, 11] Chain transfer agents are known to reduce branching and termination by ensuring a low concentration of active radicals.[7] Nonetheless, it is difficult to prepare strictly linear polymers directly from AA due to its high rate and extensive repertoire of side reactions, and branching is often overlooked in reports on pAA.[6, 8] Given the difficulties of direct polymerization of AA, pAA is often made in a two-step process starting from a precursor monomer that is less affected by transfer reactions, followed by a polymer-analogous reaction that yields pAA.

A canonical two-step method relies on the ester of acrylic acid and *tert*-butanol, the latter acting analogously to a protecting group. *tert*-Butyl acrylate (*t*BuAc) can be polymerized by anionic or radical means, and the resulting polymer is deesterified into pAA under acidic conditions, trifluoroacetic acid in DCM (TFA/DCM) being especially common.[12–17] However, even a strong molar excess yields pAA with at most 99.5% liberated carboxylic acid, the rest being still esterified with *tert*-butanol.[6, 14] The incomplete cleavage remains unaddressed, even though residual *tert*-butyl groups can affect polymer properties. Foreseeable effects are an increase of surface pressure at water-apolar interfaces and a greater tendency to form complexes through hydrophobic interactions, since the resulting structures are comparable to hydrophobically modified pAA. Thus, a means of obtaining ester-free pAA from p*t*BuAc is desirable.

In the present work, we report a cleavage reaction that yields quantitatively de-*tert*-butylated pAA rapidly, based on the work of Palladino and co-workers.[18] We apply the method to the synthesis of a triblock copolymer with a monomer that is representative[1, 19] of the use of pAA in literature, pNIPAm. Full *tert*-butyl ester cleavage

is shown by NMR. To assert the necessity of complete deprotection of p*t*BuAc precursors, we show that the ubiquitous TFA/DCM conditions yield polymers with markedly distinct flow and conformational properties, as witnessed by viscosity, dynamic light scattering (DLS) and small-angle X-ray scattering measurements (SAXS).

5.2 Experimental section

Materials 2,2'-Azobis(2-methylpropionitrile) (AIBN, 98%), *N*-isopropylacrylamide (NIPAm, 97%), *tert*-butyl acrylate (*t*BuAc, contains 10-20 ppm monomethyl ether hydroquinone as inhibitor, 98%), trioxane ($\geqslant$99.9%), trifluoroacetic acid (TFA $\geqslant$99%), concentrated HCl (37% solution in water), and dioxane (anhydrous, 99.8%) were obtained from Sigma-Aldrich, Germany, and used without further purification unless noted otherwise. NIPAm was recrystallized twice from a mixture of hexane and acetone. *t*BuAc was passed over a short column of Al_2O_3 to remove the inhibitor. AIBN was recrystallized thrice from MeOH. Bis(2-methylpropionic acid)trithiocarbonate[20, 21] (BMAT) and BMAT-terminated pNIPAm[21] were synthesized as described in literature, with NMR and SEC characterization described in Table 5.A.1. Hexafluoroisopropanol (HFIP, AR), dichloromethane (DCM, AR), tetrahydrofuran (THF, HPLC-grade), and methanol (MeOH, HPLC) were obtained from Biosolve, France.

Synthesis of pNIPAm-*b*-p*t*BuAc-*b*-pNIPAm A Schlenk flask was charged with a solution of BMAT-terminated $pNIPAm_{24}$ (0.581 g, 0.104 mmol), *t*BuAc (5.3 g, 41.4 mmol), AIBN (3.4 mg, 0.020 mmol) and trioxane (0.372 g, 4.14 mmol) in dioxane (21 mL), and was subjected to five freeze-pump-thaw cycles. The solution was magnetically stirred at 70 °C for 45 min, after which the polymerization was stopped by admitting atmosphere into the flask while cooling on an ice bath. The material was precipitated thrice in ice-cold MeOH:water 3:1 and dried under high vacuum.

TFA/DCM deprotection of pNIPAm-*b*-p*t*BuAc-*b*-pNIPAm pNIPAm-*b*-p*t*BuAc-*b*-pNIPAm (1.05 g, 0.023 mmol) was dissolved in DCM (50 mL) in a round-bottomed flask, to which was added 6 equivalents of TFA (4.2 g, 39 mmol) with respect to the amount of *t*Bu units. The mixture was stirred for 72 h at room temperature, the precipitated product was washed with fresh DCM, and extensively dried under high vacuum. The dry polymer was dispersed in water by sonication and titrated with an NaOH solution until the solution was neutral. Water was removed by freeze drying. This yielded pNIPAm-(pAA-*co*-p*t*BuAc)-*b*-pNIPAm as a white, fluffy powder.

HCl/HFIP deprotection of pNIPAM-*b*-p*t*BuAc-*b*-pNIPAm pNIPAm-*b*-p*t*BuAc-*b*-pNIPAm (3.5 g, 0.093 mmol) was dissolved in HFIP (314 mL) in a round-bottomed flask, to which concentrated HCl 37% (2.6 mL, 31.4 mmol) was added, 1.3 equivalents with respect to the amount of *t*Bu units. After 4 h, the mixture was stripped of volatiles

and the dry polymer was dispersed in water and titrated with an NaOH solution until the solution was neutral. A slight cloudiness was removed by centrifugation at 15000g, and the supernatant was dehydrated by freeze drying. pNIPAm-*b*-pAA-*b*-pNIPAm was recovered as a white fluffy powder.

Polymer characterization ^{1}H- and ^{13}C-NMR measurements were performed on a Bruker AVANCE 400 spectrometer. Fourier transform infrared absorption spectra were collected on a Bruker PLATINUM ATR mounted into a TENSOR spectrometer on powdered sample. A background was taken and subtracted from the spectra, followed by baseline correction and transformation from transmission to absorption.

Size-exclusion chromatography Size exclusion chromatography (SEC) of pNIPAm and its copolymers with p*t*BuAc was done on a Agilent 1200 HPLC equipped with a PLgel 5μm Mixed-D column with RI detection, calibrated with polystyrene standards, and HPLC-grade THF as eluent. The presence of pNIPAm blocks complicates the analyses due to column-analyte interactions. The problem is somewhat remedied in an aqueous SEC system on corresponding de-*tert*-butylated products. Aqueous size exclusion chromatography of pAA copolymers was done in an aqueous buffer of 0.01 M Na_2HPO_4/NaH_2PO_4 with 0.1 M $NaNO_3$ on an Agilent 1260 Infinity II HPLC equipped with a Waters Ultrahydrogel500 column for molecular weight analysis. Analytes were detected with a refractive index detector and by UV adsorption.

Trithiocarbonate cleavage with hydrazine In adaptation of a previous report,[22] sodium salt of BMAT-derived triblock pNIPAm-*b*-pAA-*b*-pNIPAm (0.100 g, 3.34 μmol of trithiocarbonates) was dissolved in water (11 mL), to which was added 5 equivalents of hydrazine (1 μL, 16.7 μmol). The mixture was stirred at room temperature for 72 h, and an aliquot was diluted 1:3 with 0.01 M Na_2HPO_4/NaH_2PO_4 with 0.1 M $NaNO_3$, which was analyzed with SEC over an Agilent PL AquaGel-OH 8 μm column and compared with an aliquot of non-treated sample.

DLS of triblock solutions DLS measurements on triblock networks were performed in the manner described by Bohdan et al.[23] An ALV light scattering apparatus equipped with a 632.8 nm JDSU 1145P laser and a LSE-5004 correlator was used. Temperature was controlled by means of a Julabo water bath. DLS measures the electric field autocorrelation function $g_2(t) = \langle I(0)I(t)\rangle/\langle I^2\rangle$, from which the normalized first-order correlation function $g_1(t)$ is obtained:

$$g_1(t) = \beta^{-1/2}\sqrt{g_2(t)-1} \tag{5.1}$$

in which β is a geometry-dependent constant close to unity. We describe $g_1(t)$ by a two-mode stretched exponential decay:

$$g_1(t) = \sum_{i=f,s} A_i \exp(-\frac{t_i^{\alpha}}{\tau_i}) \tag{5.2}$$

where τ is the exponential decay time and α is the stretch parameter. The latter characterises the width of the decay time distribution, with $\alpha_i = 1$ corresponding to a simple exponential decay and smaller values to a more stretched shape, and thus a broader decay time distribution. The subscripts f and s refer to, respectively, the fast and slow modes that we observe for all relaxations.[24]

Samples were made by addition of 1 mL water to 292 mg of polymer, and were filtrated over 0.2 μm regenerated cellulose (RC) syringe filters after dissolution. Correlation curves were recorded for times between 3000 and 10000 s to ensure full decay of $g_1(t)$, with higher temperatures resulting in slower decays.

Rheology Rheological measurements were recorded on an Anton Paar MCR-301, using a 1 mL Couette geometry and temperature control by a Peltier system. Evaporation was avoided by the use of a tetradecane-filled solvent trap. Viscosities were measured by monitoring stress as a function of shear rate between 0.01 and 1000 s^{-1}.

Small-angle X-ray scattering of triblock solutions Small-angle X-ray scattering experiments were performed on a SAXSLAB Ganesha 300 XL set-up with a GeniX-Cu ultra low divergence source with a wavelength of 1.54 $Å^{-1}$ and a flux of 10^8 s^{-1}, and a Pilatus 300K silicon pixel detector with 487x619 pixels of 172x172 μm^2. Temperature was controlled between 20 and 60 °C with a Julabo temperature controller. Three detector distances were used, resulting in a q-range of 0.001 to 2 $Å^{-1}$. Aqueous 292 mg mL^{-1} samples were introduced into 2 mm quartz capillaries, heated to 60 °C, equilibrated for 2 hours, then measured for 1800s at three different detector distances. This was repeated for 40 and 20 °C. The diffraction patterns were azimuthally averaged and intensities were corrected for transmission, sample thickness and detector distance. Finally, scattering from water-filled capillaries corrected in the same fashion was subtracted from the scattering of triblock solutions.

5.3 Results and discussion

We prepare pNIPAm-*b*-pAA-*b*-pNIPAm (NAN) triblock copolymers from pNIPAm-*b*-*t*BuAc-*b*-pNIPAm (NTN) precursors, as shown in Figure 5.1, and further detailed in Appendix A (Figures 5.A.1,5.A.2). One common *t*Bu-carrying precursor N_{24}-T_{330}-N_{24}, where N_{24} denotes a pNIPAm block length of 24 monomers and T_{330} denotes a p*t*BuAc block length of 330 monomers, serves to compare two acidic ester cleavage reactions: stirring with 6 equivalents of TFA in DCM for 72h and with 1.3 equivalents of HCl in HFIP for 4h. The times are sufficiently long to preclude any further reaction. For TFA/DCM, we choose conditions similar to previous reports on pAA synthesis[12–17] to allow comparison to a situation that is typical in the field.

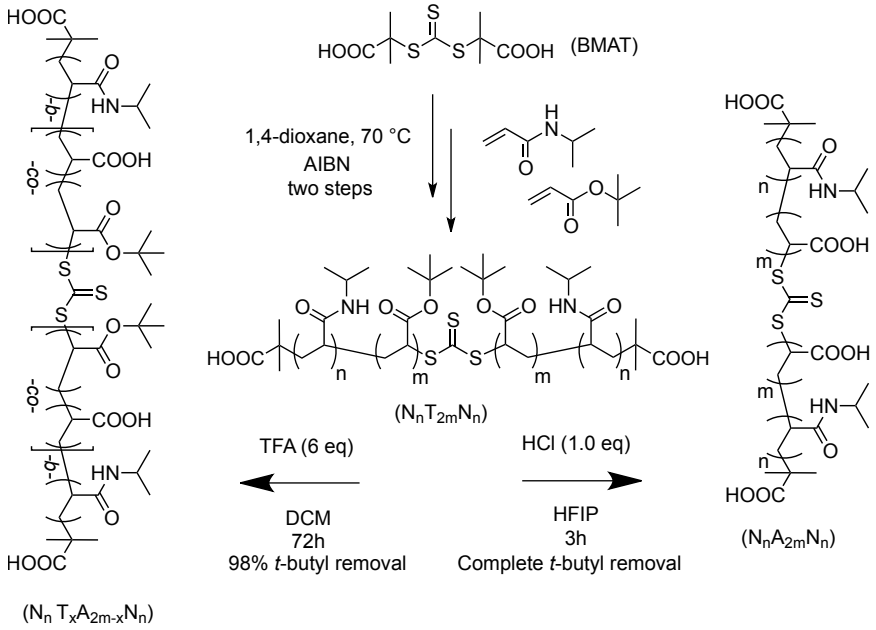

Figure 5.1: Acidic de-*tert*-butylation of the p*t*BuAc block in an ABA copolymer with pNIPAm using (left) TFA in DCM and (right) dilute stoichiometric HCl in HFIP. Characteristic degrees of *t*-butoxy group removals are given as percentages.

NMR spectroscopy on aliquots from the reaction mixtures in MeOD shows resonances characteristic of the NIPAm pendant groups at 1.16 and 3.97 ppm, as seen in the NMR spectra of Figure 5.2a. Contributions of the *t*Bu peak appear at 1.47 and 1.48 ppm, as the dominant peak in NTN precursor, and as a well-noticeable contribution for the TFA-deprotected NAN, even after 72h. Contrarily, in the HCl-treated case, the residual *t*Bu peak is sufficiently small to be indistinguishable from the tacticity features of the backbone protons, which are well-resolved in MeOD. Save for the resonances attributed to residual *tert*-butyl, the polymeric contributions to the spectra are identical, indicating no other changes to the chemical structure than de-*tert*-butylation.

In Figure 5.2b, the resonances of backbone and *t*Bu are enlarged, robustly confirming the disappearance of the latter in the case of HCl/HFIP after 3h with respect to the tacticity features. We note that the often-used D_2O does not provide an adequate environment for the *t*Bu groups to give a sharp signal, and thus leads one to underestimate its presence.

Deconvolution of the spectra between 1.4 and 1.8 ppm allows to separate the *t*Bu contribution from the backbone singlets by fitting each peak with a Gaussian-Lorentzian function. Figure 5.2c shows a representative case. A comparison of the *N*-isopropyl methine signal at 3.97 ppm to the *t*Bu contribution at 1.47 ppm gives the deprotection efficiency ϕ_D according to

$$\phi_D = 1 - \frac{\frac{1}{9} A_{t\mathrm{Bu}}}{A_{Nim}} \frac{\mathrm{DP_N}}{\mathrm{DP_T}} \tag{5.3}$$

where $A_{t\mathrm{Bu}}$ and A_{Nim} are the integrals under the deconvoluted *t*Bu contributions and the *N*-isopropyl methine signals, and DP is the degree of polymerization of the block denoted in subscript. This procedure thus provides accurate values for ϕ_D, even in cases where the area under the *t*Bu region is dominated by backbone signals.

Given the improved rate and extent of the reaction, we strongly recommend deprotection with HCl/HFIP above TFA/DCM, with deprotection efficiencies of >99.9% for HCl/HFIP and 90-98% for TFA/DCM. We summarize the deprotection efficiencies ϕ_D of the two methods in Table 5.1, ϕ_D. The entries marked with an asterisk are used for a comparison of flow properties and DLS relaxation times (*vide infra*). As seen in Table 5.1, HCl/HFIP achieves full *tert*-butyl removal down to 1.0 equivalents of HCl. We note that the polymeric contributions to the NMR spectra of all HCl/HFIP-derived products were identical for all acid loadings. Additionally, Table 5.1 shows deprotection and aqueous SEC characterization data for runs on further NAN structures with slightly varied block lengths. FT-IR data are given in Appendix A (Figure 5.A.3).

We use aqueous SEC to confirm the triblock identity of our compounds, and

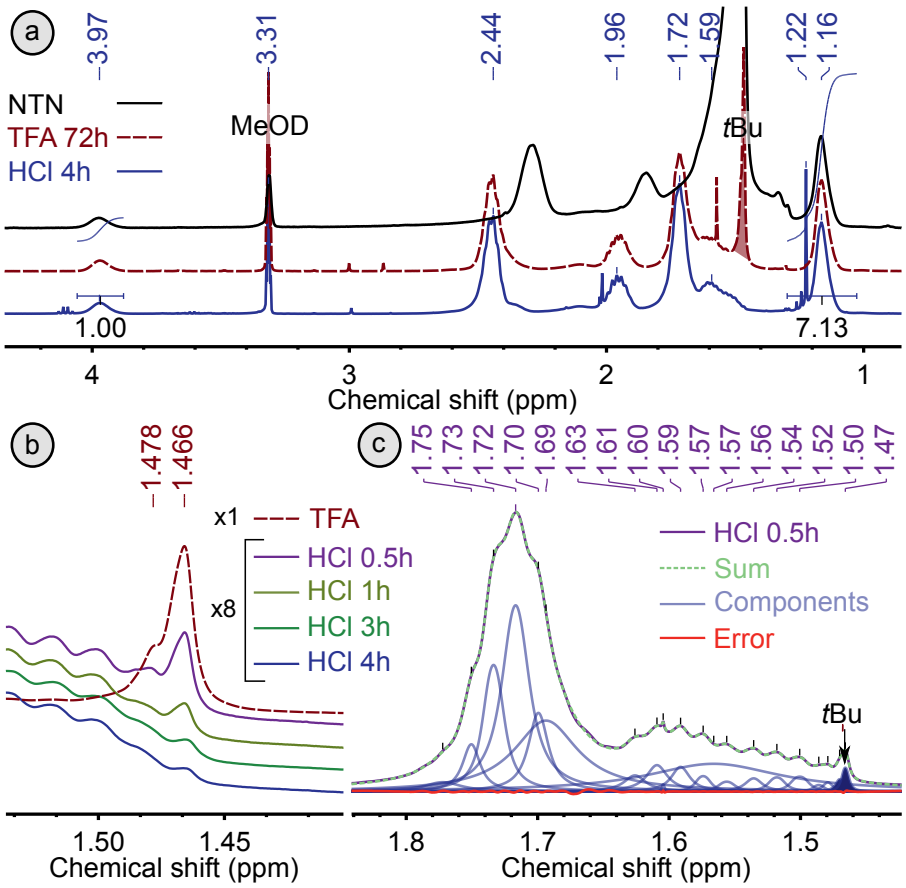

Figure 5.2: (a) ^{1}H-NMR spectra of MeOD solutions of a (top) *t*BuAc copolymer with pNIPAm, (middle) product of deprotection with 6 eq. TFA in DCM, and (bottom) crude sample of deprotection mixture with 1.3 eq. HCl in HFIP. (b) Enlarged regions of crude samples in MeOD of deprotection with TFA in DCM after 72h and with HCl in HFIP after 0.5h, 1h, 3h and 4h. Note that the HCl/HFIP spectra are inflated eight times with respect to the TFA/DCM spectrum, after normalization to the pNIPAm methine peak at 3.9 ppm. (c) Deconvolution of a spectrum taken on the deprotection in HCl/HFIP after 0.5h. The components corresponding to *tert*-butyl protons are filled.

Table 5.1: Molecular weights in kDa and deprotection efficiencies of NAN copolymers. Block lengths are based on theoretical molecular weight M_{th} that is based on monomer conversion. M_n and Đ are calculated from SEC traces after elution in 0.01 M aqueous phosphate buffer at pH 7 with 0.1 M $NaNO_3$. Entries marked with an asterisk are used further on in a comparative study of flow behavior, DLS relaxation times and SAXS.

	Polymer structure	M_{th}	M_n	Đ	Treatment	ϕ_D
	N_{26}-(A_{312}-T_5)-N_{26}	29.0	14.5	1.47	TFA 6 eq	98.4%
	N_{25}-A_{362}-N_{25}	32.5	29.0	1.52	HCl 1.2 eq	>99.9%
	N_{36}-A_{220}-N_{36}	24.3	26.8	1.59	HCl 1.0 eq	>99.9%
*	N_{24}-(A_{297}-T_{33})-N_{24}	29.5	47.4	1.37	TFA 6 eq	90.1%
*	N_{24}-A_{330}-N_{24}	29.2	44.7	1.43	HCl 1.3 eq	>99.9%

therefore the stability of the trithiocarbonate bond under conditions of deprotection and subsequent hydrolysis. We find similar values of M_n for both TFA- and HCl-deprotected species, as can be seen in Table 5.1. Additionally, we intentionally cleaved a sample of N_{24}-A_{330}-N_{24} using hydrazine.[22] Treatment with hydrazine resulted in a discoloration of the sample and a reduction of M_n by a factor of two, as shown in Figure 5.A.4. Thus, the triblocks are quantitatively cleavable, which shows that the trithiocarbonate is stable, even after deprotection and neutralization to pH 7.

We argue that two factors improve the p*t*BuAc de-esterification efficiency of HCl/HFIP with respect to TFA/DCM. DCM is not a solvent for pAA, which prevents contact between the partially deprotected intermediates (essentially pAA/p*t*BuAc copolymers) and the acidic medium. In addition, carboxylates form dimers in apolar environments,[25] further decreasing contact. Our results are not meant to capture the respective contributions of both factors, however, it is clear that TFA/DCM cannot be recommended for the synthesis of highly defined pAA. Because HFIP does not precipitate the product and since HCl is a non-carboxyl acid, both issues are not at play for HCl/HFIP de-*tert*-butylation.

Literature abounds with reports on properties of pAA (co)polymers derived from p*t*BuAc.[14, 26] We now turn to the question whether *tert*-butyl moieties influence the solution properties of our copolymers strongly, even when present at the level we found for TFA/DCM. To this end, we studied the difference in the DLS relaxation time and viscosity of aqueous solutions above overlap between triblocks cleaved with TFA and HCl, derived from a common NTN precursor, N_{26}-T_{318}-N_{26}. A common NTN precursor ensures a constant chain length between the two polymers. The NTNs employed in the comparison are labelled with an asterisk in Table 5.1. In addition,

SAXS was used to inquire into structural differences in HCl/HFIP and TFA/DCM products, respectively N_{24}-(A_{297}-T_{33})-N_{24}, where the center block in the latter is the incompletely cleaved p*t*BuAc center block. Additionally, we compared two HCl-deprotected structures of different block lengths, N_{36}-A_{220}-N_{36} and N_{24}-A_{330}-N_{24}.

At a weight concentration of 292 mg mL^{-1} without added salt, all polymers dissolved within two days on a shaking bench. Based on an estimate for R_G of 5 nm taken from DLS measurements of dilute solutions at high salt (data not shown), the overlap concentration is below 90 mg mL^{-1} for all triblocks in demineralized water. Thus, our solutions strongly exceed overlap. When heated to 60 °C, which is well above the bulk LCST for pNIPAm homopolymer around 32 °C, both solutions remain transparent. This is in marked contrast to the rapid increase in turbidity that is observed for diblock solutions with a charged block and an LCST block, where the turbidity increase is attributed to formation of micelles due to the association of pNIPAm blocks above the LCST.[14, 19, 27] In addition to the lack of a turibidty point, we note that our samples show no macroscopic phase separation, in contrast to solutions of pNIPAm homopolymer ,[28] copolymers,[29] and derived hydrogels.[30] We remind the reader than pNIPAm and pAA form complexes at a pH far lower than of these samples. Indeed, the solubility of our structures is wholly consistent with the complete deprotonation of pAA at neutral pH.[19]

We note that the mode of association of *t*Bu-free NAN triblocks above overlap is *not* related to micelle formation, as is reported for telechelic polymers with far longer stickers.[31–34] Solutions of HCl-cleaved N_{24}-A_{330}-N_{24} remain transparent even after being heated to 60 °C for three days, and show a decrease in scattering intensity at 90° when heated to 40 and 60 °C (Figure 5.A.5), precluding micellization. Under identical conditions, the TFA-cleaved N_{24}-(A_{297}-T_{33})-N_{24} solutions develop some turbidity and show occasional spikes in scattering intensity. However, SAXS measurements (*vide infra*) again preclude micellization as a cause. DLS measurements on dilute (5 mg mL^{-1}) triblock solutions show no changes in count rate or correlation times upon heating from room temperature to 60 °C, and thus show no evidence of micellization, due to the very short sticker length and high osmotic pressure due to the charged blocks.

When heated from 15 to 60 °C, a 292 mg mL^{-1} solution of N_{24}-A_{330}-N_{24} shows a strong increase in viscosity, whereas none is visually distinguishable for solutions of N_{24}-(A_{297}-T_{33})-N_{24}. This behavior is quantified in Figure 5.3 (left) by means of rotational rheology in a Couette geometry, where we plot the shear-rate dependent viscosity for both triblocks, at T above and below the bulk LCST of pNIPAm homopolymer. All viscosity curves are characterized by a wide Newtonian range, and the Newtonian viscosity of the sample increased 70-fold for N_{24}-A_{330}-N_{24}, whereas the increase is marginal for the case of N_{24}-(A_{297}-T_{33})-N_{24}.

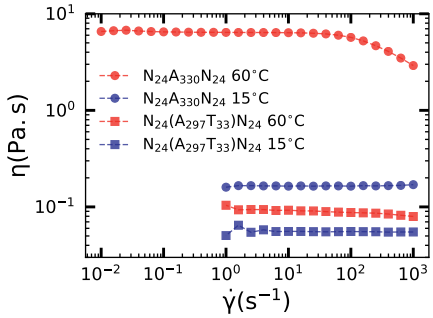

Figure 5.3: Shear rate-dependent viscosity of 292 mg mL^{-1} solutions of N_{24}-(A_{297}-T_{33})-N_{24} (squares) and N_{24}-A_{330}-N_{24} (circles) at 15 °C (blue) and 60 °C (red).

We stress that our solutions, upon heating, neither undergo a macroscopic phase transition nor have a cloud point. We merely perceive the effect of the collapse of pNIPAm as the slowed-down relaxation of a transient network. Exactly the unchanged transparency and volume of the samples allowed us to employ DLS to study differences in relaxation times between the two solutions above overlap, below and above the bulk pNIPAm LCST. In Figure 5.4(a), we show averaged first-order normalized correlation functions $g_1(t)$ for both triblocks at 20, 40 and 60 °C. At all temperatures, the correlation functions eventually decay to zero after sufficiently long measurement times (up to 10000 s).

All measured correlation functions are well described by a sum of two stretched exponentials (Equation 5.2), and thus their relaxation is characterized by one slow and one fast mean relaxation time τ_s and τ_f. The fits are plotted as solid lines in Figure 5.4a, and the relaxation times are plotted against temperature in Figure 5.4b. A third mode in $g_1(t)$ is also seen, but the acquisition of data of sufficient statistics is prohibitively long for samples at high T, as is clear from Figure 5.4a. Since its contribution is only minor, it is neglected in the analysis.

The stretch exponents of the fast mode α_f are very close to unity, and the fast modes are thus exponential. Thus, the fast relaxation times are narrowly distributed. Most of the fast relaxations contribute very little to the overall function, and only in solutions of N_{24}-(A_{297}-T_{33})-N_{24} at 20 °C does the fast mode contribute more than 1% of the signal.

The slow modes exhibit varying degrees of stretching with α_s between 0.76 and 0.95, α_s increasing with temperature. This suggests that the relaxation rates are more narrowly distributed for transient networks in which the associators have a

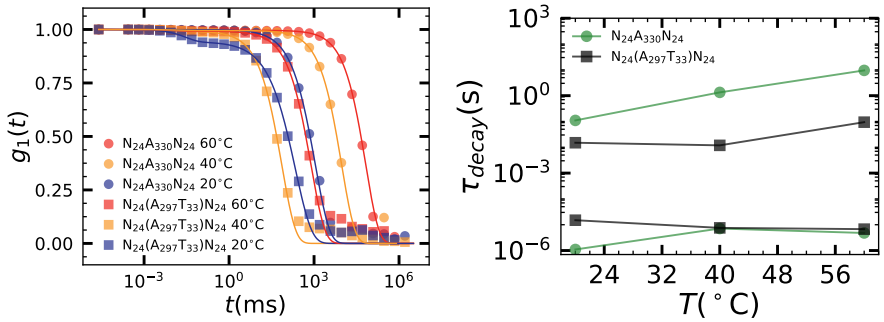

Figure 5.4: (a) First-order correlation functions from DLS on 292 mg mL^{-1} solutions of N_{24}-A_{330}-N_{24} (squares) and N_{24}-(A_{297}-T_{33})-N_{24} (circles) at 20 °C (blue), 40 °C (orange), and 60 °C (red). The lines are fitted using Equation 5.2. (b) Characteristic slow and fast relaxation times τ_s and τ_f as function of temperature as fitted using Equation 5.2. The lines are intended as a guide to the eye.

higher tendency to stick. The dependence of τ_s mirrors the chemistry-dependent thermothickening observed in viscometry. Both the absolute value of τ_s and their temperature variation mode are strongly affected by the chemistry of the middle block. For N_{24}-A_{330}-N_{24}, τ_s is always longer, and increases over more than two orders of magnitude. Its TFA-cleaved counterpart has a more rapid relaxation of the slow mode, and shows only modest growth with temperature.

Three-mode stretched exponential relaxation of $g_1(t)$ in DLS measurements of transient polymer networks has been previously described by other authors,[23, 24] where poly(ethylene glycol) networks were formed by association of aliphatic chains, which were attached to the polymers at either one or both ends, yielding “diblock” or “triblock” structures. The relaxation times of the second mode increased strongly with increasing proportion of triblock structures (thus increasing network connectivity), and is ascribed to increased node residence times. Thus, this connectivity increase is analogous to a temperature increase in our experiment. The τ of the third mode is reported to show an even stronger connectivity dependence[23] and is ascribed to diffusion of associated clusters.

Similarly, we attribute the increase of η and τ_s with T to a prolongation of the mean residence time of pNIPAm stickers in the nodes, driven by a higher segregation tendency. The collective effect of the increased residence time is a slowing down of the transient network. The wavevector q is 0.019nm^{-1}, which means that we are at length scales one order of magnitude beyond the node-node correlations.

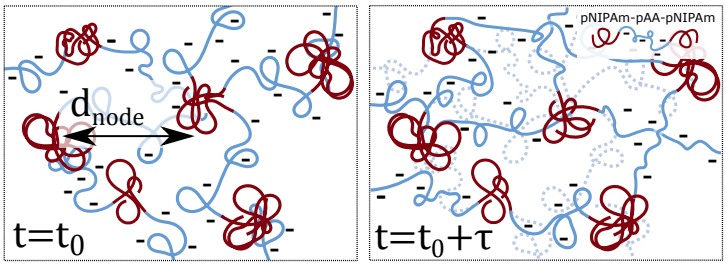

Figure 5.5: Schematic of two snapshots of a cluster of a few chains in a transient network formed by ABA triblock copolymers. Note that in the range studied, temperature and pAA purity do not change the qualitative features of the system: they change only τ, which is the waiting time between the snapshots, and is chosen to be above the node residence time and the decorrelation time of the structure on lengthscales on the order of this box size. The configuration at t_0 is drawn in the rightmost figure as dashed lines. d_{node} is the characteristic internode distance (*vide infra* for its measurement by SAXS). For clarity, the nodes have been portrayed as stationary.

Nonetheless, while τ_s cannot be trivially converted to a residence time, the relaxation time must necessarily increase with residence time.[23] We convey the relaxation of these transient networks in Figure 5.5 — one must realize that the temperature and the extent of deprotection determine the τ over which we would observe relaxation.

It is remarkable that the availability of hydrophobic groups *decreases* the residence time, since it could be argued that the hydrophobic effect would be stronger with the participation of such groups, and thus sticker association more prominent. However, we speculate that the residual esters actually improve compatibility between the pNIPAm and the pAA blocks, resulting in *weakening* the physical crosslinks. Additionally, it could be argued that the coils slightly shrink causing them to overlap less. This is consistent with the lower viscosity of the N_{24}-(A_{297}-T_{33})-N_{24} solution at low temperatures, and more prominent participation of a fast mode at room temperature.

Additional clues for the origin of short sticker residence times for identical pNIPAm moieties connected to more strongly hydrophobically contaminated pAA come from SAXS, which reveals time-averaged density fluctuations, thus structural information rather than τ-dependent observables. Here, we compare the angle-dependent absolute scattering intensities $\frac{d\Sigma}{d\Omega}(q)$ of 292 mg mL^{-1} solutions of the *tert*-butylated N_{24}-(A_{297}-T_{33})-N_{24} and fully liberated triblocks N_{36}-A_{220}-N_{36} and N_{24}-A_{330}-N_{24} at 20, 40 and 60 °C. All scattering intensities are peaked in the vicinity of q^* =0.03 Å^{-1}, as is visible in Figure 5.6. The peaks sharpen and shift to smaller q with T, which suggests

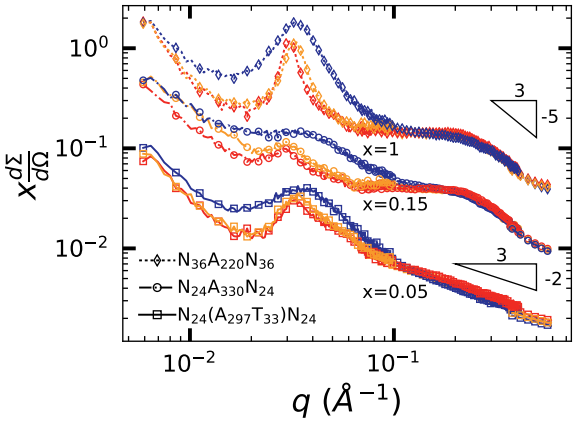

Figure 5.6: X-ray scattering intensity as function of modulus of scattering vector q for 292 mg mL^{-1} solutions of one TFA-deprotected and two HCl-deprotected NAN triblock copolymers at 20, 40 and 60 °C in respectively blue, orange and red (from bottom to top, since the scattering decreases slightly with T). The labels x = n give the scaling factor for the curves, used for better readability. The lines are plotted from the full data, while the marks are plotted only every sixth point.

their origin to be density fluctuations due to increased non-solubility of pNIPAm with a corresponding internode distance d_{node}. Indeed, a change occurs between 20 and 40 °C, in agreement with an LCST of 32°C. We attribute the presence of an internode peak below the LCST to pNIPAm-pNIPAm interactions that have been observed in scattering studies of aqueous pNIPAm before,[35] which note a decrease in excluded volume starting already from 5°C, and a consequent clustering below the LCST.[36]

Upon heating from 20 to 60 °C, the internode distance d_{node} that correspond to $q*$, at which $\frac{d\Sigma}{d\Omega}$ passes through a prominent maximum, increases from 18.5 nm to 20.4 nm for N_{36}-A_{220}-N_{36}. Thus, the pAA bridges are stretched to approximately twice their diameter of 10 nm, costing approximately one $k_B T$ assuming entropic elasticity. For N_{24}-A_{330}-N_{24} d_{node} is between 19.3 nm and 21.9 nm, in line with its longer pAA block. In other regards, the six curves for HCl-derived NAN structures are highly similar, suggesting that the qualitative picture in Figure 5.5 is correct for all cases, and that the chemistry and temperature merely cause changes in the internode distance and sticker residence time of the transient network.

The TFA-deprotected N_{24}-(A_{297}-T_{33})-N_{24} shows smaller values of d_{node}, between

17.6 nm and 19.7 nm, corresponding to a lesser stretching of the polyelectrolyte block due to more compatibility with the pNIPAm moieties. A striking feature of the curves is the high-q region, where all curves show power- laws of, in the case of N_{24}-(A_{297}-T_{33})-N_{24}, $q^{-2/3}$, and, in the case of fully liberated samples, $q^{-5/3}$, the latter corresponding to a self-avoiding walk.[37] We observe these forms up to a d of 1.5 nm, and starting from 5.4 nm for TFA and around 2 nm for the HCl-derived samples, where scattering is dominated by chain statistics ($R_g > d > l_k$).

At present, we have no interpretation of the $q^{-2/3}$ scaling for the TFA-treated case. Clearly, it is not reasonable to attribute it to an even further stretching of the chains than we would expect for a rod (q^{-1}). Thus, the observed shape is likely due to a superposition of different dependencies in the high-q scattering. Nonetheless, we stress that the high-q data witness that TFA leaves us with pAA blocks that have strongly altered conformational properties with respect to pure pAA blocks. Whereas the structure on the internode length scale is only weakly dependent on temperature and chemistry, the density fluctuations on the chain length scale are strongly altered by *tert*-butyl moieties incompletely cleaved by TFA.

Through DLS, rheology and visual observations of NAN triblocks around RT and at 60 °C, we observe a significant enhancement of sticker residence times of pNIPAm blocks when the *tert*-butyl group is removed completely, whereas association seems to be minimal when hydrophobic groups have presence. SAXS reveals internode distances of around twice the dilute coil diameter that increase slightly with pAA chain length and absence of hydrophobic groups. More strikingly, the density fluctuations on the chain length scales are dramatically different in the case when *tert*-butyl groups are not completely removed. Thus, the presence of these groups has a strong effect on the self-assembly behavior of NAN copolymers, which are prepared throughout literature through a method that we show does *not* remove *tert*-butyl up to an extent that their influence is negligible.

5.4 Conclusion

In summary, we report a facile, rapid de-*tert*-butylation scheme for the synthesis of pAA block copolymers with pNIPAm from the corresponding copolymer with p*t*BuAc. The action of stoichiometric HCl on a HFIP solution of the *tert*-butylated precursor yields pAA blocks of a chemical purity that has been inaccessible *via* the commonly used TFA/DCM mixture. In addition, we show that the presence of residual *tert*-butyl moieties, at a degree tolerated by the latter method, impacts the aqueous self-assembly properties of these polymers to such an extent that the thermothickening effect due to LCST-driven pNIPAm association is essentially disabled for polymer

solutions significantly above overlap. Thus, HCl/HFIP is an essential tool in the study of the aqueous association of pAA copolymers derived from their *tert*-butylated precursors.

Appendix

5.A Synthesis of pNIPAm-*b*-ptBuAc-*b*-pNIPAm precursors

We prepared an ABA triblock precursor by successive polymerization of pNIPAm and ptBuAc, controlled by bis(methylpropionic acid) trithiocarbonate (BMAT), as shown in Figure 5.A.1. NMR spectroscopy in $CDCl_3$ gave structure-conform spectra, as seen in Figure 5.A.2. Polymerizations were controlled, as judged by the reasonable agreement between conversion-based mean molecular weight and molecular weight distributions measured by gel permeation chromatography (GPC) in THF, see Table 5.A.1 for molecular weight averages M_n and dispersities Đ. In addition, chain extension of the BMAT-derived pNIPAm precursors with *tert*-butyl acrylate resulted in no low-molecular weight shoulder. This can be clearly seen in the GPC elugrams in Figure 5.A.2 (right).

We note that all elugrams show a slight tailing, which is due to the interaction of the pNIPAm blocks with the column material,[21] and results in underestimation of the molecular weight and overestimation of dispersity. Since these blocks are small compared to the p*t*BuAc block and dispersity values are acceptable and reasonably comparable to other block copolymers of NIPAm and styrene,[21] this level of characterization was deemed adequate for the screening of deprotection methods. In addition, we have analyzed the corresponding de-esterified polymers using aqueous SEC, which showed a somewhat lesser degree of tailing, but qualitatively similar results (see main text).

Solid-state FTIR spectra were taken on p*t*BuAc precursors and the sodium salts of the corresponding TFA/DCM and HCl/HFIP cleavage products. The spectra show the broad COO—Na stretch vibration between 3600 and 2800 cm^{-1}, and alkyl stretch vibrations at 3000 cm^{-1}. In the case of the pNIPAm—p*t* BuAc copolymer, the C=O vibration corresponding to *tert*-butyl ester appears at 1750 cm^{-1}. For the case of the sodium salts of the liberated acids, the C=O vibration is broadened and shifted to 1570 cm^{-1}. The two NIPAm N-H—C=O amide vibrations appear at 1650 and 1550 cm^{-1}, but only the former is visible in the copolymers. The TFA and HCl-treated show highly similar spectra, save for a resonance at 1680 cm^{-1} in the former, which we tentatively attribute to residual *tert*-butyl ester. Figure 5.A.3 shows representative spectra for pNIPAm-*b*-p*t*BuAc-*b*-pNIPAm and the (partially) deprotected products.

Table 5.A.1: Characteristic SEC results for pNIPAm-*b*-tBuAc-*b*-pNIPAm. Block lengths are based on theoretical molecular weight M_{th} that is based on monomer conversion. M_n and Đ are calculated from GPC traces after elution in THF. N_n designates a pNIPAm block of length n, T_m a p*t*BuAc block of length m.

Polymer structure	M_{th} (kDa)	M_n (kDa)	Đ
N_{26}-N_{26}	6.2	5.7	1.13
N_{25}-N_{25}	6.1	5.6	1.26
N_{24}-N_{24}	5.6	4.4	1.21
N_{26}-T_{318}-N_{26}	46.8	27.6	1.33
N_{25}-T_{362}-N_{25}	52.8	45.6	1.49
N_{24}-T_{330}-N_{24}	47.7	25.4	1.60

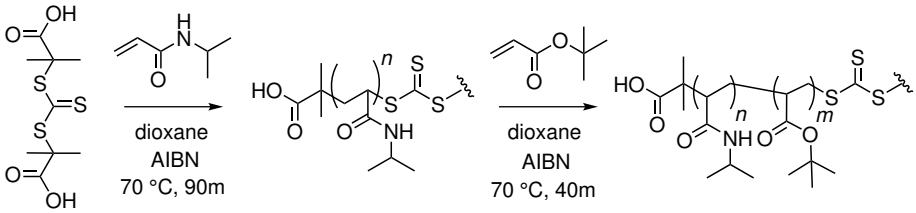

Figure 5.A.1: RAFT synthesis of pNIPAm-*b*-p*t*BuAc-*b*-pNIPAm, with p*t*BuAc as precursor for the pAA block.

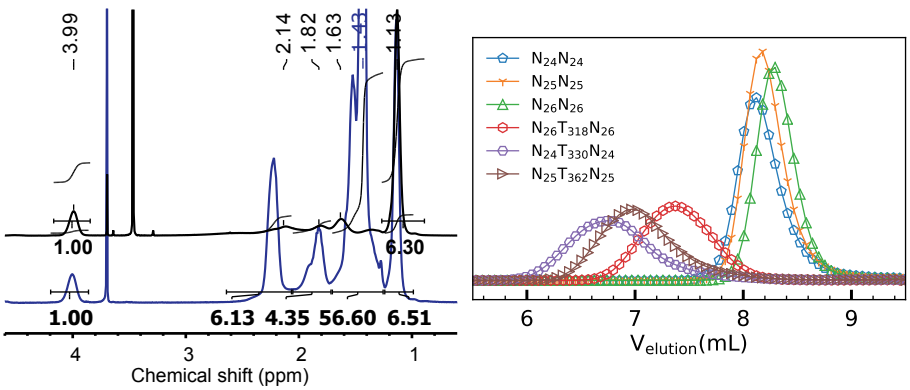

Figure 5.A.2: (left) 400 MHz ^{1}H-NMR spectra of pNIPAm$_{52}$ and pNIPAM$_{26}$-*b*-p*t*BuAc$_{318}$-*b*-pNIPAM$_{26}$ (right) SEC elugrams of pNIPAM and pNIPAM-*b*-p*t*BuAc-*b*-pNIPAm in THF with refractive index detection. N$_n$ designates a pNIPAm block of length n, T$_m$ a p*t*BuAc block of length m.

Bibliography

[1] S. J. Lue, C.-H. Chen, and C.-M. Shih, "Tuning of Lower Critical Solution Temperature (LCST) of Poly(N-Isopropylacrylamide-co-Acrylic acid) Hydrogels," *Journal of Macromolecular Science, Part B*, vol. 50, no. 3, pp. 563–579, 2011.

[2] M. K. Yoo, Y. K. Sung, Y. M. Lee, and C. S. Cho, "Effect of polyelectrolyte on the lower critical solution temperature of poly(N-isopropyl acrylamide) in the poly(NIPAAm-co-acrylic acid) hydrogel," *Polymer*, vol. 41, no. 15, pp. 5713–5719, 2000.

[3] G. Bokias, G. Staikos, and I. Iliopoulos, "Solution properties and phase behaviour of copolymers of acrylic acid with N-isopropylacrylamide: The importance of the intrachain hydrogen bonding," *Polymer*, vol. 41, no. 20, pp. 7399–7405, 2000.

[4] W. C. Blocher and S. L. Perry, "Complex coacervate-based materials for biomedicine," *Wiley Interdisciplinary Reviews: Nanomedicine and Nanobiotechnology*, vol. 9, no. 4, pp. 76–78, 2017.

[5] Y. Liu, H. H. Winter, and S. L. Perry, "Linear viscoelasticity of complex coacervates," *Advances in Colloid and Interface Science*, vol. 239, pp. 46–60, 2017.

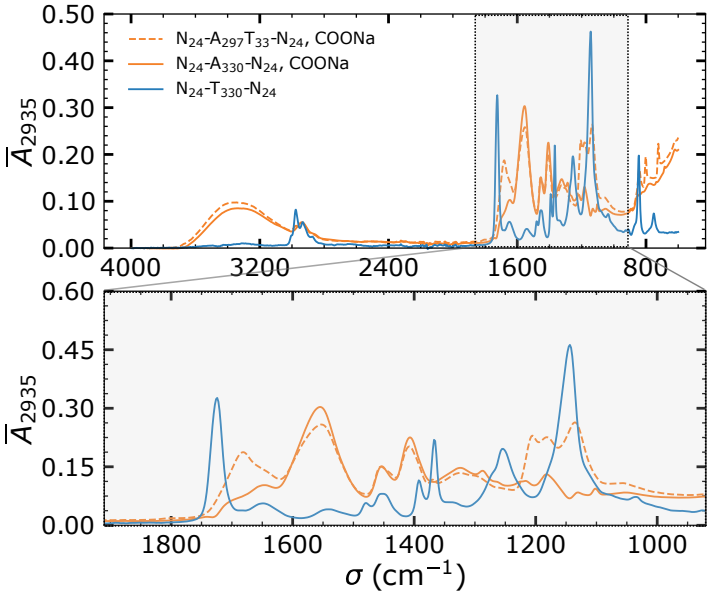

Figure 5.A.3: FTIR spectra of (blue) $N_{24}T_{330}N_{24}$, (orange) the Na salts of the deprotection products (dashed line) of TFA/DCM, $N_{24}A_{297}T_{33}N_{24}$, and (solid line) HCl/HFIP, $N_{24}A_{330}N_{24}$. All spectra have been normalized to the alkyl C-H resonance at 2935 cm^{-1}. N_n designates a pNIPAm block of length n, T_m a p*t*BuAc block of length m.

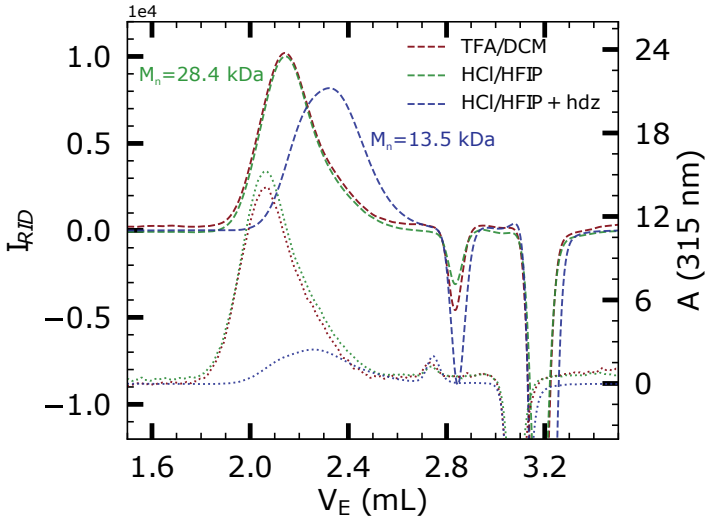

Figure 5.A.4: SEC traces of N_{24}-A_{330}-N_{24}-BMAT (green line), its TFA-treated analogue N_{24}-(A_{297}-T_{33})-N_{24}-BMAT (red line), and its hydrazine-treated cleavage product, N_{24}-A_{220}-SH (blue line). Polymers were eluted in aqueous 0.1M $NaNO_3$ on an Agilent PL AqueGel-OH 8μm column and detected by refractive index detection (left axis) and UV absorption (right axis). Numbers given are found M_n values.

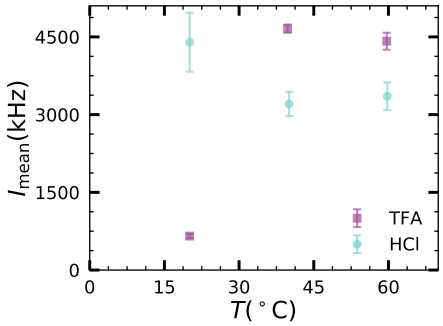

Figure 5.A.5: Raw count rates in 90° scattering of a 292 mg mL^{-1} solution of N_{24}-A_{330}-N_{24} (blue circles) and N_{24}-(A_{297}-T_{33})-N_{24} (purple squares) as function of sample temperature. Solutions are at zero salt. Error bars are the standard deviation of the count rate distribution. N_n designates a pNIPAm block of length n, T_m a p*t*BuAc block of length m.

[6] J. Loiseau, N. Doe, J. M. Suau, J. B. Egraz, M. F. Llauro, C. Ladavière, and J. Claverie, "Synthesis and Characterization of Poly(acrylic acid) Produced by RAFT Polymerization. Application as a Very Efficient Dispersant of CaCO3, Kaolin, and TiO2," *Macromolecules*, vol. 36, pp. 3066–3077, 2003.

[7] J.-B. Lena, A. K. Goroncy, J. J. Thevarajah, A. R. Maniego, G. T. Russell, P. Castignolles, and M. Gaborieau, "Effect of transfer agent, temperature and initial monomer concentration on branching in poly (acrylic acid): A study by spectroscopy and capillary electrophoresis," *Polymer*, vol. 114, pp. 209–220, 2017.

[8] M.-F. Llauro, J. Loiseau, F. Boisson, F. Delolme, C. Ladaviere, and J. Claverie, "Unexpected End-Groups of Poly(acrylic Acid) Prepared by RAFT polymerization," *Journal of Polymer Science, Part A: Polymer Chemistry*, vol. 42, pp. 5439–5462, 2004.

[9] A. R. Maniego, D. Ang, Y. Guillaneuf, C. Lefay, D. Gigmes, J. R. Aldrich-Wright, M. Gaborieau, and P. Castignolles, "Separation of poly(acrylic acid) salts according to topology using capillary electrophoresis in the critical conditions," *Analytical and Bioanalytical Chemistry*, vol. 405, pp. 9009–9020, 2013.

[10] J. M. Pelet and D. Putnam, "Poly(acrylic acid) undergoes partial esterification during RAFT synthesis in methanol and interchain disulfide bridging upon NaOH treatment," *Macromolecular Chemistry and Physics*, vol. 213, no. 23, pp. 2536–2540, 2012.

[11] I. Chaduc, O. Boyron, B. Charleux, F. D. Agosto, and M. Lansalot, "Effect of the pH on the RAFT Polymerization of Acrylic Acid in Water. Application to the Synthesis of Poly(acrylic acid)-Stabilized Polystyrene Particles by RAFT Emulsion Polymerization," *Macromolecules*, vol. 46, pp. 6013–6023, 2013.

[12] V. Dulong, Z. Souguir, C. Pottier, L. Picton, and D. Le Cerf, "Thermo- and pH-Sensitive Triblock Copolymers with Tunable Hydrophilic/Hydrophobic Properties," *Journal of Polymer Science, Part A: Polymer Chemistry*, vol. 53, pp. 2606–2616, 2015.

[13] P. Yong, Y. Yang, Z. Wang, L. Yang, and J. Chen, "Diverse nanostructures and gel behaviours contained in a thermo- and dual-pH-sensitive ABC (PNIPAM–PAA–P4VP) terpolymer in an aqueous solution," *RSC Advances*, vol. 6, pp. 88306–88314, 2016.

[14] P. Chen, J. Chen, and Y. Cao, "Self-assembly behavior of thermo- and Ph-responsive diblock copolymer of poly(N -isopropylacrylamide)-block-poly(acrylic acid) synthesized via reversible addition-fragmentation chain transfer polymerization," *Journal of Macromolecular Science, Part A: Pure and Applied Chemistry*, vol. 50, no. 5, pp. 478–486, 2013.

[15] G. Li, L. Shi, Y. An, W. Zhang, and R. Ma, "Double-responsive core-shell-corona micelles from self-assembly of diblock copolymer of poly(t-butyl acrylate-co-acrylic acid)-b-poly(N-isopropylacrylamide)," *Polymer*, vol. 47, no. 13, pp. 4581–4587, 2006.

[16] G. Li, S. E. N. Song, L. E. I. Guo, and S. Ma, "Self-Assembly of Thermo- and pH-Responsive Poly (acrylic acid)-b-poly(N-isopropylacrylamide) Micelles for Drug Delivery," *Journal of Polymer Science, Part A: Polymer Chemistry*, vol. 46, pp. 5028–5035, 2008.

[17] L. Lauber, T. Nicolai, C. Chassenieux, and O. Colombani, "Viscoelastic Properties of Hydrogels Based on Self-Assembled Multisticker Polymers Grafted with pH-Responsive Grafts," *Macromolecules*, vol. 50, pp. 8178–8184, 2017.

[18] P. Palladino and D. A. Stetsenko, "New TFA-free cleavage and final deprotection in Fmoc solid-phase peptide synthesis: Dilute HCl in fluoro alcohol," *Organic Letters*, vol. 14, no. 24, pp. 6346–6349, 2012.

[19] C. M. Schilli, M. Zhang, E. Rizzardo, S. H. Thang, . Y. Chong, K. Edwards, G. Karlsson, and A. H. Müller, "A New Double-Responsive Block Copolymer Synthesized via RAFT Polymerization: Poly (N-isopropylacrylamide)-block-poly (acrylic acid)," *Macromolecules*, vol. 37, no. 21, pp. 7861–7866, 2004.

[20] J. T. Lai, D. Filla, and R. Shea, "Functional polymers from novel carboxyl-terminated trithiocarbonates as highly efficient RAFT agents," *American Chemical Society, Polymer Preprints, Division of Polymer Chemistry*, vol. 43, no. 2, pp. 122–123, 2002.

[21] M. Cetintas, J. de Grooth, A. H. Hofman, H. M. van der Kooij, K. Loos, W. M. de Vos, and M. Kamperman, "Free-standing thermo-responsive nanoporous membranes from high molecular weight PS-PNIPAM block copolymers synthesized via RAFT polymerization," *Polymer Chemistry*, vol. 8, no. 14, pp. 2235–2243, 2017.

[22] W. Shen, Q. Qiu, Y. Wang, M. Miao, B. Li, T. Zhang, A. Cao, and Z. An, "Hydrazine as a nucleophile and antioxidant for fast aminolysis of RAFT polymers in air," *Macromolecular Rapid Communications*, vol. 31, no. 16, pp. 1444–1448, 2010.

[23] M. Bohdan, J. Sprakel, and J. Van Der Gucht, "Multiple relaxation modes in associative polymer networks with varying connectivity," *Physical Review E*, vol. 94, no. 3, pp. 1–7, 2016.

[24] K. Thuresson, S. Nilsson, A.-L. Kjøniksen, H. Walderhaug, B. Lindman, and B. Nyström, "Dynamics and Rheology in Aqueous Solutions of Associating Diblock and Triblock Copolymers of the Same Type," *The Journal of Physical Chemistry B*, vol. 103, no. 9, pp. 1425–1436, 1999.

[25] Y. Fujii, H. Yamada, and M. Mizuta, "Self-association of acetic acid in some organic solvents," *The Journal of Physical Chemistry*, vol. 92, no. 23, pp. 6768–6772, 1988.

[26] A. R. Maniego, A. T. Sutton, M. Gaborieau, and P. Castignolles, "Assessment of the Branching Quantification in Poly(acrylic acid): Is It as Easy as It Seems?," *Macromolecules*, vol. 50, no. 22, pp. 9032–9041, 2017.

[27] S. Bayati, K. Zhu, L. T. T. Trinh, A. L. Kjøniksen, and B. Nyström, "Effects of temperature and salt addition on the association behavior of charged amphiphilic diblock copolymers in aqueous solution," *Journal of Physical Chemistry B*, vol. 116, no. 36, pp. 11386–11395, 2012.

[28] M. Heskins and J. E. Guillet, "Solution Properties of Poly(N-isopropylacrylamide)," *Journal of Macromolecular Science: Part A - Chemistry*, vol. 2, pp. 1441–1455, dec 1968.

[29] M. Teodorescu, I. Negru, P. O. Stanescu, C. Drghici, A. Lungu, and A. Sârbu, "Thermogelation properties of poly(N-isopropylacrylamide)-block- poly(ethylene glycol)-block-poly(N-isopropylacrylamide) triblock copolymer aqueous solutions," *Reactive and Functional Polymers*, vol. 70, no. 10, pp. 790–797, 2010.

[30] T. Gan, Y. Guan, and Y. Zhang, "Thermogelable PNIPAM microgel dispersion as 3D cell scaffold: effect of syneresis," *Journal of Materials Chemistry*, vol. 20, no. 28, p. 5937, 2010.

[31] A. J. De Graaf, K. W. M. Boere, J. Kemmink, R. G. Fokkink, C. F. Van Nostrum, D. T. S. Rijkers, J. Van Der Gucht, H. Wienk, M. Baldus, E. Mastrobattista, T. Vermonden, and W. E. Hennink, "Looped structure of flowerlike micelles revealed by 1H NMR relaxometry and light scattering," *Langmuir*, vol. 27, no. 16, pp. 9843–9848, 2011.

[32] C. L. McCormick, B. S. Sumerlin, B. S. Lokitz, and J. E. Stempka, "RAFT-synthesized diblock and triblock copolymers: thermally-induced supramolecular assembly in aqueous media," *Soft Matter*, vol. 4, no. 9, p. 1760, 2008.

[33] S. E. Kirkland, R. M. Hensarling, S. D. McConaughy, Y. Guo, W. L. Jarrett, and C. L. McCormick, "Thermoreversible hydrogels from RAFT-synthesized BAB triblock copolymers: Steps toward biomimetic matrices for tissue regeneration," *Biomacromolecules*, vol. 9, no. 2, pp. 481–486, 2008.

[34] Z. Lin, S. Cao, X. Chen, W. Wu, and J. Li, "Thermoresponsive hydrogels from phosphorylated ABA triblock copolymers: A potential scaffold for bone tissue engineering," *Biomacromolecules*, vol. 14, no. 7, pp. 2206–2214, 2013.

[35] X. Lang, W. R. Lenart, J. E. Sun, B. Hammouda, and M. J. Hore, "Interaction and Conformation of Aqueous Poly(N-isopropylacrylamide) (PNIPAM) Star Polymers below the LCST," *Macromolecules*, vol. 50, no. 5, pp. 2145–2154, 2017.

[36] T. Kawaguchi, K. Kobayashi, M. Osa, and T. Yoshizaki, "Is a cloud-point curve in aqueous poly(N-isopropylacrylamide) solution binodal?," *Journal of Physical Chemistry B*, vol. 113, no. 16, pp. 5440–5447, 2009.

[37] P.-G. De Gennes, *Scaling concepts in polymer physics*. Cornell University Press (Ithaca and London), 1979.

Chapter 6

General discussion

In this chapter, I will critically discuss the results presented in this thesis as framed by their relationship to the central question announced in the Introduction: *how can we apply the chemistry observed in the underwater adhesives of the animal world to adapt hydrophilic synthetic polymer materials for use as biomaterials?* The topics touched organize along two themes: design parameters and practices.

On the one hand, I discuss how the work in this thesis contributes to ways to optimize important design parameters for future biomaterials. The parameters address the targets of biocompatibility of the used chemistry, the possibility for adding responsiveness to environmental stimuli, of reaching appropriate and readily adjustable linear viscoelasticity, and of robustness against high strain rates and amplitudes.

On the other hand, I evaluate the practices involved in the creation of biomaterials in laboratories, from synthesis on the basis of monomers to materials characterization. I assess the usefulness of scattering studies towards characterization of structure and dynamics of hydrophilic polymer systems. Static scattering of X-rays and static and dynamic lights scattering of light are discussed, along with microrheology using light scattering equipment. Finally, various controlled radical polymerization reactions are compared according to their ability to provide chemists with hydrophilic and polyelectrolytic polymer materials, and I discuss to what level the issue of *control* is relevant to the biomaterials community.

The last section offers a discussion of the inevitable impact of polymer technology on the human habitat and beyond. This impact is not limited to the infamous pollution of the ocean with plastic waste. Biomaterials, once adopted, are unlikely to be an exception to the resource-hungry and polluting nature of chemical industries, which presents an unacceptable risk to humans and ecosystems. A final note is reserved for questioning whether petrochemistry can and should be counted on to provide materials in the future.

6.1 Complex coacervates: biological reality, biomedical future, or a model system for academics?

In the Introduction, we have outlined the following challenges for the adoption of polymers as biomaterials: first, a biomaterial needs to have its mechanical strength matched to the tissue of interest (cohesive strength), second, it must display an appropriate level of adhesion to targets of interest (adhesive strength). Third, materials must be biocompatible in the sense that they do not provoke inflammation and that breakdown proceeds in the absence of toxic intermediates (biocompatibility). Ideally, biomaterials communicate with tissues to enhance healing following an intervention, rather than just being inert to tissues. Finally, biomaterials need to be convenient for use in the medical profession (usability). I include the presence of environmental trigger in this category, however, responsiveness could be included in one or both strength categories, or even as itself.

Below, I will outline how the work presented in this thesis aligns with overcoming these challenges, and where the alignment is still lacking and needs to be addressed in future investigations. I will provide additional data when it supports the arguments, and provide an outlook for those seeking to further the campaign that I propose.

The requirement of being compatible with tissues goes beyond the lack of acute toxicity of a materials, such as is the case for cyanoacrylates (despite their limited use in surgery).[1,2] Materials used with wet tissues also need to have appropriate surface energies to expel surface water that inevitably coats tissues, and need to adhere stronger to their targets than to surgical tools. Furthermore, biomaterials must keep their properties for as long as is required for healing to take place, which implies that there should be no (de)swelling, nor a deleterious change in the properties. Clearly, some of these "compatibility" criteria overlap with the requirements of strength and usability, and, perhaps the four of them can be more generically referred to as biocompatibility in a broader sense.[3]

Complex coacervates combine contradictory characteristics that position them at the forefront of biomaterial candidates: whilst being insoluble in water, all of their individual constituents are. As a consequence, coacervates have very low surface energy towards wet surfaces.[4,5] Furthermore, their viscoelasticity can be tuned by molecular weight, monomer choice and salt concentration.[6,7] However, the eventual salt concentration of a biomaterial will generally be physiological (around 0.15 M in humans), and one only has control over the salt concentration during application.

Sandcastle worms and mussels secrete a material that is very dense in positively charged poly(amino) proteins and negatively charged sulfated[8] proteins, to which

they add a layer of control over the modulus by incorporating high concentrations of dihydroxyphenylalanine.[9, 10] While real control over the crosslinking is elusive,[11] the adhesive is part of the organisms' highly successful strategy. Allowing for the fact that it is unclear whether these secretions should be called coacervates,[10] complex coacervates are indeed a biological reality. On a side note, this biological reality also includes the role of polyelectrolyte complexation in the nucleosome, in RNA-protein complexes, and in compartmentalization in the cell.[12]

Since tissues represent a wide range of mechanical stiffness between brain and lung around 1 kPa, to 600 kPa for blood vessels, and all the way up to 7 GPa for cartilage and 14 GPa for bone, it is clear that control over the modulus is essential to build tissue-compliant materials. Complex coacervates in equilibrium can be made up to moduli of at least 0.1 MPa. By concentrating the dense phase above equilibrium content with the use of extrusion, moduli of several MPa can be obtained,[13] and with fiber spinning it is possible to reach the GPa range.[14] Thus, coacervate "models" of essentially all tissue stiffnesses can be obtained, at least in the laboratory, where one has perfect control over the salt concentration.

In Chapter 2 and 3, we demonstrated a system where the elastic modulus was no longer a function of salt strength for salt levels close to the critical salt strength. By incorporating non-coacervate metal-ligand crosslinkers we were, like the aforementioned marine animals, able to achieve "salt-less" control over complex coacervate mechanics. Similarly, the triblock copolymers designed in Chapter 5 can be used in a similar way, where the additional structure is imparted by thermostiffening due to the aggregation of poly(*N*-isopropylacrylamide) blocks, as also implemented by the author's colleagues.[15, 16] The addition of a second, "orthogonal" structural feature is a logical step for the development of biomaterials.

However, the materials prepared in this thesis are limited by two factors. First, there is a lack of a function that can "trigger" the solidification, which is a limitations for injectable adhesives, but not for pressure-sensitive adhesion. Furthermore, there are obvious concerns regarding the biocompatibility of the molecules and ions used. We will address these issues separately.

The requirement of convenient triggers still challenges coacervates in biomedical materials

The curing of the adhesive produced by the sandcastle worms is initiated upon exposure of the secretion to sea water, which presents a higher pH and a lower salt concentration than the interior of the animal.[17] Inside the secretory glands, the components of the adhesive are stored as liquids.[18, 19] Thus, the adhesive can be

conveniently delivered, and the timing of its curing is controlled.

In synthetic systems, multiple triggered systems have been designed. Closest to bioadhesives are complex coacervates crosslinked with dopamine, which indeed solidify upon exposure to oxidative conditions.[20–23] An idea that has a great deal of practical significance is the use of polymer blocks that change their solubility with temperature (thermoresponsivity).[24] The work of Dompè and co-workers describes the incorporation of poly(*N*-isopropylacrylamide) side-chains into polyelectrolytes that form complex coacervates.[15, 25] The eventual idea is to arrive at an adhesive that is delivered as a fluid, and subsequently crosslinked simply by the physiological temperature of the tissue.

What is currently unexplored is the use of a temperature decrease, rather than an increase to trigger solidification, which would allow to use complex coacervates much like a thermoplastic adhesives. Thermostiffening materials[15] are based on lower critical solution temperature (LCST) blocks, which aggregate above a certain temperature. Thermo*softening* materials would feature upper critical solution temperature blocks (UCST). Notably, zwitterionic polymer solutions often show UCST behaviour due to self-coacervation.[26] Thermostiffening materials are exclusive to settings where the temperature of application is sufficiently low, which is far from guaranteed in in institutions without air-conditioned facilities or warm countries.

Additionally, the use of long-wave UV light has not yet been explored as a trigger. Whereas in dental adhesives, the use of UV to cure cement is commonplace, the technology seems not to have been translated to the area of complex coacervates. A host of moieties undergo crosslinking reactions when exposed to UV light,[27] and their incorporation could follow procedures analogous to those described in Chapter 2. Coumaryl dyes are a possibility, but the aforementioned 3,4-dihydroxyalanine is also known to undergo photocrosslinking.

The elephant in the room: biocompatibility

The metal-ligand reinforced polyelectrolyte complexes that we designed in Chapters 2 and 3 were not engineered with a trigger in mind, since we designed them to showcase how a salt-independent crosslinking structure impacts the flow of complex coacervates. Nonetheless, solidification could be triggered by co-injecting the high-salt terpyridylated complexes with a metal ion solution at high salt. For the metals explored in Chapters 2 and 3 this is inadmissible by any standard, since they are all toxic, a feature shared by bivalent metal ions.[28] Ferrous iron (Fe^{2+}) is to some extent an exception, which is understandable given its central role as an oxygen carrier, yet it is also toxic to some tissues.[28]

Synthetic polymers from the acrylate and acrylamide family face biocompatibility issues in general, due to their exceptional stability.[29] The problem extends to poly(acrylic acid) and poly(*N*-isopropylacrylamide), and stable hydrophilic polymers are more suitable *in vivo* as surface modifying agents, for instance to avoid foreign body reactions of implants.[30, 31] To make matters worse, most polycations are unsuitable as biomedical agents, since polycations are cytotoxic due to their tendency to complex to the phospholipids in the cell membrane, which results in hydrolysis.[29] The cytotoxicity of polycations is a serious hurdle for polyelectrolyte complexes to move forward into biomedical application, and it will be rewarded to study whether the polycation toxicity still applies after their complexation.

Complex coacervates *per se* seem to have a reasonable biocompatibility profile, though it must be cautioned that the field of their use in animals is young. Indeed, a study on a complex of a dihydroxyalanine-modified polyphosphonate with aminated collagen showed no evidence of cytotoxicity in an animal model.[32] In another study, a complex of spermine and phytic acid has also been demonstrated to work as an embolic agent *in vivo*, however, the study was not geared to address cytotoxicity.[33]

Other applications of complex coacervates, such as drug delivery,[34] will also have to learn from the advancing insight into coacervate-life interactions. In the case of drug delivery, the objective of the intervention guides the cytotoxicity that is appropriate to the material: oncological applications have cytotoxicity requirements distinct from wound recovery. As is the case in the examples cited in the previous paragraph, the use of biopolymers often implies biocompatibility. Furthermore, bio-based polymers often have swifter degradation time frames than poly(acrylamides) and poly(methacrylates). While not at the center of this thesis, degradability is not only essential for *in vivo* applications, but also to prevent adding to the already-enormous environmental burden of wasted synthetic polymers (see Section 6.5). It is essential that the lessons learnt from synthetic coacervates are applied to bio-based polymers, and other degradable macromolecules.

6.2 Scattering of light and X-rays

Throughout the thesis, we have relied on scattering of visible light and X-rays in an attempt to resolve the structure and dynamics of hydrophilic materials and their polymeric constituents. In this section, we will appraise the utility of scattering studies, but will also highlight the considerable difficulties that are inherent to the analysis of q-space data. In the final section, we will suggest further directions for the use of scattering in the field of complex coacervates.

Light scattering reveals mesh and viscoelastic decay modes

In Chapter 5, we presented X-ray scattering data for transient networks of triblock copolymer poly(*N*-isopropylacrylamide)-*b*-poly(acrylic acid)-poly(*N*-isopropylacrylamide) (pNAN), which form as a consequence of the increasing non-solubility of the poly(*N*-isopropylacrylamide) blocks with temperature. The q-dependence of the scattering intensity was peaked around an inverse scattering vector q^* of 20 nm, which we interpreted as an inter-node distance in the network. At $q \gg q^*$, we also measured the time decorrelation of visible light (dynamic light scattering). The decays featured a prominent slow mode of stretched exponential character, with a decay time that increased with temperature (0.1 s to 10 s). While the increase of the decay time increases with the lifetime of the nodes with temperature, no quantitative connection to the structure of the network is apparent. For instance, decay times extracted using Maxwell model fits of frequency sweeps were on the 10^{-3} s scale, and thus almost 10^2-fold lower than the DLS decay times.

A paper by van der Gucht et al.[35] on associative networks of micelles of a similar internodal distance also identifies a stretched exponential decay that they recognize as viscoelastic in origin, since the decay time of the mode is shown to be proportional to the time extracted from rheology. As is generally the case when scattering-based and rheological relaxation times are compared, there is a large difference between the DLS and rheological decay times, since local phenomena in soft matter do not scale up linearly to the rheological (macro) scale. While both techniques report on the same relaxation mechanisms, rheological data can often be analyzed with convenient models (such as the Maxwell fluid) to yield the residence time of a chain in a node. Decays in dynamic scattering, however, rarely connect to parameters with a straightforward physical interpretation – unless the scattering vector is sufficiently large, interactions are sufficiently small, and the objects in the sample engage in Brownian dynamics.

Similar complications plagued our attempts at analyzing the correlations of light scattered from complex coacervates. We recorded the autocorrelation function for a native complex at high salt ($\mathrm{pA/pD_{01}} - \circ$), and transiently crosslinked complex coacervates with terpyridine-metal crosslinks ($\mathrm{pA/pD_{01}}-\mathrm{Zn^{2+}}$ and $\mathrm{pA/pD_{01}}-\mathrm{Co^{2+}}$). Again, the decays could be described by a sum of three stretched exponential decays, as can be seen in Figure 6.1:

$$\sqrt{g_2(t)-1} = \sum_{k=\mathrm{A,B,C}} W_k \exp -(\Gamma_k t)^{\alpha_k} \tag{6.1}$$

where W_k is the pre-exponential weight of mode k, Γ is a decay rate which is related to the mean decay rate $\langle\Gamma\rangle$ by Equation 5.1, and α is a stretch exponent.

The initial relaxation of the complexes presents as a fast mode with a stretch exponent α_A relatively close to unity (between 0.76 and 0.9), which means that the corresponding relaxation time is narrowly distributed.[36] The corresponding apparent diffusion coefficients ($D_{\text{eff,A}} = \frac{\Gamma_A}{q^2}$) were remarkably similar for all complexes, $2.5{\cdot}10^{-12}$ m^2s^{-1} for pA/pD−∘ and pA/pD−Co^{2+}, and $1{\cdot}10^{-12}$ m^2s^{-1} for the complex with Zn^{2+}. We relied on the assertion of Spruijt and co-workers that the relaxation modes in DLS of complex coacervates are diffusive in origin, a claim which is supported by the observation that the decay rates scaled with q^2 in their work.[36] Following the same work, we identify the fast mode as a "mesh" mode, a decay that corresponds to the relaxation of chains on up to the mesh size in the coacervates.[36] The mesh structure in complex coacervates is visualized in Figure 6.2d in Section 6.3.

At long times ($t > 1$ ms), the correlations were markedly non-exponential (Figure 6.1), and we needed to add strongly stretched modes to fit the data. The late stage of the correlation function of pA/pD−∘ was described with stretched exponential modes with a mean relaxation time $\langle\tau_B\rangle$ of 40 ms and a stretch exponent α_B of 0.62. An even later contribution was also added, which we will disregard as it had a low weight W_C, close to the noise floor. The highly stretched nature of the decay, taken together with the presence of more than one mode, suggests that the late stage of the correlations do not present a well-defined relaxation time.

Similarly, the samples with added metals (transient crosslinks) presented correlation functions without a well-defined exponential late stage. For the complex pA/pD_{01}−Zn^{2+}, we also added two stretched modes to describe the correlations beyond 1 ms. For instance, the mode that contributed about 50% to the function had a $\langle\tau\rangle$ of 240 s, and was stretched with an exponent of 0.45. Thus, the addition of transient crosslinks had the effect of further broadening, as well as significantly slowing down the relaxation. We note that the use of stretched multi-exponential models is fraught with difficulty, since many sets of parameters approximate the data satisfactorily.

Since all complexes are made with the same polyelectrolytes, the inter-complex similarity of the fast mode confirms its assignment as the relaxation of the chains below a mesh size (Figure 6.2d) at which the polyelectrolytes overlap. Surprisingly, we observe that the second feature of the correlation function also exactly overlaps for the complexes with Zn^{2+} and Co^{2+}. The overlap is all the more remarkable given that the measurements were performed under different scattering angles. Thus, we renormalised the times with q^2, which implicitly assumes diffusion modes to account for the dynamics. The switch from a transient crosslink that is labile (Zn^{2+}) to a crosslink with a lifetime $\tau > 10^4$ s (Co^{2+}, see Chapter 2, Table 2) slows down only the very last portion of the density autocorrelation function. This observation supports

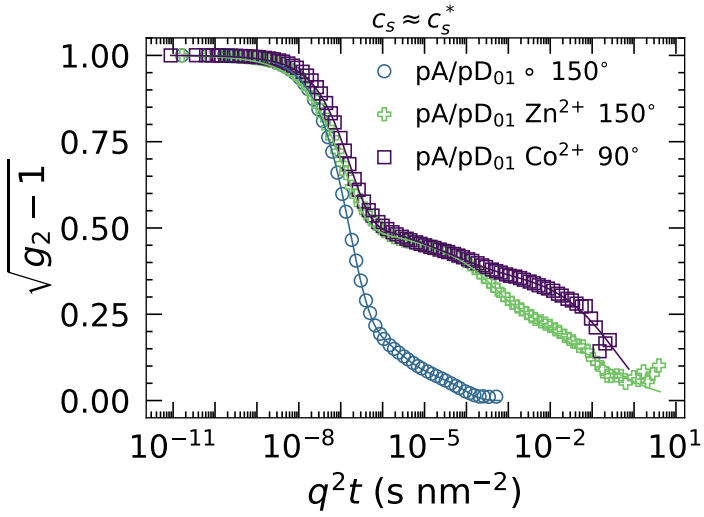

Figure 6.1: Second-order intensity autocorrelation functions of photons scattered from native (∘) and transiently crosslinked (Zn^{2+}, Co^{2+}) complex coacervates. Marks are recorded data, averaged over multiple runs in case of ∘ and Zn^{2+}. Lines are fits to a sum of three stretched exponential decays. The legend labels indicate the scattering angle. Only one in three data points are marked.

the assumption made in Chapter 2 and Chapter 3 that the local structure of the polyelectrolyte complexes is not affected by the choice of lifetime of the complexes. Conversely, the relaxation process on the node dissociation time scale is not sensitive to short-time fluctuations of the polyelectrolyte chains.

A tentative explanation for the shape of the correlation functions is as follows: the initial near-exponential decay corresponds to free diffusion over distances below the inter-crosslink distance. For the unmetalated complex, this accounts for nearly all of the decay, until the effect of long-scale density correlations becomes apparent. Spruijt et al. also report strong evidence of meso-scale heterogeneity (Figure 6.2a) in both DLS and X-ray scattering studies for pA/pD coacervates.[36] For metalated complexes, the diffusion must necessarily be hindered by the presence of crosslinks, which is reflected by the plateau-like feature starting at 50% decay. This feature is analogous to the glassy regime in supercooled fluids, and represents a barrier to diffusion. For the Zn^{2+} complex, we also witness near-complete decay that recalls the effect of long-scale density fluctuations. For Co^{2+}, it is impractical to record the correlations up to full decay.

Thus, while the quantitative analysis of our preliminary DLS study leaves much to be desired, the correlation data themselves suggest that the relaxation of the complexes is universal, and corresponds rather well to the picture painted in the conclusions to Chapter 2 and Chapter 3: the transient crosslinks do nothing else than to link together regions of the coacervate that are otherwise unperturbed. An obvious limitation is that the salt strength was near-critical for all complexes studied by DLS. At lower salt strength, the free-diffusion time can be expected to be longer, since it takes more time to exhaust the Rouse modes and enter diffusion. However, the plateau-like feature should appear at a very similar level of decay,[35, 37] since the distance between crosslinks is essentially unchanged by the salt strength.

Towards microrheology with colloids

A more fundamental limitation of using DLS microrheology to study complex fluids is that, typically, full models for density-density correlations at all times are sparse in the literature. The parsimony of models is not accidental: it reflects the challenge of accounting for correlations at all length scales.[38] Even for model networks of telechelic polymers, the physical interpretation of the observed decay modes relies either on a purely qualitative picture (as is the case here), or on stretching assumptions of more quantitative theories.[35]

An excellent way to address the problem is to incorporate nanoparticles into the complexes. When the scattering is dominated by the particles, one can rely on their Brownian dynamics. Indeed, by analyzing the correlations in DLS of telechelic

networks in which 70 nm particles dominate the scattering, Sprakel et al. resolved the dynamics of telechelic networks down to the exchange of chains between nodes, and even all the way down to the Rouse modes.[37] Furthermore, DLS microrheology holds great promise even for complex biological materials that can not be produced at the large scale required for conventional rheological measurements.[39]

We have attempted to incorporate nanoparticles to "report on" the relaxation of the coacervate complexes. The particles were 80 nm polystyrene colloids, which were subsequently stabilized by grafting neutral (pDMA), negatively charged (sodium sulfopropyl methacrylate) or positively charged (acrylamidopropyl trimethylammonium chloride) polymer brushes onto the particles with ATRP. Much to our disappointment, at high salt concentrations, the particles were inadequately incorporated into the coacervate complexes, and were depleted into the dilute phase after mixing. Likely, colloidal charges when complexed with a linear chain display a smaller two-phase region as compared to polymeric charges. Clearly, two oppositely charged coils are able to get into a more intimate contact to compensate their charges, and far more configurations are available to the two-coil situation. Then, the presence of an available polymeric counter-charge would push (most of the) colloids in the dilute phase (which is "dense" from the perspective of the colloids).

Thus, we encountered a limitation of DLS microrheology: the first-order correlation function can only be related to the mean-square displacement when the scattering is dominated by the particles. The scattering frequency with respect to undoped complexes could be increased only three-fold, which resulted in a correlation function that is a convolution of the Brownian dynamics of the particles with the relaxation dynamics of the network or coacervate. Such correlations resist analysis.

Particle-dense coacervates have been studied in our laboratory by Dompè et al.,[40] who achieved a high extent of incorporation of SiO_2 particles. Unlike the highly stabilized particles in our studies, silica particles aggregate at the c_s characteristic of liquid complex coacervates. Furthermore, SiO_2 spheres are strongly affected by depletion effects in the presence of polymers.[41] The authors circumvent the problems by exploiting the potential of poly(*N*-isopropylacrylamide) (pNIPAm), which they graft onto the polyelectrolyte constituents of the coacervate. pNIPAm adsorbs strongly and specifically to the surface of negatively charged SiO_2, which stabilizes the particles up to SiO_2 concentrations of at least 6% w/w. The concentration boosts the turbidity of the complexes appreciably.[40]

Unlike the sterically stabilized "hairy" particles of our study, which are inert with respect to the coacervate, the pNIPAm-functionalized polyelectrolytes of Dompè et al. crosslink the coacervate: one particle binds multiple pNIPAm chains, resulting in nodes where several chains meet. While this might be seen as a detrimental feature to those seeking to use the system as a microrheological platform, we note that

adsorption couples the particles' fluctuations more tightly to those of the chain, and allows to measure features on shorter timescales than inert particles. An excellent illustration is the work of Sprakel et al.,[37] where inert particles exhibit Brownian diffusion up to length scales of 10^{-7} m, at which point the particles indeed start sampling the polymeric motions. However, absorbing particles "sense" the dynamics of the polymer network on timescales short enough to allow detection of the Rouse modes ($\tau_{\text{Rouse}} \ll 1$ ms).

I suggest to take advantage of our work in Chapter 5, where we present a polymeric architecture that is sparse in pD content, yet possesses a highly defined pNIPAm triblock architecture. The pNIPAm-functionalized poly(acrylic acid) can be used in complex coacervates that bind to silica particles. Another opportunity would be to use pNIPAm microgels: temperature can then be used to turn the adsorption of the particles to the chains on or off.

DLS microrheology could potentially reveal the short-τ dynamics of complex coacervate at high salt strength. One could wonder whether such a study has any deal of practical relevance, since the short-time dynamics are routinely extrapolated from studies at lower salt.[42] Furthermore, the interest in complex coacervates more likely revolves around salt strengths at which the complexes are viscoelastic[43] or even closer to Hookean solids.[44, 45] Nonetheless, the low-viscosity regime is crucial for applications in which one wishes to deliver a coacervate as a low-viscosity fluid, after which some trigger unleashes a solidification potential.[10]

We suggest that microrheology with DLS is especially useful to resolve questions that require access to relaxation data at times below 1 ms. For instance, our rheological work in Chapter 2 and Chapter 3 did not have access to such short time scales, and we could not adequately back up our assumption that the presence of ligands and the binding of metal ions to them did not influence the structure of the coacervate. Surprisingly, even a basic attempt at a scattering study, as given in Figure 6.1, confirms that, indeed, the "orthogonality" assumption was correct, at least at high salt and low crosslink density.

An avenue that was left unexplored is the use of diffusing wave spectroscopy (DWS), which can be seen as light scattering in the limit of strong multiple scattering.[46] Since the particle density in our system did not even reach the levels required for achieving particle-dominated single scattering, reaching the levels required for DWS seems an insurmountable challenge. However, we note that systems such as that of Dompè,[40] which are characterized by a high density of particles and, correspondingly, show high turbidity, could be studied by DWS. Especially since the particles in the pA-*g*-pNIPAm/pD-SiO_2 system are *part of the material*, and not merely present as probes, DWS could reveal otherwise inaccessible short-time dynamics that are relevant to the actual complexes.

A exciting avenue is the implementation of the spatially-resolved version of DWS, known as laser speckle imaging (LSI), on coacervate systems that scatter sufficiently. A unique feature of LSI is that the Å-scale microscopic dynamics inside a material can be compared over lengthscales up to several cm, and, furthermore, that the technique can be conveniently applied while deforming a sample. For example, the formation of macroscopic cracks during delayed fracture can be predicted by an increase of dynamics that can be measured with LSI of an elastomeric sheet loaded at subcritical strain, as shown in an outstanding contribution by Van Der Kooij et al.[47] I suggest to apply the technique to failure modes that are relevant to complex coacervates in biomedical applications: adhesive failure, brittle fracture and yield. In short, future investigators will do well to harness the full spectrum of available light scattering techniques in order to study the short-τ dynamics of complex coacervates, and to use these dynamics as an observable in material optimization.

6.3 Failure mechanics of complex coacervates define their applicability range

In the previous section, I highlighted my and other[36] evidence for meso-scale ($\lambda > 100$ nm) density fluctuations in complex coacervates. Here, I make the case that long-range fluctuations are relevant for the non-linear mechanics of the hybrid complexes discussed in Chapter 3 of the thesis, and, furthermore, in complex coacervates designed towards medical applications. I will further discuss the necessity of controlling the failure mode and the strain tolerance of complex coacervates, should they be proposed as solutions to real-world problems. Finally, I will suggest that, for the coacervate field as whole, it is time to switch focus away from the linear viscoelasticity of coacervates and biomaterials in general, and instead capitalize on investigating and learning to avoid the *failure* of these materials.

Transient crosslinks bridge coacervate domains and enforce finite extensibility

In Chapter 3, we have seen that complex coacervates, when sheared beyond the highest shear rate at which the rheology is still linear $\dot{\gamma}^*$, fail in brittle fracture, confirming the observations of Spruijt et al.[42, 48] Addition of transient crosslinks widened the linear viscoelastic envelope in all complexes that we prepared. By varying the amplitude of oscillatory shear at a constant frequency, we established the character of the metal-ligand bond as a slip bond, meaning that the ratio of dissociation time and

the association time decreases with strain rate, favouring the dissociated (inactive) state of the crosslink at high strain (see Figures 3.2 and 3.3). This behaviour is the origin of shear banding in transient polymer networks, where the pull-out rate of stickers increases with respect to the rate of sticker incorporation with strain rate.[49]

The incorporation of terpyridine-metal bonds in polyelectrolyte complexes has a further effect, aside from a broadening of the LVE and manifestation of slip bonding: in a subset of complexes, we observe strain hardening in either or both of $G'(\dot{\gamma})$ and $G''(\dot{\gamma})$. Interestingly, the extent of and distribution between hardening in either component of the complex modulus depends on the choice of the metal in the crosslink (Figure 3.2). We were able to reject the hypothesis that the stiffening could be attributed to interconversion[50–52] of intra-chain (ineffective) to inter-chain (effective) crosslinks, since the relaxation time decreased with strain amplitude. Rather, we characterize the strain hardening as the chains being strained into the non-Gaussian regime of their force-extension curve, causing non-affine deformations in the sample.[53]

The occurrence of brittle fracture signatures for native coacervates can perhaps be related to the presence of the mesoscale fluctuations discussed in the scattering section of this Chapter, *vide supra*. Tabuteau et al.[54] write the critical stress σ_c at which a crack propagates during inflation of a bubble formed from a telechelic polymer solution as the stress at which the thermal fluctuations are big enough to allow growth of the already pre-existing "cracks" in the fluid. The equation for the critical stress of growing a crack is taken from the Griffiths theory of crack growth.[55] Pomeau initially suggested to allow thermal fluctuations to nucleate the cracks.[56] However, many systems to which the theory is applied do not spontaneously nucleate cracks at all, and the description is especially spurious for materials that are glassy and crystalline. However, for fluids that are structured as a (near) equilibrium distribution of telechelics, the cracks are simply regions where the connectivity is lower than the sample average.[54] Analogously, we interpret the mesoscale fluctuations measured in DLS and X-ray scattering by us and others[36] as introducing sparse, or "weak" domains in the complexes that should fracture at high shear rates. Figure 6.2 attempts to capture the mesoscale fluctuations as "dense" domains (not to be confused with the dense phase of the coacervate phase equilibrium), and "sparse" domains (not the dilute phase).

Given the premise that the structure of polyelectrolyte complexes is unchanged on length scales beneath the polyelectrolyte mesh size (Figure 6.1), the change in non-linear mechanics must indeed relate to a change on a longer length scale. If "strong" domains could somehow be bridged by covalent or slow bonds, complex coacervates should not be so predisposed to fracture. We interpret our success in Chapter 3 to take control over the fracture of high-salt coacervates as a demonstration

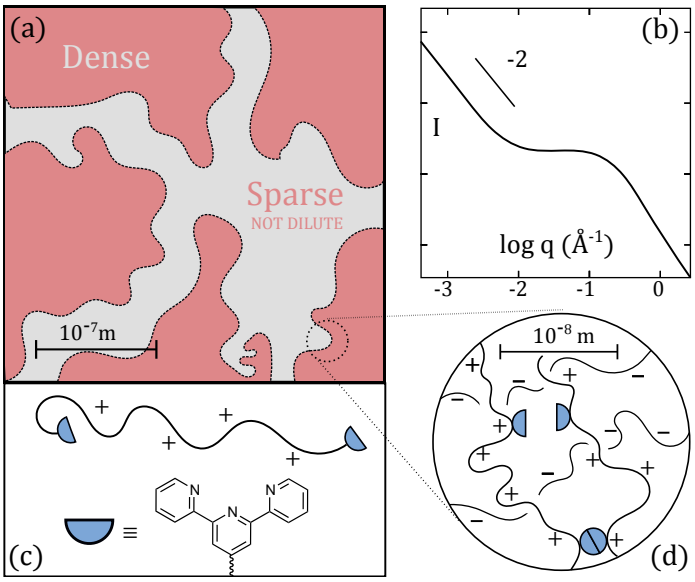

Figure 6.2: Mesoscale fluctuations of complex coacervates in (a) real space and (b) q-space. (c) suggests a way to harness the density fluctuations by linking together the dense parts, and (d) shows the fluctuations on the level of the coacervate mesh. The structure factor in (b) is drawn according to the X-ray scattering data of Spruijt et al.[36]

of the ability of transient crosslinks to bridge from one dense domain into another. However, we note that the length scales in our work are not optimized to provide bridging of the coacervate mesoscale fluctuations. In Chapter 2, we estimate the internodal length in pA/pD complexes near the critical salt strength at 20 nm. X-ray scattering studies[36] show a monotonous increase of the scattering intensity as we move to q below $\frac{1}{R_G}$, which means that the domain size is ill-defined. The same study showed a well-defined relaxation mode with a low diffusion coefficient at all q studied – if one takes this diffusion coefficient as describing the movement of the fluctuating domains, their size is 200 to 500 nm.[36] It is likely that the crosslinks follow the distribution of polyelectrolytes, and that weak spots are still present in the metal-crosslinked samples.

We suggest to investigate the effect of two further types of terpyridylated crosslinkers on the fracture resistance of complex coacervates reinforced by metal-ligand bonding. The suggestions take into account the tentative non-Gaussian origin of the strain stiffening found in metal-ligand complexes, and the presence of mesoscale fluctuations in coacervate complexes. The strain stiffening from finite extensibility could be capitalized on by the incorporation of terpyridylated semi-flexible polymers, which would already provide strain stiffening at lower strains. The predisposition of coacervates to brittle fracture could be further remedied by the use of a minority of long-chain (longer than the polyelectrolytes forming the bulk complex) terpyridylated polyelectrolytes, which allow a more effective bridging of the mesoscale density fluctuations. Figure 6.2d pictures the suggested structure as a telechelically terpyridylated polycation.

In Chapter 4, we have demonstrated the synthesis and conformations of a grafted polyelectrolyte that could address both of these suggestions at once: the dense grafting of pA chains results in a semiflexible macromolecule of a high persistence length. The graft polyelectrolyte can be terpyridylated in much the same way as described for coiled (linear) pA in Chapter 2. However, we also show that the critical salt strength of complex coacervates with semiflexible chains is lower than with coiled polyelectrolytes, an observation which we attribute to charge regulation in polymer brushes, which lead to uncharging.[57] Thus, it remains an open question whether long-chain semiflexible cross-linkers would be adequately incorporated.

In the next section, we will discuss other effects of branching that are relevant to non-linear rheology in non-coacervate materials. It remains to be seen whether the concepts are relevant to the field of complex coacervates.

Branching as an architectural hack to enhance failure-proofness

Dobrynin and co-workers published seminal work in which branching controls the elastic modulus, onset strain of non-linear elastic effects, and degree of strain stiffening in crosslinked melts of macromolecules of the bottlebrush architecture.[58–60] The crosslinked melts are represented by the amount of backbone monomers between crosslinks n_x, the amount of backbone monomers between side chains n_{sc}, and the length of the side chains n_g. The triplet of parameters $[n_x, n_{sc}, n_g]$ is referred to as a "material codon".

The bottlebrush polymer networks thus obtained have properties that are drastically different from conventional crosslinked melts (elastomers). First, the Young's modulus E of bottlebrush networks is not constrained by entanglements at the low end (normally, $E \geq k_B T \phi_e^{-3}$, ϕ_e being the entanglement density). Whereas typical flexible molecules in the molten state entangle at quite low molecular weights M_e between 10 and 100 kg mol^{-1}, the dense grafting of side-chains to a flexible backbone acts to disentangle the chains.[60] As a consequence, it becomes possible to access materials with E as low as 10 Pa that are still fully elastic. Furthermore, the maximal uniaxial strain before break λ_{max} can be tuned independently from E, which is unique for a synthetic polymer system. Finally, the extent to which strain stiffening occurs can be tuned from none to a 10^2-fold increase in strain-dependent modulus. These features allow to approach stress-strain relationships that one would want to model from a biological context, which are referred to as "material phenotypes".[61]

Elastomers made from bottlebrush polymers behave so differently from flexible coils because in the former, entanglements are avoided, and extension of elastically active chains into non-Gaussian stretching due to finite extensibility is promoted.[60, 61] The short side-chains that are grafted onto the backbone act as a diluent or a "covalent solvent", increasing M_e to above 10^3 kg mol^{-1}. At the same time, as is the case for our pA bottlebrush polyelectrolytes from Chapter 4, the backbones are already prestretched due to steric repulsion between the side chains (see, for instance, Figure 4.1 and 4.7). Thus, less strain is required to access the part of the stress-strain curve where one notices the finite extensibility.

Aside from polymer gels, complex coacervates are the only class of materials that fit the specifications for use as biomaterials. However, the stress-strain relationships that complex coacervates and their derivatives present are not ideal for use as underwater adhesives or implants. Coacervates typically fail at low strains. Thus, the above advances in taking charge of the non-linear elasticity are attractive for complex coacervates as well. It is fair to offer some critical statements in this discussion at this point.

First, polyelectrolyte bottlebrushes with a pH-dependent charge are not as charged

as their coil-like counterparts.[57] As a result, the critical salt concentration for complexes with semi-flexible chains is lower, and might perhaps not lie within the desired window of application. The lifetime of a monomer-monomer bond in a bottlebrush coacervate might also, correspondingly, be lower, resulting in more liquid-like or viscoelastic complexes. Both of these points, however, are not necessarily disadvantages, but rather ways to tune the mechanics of a coacervate. Indeed, as suggested before, bottlebrush polyelectrolytes could be considered as a diluted addition (dopant) to complex coacervates, to lower the elastic modulus, and to introduce strain hardening, as explained in the preceding section. Furthermore, polyelectrolyte bottlebrushes with permanent charges (not dependent on pH) circumvent the issue of charge regulation.

Linear viscoelasticity: searching on the bright side of the moon

A significant part of this thesis (Chapter 2) concerns the structure-property relationship between molecular parameters and linear viscoelastic functions such as the frequency-dependent complex modulus $G^*(\omega)$ and the longest relaxation time τ of complexes. The softness (modulus) and delay until flow (relaxation time) define the role that a material could play in any engineering context, and specifically in the tentative biomedical future that is suggested for coacervates.[62, 63] Nonetheless, linear viscoelasticity is given an amount of attention that I find disproportionate to its use, since it is unsuitable to advance the usefulness of materials in the world that exists outside of the rheometer gap. The characterization of small-strain rheological functions is only an initial check in the trajectory towards clearing a material for use in rehabilitating or even replacing a tissue. Subsequently, we must address the features that current biomaterials actually lack: first, practical triggers that take a material from an injectable fluid to the right viscoelasticity, and, second, an appropriate range of bond strengths.[62]

The development of triggers has been addressed in the initial section of the Discussion. The study of non-linear viscoelasticity ties in with the second. Bond strength is determined not by how stiff a material is under a small, controlled strain, but rather by how the material responds to large strains that are sufficient to change its structure.[55] Whereas structure-property relationships of linear viscoelasticity for complex coacervates and telechelic networks are widely developed,[6, 42, 64] also see Chapter 2, the connection between structure and non-linear (visco)elasticity is much harder to define.[65] The aforementioned studies of the impact of branching on the maximum strain before break and the extent of strain hardening in densely grafted molten polymers[58] set a remarkably high standard for addressing a complex, emergent property with hands-on molecular parameters.

In Chapter 3, we have embarked on a mission to take charge of the failure behaviour of complex coacervates (*vide supra*). At the same time, our study was limited by the use of amplitude sweeps and the available materials. The toughness of a material is more readily definable through the use of tension testing as a fracture energy density, which allows for easier correlation with molecular parameters. I recommend the aforementioned suggestion to use high-M dopants to "glue together" denser zones over the zones of weakness inherent to coacervate (Figure 6.2d), and correlate the fracture energy density with the amount of dopant present. Additionally, we suggest to establish structure-property relationships with more basic coacervate parameters, such as the salt strength and degrees of polymerization. The remarkable work of Schlenoff and co-workers on extruded polyelectrolyte complexes, which they coin as "saloplastics", could serve as an inspiration, since the studies take into account toughness as an important design parameter.[44, 45, 66]

Contributions by the group of Gong show another avenue into making tough biomaterials. A 2003 publication shows how intertwining two polymer networks, one soft-yet-deformable and another stiff-yet-brittle results in a hydrogel that breaks at stresses of 17 MPa, and shows strong strain hardening.[67] A disadvantage of the design is that there is no way to adjust the modulus without changing the strain hardening and fracture threshold. The same group presented subsequent results on tough hydrogels that were either covalently or physically crosslinked hydrogels of random copolymers of monomers with opposite charges.[68–70] The toughness of these polyampholyte hydrogels is related to the highly dissipative nature of the monomer-monomer interactions in the bulk: cracks are inhibited from spreading, preventing fracture. We note that our hybrid networks of Chapters 2 and 3 share similarities with double networks and polyampholyte gels: there are two distinct load-bearing structures present, and much of the materials' dissipative function relies on transient "electrostatic" bonding.

In short, polyelectrolytes and their complexes are well-positioned for the formulation of though materials. We reiterate that mechanisms to increase and control the tolerance to high strains will prove crucial to the application of polymers in biomaterials, and that incorporation of such mechanisms in complex coacervates will advance their value proposition massively.

6.4 Control, fidelity, and practical considerations in polymerization reactions for polyelectrolyte synthesis

The breakthroughs in the engineering of hydrophilic polymer materials alluded to in the above can not be achieved at a suitable scale when the chemistry required for their manufacture is prohibitively expensive due to the costs of reagents, complexity of operation, or risks to workers. Luckily, progress in the last two decades yielded polymerization reactions that tolerate milder conditions, are generalizable to a wide selection of solvents, and are easier and easier to operate. Importantly, these breakthroughs have not sacrificed the extent of control and definition that polymer scientists have learned to enjoy from ionic polymerization techniques.

In Chapters 5 of this thesis, we prepared polymer materials using reversible addition–fragmentation chain-transfer polymerization (RAFT). In Chapter 2 and 3 we used only techniques based on atom transfer radical polymerization (ATRP), also known by the mechanism-agnostic homonym copper-catalyzed radical polymerization. In Chapter 4, a combination was used. In this section, I will reflect on how the choice of one over the other might affect experiments. Furthermore, I will discuss chemical definition in polymers, or how chemists should be wary of even marginally present groups such as end groups or impurities. On a side note, I use the term ATRP in the broad sense to mean any kind of Cu-based polymerization that includes atom transfer as a part of its mechanism. An undecided debate[71, 72] rages on about whether the reactions used in Chapter 2 are accurately described by the original ATRP mechanism.

Controlled radical polymerization facilitates direct or indirect polyelectrolyte synthesis

Before the advent of controlled radical polymerization techniques, polymerization reactions were only feasible for monomers that do not react with ionic propagating species – carbanions[73] or carbocations.[74] This constraint excludes one-step synthesis of poly(anions), but weak polycations such as poly(*N*,*N*-dimethylaminoethyl methacrylate) (pD) can be prepared with anionic polymerization.[75, 76] Selected poly(anions) can be prepared by polymerization of a neutral precursor, followed by a polymer analogous reaction, for instance, the de-*tert*-butylation of *tert*-butyl acrylate to poly(acrylic acid) (pA).

We opted for the use of controlled radical polymerization techniques in this thesis, given the ease of operation that they offer, and their compatibility with direct

synthesis of polymers from ionic monomers, which we ended up using in only a few cases (*vide infra*). Both RAFT[77–83] and copper-catalyzed techniques[80, 84] are suitable to the direct synthesis of polyelectrolytes. Generally, the latter requires careful optimization and sometimes specialized conditions, especially if one wishes to polymerize acidic monomers.[85] Nonetheless, we were able to polymerize *N,N*-dimethyl acrylamide brushes with 5% of acrylamidopropyl trimethylammonium chloride or sodium sulfopropyl methacrylate onto crosslinked poly(styrene) particles, in which we had also incorporated the acrylate ester of 2,2-dimethyl-*iso*-bromo butyrate, which acts as an ATRP initiator. We also added a sacrificial initiator, the ligand Me_6TREN, and CuBr. While it remains uncertain whether the success translates to well-characterized, linear polymers, the brushes were highly effective at sterically stabilizing the particles in solutions of 1.5 M NaCl.

We used RAFT to directly polymerize 2,2-acrylamido propylsulfonic acid for the work in Chapters 2 and 3 (full procedure in the Appendix), which yields a strong poly(anion). The polymerization was sufficiently controlled, however, we were not able to extend the reaction to block copolymer formation with poly(acrylamide). Additionally, it is not clear whether it would have been possible to synthesize polymers of higher M.

Even though RAFT and ATRP offer the direct synthesis of pA directly from the carboxylic acid, we opted for the two-step scheme that is described in detail in Chapter 5: synthesis of poly(*tert*-butyl acrylate) with either RAFT (Chapter 5) or ATRP (Chapter 2, 3, 4) followed by removal of the *tert*-butyl ester with HCl in hexafluoroisopropanol. The introduction to Chapter 5 highlights the many side reactions that are inherent to direct polymerization of acrylic acid with any form of radical polymerization. Furthermore, both RAFT and ATRP can yield poly(*tert*-butyl acrylate) of a good definition up to high molecular weight, whereas it is doubtful that the same is true for poly(acrylic acid).

Copper-based radical polymerization has one obvious drawback in the context of this thesis: the presence of copper. It remains very difficult to remove copper from polymer residues adequately, even in polymerization in which small amounts are used. From the fact that the rheological signatures of supposedly unmetalated samples in Chapter 3 show clear signs of metal terpyridine-binding, it is clear that simply passing the solution of the product through a column of Al_2O_3 does not clear the mixture of Cu^{2+}. Likewise, dialysis against water is ineffective, however, addition of excesses of EDTA to the dialysate accomplishes a gradual removal of Cu^{2+}. Only clean samples were used in Chapter 2.

While RAFT is not plagued by the presence of copper, it has other, subtle, drawbacks. Whereas we show in Chapter 5 that the trithiocarbonate moiety is stable to at least dissolution in water, neutralization with NaOH, and to general handling, we

know that it is photolabile in the long term, since visible light initiates RAFT polymerization.[86] For polymers that have the trithiocarbonate moiety in the center of the chain, such as in Chapter 5, this would result in a slow halving of the molecular weight distribution, a complication that was not acceptable to us in the long-time rheological studies of Chapters 2 and 3. Photolability of end groups is similarly undesirable, since the removal of RAFT end-groups results in free thiols.[87] Ultimately, we opted to synthesize the precursor for the poly(acrylic acid) with a Cu^0-based method[71] with low copper concentration. Given the waste of water and material for the removal of residual Cu^{2+}, we can not give the method a recommendation, despite the great ease of the polymerization itself.

Ideally, the polymerization of poly(*tert*-butyl acrylate) would have been done with a RAFT agent with a short alkyl or hydroxyalkyl Z-group, and a 2-methylpropionic acid R-group, followed by end group removal (*vide infra*). However, the correct RAFT agent was not available to us at the time, and end group removal involves an extra step. Despite considerable progress, the selection of a polymerization technique remains an ever subtle art, perhaps due to the availability of a growing selection of equally qualified methods.

Increased control over radical polymerizations under increasingly mild conditions

The conditions used in the first few ATRP papers by Wang and Matyjaszewski[88] must have been a great relief to those looking to start a career in polymer chemistry: gone was the need for high vacuum, immaculately clean monomers, and the specialised chemistry that tailoring an anionic polymerization entailed.[73] Nonetheless, the initial iteration of ATRP studies utilized temperatures between 60–130 °C, catalyst loadings at least stoichiometric to the initiator, and were performed in neat liquid monomers or ethyl acetate. While the system could be used to polymerize styrene, acrylates and methacrylates, Đ was only low for styrene.

A plethora of discoveries made the conditions milder, more readily generalizable to a broad class of solvents and monomers, and the operation easier.[76, 89] Here, I will focus on those discoveries that are especially relevant to the synthesis of hydrophilic polymers. First of all, the discovery of highly active ATRP ligands, such as the three-armed, quadridentate ligand tris[2-(dimethylamino)ethyl]amine (Me_6TREN), allowed to carry out polymerizations at room temperature.[90] A concurrent benefit of more active ligands is that the concentration of catalyst can be lowered, which simplifies work-up, and *increases* the extent to which the polymerization is controlled[91] by decreasing the contribution of side reactions.[92] Second, the dramatic influence of

solvent choice on the polymerization rate and degree of control[93] enabled a wider variety of monomers and copolymers to be synthesized, with more polar solvents generally leading to higher activation and polymerization rates.[93] In particular, water is reported to yield fast, controlled polymerization, despite a few challenges specific to this solvent.[94–96] Finally, the use of zerovalent copper (Cu^0) also allows to lower the amount of catalyst.[97]

The use of Cu^0 is especially common in combination with polar solvents (including water), and is particularly effective when attempting to polymerize hydrophilic monomers in a controlled manner.[71, 96, 98] It is quite common to encounter an alternative mechanism to ATRP[88] for copper-catalyzed polymers in polar solvents: that of Single Electron Transfer Living Radical Polymerization (SET-LRP).[72] The central point of contention is whether Cu^0 merely reduces Cu^{II} into the ATRP-active Cu^I (ATRP mechanism), or whether complexes with Cu^0 itself act as a catalyst. A full summary of the immense bibliography that documents the ever-raging debate over whether use of the SET-LRP terminology is qualified is outside of the scope of this thesis. Moreover, the debate is now stranded at a point were advocates of both – conflicting – models have conclusively proven their point.[99] I suggest the work of Anastasaki and co-workers for a particularly fair depiction of both sides.[96]

A more recent development in Cu-catalyzed polymerization shows that, perhaps, more is uncertain than we would like to think: initiating radicals can also be generated in the *absence* of both Cu^0 and Cu^I, with Me_6TREN and "deactivating" Cu^{II} in the presence of light in the UV or visible spectrum.[100] We used this much overlooked "activator-less", photomediated method for the multi-gram synthesis of pD for Chapters 2 and 3. Unfortunately, we were confronted with quite a mismatch between theoretical and SEC-derived values for the molecular weight. Nonetheless, the procedure could undoubtedly be optimized further, and represents a further decrease in complexity and reagent costs. We note that we were also able to synthesize a co-polymer of pentafluorophenyl acrylate and *tert*-butyl acrylate, a combination that resisted all conventional RAFT and ATRP methodologies attempted.

The original RAFT reaction reported by Moad et al. in 1998[101] underwent a similar revolution.[78, 102] The extension of RAFT to all classes of acrylic monomers, ambient temperatures, and broad solvent tolerance has for a large part been driven by the wide assortment of RAFT agents.[103] Nonetheless, RAFT agents are more expensive than reagents for copper-catalyzed polymerization, and this drove us to use ATRP for a significant part of our work. For instance, the synthesis of bottlebrush polyelectrolytes by grafting-from with ATRP was cheap: the initiating 2-bromo-*iso*-butyrate groups were installed *via* trivial ester formation using universally available reagents. Doing the same with RAFT would have incurred much higher costs.

A particularly attractive feature of RAFT is the recent development of photome-

diated initiation of the reaction,[104] which we were happy to implement in Chapter 5. Despite the fact that RAFT agents, per definition, comprise a homolytically labile group that could initiate polymerization, polymerizations are performed with the aid of additional radicals initiators, typically azo compounds such as azo-*iso*-butyronitrile (AIBN). When one wishes to perform the polymerization at room temperature, the list of initiators is very short, and their availability is highly limited due to the inherent risks of room-temperature initiators. However, with photo-mediated RAFT polymerization, it is possible to use any water-soluble RAFT agent, and initiate the reaction with long-wave UV or visible light. The process has been used to prepare ultra-high M polymers of the acrylamide class.[86, 105] The use of unnecessary azo initiators will rapidly be abolished, so that chemists can enjoy the improved capacities and ease of operation that photo-mediated RAFT provides.

An exciting prospect is the work towards oxygen tolerance in RAFT[106] and ATRP.[107] Improving the ease at which polymerizations can be done allows the desired polymer structure to be accessed early on in research projects. As a consequence, more effort can be allotted to studying polymer properties, and improving materials.

On a final note, an oft-ignored question is whether it is always necessary to synthesize polymers that are narrowly dispersed. Even with the most controlled radical polymerization techniques, the products come nowhere near the Đ= 1 polymers produced in the ribosome. Indeed, all industrial polymers applied to this day are polydisperse. Nonetheless, the molecular weight distribution is a parameter with an importance similar to the choice of monomer and the average molecular weight. I reiterate the point of Grubbs[76] that there are few key advantages to having a minimal value of Đ in real-world applications of polymers. We note that free radical polymerization, although often disregarded as outmoded, continues to expand the mechanical parameter space that can be addressed with hydrogels, such as in the work of Gong.[67]

The RAFT end-group provides a reactive handle that can addressed quantitatively

An important distinction between free radical polymerization and controlled techniques, such as RAFT and ATRP, is the fate of the polymer ends. The moiety that starts the radical chain reaction (the R-group in RAFT, and the initiator radical after homolytic dehalogenation in ATRP) is often called the α-end, whereas the opposite end is called the ω-end or, simply, the end-group. Because in both methods growing chains are repeatedly deactivated and then re-activated by transfer of a group (RAFT) or halogen atom (ATRP), the end group is defined, or "faithful" in an ideal polymeriza-

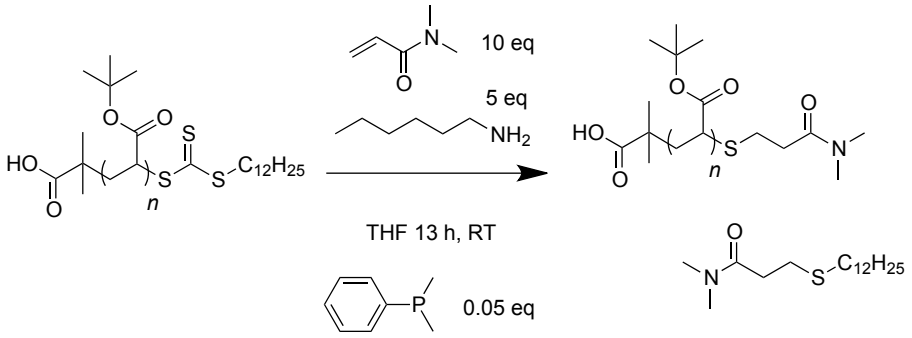

Figure 6.3: Reaction conditions for modification of dodecyl trithiocarbono-capped chains by liberation of the thiol, followed by thio-Michael addition of the thiol to an activated alkene.

tion. Indeed, end-group fidelity is a well-discussed topic in the world of RAFT[87, 108] and ATRP,[98, 109, 110] because the chain ends can impart physical or chemically reactive properties to the chains, or because it can be desirable to transform the end groups in a subsequent step.

In an early phase of the experimentation for this thesis, we had an interest in stabilizing RAFT end groups to address the issue of hydrolytic lability.[111] For this purpose, we synthesized oligomeric fragments of poly(*tert*-butyl acrylate) (pT) under the control of 2-methyl-2-propionic acid dodecyl trithiocarbonate (DMP), and subsequently exposed them to conditions that, first, unmask the thiol by aminolysis with hexylamine, and, second, enable Michael addition of the resulting thiol to *N*,*N*-dimethyl acrylamide (DMA). The chemistry is depicted in Figure 6.3 and was executed as described by Haddleton and co-workers.[112]

The procedure successfully resulted in a quantitative passivization of the RAFT functionality and replaced the trithio moiety with a DMA residue. Whereas GPC traces from runs in tetrahydrofuran were identical, mass spectrometry confirmed the successful removal of the CS_2–$C_{12}H_{25}$ group and its replacement with a DMA residue, as can be seen by the shift of -146 mass units between peaks of pT-$S_3C_{12}H_{25}$ and pT-DMA in Figure 6.4. All peak masses could be attributed to expected structures — the masses for pT^7-DMA (7 units of *tert*-butyl acrylate) correspond to the formula $nM_{t\mathrm{BuAc}} + M_{\mathrm{MPA}} + M_{\mathrm{DMA}} + M_{\mathrm{Na}^+}$, where M_{MPA} refers to the 2-methylpropionic acid radical from the RAFT R-group (87 g mol^{-1}), whereas the masses for the untreated residues correspond to $nM_{t\mathrm{BuAc}} + M_{\mathrm{DMP}}$. Finally, the spectrum of the modified sample showed no signals that correspond to chains with the RAFT group still intact.

Despite the unambiguous demonstration that every chain was indeed modified,

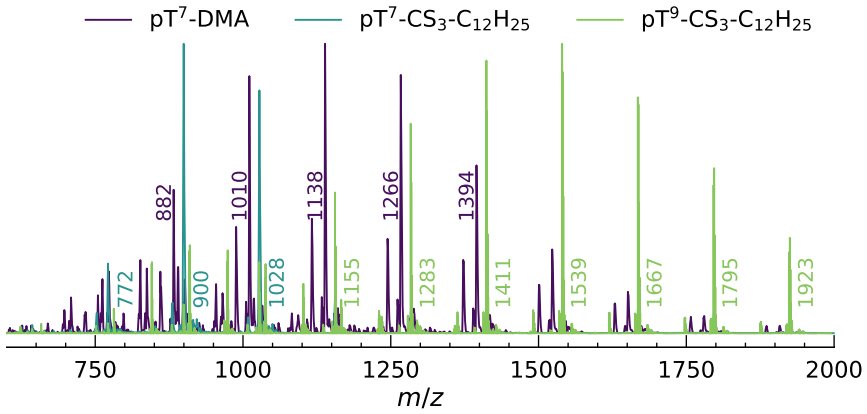

Figure 6.4: Mass spectra for unmodified pT with median degrees of polymerization of 7 (pT^7-$S_3C_{12}H_{25}$) and 9 (pT^9-$S_3C_{12}H_{25}$) and end-group modified pT^7-DMA, which has the RAFT functionality replaced by a DMA residue. We included the unmodified nonamer for the reason that it present a clearer mass spectrum for comparison with the modified heptamer. The mass spectra were recorded in positive ion mode, using soft ionization on an LXQ machine.

we deemed the method impractical for large-scale use: it requires the hazardous and labile dimethylphenyl phosphine, and, crucially, chromatography on SiO_2 to separate the oligomer fragments from the Michael product of dodecyl thiol and DMA. The latter is not reasonable for large batches of high M pT. As such, we settled for the intrinsically more passive ω-brominated products of Cu^0-catalyzed polymerization described above.

Nonetheless, the modification of polymers in this way promises facile synthesis of α,ω telechelic terpyrdidylated products, which have been suggested above to improve the fracture energy density of complex coacervates. To this end, however, one must start with two RAFT agents coupled together via their R-groups, for instance by dimerizing DMP through amide bond formation or esterification. Our group has not met great success in the synthesis of said structure with carbodiimide-facilitated amide coupling, however, there is literature on similar structures.[113] Alternatively, bis-2-(2-bromobutyryl) ATRP-type initiators are available commercially, or can be prepared cheaply. The subsequent modification of the α,ω chain end bromines could proceed via azide formation, followed by a azido-alkyne "click" reaction with a terpyridylated alkyne.[109] The ability to control both α- and ω- ends should be considered as a prime target in controlled radical polymerization.

The *tert*-butyl ester: fidelity on the monomer level

A more overlooked fidelity issue in polymer chemistry seems to be that of the monomers *themselves* — Chapter 5 presented a cautionary tale of how the presence of residual *tert*-butyl acrylate residues is often overlooked in literature describing the properties of poly(acrylic acid) derived from pT using TFA/DCM de-esterification. To the surprise of the author, even after publication of the chapter,[114] the use of TFA/DCM in de-*tert*-butylation for poly(acrylic acid) synthesis is commonplace.

Fidelity in polymers is not limited to the control over a molecular weight distribution or even an end group. Controlled radical polymerization entails that the chemical structure of the actual chains is accurately reflected in the chemical drawings. This is not merely for the sake of purism: we have shown in Chapter 5 that the conformational properties of the contaminated polymers were markedly altered, as was the assembly behaviour of the triblocks. The author urges chemists to always look critically at their own methods and those of their peers, and at all times expect the unexpected, even in old, "trusted" reactions.

6.5 The ecological and societal impact of chemistry

The ecological ramifications of the rapidly increasing production of polymer products and their release into the environment can not be overstated. Since the 1950s, plastic has been dumped into the ocean, and in 2010 alone an estimated 10^{13} kg of plastic escaped from coastal landfills into oceans.[115] Estimates of the total mass of plastic in the marine environment are difficult to give due to the lack of data in earlier decades, but modelling suggests that between 2010 and 2025, $0.25 \cdot 10^{15}$ kg will be released cumulatively into the seas. Analysis of socioeconomic data predicts that peak waste will be not achieved before 2100, if reasonable predictions of population growth and consumption are met.[116]

The effects of this enormous amount of wasted material are devastating to organisms that inhabit the sees: animals ingest material, get entangled into waste, and are affected by leeching of harmful plasticizers.[117] Furthermore, the problem threatens humans directly, since plastic can accumulate in dams and riverbeds, contributing to floods.[118] The impacts of flood-driven mobilization of riverine plastic are similarly devastating as plastic discharge into the ocean: the release of plastics into rivers severely harms local populations by taking away food sources and access to clean drinking water.[118]

While it is indisputable that cheap plastics have contributed to the quality of life of humans around the world, for instance through single-use items making medical care cheaper and more convenient, as barrier materials in the COVID-19 crisis, and in making consumer goods more available throughout socioeconomic classes, it is inevitable that this contribution comes at a grave cost. The industrial lobby is quick to lay the blame on consumers. However, the civil court of The Hague recently ruled that consumer choices do not deprive Shell of their responsibility to not harm people by their conduct in a widely popularised case.[119] Likewise, the industrio-economic complex that drives plastic consumption likely breaks legal norms, and their profits are a major force behind humanity's devastating effect on their environment.

Clearly, the world is becoming a victim of polymer science's success. I urge polymer chemist to take responsibility, stimulate research into materials that can circumvent the devastating impacts of "forever" plastics, and call out industries on their complicity in the plastic crisis.

To an ever-more ecologically minded generation, synthetic polymers are becoming a new iteration of Alfred Nobel's dynamite. The violent application of his morally neutral invention – dynamite – made him lose faith in mankind. Nobel eventually calmed his guilt by investing all his money in savings so that the eponymous award could be financed annually from the interest alone. However, progress in science can not be paid by human lives, and in that sense one can not redeem Nobel. In

fact, his investment eerily echoes the greenwashing practices employed by polluting industries in the 21st century, by which they wish to market an impossible future to a generation of consumers who are getting increasingly worried about living conditions on Earth.

Polymers and the end of petrochemistry

A more subtle question sits uncomfortably in the mind of chemists: given that petrochemical sources are due to run out eventually, and that the practice of oil extraction has countless negative by-effects, how will we go about doing chemistry in the future? The question is pressing for polymer chemists, too: 90% of resin is synthesized directly from virgin oil,[115] a practice that is only affordable in times of cheap oil.

As reserves of clean oil run out, chemistry will have to adapt and source its materials from other sources. Likewise, it is unwise to presume that we could simply use plants for our chemical needs, since the purification of pure organics from plant matter is extremely energy-intensive, and energy will likely be more expensive in times of oil scarcity. Furthermore, it is undesirable that arable land will be competed for by the chemical industry at any great scale.

The field called "green chemistry" concerns itself with future-proofing chemical practices. It is the opinion of the author that *all* of chemistry will have to "go green", since the value of discoveries that are relevant only to a petrochemically dominated world might be of a short shelf life. Without wishing to constrain the debate to a certain technology (there are many), I would like to end this discussion by challenging the reader to set goals for achieving chemistry that will be of use in a defossilized world.

6.6 Concluding remarks

In short, this thesis explores the use of chemistry inspired by the adhesives of underwater animals, such as mussels and sandcastle worms, to improve the mechanical and stimulus-responsive capabilities of hydrophilic polymer materials. Polyelectrolytes constitute a major component of biological underwater adhesives, and the ability of opposite, polymeric charges to form complexes contributes to the unique combination of features that enable effective contact formation and strong cohesion underwater. Accordingly, I argue in this thesis that polyelectrolyte complexes are central to the future of biomaterials.

Complex coacervates are mechanically versatile, since their viscoelasticity can be varied from that of liquids of low viscosity to that of elastic solids of appreciable elastic

modulus (in the MPa range). The parameters that control coacervate viscoelasticity are the chemistry of the monomers, the architectural features of the polymers (such as branching), and the salt concentration of the environment. Because there are limits to which materials are tolerated in applications, and because the salt concentration can not always be chosen freely, the application of complex coacervates requires an enlarged toolkit of means to take control over mechanics.

Complex coacervates display a unique combination of features due to their low surface energy and hydrophilicity, two characteristics that contradict the insolubility of complex coacervates in water. However, coacervates *per se* do not offer sufficient handles for bringing them up to the exacting specifications of biomaterial applications. The engineering of transient crosslinking and semiflexibility into coacervates offers eminent opportunities to prepare polyelectrolyte complexes for the real world. It is imperative that further work on biomaterials addresses issues of biocompatibility, but also of degradability, and the question of how to conduct chemistry within planetary boundaries.

Bibliography

[1] G. Bot, K. Bot, J. Ogunranti, J. Onah, A. Sule, I. Hassan, and E. Dung, "The use of cyanoacrylate in surgical anastomosis: An alternative to microsurgery," *Journal of Surgical Technique and Case Report*, vol. 2, no. 1, p. 44, 2010.

[2] G. Pascual, S. Sotomayor, M. Rodríguez, B. Pérez-Köhler, A. Kühnhardt, M. Fernández-Gutiérrez, J. S. Román, and J. M. Bellón, "Cytotoxicity of cyanoacrylate-based tissue adhesives and short-term preclinical in vivo biocompatibility in abdominal hernia repair," *PLoS ONE*, vol. 11, no. 6, pp. 1–22, 2016.

[3] D. F. Williams, "On the mechanisms of biocompatibility," *Biomaterials*, vol. 29, no. 20, pp. 2941–2953, 2008.

[4] J. Qin, D. Priftis, R. Farina, S. L. Perry, L. Leon, J. Whitmer, K. Hoffmann, M. Tirrell, and J. J. De Pablo, "Interfacial tension of polyelectrolyte complex coacervate phases," *ACS Macro Letters*, vol. 3, no. 6, pp. 565–568, 2014.

[5] E. Spruijt, J. Sprakel, M. A. Cohen Stuart, and J. Van Der Gucht, "Interfacial tension between a complex coacervate phase and its coexisting aqueous phase," *Soft Matter*, vol. 6, no. 1, pp. 172–178, 2009.

[6] E. Spruijt, M. A. Cohen Stuart, and J. Van Der Gucht, "Linear viscoelasticity of polyelectrolyte complex coacervates," *Macromolecules*, vol. 46, no. 4, pp. 1633–1641, 2013.

[7] M. Yang, J. Shi, and J. B. Schlenoff, "Control of Dynamics in Polyelectrolyte Complexes by Temperature and Salt," *Macromolecules*, vol. 52, no. 5, pp. 1930–1941, 2019.

[8] E. Hennebert, E. Gregorowicz, and P. Flammang, "Involvement of sulfated biopolymers in adhesive secretions produced by marine invertebrates," *Biology Open*, vol. 7, no. 11, p. bio037358, 2018.

[9] R. J. Stewart, T. C. Ransom, and V. Hlady, "Natural underwater adhesives," *Journal of Polymer Science, Part B: Polymer Physics*, vol. 49, no. 11, pp. 757–771, 2011.

[10] R. J. Stewart, C. S. Wang, and H. Shao, "Complex coacervates as a foundation for synthetic underwater adhesives," *Advances in Colloid and Interface Science*, vol. 167, no. 1-2, pp. 85–93, 2011.

[11] J. Yang, M. A. Cohen Stuart, and M. Kamperman, "Jack of all trades: versatile catechol crosslinking mechanisms," *Chem. Soc. Rev.*, vol. 43, no. 24, pp. 8271–8298, 2014.

[12] S. F. Banani, H. O. Lee, A. A. Hyman, and M. K. Rosen, "Biomolecular condensates: Organizers of cellular biochemistry," *Nature Reviews Molecular Cell Biology*, vol. 18, no. 5, pp. 285–298, 2017.

[13] F. Sciortino, S. H. Mir, A. Pakdel, A. Oruganti, H. Abe, A. Witecka, D. N. Awang Shri, G. Rydzek, and K. Ariga, "Saloplastics as multiresponsive ion exchange reservoirs and catalyst supports," *Journal of Materials Chemistry A*, vol. 8, no. 34, pp. 17713–17724, 2020.

[14] Q. Wang and J. B. Schlenoff, "Tough strained fibers of a polyelectrolyte complex: Pretensioned polymers," *RSC Advances*, vol. 4, no. 87, pp. 46675–46679, 2014.

[15] M. Dompe, M. Vahdati, F. V. Ligten, F. J. Cedano-serrano, D. Hourdet, C. Creton, M. Zanetti, P. Bracco, J. V. D. Gucht, T. Kodger, and M. Kamperman, "Enhancement of the Adhesive Properties by Optimizing the Water Content in PNIPAM-Functionalized Complex Coacervates," *ACS Applied Polymer Materials*, vol. 2, pp. 1722–1730, 2020.

[16] I. A. V. Hees, P. J. M. Swinkels, R. G. Fokkink, A. H. Velders, I. K. Voets, J. V. D. Gucht, and M. Kamperman, "Polymer Chemistry Self-assembly of oppositely charged polyelectrolyte block copolymers containing short thermoresponsive blocks," *Polymer Chemistry*, vol. 10, no. 23, pp. 3127–3134, 2019.

[17] C. S. Wang and R. J. Stewart, "Multipart copolyelectrolyte adhesive of the sandcastle worm, Phragmatopoma californica (Fewkes): Catechol oxidase catalyzed curing through peptidyl-DOPA," *Biomacromolecules*, vol. 14, no. 5, pp. 1607–1617, 2013.

[18] H. Zhao, C. Sun, R. J. Stewart, and J. H. Waite, "Cement proteins of the tube-building polychaete Phragmatopoma californica," *Journal of Biological Chemistry*, vol. 280, no. 52, pp. 42938–42944, 2005.

[19] C. S. Wang, K. K. Svendsen, and R. J. Stewart, *Morphology of the Adhesive System in the Sandcastle Worm, Phragmatopoma californica*, pp. 169–179. Vienna: Springer Vienna, 2010.

[20] L. Zhang, V. Lipik, and A. Miserez, "Complex coacervates of oppositely charged co-polypeptides inspired by the sandcastle worm glue," *J. Mater. Chem. B*, vol. 4, no. 8, pp. 1544–1556, 2016.

[21] S. Kaur, G. M. Weerasekare, and R. J. Stewart, "Multiphase adhesive coacervates inspired by the sandcastle worm," *ACS Applied Materials and Interfaces*, vol. 3, no. 4, pp. 941–944, 2011.

[22] H. Shao, K. N. Bachus, and R. J. Stewart, "A water-borne adhesive modeled after the sandcastle glue of P. californica," *Macromolecular Bioscience*, vol. 9, no. 5, pp. 464–471, 2009.

[23] B. K. Ahn, S. Das, R. Linstadt, Y. Kaufman, N. R. Martinez-Rodriguez, R. Mirshafian, E. Kesselman, Y. Talmon, B. H. Lipshutz, J. N. Israelachvili, and J. H. Waite, "High-performance mussel-inspired adhesives of reduced complexity," *Nature Communications*, vol. 6, p. 8663, 2015.

[24] E. Siband, Y. Tran, and D. Hourdet, "Thermoresponsive interpolyelectrolyte complexation: Application to macromolecular assemblies," *Macromolecules*, vol. 44, no. 20, pp. 8185–8194, 2011.

[25] M. Dompé, F. J. Cedano-Serrano, O. Heckert, N. van den Heuvel, J. van der Gucht, Y. Tran, D. Hourdet, C. Creton, and M. Kamperman, "Thermoresponsive Complex Coacervate-Based Underwater Adhesive," *Advanced Materials*, p. 1808179, 2019.

[26] J. Niskanen and H. Tenhu, "How to manipulate the upper critical solution temperature (UCST)?," *Polymer Chemistry*, vol. 8, no. 1, pp. 220–232, 2017.

[27] K. S. Lim, J. H. Galarraga, X. Cui, G. C. Lindberg, J. A. Burdick, and T. B. Woodfield, "Fundamentals and Applications of Photo-Cross-Linking in Bioprinting," *Chemical Reviews*, vol. 120, no. 19, pp. 10662–10694, 2020.

[28] W. H. Shaw, "Cation toxicity and the stability of transition-metal complexes," *Nature*, vol. 192, no. 4804, pp. 754–755, 1961.

[29] S. Lanzalaco and E. Armelin, "Poly(N-isopropylacrylamide) and Copolymers: A Review on Recent Progresses in Biomedical Applications," *Gels*, vol. 3, no. 4, p. 36, 2017.

[30] M. Xu, J. Zhu, F. Wang, Y. Xiong, Y. Wu, Q. Wang, J. Weng, Z. Zhang, W. Chen, and S. Liu, "Improved In Vitro and In Vivo Biocompatibility of Graphene Oxide through Surface Modification: Poly(Acrylic Acid)-Functionalization is Superior to PEGylation," *ACS Nano*, vol. 10, no. 3, pp. 3267–3281, 2016.

[31] B. D. Ratner, "Biomaterials: Been There, Done That, and Evolving into the Future," *Annual Review of Biomedical Engineering*, vol. 21, pp. 171–191, 2019.

[32] B. D. Winslow, H. Shao, R. J. Stewart, and P. A. Tresco, "Biocompatibility of adhesive complex coacervates modeled after the sandcastle glue of Phragmatopoma californica for craniofacial reconstruction," *Biomaterials*, vol. 31, no. 36, pp. 9373–9381, 2010.

[33] J. P. Jones, M. Sima, R. G. O'Hara, and R. J. Stewart, "Water-Borne Endovascular Embolics Inspired by the Undersea Adhesive of Marine Sandcastle Worms," *Advanced Healthcare Materials*, vol. 5, no. 7, pp. 795–801, 2016.

[34] W. C. Blocher and S. L. Perry, "Complex coacervate-based materials for biomedicine," *Wiley Interdisciplinary Reviews: Nanomedicine and Nanobiotechnology*, vol. 9, no. 4, pp. 76–78, 2017.

[35] M. Bohdan, J. Sprakel, and J. Van Der Gucht, "Multiple relaxation modes in associative polymer networks with varying connectivity," *Physical Review E*, vol. 94, no. 3, pp. 1–7, 2016.

[36] E. Spruijt, F. A. Leermakers, R. Fokkink, R. Schweins, A. A. Van Well, M. A. Cohen Stuart, and J. Van Der Gucht, "Structure and dynamics of polyelectrolyte complex coacervates studied by scattering of neutrons, X-rays, and light," *Macromolecules*, vol. 46, no. 11, pp. 4596–4605, 2013.

[37] J. Sprakel, J. Van Der Gucht, M. A. Cohen Stuart, and N. A. Besseling, "Brownian particles in transient polymer networks," *Physical Review E - Statistical, Nonlinear, and Soft Matter Physics*, vol. 77, no. 6, 2008.

[38] M. Doi and S. F. Edwards, *The theory of polymer dynamics*. New York: Oxford University Press, first ed., jun 1988.

[39] B. A. Krajina, C. Tropini, A. Zhu, P. Digiacomo, J. L. Sonnenburg, S. C. Heilshorn, and A. J. Spakowitz, "Dynamic Light Scattering Microrheology Reveals Multiscale Viscoelasticity of Polymer Gels and Precious Biological Materials," *ACS Central Science*, vol. 3, pp. 1294–1303, 2017.

[40] M. Dompé, F. J. Cedano-Serrano, M. Vahdati, D. Hourdet, J. Van der Gucht, M. Kamperman, and T. E. Kodger, "Hybrid complex coacervate," *Polymers*, vol. 12, no. 2, 2020.

[41] M. J. Snowden, S. M. Clegg, P. A. Williams, and I. D. Robb, "Flocculation of silica particles by adsorbing and non-adsorbing polymers," *Journal of the Chemical Society, Faraday Transactions*, vol. 87, no. 14, pp. 2201–2207, 1991.

[42] E. Spruijt, J. Sprakel, M. Lemmers, M. A. Stuart, and J. Van Der Gucht, "Relaxation dynamics at different time scales in electrostatic complexes: Time-salt superposition," *Physical Review Letters*, vol. 105, no. 20, 2010.

[43] Q. Wang and J. B. Schlenoff, "The polyelectrolyte complex/coacervate continuum," *Macromolecules*, vol. 47, no. 9, pp. 3108–3116, 2014.

[44] R. F. Shamoun, A. Reisch, and J. B. Schlenoff, "Extruded saloplastic polyelectrolyte complexes," *Advanced Functional Materials*, vol. 22, no. 9, pp. 1923–1931, 2012.

[45] H. H. Hariri and J. B. Schlenoff, "Saloplastic macroporous polyelectrolyte complexes: Cartilage mimics," *Macromolecules*, vol. 43, no. 20, pp. 8656–8663, 2010.

[46] D. A. Deitz, J. X. Zhu, D. J. Durian, H. Gang, and D. J. Pine, "Diffusing-Wave Spectroscopy: The Technique and Some Applications," *Physica Scripta*, vol. T49, pp. 610–621, 1993.

[47] H. M. Van Der Kooij, S. Dussi, G. T. Van De Kerkhof, R. A. Frijns, J. Van Der Gucht, and J. Sprakel, "Laser Speckle Strain Imaging reveals the origin of delayed fracture in a soft solid," *Science Advances*, vol. 4, no. 5, 2018.

[48] E. Spruijt, *Strength, structure and stability of polyelectrolyte complex coacervates*. PhD thesis, Wageningen University, 2012.

[49] J. Sprakel, E. Spruijt, M. A. Cohen Stuart, N. A. Besseling, M. P. Lettinga, and J. Van Der Gucht, "Shear banding and rheochaos in associative polymer networks," *Soft Matter*, vol. 4, no. 8, pp. 1696–1705, 2008.

[50] D. Xu and S. L. Craig, "Strain hardening and strain softening of reversibly cross-linked supramolecular polymer networks," *Macromolecules*, vol. 44, no. 18, pp. 7478–7488, 2011.

[51] D. Xu, J. L. Hawk, D. M. Loveless, S. L. Jeon, and S. L. Craig, "Mechanism of shear thickening in reversibly cross-linked supramolecular polymer networks," *Macromolecules*, vol. 43, no. 7, pp. 3556–3565, 2010.

[52] D. Xu and S. L. Craig, "Multiple Dynamic Processes Contribute to the Complex Steady Shear Behavior of Cross-Linked Supramolecular Networks of Semidilute Entangled Polymer Solutions," *Journal of Physical Chemistry Letters*, vol. 1, no. 11, pp. 1683–1686, 2010.

[53] R. D. Groot, A. Bot, and W. G. Agterof, "Molecular theory of the yield behavior of a polymer gel: Application to gelatin," *Journal of Chemical Physics*, vol. 104, no. 22, pp. 9220–9233, 1996.

[54] H. Tabuteau, S. Mora, G. Porte, M. Abkarian, and C. Ligoure, "Microscopic mechanisms of the brittleness of viscoelastic fluids," *Physical Review Letters*, vol. 102, no. 15, pp. 1–4, 2009.

[55] C. Creton and M. Ciccotti, "Fracture and adhesion of soft materials: a review," *Reports on Progress in Physics*, vol. 79, no. 4, p. 046601, 2016.

[56] Y. Pomeau, "Brisure spontanee de cristaux bidimensionnels courbes," *Comptes Rendus - Academie des Sciences, Serie II*, vol. 314, no. 6, pp. 553–556, 1992.

[57] G. Ferrand-Drake Del Castillo, R. L. Hailes, and A. Dahlin, "Large Changes in Protonation of Weak Polyelectrolyte Brushes with Salt Concentration-Implications for Protein Immobilization," *Journal of Physical Chemistry Letters*, vol. 11, no. 13, pp. 5212–5218, 2020.

[58] S. S. Sheiko and A. V. Dobrynin, "Architectural Code for Rubber Elasticity: From Supersoft to Superfirm Materials," *Macromolecules*, vol. 52, no. 20, pp. 7531–7546, 2019.

[59] H. Liang, S. S. Sheiko, and A. V. Dobrynin, "Supersoft and Hyperelastic Polymer Networks with Brushlike Strands," *Macromolecules*, vol. 51, pp. 638–645, 2018.

[60] H. Liang, B. J. Morgan, G. Xie, M. R. Martinez, E. B. Zhulina, K. Matyjaszewski, S. S. Sheiko, and A. V. Dobrynin, "Universality of the Entanglement Plateau Modulus of Comb and Bottlebrush Polymer Melts," *Macromolecules*, vol. 51, pp. 10028–10039, 2018.

[61] M. Vatankhah-Varnosfaderani, W. F. Daniel, M. H. Everhart, A. A. Pandya, H. Liang, K. Matyjaszewski, A. V. Dobrynin, and S. S. Sheiko, "Mimicking biological stress–strain behaviour with synthetic elastomers," *Nature*, vol. 549, no. 7673, pp. 497–501, 2017.

[62] L. P. Bré, Y. Zheng, A. P. Pêgo, and W. Wang, "Taking tissue adhesives to the future: from traditional synthetic to new biomimetic approaches," *Biomater. Sci.*, vol. 1, no. 3, pp. 239–253, 2013.

[63] A. H. Hofman, I. A. van Hees, J. Yang, and M. Kamperman, "Bioinspired Underwater Adhesives by Using the Supramolecular Toolbox," *Advanced Materials*, vol. 1704640, p. 1704640, 2018.

[64] F. G. Hamad, Q. Chen, and R. H. Colby, "Linear Viscoelasticity and Swelling of Polyelectrolyte Complex Coacervates," *Macromolecules*, vol. 51, no. 15, pp. 5547–5555, 2018.

[65] C. W. Macosko, *Rheology principles, measurements and applications*. Wiley-VCH, 1994.

[66] A. Reisch, E. Roger, T. Phoeung, C. Antheaume, C. Orthlieb, F. Boulmedais, P. Lavalle, J. B. Schlenoff, B. Frisch, and P. Schaaf, "On the benefits of rubbing salt in the cut: Self-healing of saloplastic PAA/PAH compact polyelectrolyte complexes," *Advanced Materials*, vol. 26, no. 16, pp. 2547–2551, 2014.

[67] J. P. Gong, Y. Katsuyama, T. Kurokawa, and Y. Osada, "Double-network hydrogels with extremely high mechanical strength," *Advanced Materials*, vol. 15, no. 14, pp. 1155–1158, 2003.

[68] P. Rao, T. L. Sun, L. Chen, R. Takahashi, G. Shinohara, H. Guo, D. R. King, T. Kurokawa, and J. P. Gong, "Tough Hydrogels with Fast, Strong, and Reversible Underwater Adhesion Based on a Multiscale Design," *Advanced Materials*, vol. 30, no. 32, pp. 1–8, 2018.

[69] K. Cui, T. L. Sun, X. Liang, K. Nakajima, Y. N. Ye, L. Chen, T. Kurokawa, and J. P. Gong, "Multiscale Energy Dissipation Mechanism in Tough and Self-Healing Hydrogels," *Physical Review Letters*, vol. 121, no. 18, p. 185501, 2018.

[70] T. L. Sun, T. Kurokawa, S. Kuroda, A. B. Ihsan, T. Akasaki, K. Sato, M. A. Haque, T. Nakajima, and J. P. Gong, "Physical hydrogels composed of polyampholytes demonstrate high toughness and viscoelasticity," *Nature Materials*, vol. 12, no. 10, pp. 932–937, 2013.

[71] A. Anastasaki, V. Nikolaou, G. Nurumbetov, P. Wilson, K. Kempe, J. F. Quinn, T. P. Davis, M. R. Whittaker, and D. M. Haddleton, "Cu(0)-Mediated Living Radical Polymerization: A Versatile Tool for Materials Synthesis," *Chemical Reviews*, vol. 116, no. 3, pp. 835–877, 2016.

[72] Y. Gao, T. Zhao, and W. Wang, "Is it ATRP or SET-LRP? Part I: Cu0&CuII/PMDETA-mediated reversible-deactivation radical polymerization," *RSC Advances*, vol. 4, no. 106, pp. 61687–61690, 2014.

[73] D. Baskaran and A. H. Müller, "Anionic vinyl polymerization-50 years after Michael Szwarc," *Progress in Polymer Science (Oxford)*, vol. 32, no. 2, pp. 173–219, 2007.

[74] S. Aoshima and S. Kanaoka, "A renaissance in living cationic polymerization," *Chemical Reviews*, vol. 109, no. 11, pp. 5245–5287, 2009.

[75] S. Antoun, P. Teyssié, and R. Jérôme, "Lithium diisopropylamide as initiator for the anionic polymerization of methacrylates," *Macromolecules*, vol. 30, no. 6, pp. 1556–1561, 1997.

[76] R. B. Grubbs and R. H. Grubbs, "50th Anniversary Perspective: Living Polymerization - Emphasizing the Molecule in Macromolecules," *Macromolecules*, vol. 50, no. 18, pp. 6979–6997, 2017.

[77] F. Chen, D. Dai, J. Yang, Z. Fei, and M. Zhong, "Controlled synthesis of polyelectrolytes by 4-cyanopentanoic acid dithiobenzoate mediated RAFT polymerization," *Journal of Macromolecular Science, Part A: Pure and Applied Chemistry*, vol. 50, no. 9, pp. 1002–1006, 2013.

[78] S. Perrier, "50th Anniversary Perspective: RAFT Polymerization - A User Guide," *Macromolecules*, vol. 50, no. 19, pp. 7433–7447, 2017.

[79] C. C. Fouillet, T. L. Greaves, J. F. Quinn, T. P. Davis, J. Adamcik, M. A. Sani, F. Separovic, C. J. Drummond, and R. Mezzenga, "Copolyampholytes Produced from RAFT Polymerization of Protic Ionic Liquids," *Macromolecules*, vol. 50, no. 22, pp. 8965–8978, 2017.

[80] A. Laschewsky, "Recent trends in the synthesis of polyelectrolytes," *Current Opinion in Colloid and Interface Science*, vol. 17, no. 2, pp. 56–63, 2012.

[81] X. Cao and Z. An, "RAFT synthesis in water of cationic polyelectrolytes with tunable UCST," *Macromolecular Rapid Communications*, vol. 36, no. 23, pp. 2107–2110, 2015.

[82] C. L. McCormick, B. S. Sumerlin, B. S. Lokitz, and J. E. Stempka, "RAFT-synthesized diblock and triblock copolymers: thermally-induced supramolecular assembly in aqueous media," *Soft Matter*, vol. 4, no. 9, p. 1760, 2008.

[83] S. E. Morgan, P. Jones, A. S. Lamont, A. Heidenreich, and C. L. McCormick, "Layer-by-layer assembly of pH-responsive, compositionally controlled (Co)polyelectrolytes synthesized via RAFT," *Langmuir*, vol. 23, no. 1, pp. 230–240, 2007.

[84] F. Lorandi, M. Fantin, Y. Wang, A. A. Isse, A. Gennaro, and K. Matyjaszewski, "Atom Transfer Radical Polymerization of Acrylic and Methacrylic Acids: Preparation of Acidic Polymers with Various Architectures," *ACS Macro Letters*, vol. 9, no. 5, pp. 693–699, 2020.

[85] L. Fu, A. Simakova, M. Fantin, Y. Wang, and K. Matyjaszewski, "Direct ATRP of Methacrylic Acid with Iron-Porphyrin Based Catalysts," *ACS Macro Letters*, vol. 7, no. 1, pp. 26–30, 2018.

[86] R. W. Lewis, R. A. Evans, N. Malic, K. Saito, and N. R. Cameron, "Ultra-fast aqueous polymerisation of acrylamides by high power visible light direct photoactivation RAFT polymerisation," *Polymer Chemistry*, pp. 60–68, 2017.

[87] H. Willcock and R. K. O'Reilly, "End group removal and modification of RAFT polymers," *Polymer Chemistry*, vol. 1, no. 2, pp. 149–157, 2010.

[88] J. S. Wang and K. Matyjaszewski, "Controlled/"Living" Radical Polymerization. Halogen Atom Transfer Radical Polymerization Promoted by a Cu(I)/Cu(II) Redox Process," *Macromolecules*, vol. 28, no. 23, pp. 7901–7910, 1995.

[89] G. Lligadas, S. Grama, and V. Percec, "Recent Developments in the Synthesis of Biomacromolecules and their Conjugates by Single Electron Transfer-Living Radical Polymerization," *Biomacromolecules*, vol. 18, no. 4, pp. 1039–1063, 2017.

[90] J. Xia, S. G. Gaynor, and K. Matyjaszewski, "Controlled/"Living" Radial Polymerizatioin. Atom Transfer Radical Polymerization of Acrylates at Ambient Temperature.," *Macromolecules*, vol. 31, no. Figure 2, pp. 5958–5959, 1998.

[91] Y. Wang, N. Soerensen, M. Zhong, H. Schroeder, M. Buback, and K. Matyjaszewski, "Improving the "livingness" of ATRP by reducing Cu catalyst concentration," *Macromolecules*, vol. 46, no. 3, pp. 683–691, 2013.

[92] A. E. Enciso, F. Lorandi, A. Mehmood, M. Fantin, G. Szczepaniak, B. G. Janesko, and K. Matyjaszewski, "p-Substituted Tris(2-pyridylmethyl)amines as Ligands for Highly Active ATRP Catalysts: Facile Synthesis and Characterization," *Angewandte Chemie*, vol. 132, no. 35, pp. 15020–15030, 2020.

[93] K. Matyjaszewski, Y. Nakagawa, and C. B. Jasieczek, "Polymerization of n-butyl acrylate by atom transfer radical polymerization. Remarkable effect of ethylene carbonate and other solvents," *Macromolecules*, vol. 31, no. 5, pp. 1535–1541, 1998.

[94] D. Konkolewicz, Y. Wang, P. Krys, M. Zhong, A. A. Isse, A. Gennaro, and K. Matyjaszewski, "SARA ATRP or SET-LRP. End of controversy?," *Polymer Chemistry*, vol. 5, no. 15, pp. 4396–4417, 2014.

[95] N. H. Nguyen, C. Rodriguez-Emmenegger, E. Brynda, Z. Sedlakova, and V. Percec, "SET-LRP of N-(2-hydroxypropyl)methacrylamide in H2O," *Polymer Chemistry*, vol. 4, no. 8, pp. 2424–2427, 2013.

[96] A. Anastasaki, V. Nikolaou, and D. M. Haddleton, "Cu(0)-mediated living radical polymerization: recent highlights and applications; a perspective," *Polym. Chem.*, vol. 7, no. 5, pp. 1002–1026, 2016.

[97] K. Matyjaszewski, S. Coca, S. G. Gaynor, M. Wei, and B. E. Woodworth, "Zerovalent metals in controlled/"living" radical polymerization," *Macromolecules*, vol. 30, no. 23, pp. 7348–7350, 1997.

[98] G. Lligadas, S. Grama, and V. Percec, "Single-Electron Transfer Living Radical Polymerization Platform to Practice, Develop, and Invent," *Biomacromolecules*, vol. 18, no. 10, pp. 2981–3008, 2017.

[99] D. Konkolewicz, Y. Wang, P. Krys, M. Zhong, A. A. Isse, A. Gennaro, and K. Matyjaszewski, "SARA ATRP or SET-LRP. End of controversy?," *Polymer Chemistry*, vol. 5, no. 15, p. 4409, 2014.

[100] A. Anastasaki, V. Nikolaou, Q. Zhang, J. Burns, S. R. Samanta, C. Waldron, A. J. Haddleton, R. McHale, D. Fox, V. Percec, P. Wilson, and D. M. Haddleton, "Copper(II)/tertiary amine synergy in photoinduced living radical polymerization: Accelerated synthesis of ω-functional and α,ω-heterofunctional poly(acrylates)," *Journal of the American Chemical Society*, vol. 136, no. 3, pp. 1141–1149, 2014.

[101] J. Chiefari, Y. K. B. Chong, F. Ercole, J. Krstina, J. Jeffery, T. P. T. Le, R. T. A. Mayadunne, G. F. Meijs, C. L. Moad, G. Moad, E. Rizzardo, and S. H. Thang, "Living Free-Radical Polymerization by Reversible Addition - Fragmentation Chain Transfer: The RAFT Process," *Macromolecules*, vol. 31, no. 16, pp. 5559–5562, 1998.

[102] A. Gregory and M. H. Stenzel, "Complex polymer architectures via RAFT polymerization: From fundamental process to extending the scope using click chemistry and nature's building blocks," *Progress in Polymer Science (Oxford)*, vol. 37, no. 1, pp. 38–105, 2012.

[103] D. J. Keddie, G. Moad, E. Rizzardo, and S. H. Thang, "RAFT agent design and synthesis," *Macromolecules*, vol. 45, no. 13, pp. 5321–5342, 2012.

[104] S. Li, G. Han, and W. Zhang, "Photoregulated reversible addition-fragmentation chain transfer (RAFT) polymerization," *Polymer Chemistry*, vol. 11, no. 11, pp. 1830–1844, 2020.

[105] R. N. Carmean, T. E. Becker, M. B. Sims, and B. S. Sumerlin, "Ultra-High Molecular Weights via Aqueous Reversible-Deactivation Radical Polymerization," *Chem*, vol. 2, no. 1, pp. 93–101, 2017.

[106] N. Zaquen, A. M. Kadir, A. Iasa, N. Corrigan, T. Junkers, P. B. Zetterlund, and C. Boyer, "Rapid Oxygen Tolerant Aqueous RAFT Photopolymerization in Continuous Flow Reactors," *Macromolecules*, vol. 52, no. 4, pp. 1609–1619, 2019.

[107] G. Szczepaniak, L. Fu, H. Jafari, K. Kapil, and K. Matyjaszewski, "Making ATRP More Practical: Oxygen Tolerance," *Accounts of Chemical Research*, vol. 54, no. 7, pp. 1779–1790, 2021.

[108] Q. Zhang, L. Voorhaar, B. G. De Geest, and R. Hoogenboom, "One-pot preparation of inert well-defined polymers by RAFT polymerization and in situ end group transformation," *Macromolecular Rapid Communications*, vol. 36, no. 12, pp. 1177–1183, 2015.

[109] A. Anastasaki, J. Willenbacher, C. Fleischmann, W. R. Gutekunst, and C. J. Hawker, "End group modification of poly(acrylates) obtained: Via ATRP: A user guide," *Polymer Chemistry*, vol. 8, no. 4, pp. 689–697, 2017.

[110] A. P. Vogt and B. S. Sumerlin, "An efficient route to macromonomers via ATRP and click chemistry," *Macromolecules*, vol. 39, no. 16, pp. 5286–5292, 2006.

[111] D. B. Thomas, A. J. Convertine, R. D. Hester, A. B. Lowe, and C. L. McCormick, "Hydrolytic Susceptibility of Dithioester Chain Transfer Agents and Implications in Aqueous RAFT Polymerizations," *Macromolecules*, vol. 37, no. 5, pp. 1735–1741, 2004.

[112] G.-Z. Li, R. K. Randev, A. H. Soeriyadi, G. Rees, C. Boyer, Z. Tong, T. P. Davis, C. R. Becer, and D. M. Haddleton, "Investigation into thiol-(meth)acrylate Michael addition reactions using amine and phosphine catalysts," *Polymer Chemistry*, vol. 1, no. 8, p. 1196, 2010.

[113] X. P. Qiu and F. M. Winnik, "Synthesis of α,ω-dimercapto poly(N-isopropylacrylamides) by RAFT polymerization with a hydrophilic difunctional chain transfer agent," *Macromolecules*, vol. 40, no. 4, pp. 872–878, 2007.

[114] A. Filippov, I. Van Hees, R. Fokkink, I. Voets, and M. Kamperman, "Rapid and Quantitative De-tert-butylation for Poly(acrylic acid) Block Copolymers and Influence on Relaxation of Thermoassociated Transient Networks," *Macromolecules*, vol. 51, no. 20, pp. 8316–8323, 2018.

[115] S. A. Elias, *Plastics in the ocean*, vol. 1-5. Elsevier Inc., 2017.

[116] D. Hoornweg, P. Bhada-Tata, and C. Kennedy, "Waste production must peak this century," *Nature*, vol. 502, no. 7473, pp. 615–617, 2013.

[117] W. C. Li, H. F. Tse, and L. Fok, "Plastic waste in the marine environment: A review of sources, occurrence and effects," *Science of the Total Environment*, vol. 566-567, pp. 333–349, 2016.

[118] C. T. Roebroek, S. Harrigan, T. H. Van Emmerik, C. Baugh, D. Eilander, C. Prudhomme, and F. Pappenberger, "Plastic in global rivers: Are floods making it worse?," *Environmental Research Letters*, vol. 16, no. 2, 2021.

[119] “Case nr. C/09/571932 / HA ZA 19-379,” 2021.

Summary

The design of the molecules from which life emerges is the polymeric architecture. Genetic information is written down on DNA and RNA, proteins catalyze a web of reactions of an unimaginable complexity, and at the same time enable the mechanical integrity of structures as small as viruses, the nucleosome and organelles, and as large as entire organisms. Often, the ingenuity of natural polymers takes chemists by surprise. While it is inconceivable that one recreates in the laboratory all the lushly orchestrated processes that make up an entire ecosystem, or even a cell, the solutions that organisms find to adapt to the hardships of their everyday life can inspire breakthroughs in designing materials to solve problems in the sphere of human life.

The problem that this thesis relates to is the problem of underwater adhesion. Many animals from marine environments rely on robust adhesion to underwater surfaces to adapt to their turbulent habitat. The threads that mussels employ to anchor themselves to rocks are known to many, but natural implementations of underwater adhesion are much more diverse. For instance, sandcastle worms can inhabit the shorelines of California forming dense colonies by excreting a glue that they use to glue together sand grains. Caddisfly larvae "dress" themselves in protective hulls that they glue together from materials found in streams, and barnacles are notorious in the shipping industry for their robust attachment to ship hulls.

Underwater adhesion would also help humans to adapt to the circumstances of our life: in the Introduction (Chapter 1), I describe them as biomaterials that can act instead of sutures to recover wounds, and as sealants for torn tissues. Moreover, uncovering a composition that would enable a material to adhere to biological tissues will advance possibilities for future implants and tissue engineering. However, few materials made by humans fit the specifications that biomaterials have: to stick to tissues, their interface must be very hydrophilic, yet, the material must not dissolve in water. On of the few classes of materials to bridge this contradiction is the complex coacervate: a complex of oppositely charged polymers in water. Whereas complex coacervate are already quite versatile in their mechanics, there is a need to create ways to make them harder, and more resistant to big deformations. As I argue in Chapter 1, this is necessary for two reasons: to allow the adjustment of mechanical parameters to fit a certain target tissue, and to allow on-demand changes of these parameters upon a certain stimulus.

In Chapter 2, transient crosslinks, bonds that are in equilibrium between an "open"

and "closed" state, are shown to be a complementary entity to set the viscoelastic parameters of complex coacervates. Normally, salt concentration and the chemistry of the polyelectrolyte chains alone determine the mechanics of coacervate complexes. However, the incorporation of ligands into polyelectrolyte chains allows metal ions such as Zn^{2+} and Ni^{2+} to set rheological fate of a coacervate independently of its salt concentration and monomer chemistry. We show that this promise of orthogonality is approached when the viscoelasticity of the coacervate contributes less to the rheology than the metal-ligand network, which forms as a consequence of a sufficient density of metal-ligand bonds. Contrarily, the complex coacervate dominates the transient crosslinks when the relaxation times that the coacervate provides outlive the metal-ligand bonds. Notably, the relaxation times of "hybrid" complexes were longer than the times of either metal-ligand complex or coacervate complex.

Taking control of the *linear* viscoelasticity, or the flow behaviour when small (model) deformations are applied, of coacervates is only a preliminary step. In Chapter 3, we show that the incorporation of transient bonds may also help to increase the tolerance of coacervates to high strain rates and amplitudes, and thus postpone the incidence of failure. Arriving at coacervates with sufficient toughness for biomaterial applications will require building blocks that are not just resistant to large deformations, but also incorporate strain hardening by design. The complexes of Chapter 2 and 3 show strain hardening, but only to limited extent, control over which seems elusive. In Chapter 4, we show that polyelectrolytes of bottlebrush architecture display characteristics of built-in semiflexibility, and that they are able to form complexes. Future studies must address the impact of semiflexibility on the non-linear mechanics of coacervates, and thus uncover whether semiflexible polyelectrolytes indeed contribute to high-strain tolerance and strain hardening in coacervate complexes.

A crucial aspect of the glue of sandcastle worms is the transformation from a liquid to a solid upon its delivery — an example of a "triggered" response. In Chapter 5, we describe the synthesis of a polyelectrolyte that is designed to enable a complex coacervate to respond with solidification upon an increase of temperature. To this end, we polymerized *tert*-butyl acrylate (pT) "into" a poly(*N*-isopropylacrylamide) (pN) chain transfer agent using RAFT polymerization. pN is known to undergo a solubility transition, in which it is rendered water-insoluble above a certain temperature. The result is the triblock copolymer pNTN, which can be transformed into the corresponding poly(acrylic acid) (pA) block copolymer. However, we found that the common method of de-esterification (removal of the *tert*-butyl group) did not cleanly yield pNAN. Thus, we took upon us the task to find a reliable method to be able to synthesize pNAN, and related "blocky" pA-based macromolecules. The novelty of Chapter 5 is the quantitative removal of polymeric *tert*-butyl esters us-

ing HCl in hexafluoroisopropanol (HFIP). We show that cleanly (with HCl/HFIP) deprotected solutions of pNAN show the expected solidification upon heating to a temperature above which pN becomes insoluble. pNAN residues deprotected with the commonly used trifluoroacetic acid in dichloromethane showed the presence of residual *tert*-butyl ester, and, importantly, showed a much reduced response to increased temperatures. Thus, we provide the biomaterials community with an improved deprotection chemistry, which turns out to be highly relevant for the synthesis of macromolecules for the use in responsive coacervates.

In Chapter 6 (General Discussion), I confront the work done in this thesis with the real-world requirements for biomaterials, and with the evolution of macromolecules towards use in them. I address the lack of biocompatibility of the structures used in this thesis and elsewhere, highlight the importance of testing the behaviour of candidate biomaterials at high strains, and in realistic deformation conditions, and reflect on the use of scattering studies in this thesis, and inquiries into the structure and dynamics of hydrophilic polymer structures in general. The practice of polymerization chemistry in academic labs is also subjected to criticism, and I point out the need for safe, cheap, and mild chemistries for the synthesis of polyelectrolytes to enable the manufacture of potential biomaterials at a large scale.

List of publications

S. P. Pujari, A. D. Filippov, S. Gangarapu, H. Zuilhof, "High-Density Modification of H-Terminated Si(111) Surfaces Using Short-Chain Alkynes"
Langmuir, 2017, **33** (51), 14599–14607

J. Yang, M. K. Włodarczyk-Biegun, A. Filippov, S. Akerboom, M. Dompè, I. A. van Hees, M. Mocan, M. Kamperman, "Functional Polymeric Materials Inspired by Geckos, Mussels, and Spider Silk"
Macromolular Chemistry and Physics, 2018, **219**, 1800051

A. D. Filippov, I. van Hees, R. Fokkink, I. Voets, M. Kamperman, "Rapid and quantitative de-tert-butylation for poly(acrylic acid) block copolymers and influence on relaxation of thermoassociated transient networks"
Macromolecules, 2018, **51** (20), 8316–8323

M. Kamperman, M. Dompè, A.D. Filippov, "Adhesive composition"
Patent No. WO2019172764, 2019

A. D. Filippov, J. Sprakel, M. Kamperman, "Complex coacervation and metal–ligand bonding as synergistic design elements for aqueous viscoelastic materials"
Soft Matter, 2021, **17**, 3294-3305

About the author

Alexei Dmitrievitsj Filippov (Aljosha) was born in Moscow, Russian Federation, on the 12th of February, 1992. He received his primary and secondary education in Leiden, The Netherlands, and graduated from the Stedelijk Gymansium Leiden in 2010.

He then enrolled at Wageningen University for the BSc programme in Molecular Life Sciences, which he finished *cum laude* in 2013. Subsequently, he continued with the eponymous Master's degree, which he received *cum laude* in 2015. Alexei's MSc programme involved a six-month internship at the Institut Charles Sadron in Strasbourg and two theses, one at the Laboratory of Organic Chemistry, and the other at the Laboratory of Physical Chemistry. The latter was awarded the Unilever Research Prize, and he continued to study with the same chair group, now as a PhD candidate under the supervision of Marleen Kamperman and Joris Sprakel.

During his PhD study, Alexei developed polymeric architectures for use in future underwater adhesives. In 2019, he was part of the Lindau Nobel Laureate Meetings, and worked for three months in the Catalan Institute for Nanoscience and Nanotechnology with Daniel Ruiz-Molina. He also taught a BSc course in quantum mechanics for six months in 2020. Following his promotion, Alexei pursues an academic career on the interface between chemistry and physics. Beyond his studies, he organizes folk dance events, goes rock climbing, and records music in his home studio.

Acknowledgements

The past five-and-a-half years of my life were dedicated to research in the Laboratory of Physical Chemistry and Soft Matter, the result of which is this thesis. Over these years I have become indebted to many people, both on a professional and personal level. What follows here is my futile attempt to express the deep gratitude I feel towards you all.

Marleen, thank you for seeing a researcher in me, a year ahead of the end of my Master's programme, for always believing in me through the course of the past years, and for supporting me through many doubts. Thank you for laying the inspiring foundation under this (and more) work, and opening the world of coacervates for me.

Joris, I am grateful for you joining halfway through the project, and for taking on the role of my promotor. You uniquely combine a no-nonsense attitude towards research with your endless reservoir of ideas. The former was instrumental in shifting into the right gear towards the end. May the latter be a gift that keeps on giving – I wish you all the best in your fascinating new research direction!

Daan, брат, thank you for your friendship and loyalty, and for sharing music, climbing, as well as countless trips through the mountains. May countless more follow. I'm proud that we both make it through our PhDs as peers, and feel our mutual paranymphship as a fitting conclusion.

Riccardo, grazie mille for taking on the role of paranymph. Before your arrival at PCC, I already drank too much coffee, and this did not change after you arrived. I will remember all the lunches and breaks fondly, as well as your support, kindness, gnocchi and pasta. And I'm looking forward to our climb in Italy. Best of luck for the remainder of your PhD!

Jasper, my first steps in the field of soft matter were under your guidance, and my choice to steer away from "pure" organic chemistry had a lot to do with your course Advanced Soft Matter. You supervised the initial stretch of the work in this book, and helped me get on board the PCC ship. Thank you being my teacher – you are an absolute giant in the field.

Frans, you were the first to focus my curiosity towards polymers and physics in general, and opened the door to any understanding of thermodynamics that I have. We really should have worked together more – maybe we should take another look at these `sfbox` results from last decade. Thank you for the courage and inspiration!

Ilja Voets, thank you for your contribution to Chapter 5, the first published work

in this thesis. Your positive attitude towards the manuscript and support in the form of X-ray radiation transformed it into a piece of work that I am proud of.

Joshua, thank you for your input in rheological matters, and for your frankness in conversation. Remco, how can I even think of writing this thesis without acknowledging your never-ending support in the light scattering aspects of my work. Half of the chapters in this work are a witness to your understanding of scattering techniques. I also remember our trip to Grenoble with Marco and Ilse, and innumerable lunch-hour discussions. Diane, you taught me during my first attempts at Schlenk technique and polymer synthesis. It was a lot of fun, and I feel grateful for you sharing your experience.

Mara, Leonie, thank you for handling the administrative side, and sorry for my occasional disregard for punctuality. Mara, you always made me feel welcome and understood during all this time at PCC. I wish you the best in your new career, and it is so inspiring to see you chase your dreams. Leonie, thank you for your help and kindness. Josie, you have left behind something in the hearts of all people that worked with you around. Thanks for all the sunshine you brought into this place.

To my coacervate colleagues Macro, Ilse, and Anton – thanks for the countless exchanges, and for always being ready to discuss work and life. All of you delivered good work way ahead of me, and I wish you the best in your new jobs and lives.

To my early officemates Marco, Nicolò, Slav, and Simone, thanks for the vibe in 7062. I'm sorry for the coffee requests. It won't happen again. But never say never. Speaking of which, Nicolò, thank you for the dinner invitations of the past years. Our office hours were not necessarily well-aligned, but our dinner times, man! I remember our conversations dearly.

To my colleagues in Barcelona - Dani, Josep, Miguel, thank you for the warm welcome and the collaboration.

During the post-2020 era a lot of *unprecedented* changes occurred, including a change in the 7062 shift. But I am grateful to have returned, because now I have the pleasure of thanking Chandan, Larry, and José for their company. Unfortunately I finished my PhD now, but, once again, never say never. Good luck with your pursuits. The future of 7062 rests in your hands.

To those who frequented 7070 in the past years, I am looking at you Qimeng, Tom, Marco, Vadid, thanks for tolerating repeated plays of João Gilberto's "Chega de Saudade", and further breaches of GLP. Vahid, I will remember our many encounters in the lab and the office. It was a pleasure to converse around the topics of our work and our lives with someone as kind as you. Tom, thank you for always leaving your office door open to discuss science. You contributed more than you perhaps imagine to the work in this thesis, but very possibly also to future projects. I did not always take your kind critique to heart, which in retrospect I probably should have! It

would be my pleasure to work together more. Qi Meng, I will remember countless exchanges in offices and hallways. You have the unique quality to turn pessimism into, paradoxically, an uplifting art form. Wherever you are, hope we meet soon.

Hanne, we shared much conversation time since our very first hallway chat in, I don't know, 2014? You also made me feel very understood, and I appreciated this sense of unguardedness that our chats had. I am still grateful to have been your colleague for so long. You are very supportive, but at the same time a deep thinker that reaches very far into many spaces. I am so glad you have a spot amongst the illustrious PCC *permanents*, for your incredible talent as a scientist, but just as much for the level of humanity and respect you extend to everyone. Marcel, you are so *real*. I am impressed by your constructions and engineering mindset. I hope you follow the path of the *true Sashimi*. Martijn, thank you for your friendship and interest. Too bad our summer plans didn't work out... yet, hopefully! I hope you keep cultivating your interest in *tonal* music, next to your awesome work in science. Justin, we share so many of our scientific interests, and probably even more when it comes to non-scientific ones. I hope we get to talk soon again, four years of colleagueship was too short for me!

Ruben, JB, Julia, thanks for all the climbing and the colleagueship. It was great to share the passion of doing climbs and science with you. Jan Maarten, Ties, Pieter, Justin, Joanne, Jessica, you constitute the old school of PCC colleagues, and I remember you for your fun at lunch tables and elsewhere on the grey floors of Helix. Thanks for keeping the office doors open, and for sharing drinks. In particular, Wolf, Lione, I acknowledge you for introducing me to road biking. My health thanks you! Raoul, Ralph, Inge, Justine, Niek, Rob, Dana, I always felt your contribution to the social fabric of PCC, thank you for that. Ali, thank you for our frank conversations. Akankshya, thanks for discussing (*real*) literature with me! Zohreh, Ketan, Siddharth, welcome to the group, I wish I got to now you better, good luck in your endeavours here and elsewhere!

To the ORC colleagues – you were the best neighbours. Thanks for all the chats, reagents, solvents, and effortless access to the spectroscopic facilities. Maarten, thank you for helping out in the initial planning for Chapter 2. Sidhu, I am really glad you stayed around in Wageningen. Thank you for your continued encouragements and kindness.

Mariska, you joined me for your bachelor's thesis, and together we installed a solid foundation underneath Chapter 2. Your efforts proved invaluable, and I really enjoyed working with you. Emma, thanks for working with me for the first few miles towards the destination that is Chapter 4. Lennart, Sjoerd, it was a pleasure to supervise you. I wish all of you the best in your careers.

Charlotte, Laetitia, Daan, Solina, Kiki, Eric, Arvi, you are the *inner circle* of the

Droev family, and I am forever grateful to you for sharing so much together over the past years. New arrivals Eva, Jolan, Brechje, Fiete, thank you for the great vibes living together and many shared interests. Further thanks to the wider Droev family, which is far too numerous to exhaustively mention here. Johanna, thanks for showing me the good life. Nico, let's make some music together. Kris, we should celebrate a decade of music together. Djoerd, Maureen, Eli, thank you for your endless neighborhood and hospitality. Renske, thank you for everything we share, and for being a bal folk co-organizer partner *par excellence* in crime. Linda, not one but *two* of your designs grace the work in this book, and I look forward to celebrating the first decade of our friendship. Joeri, I miss our times in Gruismachine. I'm glad you are my friend. Lieuwe, thank you for your friendship and insight.

Lieve Wendy, I feel overwhelming gratitude for your love and company. You have always supported me, and I feel lucky to have you by my side.

Юля и Дима, thank you for taking care of me always and everywhere. This book is dedicated to you.

List of completed training activities

Discipline-specific activities

- Physics @ FOM, FOM, Veldhoven, 2015
- Wageningen Organic Chemistry Symposium, KNCV, Wageningen, 2016
- Dutch Polymer Days, NWO, Lunteren, 2016†
- CHAINS, NWO, Veldhoven, 2016†
- Han sur Lesse winterschool, Han sur Lesse, 2016
- Dutch Polymer Days, NWO, Lunteren, 2017†
- Han sur Lesse winterchool, Han sur Lesse, 2017
- Dutch Polymer Days, NWO, Lunteren, 2018‡
- RPK B: Polymer Physics training, RPK, Utrecht, 2018
- IACIS conference, IACIS, Rotterdam, 2018†
- International Symposium on Polyelectrolytes Pre-school, VLAG, Wageningen, 2018
- International Symposium on Polyelectrolytes, VLAG, Wageningen, 2018‡
- BioSmartTrainee Paris School, BioSmartTrainee, Paris, 2018
- Dutch Polymer Days, NWO, Lunteren, 2019‡
- 69th Lindau Nobel Laureate Meeting dedicated to Physics, Lindau Nobel Laureate Meetings, Lindau, 2019

General courses

- Teaching and Supervising Thesis Students, WGS, Wageningen, 2017
- Bridging across Cultural Differences, WGS, Wageningen, 2018
- Brain training, WGS, Wageningen, 2018
- Brain-friendly working and writing, WGS, Wageningen, 2018
- Writing Grant Proposals, WGS, Wageningen, 2018
- Career Perspectives, WGS, Wageningen, 2021

Other activities

- Preparation of research proposal, PCC, Wageningen, 2017
- Participation in PCC group meetings, PCC, Wageningen, 2017-2021
- PCC seminars, PCC, Wageningen, 2017-2021
- PCC Journal Club, PCC, Wageningen, 2017-2021

† poster presentation
‡ oral presentation

The research described in this thesis was financially supported by the Netherlands Organisation for Scientific Research (NWO) through VIDI grant number 723.013.005.

Cover design by Linda Calciolari
Printed by proefschriftmaken.nl